Universidade do Minho
Escola de Medicina

Ana Isabel de Araújo Coelho

The human brain connectome in aging: MRI biomarkers of cognitive preservation and decline

maio de 2021

The human brain connectome in aging:
MRI biomarkers of cognitive preservation and decline

Ana Isabel de Araújo Coelho

UMinho | 2021

Universidade do Minho
Escola de Medicina

Ana Isabel de Araújo Coelho

The human brain connectome in aging: MRI biomarkers of cognitive preservation and decline

Tese de Doutoramento

Ciências da Saúde

Trabalho efetuado sobre a orientação de

Professor Doutor Nuno Jorge Carvalho Sousa

maio de 2021

DIREITOS DE AUTOR E CONDIÇÕES DE UTILIZAÇÃO DO TRABALHO POR TERCEIROS

Este é um trabalho académico que pode ser utilizado por terceiros desde que respeitadas as regras e boas práticas internacionalmente aceites, no que concerne aos direitos de autor e direitos conexos.

Assim, o presente trabalho pode ser utilizado nos termos previstos na licença abaixo indicada.

Caso o utilizador necessite de permissão para poder fazer um uso do trabalho em condições não previstas no licenciamento indicado, deverá contactar o autor, através do RepositóriUM da Universidade do Minho.

Licença concedida aos utilizadores deste trabalho

Atribuição-NãoComercial-SemDerivações

CC BY-NC-ND

https://creativecommons.org/licenses/by-nc-nd/4.0/

Acknowledgments

First, I would like to thank my parents for all the love, care and support, you are the main responsible of who I am today. To my sister Cláudia for all the support and shared experience, especially given that we entered in the PhD journey at the same time. To Tiago for all the encouragement in the good and bad moments, for always being by my side and motivate me to give my best.

To Professor Nuno Sousa, my supervisor, for all the mentorship, guidance and trust placed in me. I really appreciate all our discussions and I believe you made me grow in several aspects of my life.

To Professor Henrique Fernandes for all the support, contributions and all the enlightening discussions. I am very thankful that you accepted to take part in this journey. This work would not be possible without your help.

To the marvelous neuroimaging team for being so supportive in every moment. I believe we are a great team (in and out of work) and it will only get better. A special word to Paulo, Pedro and Ricardo for welcoming me to the team and teaching me everything they could.

To Ed Ganz for all the support and always being available to revise my manuscripts.

To the School of Medicine and ICVS for accepting me into the PhD program and providing all the necessary tools.

To the staff from 2CA and Hospital de Braga for the assistance in the magnetic resonance imaging acquisitions.

To all the participants from the SWITCHBOX project.

This work was financially supported by a grant of the project NORTE-08-5369-FSE-000041, supported by Norte Portugal Regional Operational Programme (NORTE 2020), under the PORTUGAL 2020 Partnership Agreement, through the European Regional Development Fund (ERDF) (grant UMINHO/BD/51/2017).

STATEMENT OF INTEGRITY

I hereby declare having conducted this academic work with integrity. I confirm that I have not used plagiarism or any form of undue use of information or falsification of results along the process leading to its elaboration.

I further declare that I have fully acknowledged the Code of Ethical Conduct of the University of Minho.

Assinado por : **ANA ISABEL DE ARAÚJO COELHO**
Num. de Identificação Civil: BI141404779
Data: 2021.05.07 11:55:26 +0100

O conectoma cerebral humano no envelhecimento: biomarcadores de RM de preservação e declínio cognitivo

Resumo

O envelhecimento normal é caracterizado por alterações no cérebro e na cognição, mesmo na ausência de doença. Visivelmente, as trajetórias de desempenho cognitivo no envelhecimento apresentam alta variabilidade inter-individual e vários fatores são conhecidos por contribuir para essa variabilidade. No entanto, os mecanismos neurais que provocam diferentes níveis de desempenho cognitivo em idosos ainda são mal compreendidos. O surgimento de novas ferramentas de análise na investigação em neuroimagem, tais como a análise de redes e parcelamento baseado em conectividade, pode ajudar a clarificar o envelhecimento do cérebro e as trajetórias cognitivas diferenciais. Contudo, até ao momento, poucos estudos aplicaram essas novas ferramentas para estudar alterações relacionadas com a idade nas redes cerebrais estruturais de matéria branca. O objetivo principal desta tese foi fornecer novo conhecimento sobre as mudanças induzidas pelo envelhecimento nas redes cerebrais estruturais de matéria branca e a sua associação com o estado cognitivo, através do uso de novas ferramentas de neuroimagem e estudos longitudinais. Os resultados obtidos revelaram que o envelhecimento é caracterizado por uma deterioração da integridade de matéria branca, que está associada a mudanças longitudinais na cognição. Também identificamos pela primeira vez uma sub-rede com mudanças significativas na conectividade estrutural ao longo do envelhecimento, que englobou diminuições sobretudo nas conexões intra-hemisféricas e aumentos principalmente nas conexões inter-hemisféricas. A análise das propriedades topológicas das redes cerebrais revelou uma diminuição na integração e aumento na segregação, sugerindo um cérebro mais "desconectado" com o envelhecimento. Por fim, também desenvolvemos um novo método para criar um parcelamento do cérebro baseado em conectividade e aplicámo-lo para estudar o envelhecimento do cérebro. Replicando o nosso resultado anterior, encontramos uma sub-rede com diminuições significativas nas conexões intra-hemisféricas e aumentos nas conexões inter-hemisféricas. A análise das características topológicas revelou resultados desafiadores que podem ser explicados pela maior resolução do parcelamento desenvolvido. De um modo geral, estes resultados podem ajudar a identificar os principais impulsionadores das alterações de matéria branca em diferentes níveis cognitivos, o que pode levar ao desenvolvimento de novos biomarcadores cerebrais in vivo de variabilidade inter-individual em trajetórias cognitivas.

Palavras-chave: envelhecimento; RM de difusão; matéria branca; performance cognitiva; rede cerebral; parcelamento cerebral

The human brain connectome in aging: MRI biomarkers of cognitive preservation and decline

Abstract

Normal aging is characterized by alterations in the brain and in cognition, even in the absence of disease. Noticeably, cognitive performance trajectories in aging exhibit high inter-individual variability and multiple factors are known to contribute to this variability. Still, the neural mechanisms which elicit different levels of cognitive performance in older adults are yet poorly understood. The emergence of new analytical tools in neuroimaging research, such as network analysis and connectivity-based parcellation, can help shed new light regarding the aging brain and the differential cognitive trajectories. However, to date few studies have applied these new tools to study age-related alterations in white matter structural brain networks. The main goal of this thesis was to provide new insights about the changes induced by aging in white matter structural brain networks and their association with cognitive status, through the use of new neuroimaging tools and longitudinal designs. Our findings revealed that aging is characterized by a deterioration of white matter integrity which is associated with longitudinal changes in cognition. We also identified for the first time a sub-network with significant changes in structural connectivity along aging, which encompassed decreases mainly in intra-hemispheric connections and increases mostly in inter-hemispheric connections. The analysis of the topological properties of brain networks revealed a decrease in integration and an increase in segregation, suggesting a more "disconnected" brain along aging. Finally, we also developed a new method to create a connectivity-based parcellation of the brain and applied it to study the aging brain. Replicating our previous result, we found a sub-network with significant decreases in intra-hemispheric connections and increases in inter-hemispheric connections. The analysis of the topological features revealed challenging results which could be explained by the higher resolution of the developed parcellation. Altogether, these findings may help identify the main drivers of white matter alterations at different cognitive levels, which could lead to the development of new in-vivo brain biomarkers of inter-individual variability in cognitive trajectories.

Keywords: aging; diffusion MRI; white matter; cognitive performance; brain network; brain parcellation

Table of Contents

List of Abbreviations

A

AAL – Automated Anatomical Labeling

AD – Axial diffusivity

AD – Alzheimer's Disease

ANCOVA – Analysis of Covariance

ANTs – Advanced Normalization Tools

ATR – Anterior thalamic radiation

B

BOLD – Blood oxygen level dependent

C

CBP – Connectivity-based parcellation

CGC – Cingulate gyrus part of cingulum

CHF – Connectivity homogeneity fingerprint

CLTR – Consistent long-term retrieval

CRUNCH – Compensation-related utilization of neural circuits hypothesis

CSF – Cerebrospinal fluid

CST – Corticospinal tract

D

DLPFC – Dorsolateral prefrontal cortex

DMN – Default mode network

DR – Delayed-recall

DTI – Diffusion tensor imaging

DWI – Diffusion weighted imaging

E

EXEC – General cognition and executive functioning dimension

F

FA – Fractional Anisotropy

FC – Functional connectivity

FDT – FMRIB Diffusion Toolbox

FDR – False discovery rate

FMI – Forceps minor

fMRI – Functional magnetic resonance imaging

FWER – Family-wise error rate

G

GM – Gray matter

H

HAROLD – Hemispheric asymmetric reduction in older adults

I

IFOF – Inferior fronto-occipital fasciculus

IPC – Inferior parietal cortex

L

LTS – Long-term storage

M

MACM – Meta-analytic connectivity modeling

MCI – Mild cognitive impairment

MD – Mean diffusivity

MEM – Memory dimension

MLMV – Maximum likelihood mean- and variance- adjusted

MMSE – Mini Mental State Examination

MNI – Montreal Neurological Institute

MRI – Magnetic resonance imaging

N

NBS – Network-based statistics

P

PASA – Posterior-anterior shift in aging

PC – Participation coefficient

PC – Principal components

PCA – Principal Component Analysis

PFC – Prefrontal cortex

POMS – Proportion of maximum scaling

R

RD – Radial Diffusivity

ROI – Region of interest

rs-fMRI – Resting-state functional magnetic resonance imaging

RSN – Resting-state networks

S

SC – Structural connectivity

SC – Stroop Colors

SD – Standard deviation

SE-EPI – Spin-echo echo-planar imaging

SLF – Superior longitudinal fasciculus

SNR – Signal to noise ratio

SOM – Self-Organizing Maps

SRT – Selective reminding test

STAC – Scaffolding theory of aging and cognition

SW – Stroop Words

SWC – Stroop Words/Colors

T

TC – Timepoint consistency

TFCE – Threshold-free cluster enhancement

U

UF – Uncinate fasciculus

W

WM – White matter

List of Figures

CHAPTER II

associated with higher LTS scores. For AD, RD and MD clusters, a negative correlation was found, showing that lower AD, RD or MD values are associated with higher SC scores. Regarding SWC, FA cluster 1 was positively correlated and AD was negatively correlated. Overall, these results suggest that higher WM integrity is associated with higher cognitive performance in the executive function domain.

Figure 5. Significant repeated measures correlations between Mini-Mental State Examination (MMSE) and DTI metrics (FA and RD) of clusters with significant changes between timepoints. The x-axis represents average values of each DTI metric and y-axis, the average values of MMSE. Observations from the same individual are represented with the same color, with corresponding lines showing the repeated measures correlation fit for each subject. Dashed black line represents the overall regression line. Only FA cluster 2 and RD cluster 1 were significantly associated with MMSE. FA exhibited a positive correlation, meaning that higher FA values are associated with higher MMSE scores. RD was negatively correlated with MMSE, showing that lower RD values are associated with higher MMSE scores. Overall, these results suggest that higher WM integrity is associated with higher general cognition.

Figure S1. Trajectories of cognitive test scores for memory (LTS, CLTR, DR), executive function (SW, SC, SWC) and general cognition (MMSE) along time. The x-axis represents time of assessment and y-axis, the average values of each test. Error bars represent standard deviation. All cognitive test scores exhibit a decrease between timepoints, with the exception of SW that remains practically constant.

Figure S2. Statistically significant changes along time in a) FA Cluster 1, b) FA Cluster 2, c) RD Cluster 1 and d) RD Cluster 2. Blue/light-blue gradient indicates decreases along time. Red/yellow gradient indicate increases along time. All results were considered significant at $p<0.05$ (FWE corrected for multiple comparisons).

CHAPTER III

Figure 1. Significant changes in structural connectivity between timepoints. A) Binarized version of the connected component of significantly altered structural connectivity. B) Weighted version of A), with edge thickness representing the amplitude of differences. Blue represents decreases in connectivity strength between timepoints and red represents increases. Connections with decreases are mostly intra-hemispheric, while most of the increases are composed of intra-hemispheric connections. Both increases and decreases are mainly composed by links between subcortical and frontal regions.

Figure 2. Mean connectivity values of the significant connected component. (A) all the connections; (B) connections with increases in connectivity along time; (C) connections with decreases in connectivity. For each plot, we present the connectivity values for all connections (black), intra-left (red), intra-right (green) and inter-hemispheric (purple) connections. Intra-hemispheric connections exhibit a decrease along time, while inter-hemispheric links show an increase. Most of the decreases in SC are due to connections within the right hemisphere.

Figure 3. Proportion of change between timepoints in the mean number of streamlines of the overlap between each seed region of the sub-network with decreases in structural connectivity and WM tract. Seed regions are presented in rows and white matter tracts in columns. For most of the connections, we found a common WM tract and the majority were association fibers.

Figure 4. Proportion of change between timepoints in the mean number of streamlines of the overlap between each seed region of the sub-network with increases in structural connectivity and WM tract. Seed regions are presented in rows and white matter tracts in columns. There were more than a single WM tract connecting the regions, probably due to the fact that almost all the connections were inter-hemispheric.

Figure 5. Global hubs identified in the two timepoints as measured by the normalized nodal efficiency. Here, we observe the plot of the normalized nodal efficiency for all the 90 AAL regions, sorted in descending order of efficiency values, for timepoint 1 (left) and timepoint 2 (right). We observe a reorganization of brain structural networks in aging, characterized by the loss of two hubs (left inferior parietal cortex and left fusiform gyrus).

Figure 6. Global hubs identified in the two timepoints as measured by the normalized nodal efficiency. Here, we represent in the brain the identified hubs for timepoint 1 (top row) and timepoint 2 (bottom row). We observe a reorganization of brain structural networks in aging, characterized by the loss of two hubs (left inferior parietal cortex and left fusiform gyrus).

Figure 7. Modularity structure (A), connector-hub connectivity (B) and matrices of RSNs overlap (C) at timepoint 1 (top row) and timepoint 2 (bottom row). Filled circles represent connector hubs and unfilled circles represent provincial hubs. Although very similar modular arrangements were found at both timepoints (A, B), the undirected structural connectivity profile for the connector hubs was different (C). These differences are probably due to the loss of two connector hubs from first to last timepoint, namely

left caudate and right midcingulate cortex, while left middle occipital gyrus was identified as a connector hub only in the last timepoint. Giving the role of connector hubs in inter-modular communication, the reduction in their number between timepoints reflects a decrease in integration of brain structural networks in aging.

Figure 8. Fingerprints of modular connectivity at timepoint 1 (top row) and timepoint 2 (bottom row). Left column represents the inter-modular connectivity, middle column the intra-module connectivity and right column the connector-hub driven inter-modular connectivity. Modular connectivity strength is quantified as the total number of connections (degree) of all nodes forming a module. Community structure of timepoint 2 was selected as the reference scheme, since it had higher group goodness-of-fit. We observe different patterns only in connector-hub driven inter-modular connectivity. Overall, there was a decrease of around 19% in this connectivity between timepoints, which is probably due to the loss of one connector hub. This results again suggests a decrease in integration of brain SC during aging.

Figure S1. Correlation between head-motion relative displacement values and age for all subjects and both timepoints. Head-motion displacement values were extracted using FSL tools and averaged across all volumes acquired for one subject. Correlation is not significant ($r = 0.019$, $p = 0.85$) meaning that age is not associated with head-motion.

Figure S2. Comparison of head-motion relative displacement values between timepoints. A paired t-test was performed, and it was not significant ($p = 0.95$) meaning that head-motion values did not differ between timepoints.

Figure S3. Percentage of connections lost in each subject when applying consistency-based thresholding. Percentage is calculated as the proportion of connections removed in the subject SC matrix relative to the total number of connections removed in the group consistency mask. Plot on the left illustrates results for timepoint 1 and on the right, results for timepoint 2.

Figure S4. Frequency distribution for the connection strength of the links removed when applying consistency-based thresholding. Plot on the left illustrates results for timepoint 1 and on the right, results for timepoint 3.

Figure S5. Percentage of connections that were present in the group consistency mask but were not present in all subjects' SC matrices. Percentage is calculated as the proportion of connections not present

in the subject SC matrix relative to the total number of connections in the group consistency mask. Plot on the left illustrates results for timepoint 1 and on the right, results for timepoint 2.

Figure S6. Frequency distribution for the connection strength of the links from the group consistency mask not present in all subjects, when applying consistency-based thresholding. Plot on the left illustrates results for timepoint 1 and on the right, results for timepoint 3.

Figure S7. Consistent signatures of SC for M1 and M2 timepoints. Left panel shows intra-timepoint consistency measured as the association between individual SC signatures and timepoint average SC and we can observe that the two timepoints reveal a very high level of intra-timepoint consistency (M1: 97.6%; M2: 97.5%). Right panel shows the degree of association between the signatures of SC for all pairs of subjects in the same timepoint. Once again, we notice a high level of timepoint consistency in SC (100% and 99.8% of all pairwise combinations in M1 and M2 timepoints respectively have a correlation higher than r=0.9137, with number of occurrences peaking at approximately r=0.96 for both timepoints). The overlap between the distributions of intra-timepoint consistency of both timepoints is additionally confirmed by the inter-timepoint consistency distribution (M1-M2: peak at approximately r=0.95). Taken together, these results suggest that, at a global level, the patterns of SC are highly consistent within and between timepoints, and thus potential differences due to age and sex do not have a significant impact on the estimation of SC patterns.

Figure S8. Relationship between F-threshold and number of connections/nodes, that detected a significant component. The F-threshold used in this study (17.0) was selected based on the maximal F-threshold that detected a single component with more than two connections. This generated an NBS component with 19% nodes of the network and 16 links.

Figure S9. Repeated measures correlation between mean SC values of the network with increases and mean factor scores of general cognition and executive function.

Figure S10. Values of the mean number of streamlines for seed regions of the sub-network with decreases in structural connectivity. Top row shows values for timepoint M1 and bottom row shows values for timepoint M2. Seed regions are presented in rows and white matter tracts in columns.

Figure S11. Values of the mean number of streamlines for seed regions of the sub-network with increases in structural connectivity. Top row shows values for timepoint M1 and bottom row shows values for timepoint M2. Seed regions are presented in rows and white matter tracts in columns.

CHAPTER IV

Figure 1. Overview of the workflow employed for the CBP method. Yellow boxes represent the initial input, blue boxes represent intermediate outputs and green boxes the final output.

Figure 2. Example of silhouette scores of one brain region for different clustering algorithms (hierarchical and *k*-means clustering) and different clustering algorithms in conjunction with different data dimensionality reduction techniques (PCA and SOM). Different clustering solutions (2 to 6 clusters) were tested. SOM + *k*-means clustering is the solution with the highest values of silhouette coefficient and with more balanced cluster sizes.

Figure 3. Final group parcellations for the different validity metrics: A) silhouette, B) Davies-Bouldin, C) Calinski-Harabasz. Parcellations are displayed in MNI standard space.

Figure 4. Mean connectivity homogeneity fingerprint (CHF) scores of the different group parcellations for all subjects. The three solutions resulted in parcellations with higher CHF in comparison to the original partition. Calinski-Harabasz parcellation had the highest homogeneity values but also the highest number of clusters.

Figure 5. Mean CHF values for the two timepoints and the initial parcellation. At both timepoints, the homogeneity is higher in comparison to the original partition.

Figure 6. Significant changes in structural connectivity between timepoints. A) Binarized version of the connected component of significantly altered structural connectivity. B) Weighted version of A), with edge thickness representing the amplitude of differences. Blue represents decreases in connectivity strength between timepoints and red represents increases. Connections with decreases are mostly intra-hemispheric, while most of the increases are composed of intra-hemispheric connections.

Figure 7. Modularity structure (A) and connector-hub connectivity (B) at timepoint 1 (top row) and timepoint 2 (bottom row). Filled circles represent connector hubs and unfilled circles represent provincial

hubs. The same number of modules was found at both timepoints but there were evident differences in modular arrangements (A, B) and in the undirected structural connectivity profile for the connector hubs (C). These differences are probably due to the higher number of connector hubs at the last timepoint. Giving the role of connector hubs in inter-modular communication, the increase in their number between timepoints reflects an increase in integration of brain structural networks in aging.

Figure 8. Hubs (global, provincial and connector) identified in the two timepoints. Blue represents hubs only identified at timepoint 1, green represents hubs only identified at timepoint 2 and red represents hubs identified at both timepoints. We observe an increase in all type of hubs (global, provincial and connector) between timepoints. Furthermore, some hubs change their role between timepoints (from provincial to connector – left precuneus 2, right precuneus 2 and right precentral 1; and from connector to provincial – left putamen 2 and right putamen 1).

Figure 9. Fingerprints of modular connectivity at timepoint 1 (top row) and timepoint 2 (bottom row). Left column represents the inter-modular connectivity, middle column the intra-module connectivity and right column the connector-hub driven inter-modular connectivity. Modular connectivity strength is quantified as the total number of connections (degree) of all nodes forming a module. Community structure of timepoint 2 was selected as the reference scheme, since it had higher group goodness-of-fit. We observe different patterns only in connector-hub driven inter-modular connectivity. Overall, there was an increase of around 33% in this connectivity between timepoints, which is probably due to the increase in the number of connector hub. This results again suggests an increase in integration of brain SC during aging.

Figure S1. Example of the distribution of structural connectivity values for a region and the different transforms applied to normalize values. The BoxCox transform is the one achieving a distribution more approximated to a normal distribution.

Figure S2. Plot with the minimum cluster size of all subjects for each threshold and each metric. The threshold of 300 voxels gives a minimum cluster size above 5 voxels for all metrics.

Figure S3. Structural connections surviving the different methods accounting for intra-cluster connectivity. 1 represents connections with intra-cluster connectivity set to 0; 2 represents connections with intra-cluster connectivity set to 1; 3 represents connections with original intra-cluster connectivity values; 4 represents connections common to intra-cluster connectivity set to 0 and 1; 5 represents

connections common to intra-cluster connectivity set to 0 and original values; 6 represents connections common to intra-cluster connectivity set to 1 and original values; 7 represents connections common to the three strategies.

Figure S4. Relationship between F-threshold and number of connections/components, that detected a significant component. The F-threshold used in this study (7.0) was selected based on the maximal F-threshold that detected a single component with more than two connections. This generated an NBS component with 59% nodes of the network (100 nodes) and 122 links.

Figure S5. Davies-Bouldin parcellation with the region displaying a checkerboard pattern highlighted.

List of Tables

CHAPTER II

CHAPTER III

CHAPTER IV

CHAPTHER I

Introduction

1. Introduction

Population aging is a phenomenon occurring worldwide and can be considered a story of success. It reflects the evolution of different areas, such as medicine, public health, economic and social development, that contributed to the extension of human longevity. This has led to a growth both in size and in proportion of older persons in the population. In 2019, the number of persons aged 65 years or over in the global population was 703 million, and this number is expected to double to 1.5 billion in 2050. This shift in the population age distribution is known to have a considerable impact on societies and should be taken into account in order to assure a sustainable development (United Nations, 2019).

Normal aging is characterized by functional and structural alterations at the brain level accompanied with changes in cognition, even in the absence of disease (Andrews-Hanna et al., 2007; Davis et al., 2009; Fjell et al., 2016a; Madden et al., 2017; Meunier et al., 2014; O'Sullivan et al., 2001a). Importantly, cognitive trajectories in aging present high inter-individual variability. In fact, while some individuals maintain relatively high levels of cognitive performance, others exhibit steep trajectories of cognitive decline (Ghisletta et al., 2012; Habib et al., 2007; Josefsson et al., 2012). Several factors, such as genetic, environmental, health and lifestyle factors, are known to contribute to these individual differences in the response to the aging process (Barter and Foster, 2018; Josefsson et al., 2012; Paulo et al., 2011; Santos et al., 2014). Understanding the factors and neural pathways that affect inter-individual variability, leading to either cognitive preservation or decline, is of paramount importance to promote healthier cognitive aging.

Of relevance for this Thesis, neuroimaging techniques, particularly Magnetic Resonance Imaging (MRI), can be used to understand how functional and structural brain changes that occur in aging relate with alterations in cognition (Antonenko and Flöel, 2013; Fjell et al., 2016b; Grady, 2012; Madden et al., 2017; Salat, 2011). The results obtained with these techniques open the possibility for the identification of *in vivo* brain biomarkers of inter-individual variability in cognitive trajectories, that could help to provide a healthier aging to the population.

2. Aging and Cognition

Normal aging is associated with alterations in cognition, that could be either a decline, which is the case for many individuals, or preservation of cognitive performance (Cabeza et al., 2018). One of the research goals for cognitive neuroscience in aging is to understand the brain mechanisms that could underlie these distinct cognitive trajectories (Grady, 2012).

Cognition is composed of different dimensions, which display also distinct patterns of age-related changes. As an example, memory is one of these cognitive dimensions, being particularly affected by age. There are several classifications for memory sub-types, including its temporal attributes (e.g., acute- versus long-term memory). Long-term memory can be further divided into declarative/explicit memory (conscious recollections of factual information and events) and nondeclarative/implicit memory (collection of unconscious memory abilities) (Schacter and Tulving, 1994). Declarative memory can be even further divided into episodic (memories related with past personal experiences) and semantic memory (memories related with general world knowledge) (Shachter et al., 2020). Aging studies in the different types of memory systems have demonstrated that episodic memory shows greater decline in comparison to semantic and nondeclarative memory (for a review, see (Lighthall et al., 2019)). In contrast, semantic memory appears to be relatively spared throughout the lifespan, even though there exist some age differences, particularly with increasing task demands. Regarding nondeclarative memory, many earlier studies claimed that this type of memory is quite preserved in normal aging; recent studies, however, have disputed this view, though the effect is smaller in comparison to that observed for explicit memory, which is one of the reasons why previous studies may have failed to find an age effect (Ward et al., 2020, 2013). In summary, the effect of normal aging in memory is heterogeneous, ranging from steep declines (e.g., episodic memory) to relatively spared (e.g., semantic memory), but in general, all memory systems are susceptible to age effects.

Another cognitive dimension that exhibits declines during aging is executive function. Executive function typically encompasses a set of cognitive processes, such as working memory, inhibitory control, cognitive flexibility, planning, reasoning and problem solving, which are essential to formulate, plan and achieve goals, adapt to novel, unanticipated daily life situations and manage social relationships (Cristofori et al., 2019). These abilities are critical for everyday life, having an impact in mental and physical health, quality of life, school and job success, as well as social interactions (Diamond, 2013). Other cognitive functions remain stable or, even, improve with age - one example is language. In fact, despite some observed age-

related declines in language production, language comprehension is preserved in aging, and vocabulary knowledge improves throughout the adult lifespan (Shafto and Tyler, 2014). Another case of improved cognitive function with aging is emotion regulation, where older adults display a bias toward positive stimuli which may contribute to explain the increased emotional well-being and life satisfaction reported in some older subjects (Carstensen et al., 2011; Kim et al., 2019).

In conclusion, aging affects multiple aspects of cognition in quite different ways. Various factors influence cognitive aging and its inter-individual variability, such as brain functional and structural alterations, life experiences, education, diet, physical activity, genetic factors, among others (Grady, 2012). Studies integrating multiple influencing factors can help advance our understanding of aging and what causes individuals to present distinct cognitive trajectories.

3. The Aging Brain

The aging process affects both brain structure and function. These alterations occurring at the brain level are thought to account for age-related cognitive changes (Cabeza et al., 2017; Craik and Salthouse, 2008). Therefore, understanding the neural mechanisms underlying these brain alterations and how they associate with cognition can help to identify in-vivo brain biomarkers of cognitive preservation and decline (Cabeza et al., 2018; Grady, 2012).

3.1. Structural alterations

Brain structural alterations are usually reported in terms of volume or cortical thickness. The global patterns of structural changes most consistently reported with aging are gray matter (GM) and white matter (WM) atrophy and concomitant increases in cerebrospinal fluid (CSF) and ventricular volumes (Fjell et al., 2014; Good et al., 2001; Resnick et al., 2003; Shaw et al., 2016; Storsve et al., 2014; Thambisetty et al., 2010; Vinke et al., 2018) (for a review see (Toepper, 2017)).

GM alterations can be described with three neuroimaging metrics: volume, cortical thickness and surface area. Previous studies found evidence of GM atrophy with aging, characterized by decreases in all these metrics, with surface area exhibiting the weakest association with age (Fleischman et al., 2014; Lemaitre et al., 2012; Rettmann, 2005; Storsve et al., 2014). Furthermore, observed age-effects on cortical thinning are more widespread in comparison to GM volume, which may indicate higher sensitivity of this

metric to the effects of aging in brain's structure. In fact, volume is calculated from the product of cortical thickness and surface area, which can explain its reduced sensitivity due to the attenuation exerted by the surface area component. Thus, the evaluation of different morphological measures is important since they might reflect different age-related brain structural changes (Fleischman et al., 2014; Lemaitre et al., 2012). Of notice, associations between all these metrics of GM alterations and cognitive decline were found for distinct cognitive domains (executive function, processing speed and episodic memory) (Fjell and Walhovd, 2010; Fleischman et al., 2014; Head et al., 2008; Kalpouzos et al., 2009; Zimmerman et al., 2006).

When looking at individual brain regions we observe distinct patterns of age-related structural brain changes. This regional variability, reported in several previous studies (Fjell et al., 2009; Fjell and Walhovd, 2010; Raz, 1997; Raz et al., 2005; Resnick et al., 2003; Salat, 2004), is the basis for the formulation of different hypothesis that try to explain the heterogeneity of aging processes in the brain. One of such hypothesis is the "last-in, first-out" which postulates that regions reaching complete myelination later, such as association cortices or the neostriatum, are more vulnerable to the effects of aging (Raz, 2005, 1999). Previous studies found evidence supporting this hypothesis in terms of regional brain volumes (Good et al., 2001; Grieve et al., 2005; Raz et al., 2005) and cortical thickness (Fjell et al., 2009; Salat, 2004; Yang et al., 2014). This theory was later extended to the "developmental-sensory" hypothesis which suggests that early aging is associated with atrophy in heteromodal association regions, as stated in the "last-in, first-out" hypothesis, while later aging processes are marked by declines in primary sensory/motor regions (McGinnis et al., 2011).

Age-associated brain structural changes, however, are not confined to GM. The WM is also affected by age and there are several neuroimaging metrics to measure such changes. One of these metrics is WM lesion volume. These WM lesions are thought to reflect axonal loss and demyelination as a result of ischemic events (Prins and Scheltens, 2015). Its prevalence and severity increase as a function of age (Breteler et al., 1994; Prins and Scheltens, 2015; Zupan, 2016), and they have been associated with vascular risk factors (Debette et al., 2011; Habes et al., 2018). Past studies have found a clear link between WM lesions and cognitive impairment in domains such as processing speed, executive function and general cognition (Deary et al., 2003; Debette and Markus, 2010; Prins et al., 2005).

WM changes in aging can be further characterized through diffusion imaging methods, which allow the characterization of WM microstructural integrity. Degradation of WM integrity with aging has been reported across multiple cross-sectional (de Groot et al., 2015; de Lange et al., 2016; Lebel et al., 2012; Salat et

al., 2005; Westlye et al., 2010) and longitudinal studies (Sexton et al., 2014; Vinke et al., 2018). Importantly, WM integrity changes during aging have also been associated with cognitive decline (Andrews-Hanna et al., 2007; Bartzokis, 2004; Bennett and Madden, 2014; Fjell et al., 2016a; Madden et al., 2017; Marques et al., 2015; O'Sullivan et al., 2001a). Moreover, distinct patterns of deterioration are also observed for different WM tracts. Interestingly, these are, at least in part, consistent with the "last-in, first-out" hypothesis (Bender et al., 2016; Brickman et al., 2012; Davis et al., 2009; Slater et al., 2019), as association fibers (WM tracts connecting different regions within a hemisphere) which reach the peak of maturation later in comparison to commissural fibers (WM tracts connecting regions between the two hemispheres) had increased vulnerability to age effects. These WM neuroimaging findings, and their association with cognitive results, constitute the basis for one of the most prevalent hypothesis in brain aging - the "disconnection" hypothesis. According to this theory, originally proposed by Geschwind (Geschwind, 1965a, 1965b), the disruption of communication between distinct cortical regions is the potential sources of cognitive decline. Simply, WM tracts provide the anatomical connections between cortical regions and disruption of their integrity can lead to a "disconnected" brain and, consequently, to cognitive impairments (O'Sullivan et al., 2001a). A note to highlight that all these theories are not mutually exclusive and most likely, there is truth in each of these perspectives.

Noticeable, network analysis has emerged as a tool to characterize brain's structural and functional organization (Bullmore and Sporns, 2009). In this framework, the brain is conceptualized as a complex network of inter-connected regions. Using graph theory analysis, the brain network can be modeled as a graph where nodes represent brain regions and edges characterize the structural/functional connections between regions. Then, quantifiable topological properties of the graph can be estimated which can help elucidate about the organization and function of the brain network (Rubinov and Sporns, 2010). Several non-trivial topological properties of the human brain network have been identified with these tools, such as small-worldness, modular architecture, hubs and cores and rich club structure (Bullmore and Sporns, 2009; van den Heuvel and Sporns, 2011; Wang et al., 2010). Structural networks can be estimated from structural or diffusion imaging methods. For the case of structural data, the structural connectivity measure is defined as the structural covariance of gray matter volumes or cortical thickness (Bassett et al., 2008). Regarding diffusion data, the structural connectivity measure could be either the number of WM fibers connecting a pair of brain regions, or the probability that a connection between two brain regions exists (Damoiseaux, 2017). Importantly, all these tools are of relevance for aging studies. In fact, studies exploring the effects of the aging process in structural covariance networks have consistently reported a shift from distributed to a more localized organization (Li et al., 2013; Montembeault et al.,

2012; Wu et al., 2012). Other studies described a decrease in integrity of structural covariance patterns in networks that support different cognitive functions, such as executive function, language-related semantics and visual imagery and mentalization (default mode network) (Chen et al., 2011; DuPre and Spreng, 2017; Li et al., 2013; Montembeault et al., 2012; Spreng and Turner, 2013). Regarding white matter structural networks estimated from diffusion data, evidence suggests a decrease in connectivity strength (Gong et al., 2009; Madden et al., 2020) and topological efficiency of the whole-brain network during aging (Betzel et al., 2014; Madden et al., 2020; Wen et al., 2011; Zhao et al., 2015), and also a regional pattern of decreased efficiency most prominent in frontal and temporal regions (Gong et al., 2009; Zhao et al., 2015). Recent reports also describe a decline in connectivity strength within and between network modules (Madden et al., 2020; Zhao et al., 2015). Moreover, the topological properties of the white matter structural network have been associated with distinct cognitive functions, such as information processing speed, visuospatial reasoning, crystallized ability and executive function (Wen et al., 2011; Wiseman et al., 2018). In summary, the use of these tools has significantly contributed to our knowledge of the impact of age upon brain structure and has provided a more comprehensive perspective of the morphological phenomena underpinning age-associated cognitive trajectories.

3.2. Functional alterations

The aging process also induces changes in brain function. One of the most important patterns observed across age-related functional studies is neural dedifferentiation. This process is characterized by a reduction in neural specificity, meaning that regions which are selectively recruited for a preferred stimulus in younger adults will activate/respond to a broader range of stimuli in older adults (Koen and Rugg, 2019; Park and Reuter-Lorenz, 2009). Neural dedifferentiation can manifest in different forms, such as: i) contralateral recruitment, in which older adults engage homologous brain regions compared to young adults, ii) unique recruitment, where different brain regions are additionally recruited and iii) substitution, where a completely new neural network is engaged for a specific function (Spreng and Turner, 2019). This pattern of changes has been observed across multiple cognitive tasks (Eyler et al., 2011; Spreng et al., 2010; Turner and Spreng, 2012). Still, there is no consensus if neural dedifferentiation reflects compensatory mechanisms or is the cause of cognitive impairment. While that is being investigated, several theoretical perspectives/models have been developed to encapsulate the age-associated functional findings.

One of the first models proposed was the Hemispheric Asymmetry Reduction in Older Adults (HAROLD) developed in 2002 by Roberto Cabeza (Cabeza, 2002). It posits that under similar conditions (i.e., when performing the same cognitive task), older adults exhibit a pattern of less lateralized prefrontal activity in comparison to younger adults. This pattern was observed across multiple cognitive tasks, such as episodic memory, semantic memory, working memory, perception and inhibitory control, and was suggested to reflect either compensatory mechanisms or a struggle to recruit specialized neural circuitry (Cabeza, 2002). The HAROLD model was revised in 2012, to include a distinction between successful and unsuccessful compensation. Briefly, successful compensation occurs when the increase in neural activity, as an attempt to counteract the mismatch between task demands and cognitive processing, results in improved cognitive performance, whereas in the case of unsuccessful compensation it leads to no change or even worse performance (Cabeza and Dennis, 2012).

Another proposed model is the Posterior-Anterior Shift in Aging (PASA) formulated by Davis in 2008 (Davis et al., 2008). It considers two patterns co-occurring in older adults: i) diminished activation of posterior brain regions and ii) increased activation of anterior brain regions. The frontal overactivation is suggested to be compensatory as evidence demonstrates that this increased frontal activation is usually positively correlated with performance and negatively correlated with decreased occipital activity (Davis et al., 2008). Of relevance, the PASA pattern has been observed in distinct cognitive tasks (e.g., visual perception, memory encoding, working memory, episodic memory retrieval) (Festini et al., 2018).

Of notice, both HAROLD and PASA models were applied only to older adults and HAROLD was restricted to differences in prefrontal cortex. However, not all models suffer from these constraints; one of these is the Compensation-Related Utilization of Neural Circuits Hypothesis (CRUNCH) model (Reuter-Lorenz and Mikels, 2006; Reuter-Lorenz and Cappell, 2008; Reuter-Lorenz and Lustig, 2005). It interprets overactivation as a compensation for inefficiencies in neural processing and that it is influenced by the level of task demand. Briefly, it postulates that at lower levels of task demands, older adults exhibit increased activation compared to younger adults with minimal differences or equivalent performance. In contrast, at higher levels of task demands, older adults show decreased activation and worse performance, and this is thought to occur due to the fact that older adults have reached their capacity for compensatory recruitment (Reuter-Lorenz and Mikels, 2006; Reuter-Lorenz and Cappell, 2008; Reuter-Lorenz and Lustig, 2005). The CRUNCH pattern is not limited to older adults, as it can occur whenever the recruitment of additional neural resources is necessary to meet cognitive challenge, and it can also happen in any region of the brain (Festini et al., 2018).

One last model of brain function in aging is the Scaffolding Theory of Aging and Cognition (STAC), which differs from the previous models above described because it incorporates both structural and functional brain changes to predict cognitive function. It hypothesizes that as a response to declines in structure and function, the adaptive brain recruits compensatory scaffolding, which involves the enrollment of additional neural resources to preserve cognitive performance (Park and Reuter-Lorenz, 2009). Thus, the levels of neural degeneration, neural challenge, and the capacity for compensatory scaffolding will determine the cognitive function of an individual. This theory can also be applied to any age and can occur at any brain region. It was revised in 2014 to include life-course experiences as factors that can influence brain structure and function, and the capacity for compensatory scaffolding (Reuter-Lorenz and Park, 2014). These factors can either enhance (e.g., education, physical fitness, multilingualism, intellectual engagement) or deplete (e.g., stress, vascular disease, depression) neural resources. This revision also included longitudinal changes in cognition and in brain's structure and function. In sum, the revised STAC model postulates that life-course experiences can enhance, preserve or compromise brain status and the potential for compensatory scaffolding, which altogether influence cognitive function over time. Interestingly, it is the only model that incorporates longitudinal changes.

In summary, all these theoretical perspective/models helped advance research in the neurocognitive aging field and are partially supported by neuroimaging studies. Still, future research will benefit from more longitudinal studies and interference studies which allow causal inferences, to clarify if age-related changes in functional activation are truly part of a compensatory mechanism or simply a result of the aging process (Festini et al., 2018).

4. Neuroimaging techniques and data analysis

Neuroimaging techniques allow the study of the brain structure and function *in vivo* and non-invasively. As already stated, their emergence was crucial in advancing our knowledge of the processes triggered by aging upon the brain. Recently, the application of analytical tools from other fields, such as graph theory or machine learning, to study the brain have opened the possibility to combine measures of brain structure and function with the ultimate goal of developing personalized biomarkers of age-related cognitive preservation and decline (Spreng and Turner, 2019). In the next paragraphs, a brief description of the most commonly used neuroimaging techniques for studying the age-associated processes in the brain is provided.

4.1. Image acquisition

MRI has the advantage of allowing structural and functional acquisitions within the same imaging session and scanner, which makes it adequate to investigate the aging brain. T1-weighted acquisitions are a particular type of structural MRI that is often used to study whole-brain or regional brain volumes and cortical thickness (Yousaf et al., 2018). On the other hand, T2-weighted acquisitions allow, amongst others, the quantification of WM lesion volumes through the identification of WM hyperintensities (Prins and Scheltens, 2015).

Diffusion Weighted Imaging (DWI) enables the study of WM microstructural integrity based on the principle that the diffusion of water molecules in the brain has different directionality according to the tissue type (Basser et al., 1994; Le Bihan, 2003; Pierpaoli and Basser, 1996). By applying the Diffusion Tensor Imaging (DTI) model to DWI data it is possible to extract different metrics to evaluate microstructural integrity. The most frequently reported is fractional anisotropy (FA), which measures the anisotropic (i.e., directional diffusion) fraction of the total diffusion, and higher values indicate higher tissue integrity (Bennett and Madden, 2014). Other metrics are mean diffusivity (MD) which measures the average rate of diffusion and lower values are associated with higher tissue integrity (Bennett and Madden, 2014), axial diffusivity (AD) which indexes the rate of diffusion along the principal direction and is assumed to be sensitive to axonal integrity (Budde et al., 2007; Song et al., 2003, 2002; Sun et al., 2008), and radial diffusivity (RD) which measures the average rate of diffusion orthogonal to the principal direction and is usually associated with the degree of myelination (Klawiter et al., 2011; Song et al., 2005, 2003, 2002). Moreover, DWI allows the reconstruction of WM pathways, a technique called tractography (Jbabdi and Johansen-Berg, 2011; Jones, 2010). This can be used to estimate the structural connectivity (SC) between brain regions, which can be either the number of reconstructed WM tracts or the probability that a connection exists between each pair of regions (Damoiseaux, 2017). In the end, structural connectivity networks can be built by combining the SC of all regions of the brain and topologic properties of these networks can be assessed using network analysis tools.

Functional MRI (fMRI) provides an indirect measure of brain activity through the blood oxygen level dependent (BOLD) contrast. This contrast appears due to differences in the levels of oxyhemoglobin and deoxyhemoglobin, which are a result of the increased supply of oxygenated blood to a brain region when it is active (Sutton et al., 2009). The BOLD contrast can be captured while the individual is at rest or performing a task. The former is known as resting state fMRI (rs-fMRI) and allows the estimation of

functional connectivity (FC) which represents the inter-correlations between temporal fluctuations in the BOLD signal across brain regions (Damoiseaux, 2017). As in SC networks, the FC of all pairs of regions can be combined to create FC networks that can be further analyzed with network analysis tools.

4.2. Network analysis

Network analysis tools emerged from the conceptualization of the brain as a complex network of inter-connected regions. It enables the characterization of brain's structural and functional organization (Bullmore and Sporns, 2009). In this framework, the brain network is modeled as a graph constituted by nodes and edges. The nodes are the different brain regions, usually defined from a pre-existing atlas, while the edges are the functional or structural connectivity measures between brain regions, which were described in previous sections. Using graph theory analysis, it is possible to extract quantifiable topological properties which can shed light on the organization and function of the brain network (Rubinov and Sporns, 2010). This analysis can be performed at distinct levels, namely edge, local and global level.

At the edge level, it is possible to identify which connections are significantly altered under a specific condition or pathology. A powerful technique to perform this analysis is the network-based statistics (NBS) procedure implemented in the NBS toolbox (https://sites.google.com/site/bctnet/comparison/nbs). It is a non-parametric statistical method that allows the identification of significantly altered sub-networks, while controlling for the family-wise error rate (FWER) (Zalesky et al., 2010). This is important, since testing the hypothesis of interest at the edge level poses a multiple comparisons problem.

Different measures can be extracted to quantitatively describe the brain network topology, which characterize global and local features of brain connectivity. These metrics can reflect aspects of integration (e.g., shortest path length, global efficiency), segregation (e.g., modularity, clustering coefficient), centrality (e.g., node degree, participation coefficient, betweenness centrality), patterns of local connectivity (e.g., network motifs) and resilience (e.g., degree distribution, assortativity coefficient) (Rubinov and Sporns, 2010).

Several studies already employed network analysis tools to characterize the aging brain. They found a reorganization of the brain's structural and functional network during aging, characterized as reduced global and local efficiency (Gong et al., 2009; Wu et al., 2012; Zhao et al., 2015), increased shortest path length and clustering coefficient (Otte et al., 2015; Sala-Llonch et al., 2014), and modularity architecture reorganization (Betzel et al., 2014; Wu et al., 2012). Moreover, significant associations

between these topological properties of brain networks and cognitive function have been reported (Bernard et al., 2015; Wen et al., 2011; Wiseman et al., 2018). Still, at the edge level, the existing studies have focused on the connectivity of the whole-brain or of specific networks usually associated with some cognitive dimension. To date, and to the best of our knowledge, no study has explored the existence of sub-networks with significant age-related changes in connectivity using the NBS approach.

4.3. Connectivity-based Parcellation

Functional integration and segregation are the two main principles of brain organization, with functional integration characterized through long-range connections and functional segregation through local differentiation (Tononi et al., 1994). The notion that these two concepts are entangled, since each specialized brain region might be depicted by a different set of long-range connections, inspired the development of a new neuroimaging method known as connectivity-based parcellation (CBP) (Eickhoff et al., 2015). CBP divides a brain region according to its voxels' connectivity profiles (Eickhoff et al., 2015; Reuter et al., 2020). Specifically, first the connectivity profiles are estimated by computing the connection strengths between each voxel in the region of interest (ROI) and a set of target voxels. Then, ROI voxels are grouped in a way that voxels within a group have similar connectivity profiles and voxels between groups have distinct connectivity profiles. Usually, the grouping of voxels is performed using clustering algorithms and the resulting clusters/parcels represent homogeneous units with respect to the measured connectivity. Connectivity between voxels is often derived from rs-fMRI which represents functional connectivity, DWI that characterizes anatomical connectivity or meta-analytic connectivity modeling (MACM) which measures task-dependent functional connectivity and co-activation patterns (Reuter et al., 2020). Another option is to compute connectivity from structural covariance, but its use is very limited, probably due to its complex interpretation (Eickhoff et al., 2018).

CBP method can be fundamental to advance our understanding of brain organization and function. It can lead to the development of new hypotheses on regional differentiation (Eickhoff et al., 2015) and can be used as biologically informed strategies of data reduction (Eickhoff et al., 2018). The latter has a relevant importance in network analysis, since these tools require the division of the brain in nodes. The typical approach is to define the nodes using parcellations derived from local properties (e.g., anatomical landmarks or cytoarchitectonic information). Although these parcellations provide biologically significant nodes, they may not adequately reflect brain organization and inter-individual variability (Arslan et al., 2018). Nodes derived from CBP will be more adequate for network analysis due to its data-driven

approach which originates clusters with high homogeneity and functional coherence and with different connectivity patterns between them (Arslan et al., 2018). Additionally, the data reduction feature of CBP can be applied to study brain-behavior associations in big-data projects (Eickhoff et al., 2018).

There are already numerous parcellations derived from CBP using both functional and structural connectivity measures (for a review see (Arslan et al., 2018; Eickhoff et al., 2018). Moreover, some studies suggest that individual brain parcellations can predict inter-individual variability in demographics, cognition, emotion, personality and behavior (Bijsterbosch et al., 2018; Kong et al., 2018; Salehi et al., 2018). Nevertheless, the high heterogeneity in the procedures that were developed, since different approaches can be applied at different steps within the CBP method, combined with the lack of a ground truth makes it difficult to evaluate the proposed solutions (Arslan et al., 2018; Reuter et al., 2020). As a result, to date there is no universal method to perform CBP. Furthermore, the application of CBP methods to study the aging brain is very scarce and limited to particular brain regions (Fritz et al., 2019).

5. Objectives

Despite age-related changes in brain network are already described in several studies, most of them use cross-sectional designs and conventional analysis methods. The aim of this thesis is *to provide new insights about the changes induced by the aging process in brain networks and how these changes associate with cognitive trajectories, through the use of sophisticated neuroimaging tools and longitudinal designs*. The identification of brain correlates of cognitive dysfunction in aging is of relevance, as it could drive the development of new *in vivo* brain biomarkers of inter-individual variability in cognitive trajectories and, ultimately, customized interventions.

In order to achieve this goal, network analysis and CBP methods were applied to MRI data of a group of older subjects followed longitudinally. This sample is part of the Switchbox project (www.switchbox-online.eu/) and, at each evaluation, cognitive and neuroimaging characterization was performed.

In order to accomplish the main aim of this thesis, different tasks were performed:

1. Characterize whole-brain signatures of white-matter microstructural change during aging and its association with cognition (Chapter 2)
2. Characterize longitudinal changes in the organization of structural brain networks and explore its relationship with cognitive trajectories (Chapter 3)
3. Describe the organization of structural brain networks in aging using CBP and investigate its advantages over conventional analysis methods (Chapter 4)

6. References

Andrews-Hanna, J.R., Snyder, A.Z., Vincent, J.L., Lustig, C., Head, D., Raichle, M.E., Buckner, R.L., 2007. Disruption of Large-Scale Brain Systems in Advanced Aging. Neuron 56, 924–935. https://doi.org/10.1016/j.neuron.2007.10.038

Antonenko, D., Flöel, A., 2013. Healthy aging by staying selectively connected: A mini-review. Gerontology 60, 3–9. https://doi.org/10.1159/000354376

Arslan, S., Ktena, S.I., Makropoulos, A., Robinson, E.C., Rueckert, D., Parisot, S., 2018. Human brain mapping: A systematic comparison of parcellation methods for the human cerebral cortex. NeuroImage 170, 5–30. https://doi.org/10.1016/j.neuroimage.2017.04.014

Barter, J.D., Foster, T.C., 2018. Aging in the Brain: New Roles of Epigenetics in Cognitive Decline. The Neuroscientist 24, 516–525. https://doi.org/10.1177/1073858418780971

Bartzokis, G., 2004. Age-related myelin breakdown: a developmental model of cognitive decline and Alzheimer's disease. Neurobiology of Aging 25, 5–18. https://doi.org/10.1016/j.neurobiolaging.2003.03.001

Basser, P.J., Mattiello, J., LeBihan, D., 1994. MR diffusion tensor spectroscopy and imaging. Biophysical Journal 66, 259–267. https://doi.org/10.1016/S0006-3495(94)80775-1

Bassett, D.S., Bullmore, E., Verchinski, B.A., Mattay, V.S., Weinberger, D.R., Meyer-Lindenberg, A., 2008. Hierarchical Organization of Human Cortical Networks in Health and Schizophrenia. Journal of Neuroscience 28, 9239–9248. https://doi.org/10.1523/JNEUROSCI.1929-08.2008

Bender, A.R., Völkle, M.C., Raz, N., 2016. Differential aging of cerebral white matter in middle-aged and older adults: A seven-year follow-up. NeuroImage 125, 74–83. https://doi.org/10.1016/j.neuroimage.2015.10.030

Bennett, I.J., Madden, D.J., 2014. Disconnected aging: Cerebral white matter integrity and age-related differences in cognition. Neuroscience 276, 187–205. https://doi.org/10.1016/j.neuroscience.2013.11.026

Bernard, C., Dilharreguy, B., Helmer, C., Chanraud, S., Amieva, H., Dartigues, J.-F., Allard, M., Catheline, G., 2015. PCC characteristics at rest in 10-year memory decliners. Neurobiology of Aging 36, 2812–2820. https://doi.org/10.1016/j.neurobiolaging.2015.07.002

Betzel, R.F., Byrge, L., He, Y., Goñi, J., Zuo, X.N., Sporns, O., 2014. Changes in structural and functional connectivity among resting-state networks across the human lifespan. NeuroImage 102, 345–357. https://doi.org/10.1016/j.neuroimage.2014.07.067

Bijsterbosch, J.D., Woolrich, M.W., Glasser, M.F., Robinson, E.C., Beckmann, C.F., Van Essen, D.C., Harrison, S.J., Smith, S.M., 2018. The relationship between spatial configuration and functional connectivity of brain regions. eLife 7. https://doi.org/10.7554/eLife.32992

Breteler, M.M.B., van Swieten, J.C., Bots, M.L., Grobbee, D.E., Claus, J.J., van den Hout, J.H.W., van Harskamp, F., Tanghe, H.L.J., de Jong, P.T.V.M., van Gijn, J., Hofman, A., 1994. Cerebral white matter lesions, vascular risk factors, and cognitive function in a population-based study: The Rotterdam Study. Neurology 44, 1246–1246. https://doi.org/10.1212/WNL.44.7.1246

Brickman, A.M., Meier, I.B., Korgaonkar, M.S., Provenzano, F.A., Grieve, S.M., Siedlecki, K.L., Wasserman, B.T., Williams, L.M., Zimmerman, M.E., 2012. Testing the white matter retrogenesis hypothesis of cognitive aging. Neurobiology of Aging 33, 1699–1715. https://doi.org/10.1016/j.neurobiolaging.2011.06.001

Budde, M.D., Kim, J.H., Liang, H.-F., Schmidt, R.E., Russell, J.H., Cross, A.H., Song, S.-K., 2007. Toward accurate diagnosis of white matter pathology using diffusion tensor imaging. Magnetic Resonance in Medicine 57, 688–695. https://doi.org/10.1002/mrm.21200

Bullmore, E.T., Sporns, O., 2009. Complex brain networks: graph theoretical analysis of structural and functional systems. Nature reviews. Neuroscience 10, 186–198. https://doi.org/10.1038/nrn2575

Cabeza, R., 2002. Hemispheric asymmetry reduction in older adults: The HAROLD model. Psychology and Aging 17, 85–100. https://doi.org/10.1037//0882-7974.17.1.85

Cabeza, R., Albert, M., Belleville, S., Craik, F.I.M., Duarte, A., Grady, C.L., Lindenberger, U., Nyberg, L., Park, D.C., Reuter-Lorenz, P.A., Rugg, M.D., Steffener, J., Rajah, M.N., 2018. Maintenance, reserve and compensation: the cognitive neuroscience of healthy ageing. Nature Reviews Neuroscience 19, 701–710. https://doi.org/10.1038/s41583-018-0068-2

Cabeza, R., Dennis, N.A., 2012. Frontal Lobes and Aging, in: Stuss, D.T., Knight, R.T. (Eds.), Principles of Frontal Lobe Function. Oxford University Press, pp. 628–652. https://doi.org/10.1093/med/9780199837755.003.0044

Cabeza, R., Nyberg, L., Park, D.C. (Eds.), 2017. Cognitive neuroscience of aging: linking cognitive and cerebral aging, Second edition. ed. Oxford University Press, New York, NY, United States of America.

Carstensen, L.L., Turan, B., Scheibe, S., Ram, N., Ersner-Hershfield, H., Samanez-Larkin, G.R., Brooks, K.P., Nesselroade, J.R., 2011. Emotional experience improves with age: Evidence based on over 10 years of experience sampling. Psychology and Aging 26, 21–33. https://doi.org/10.1037/a0021285

Chen, Z.J., He, Y., Rosa-Neto, P., Gong, G., Evans, A.C., 2011. Age-related alterations in the modular organization of structural cortical network by using cortical thickness from MRI. NeuroImage 56, 235–245. https://doi.org/10.1016/j.neuroimage.2011.01.010

Craik, F.I.M., Salthouse, T.A. (Eds.), 2008. The handbook of aging and cognition, 3. ed. ed. Psychology Press, New York, NY.

Cristofori, I., Cohen-Zimerman, S., Grafman, J., 2019. Executive functions, in: Handbook of Clinical Neurology. Elsevier, pp. 197–219. https://doi.org/10.1016/B978-0-12-804281-6.00011-2

Damoiseaux, J.S., 2017. Effects of aging on functional and structural brain connectivity. NeuroImage 1–9. https://doi.org/10.1016/j.neuroimage.2017.01.077

Davis, S.W., Dennis, N.A., Buchler, N.G., White, L.E., Madden, D.J., Cabeza, R., 2009. Assessing the effects of age on long white matter tracts using diffusion tensor tractography. NeuroImage 46, 530–541. https://doi.org/10.1016/j.neuroimage.2009.01.068

Davis, S.W., Dennis, N.A., Daselaar, S.M., Fleck, M.S., Cabeza, R., 2008. Que PASA? The Posterior-Anterior Shift in Aging. Cerebral Cortex 18, 1201–1209. https://doi.org/10.1093/cercor/bhm155

de Groot, M., Ikram, M.A., Akoudad, S., Krestin, G.P., Hofman, A., van der Lugt, A., Niessen, W.J., Vernooij, M.W., 2015. Tract-specific white matter degeneration in aging: The Rotterdam Study. Alzheimer's & Dementia 11, 321–330. https://doi.org/10.1016/j.jalz.2014.06.011

de Lange, A.-M.G., Bråthen, A.C.S., Grydeland, H., Sexton, C., Johansen-Berg, H., Andersson, J.L.R., Rohani, D.A., Nyberg, L., Fjell, A.M., Walhovd, K.B., 2016. White matter integrity as a marker for cognitive plasticity in aging. Neurobiology of Aging 47, 74–82. https://doi.org/10.1016/j.neurobiolaging.2016.07.007

Deary, I.J., Leaper, S.A., Murray, A.D., Staff, R.T., Whalley, L.J., 2003. Cerebral white matter abnormalities and lifetime cognitive change: A 67-year follow-up of the Scottish Mental Survey of 1932. Psychology and Aging 18, 140–148. https://doi.org/10.1037/0882-7974.18.1.140

Debette, S., Markus, H.S., 2010. The clinical importance of white matter hyperintensities on brain magnetic resonance imaging: systematic review and meta-analysis. BMJ 341, c3666–c3666. https://doi.org/10.1136/bmj.c3666

Debette, S., Seshadri, S., Beiser, A., Au, R., Himali, J.J., Palumbo, C., Wolf, P.A., DeCarli, C., 2011. Midlife vascular risk factor exposure accelerates structural brain aging and cognitive decline. Neurology 77, 461–468. https://doi.org/10.1212/WNL.0b013e318227b227

Diamond, A., 2013. Executive Functions. Annual Review of Psychology 64, 135–168. https://doi.org/10.1146/annurev-psych-113011-143750

DuPre, E., Spreng, R.N., 2017. Structural covariance networks across the life span, from 6 to 94 years of age. Network Neuroscience 1, 302–323. https://doi.org/10.1162/NETN_a_00016

Eickhoff, S.B., Thirion, B., Varoquaux, G., Bzdok, D., 2015. Connectivity-based parcellation: Critique and implications. Human Brain Mapping 36, 4771–4792. https://doi.org/10.1002/hbm.22933

Eickhoff, S.B., Yeo, B.T.T., Genon, S., 2018. Imaging-based parcellations of the human brain. Nature Reviews Neuroscience 19, 672–686. https://doi.org/10.1038/s41583-018-0071-7

Eyler, L.T., Sherzai, A., Kaup, A.R., Jeste, D.V., 2011. A Review of Functional Brain Imaging Correlates of Successful Cognitive Aging. Biological Psychiatry 70, 115–122. https://doi.org/10.1016/j.biopsych.2010.12.032

Festini, S.B., Zahodne, L., Reuter-Lorenz, P.A., 2018. Theoretical Perspectives on Age Differences in Brain Activation: HAROLD, PASA, CRUNCH—How Do They STAC Up?, in: Oxford Research Encyclopedia of Psychology. Oxford University Press. https://doi.org/10.1093/acrefore/9780190236557.013.400

Fjell, A.M., Sneve, M.H., Grydeland, H., Storsve, A.B., Walhovd, K.B., 2016a. The Disconnected Brain and Executive Function Decline in Aging. Cerebral Cortex bhw082. https://doi.org/10.1093/cercor/bhw082

Fjell, A.M., Sneve, M.H., Storsve, A.B., Grydeland, H., Yendiki, A., Walhovd, K.B., 2016b. Brain Events Underlying Episodic Memory Changes in Aging: A Longitudinal Investigation of Structural and Functional Connectivity. Cerebral Cortex 26, 1272–1286. https://doi.org/10.1093/cercor/bhv102

Fjell, A.M., Walhovd, K.B., 2010. Structural Brain Changes in Aging: Courses, Causes and Cognitive Consequences. Reviews in the Neurosciences 21. https://doi.org/10.1515/REVNEURO.2010.21.3.187

Fjell, A.M., Westlye, L.T., Amlien, I., Espeseth, T., Reinvang, I., Raz, N., Agartz, I., Salat, D.H., Greve, D.N., Fischl, B., Dale, A.M., Walhovd, K.B., 2009. High Consistency of Regional Cortical Thinning in Aging across Multiple Samples. Cerebral Cortex 19, 2001–2012. https://doi.org/10.1093/cercor/bhn232

Fjell, A.M., Westlye, L.T., Grydeland, H., Amlien, I., Espeseth, T., Reinvang, I., Raz, N., Dale, A.M., Walhovd, K.B., for the Alzheimer Disease Neuroimaging Initiative, 2014. Accelerating Cortical Thinning: Unique to Dementia or Universal in Aging? Cerebral Cortex 24, 919–934. https://doi.org/10.1093/cercor/bhs379

Fleischman, D.A., Leurgans, S., Arfanakis, K., Arvanitakis, Z., Barnes, L.L., Boyle, P.A., Han, S.D., Bennett, D.A., 2014. Gray-matter macrostructure in cognitively healthy older persons: associations with age and cognition. Brain Structure and Function 219, 2029–2049. https://doi.org/10.1007/s00429-013-0622-7

Fritz, H.J., Ray, N., Dyrba, M., Sorg, C., Teipel, S., Grothe, M.J., 2019. The corticotopic organization of the human basal forebrain as revealed by regionally selective functional connectivity profiles. Human Brain Mapping 40, 868–878. https://doi.org/10.1002/hbm.24417

Geschwind, N., 1965a. Disconnexion syndromes in animal and man. Part I. Brain 88, 237–294.

Geschwind, N., 1965b. Disconnexion syndromes in animal and man. Part II. Brain 88, 585–644.

Ghisletta, P., Rabbitt, P., Lunn, M., Lindenberger, U., 2012. Two thirds of the age-based changes in fluid and crystallized intelligence, perceptual speed, and memory in adulthood are shared. Intelligence 40, 260–268. https://doi.org/10.1016/j.intell.2012.02.008

Gong, G., Rosa-Neto, P., Carbonell, F., Chen, Z.J., He, Y., Evans, A.C., 2009. Age- and Gender-Related Differences in the Cortical Anatomical Network. Journal of Neuroscience 29, 15684–15693. https://doi.org/10.1523/JNEUROSCI.2308-09.2009

Good, C.D., Johnsrude, I.S., Ashburner, J., Henson, R.N.A., Friston, K.J., Frackowiak, R.S.J., 2001. A Voxel-Based Morphometric Study of Ageing in 465 Normal Adult Human Brains. NeuroImage 14, 21–36. https://doi.org/10.1006/nimg.2001.0786

Grady, C., 2012. The cognitive neuroscience of ageing. Nature Reviews Neuroscience 13, 491–505. https://doi.org/10.1038/nrn3256

Grieve, S.M., Clark, C.R., Williams, L.M., Peduto, A.J., Gordon, E., 2005. Preservation of limbic and paralimbic structures in aging. Human Brain Mapping 25, 391–401. https://doi.org/10.1002/hbm.20115

Habes, M., Erus, G., Toledo, J.B., Bryan, N., Janowitz, D., Doshi, J., Völzke, H., Schminke, U., Hoffmann, W., Grabe, H.J., Wolk, D.A., Davatzikos, C., 2018. Regional tract-specific white matter hyperintensities are associated with patterns of aging-related brain atrophy via vascular risk factors, but also independently. Alzheimer's & Dementia: Diagnosis, Assessment & Disease Monitoring 10, 278–284. https://doi.org/10.1016/j.dadm.2018.02.002

Habib, R., Nyberg, L., Nilsson, L.-G., 2007. Cognitive and Non-Cognitive Factors Contributing to the Longitudinal Identification of Successful Older Adults in the *Betula* Study. Aging, Neuropsychology, and Cognition 14, 257–273. https://doi.org/10.1080/13825580600582412

Head, D., Rodrigue, K.M., Kennedy, K.M., Raz, N., 2008. Neuroanatomical and cognitive mediators of age-related differences in episodic memory. Neuropsychology 22, 491–507. https://doi.org/10.1037/0894-4105.22.4.491

Jbabdi, S., Johansen-Berg, H., 2011. Tractography: Where Do We Go from Here? Brain Connectivity 1, 169–183. https://doi.org/10.1089/brain.2011.0033

Jones, D.K., 2010. Challenges and limitations of quantifying brain connectivity in vivo with diffusion MRI. Imaging in Medicine 2, 341–355. https://doi.org/10.2217/iim.10.21

Josefsson, M., de Luna, X., Pudas, S., Nilsson, L.-G., Nyberg, L., 2012. Genetic and Lifestyle Predictors of 15-Year Longitudinal Change in Episodic Memory. Journal of the American Geriatrics Society 60, 2308–2312. https://doi.org/10.1111/jgs.12000

Kalpouzos, G., Chételat, G., Landeau, B., Clochon, P., Viader, F., Eustache, F., Desgranges, B., 2009. Structural and Metabolic Correlates of Episodic Memory in Relation to the Depth of Encoding in Normal Aging. Journal of Cognitive Neuroscience 21, 372–389. https://doi.org/10.1162/jocn.2008.21027

Kim, J.U., Weisenbach, S.L., Zald, D.H., 2019. Ventral prefrontal cortex and emotion regulation in aging: A case for utilizing transcranial magnetic stimulation. International Journal of Geriatric Psychiatry 34, 215–222. https://doi.org/10.1002/gps.4982

Klawiter, E.C., Schmidt, R.E., Trinkaus, K., Liang, H.-F., Budde, M.D., Naismith, R.T., Song, S.-K., Cross, A.H., Benzinger, T.L., 2011. Radial diffusivity predicts demyelination in ex vivo multiple sclerosis spinal cords. NeuroImage 55, 1454–1460. https://doi.org/10.1016/j.neuroimage.2011.01.007

Koen, J.D., Rugg, M.D., 2019. Neural Dedifferentiation in the Aging Brain. Trends in Cognitive Sciences 23, 547–559. https://doi.org/10.1016/j.tics.2019.04.012

Kong, R., Li, J., Orban, C., Sabuncu, M.R., Liu, H., Schaefer, A., Sun, N., Zuo, X.-N., Holmes, A.J., Eickhoff, S.B., Yeo, B.T.T., 2018. Spatial Topography of Individual-Specific Cortical Networks Predicts Human Cognition, Personality, and Emotion. Cerebral Cortex 19.

Le Bihan, D., 2003. Looking into the functional architecture of the brain with diffusion MRI. Nature Reviews Neuroscience 4, 469–480. https://doi.org/10.1038/nrn1119

Lebel, C., Gee, M., Camicioli, R., Wieler, M., Martin, W., Beaulieu, C., 2012. Diffusion tensor imaging of white matter tract evolution over the lifespan. NeuroImage 60, 340–352. https://doi.org/10.1016/j.neuroimage.2011.11.094

Lemaitre, H., Goldman, A.L., Sambataro, F., Verchinski, B.A., Meyer-Lindenberg, A., Weinberger, D.R., Mattay, V.S., 2012. Normal age-related brain morphometric changes: nonuniformity across cortical thickness, surface area and gray matter volume? Neurobiology of Aging 33, 617.e1-617.e9. https://doi.org/10.1016/j.neurobiolaging.2010.07.013

Li, X., Pu, F., Fan, Y., Niu, H., Li, S., Li, D., 2013. Age-related changes in brain structural covariance networks. Frontiers in Human Neuroscience 7. https://doi.org/10.3389/fnhum.2013.00098

Lighthall, N.R., Conner, L.B., Giovanello, K.S., 2019. Learning and memory in the aging brain: The function of declarative and nondeclarative memory over the lifespan., in: The Aging Brain: Functional Adaptation across Adulthood. American Psychological Association, Washington, DC, US, pp. 73–109. https://doi.org/10.1037/0000143-004

Madden, D.J., Jain, S., Monge, Z.A., Cook, A.D., Lee, A., Huang, H., Howard, C.M., Cohen, J.R., 2020. Influence of structural and functional brain connectivity on age-related differences in fluid cognition. Neurobiology of Aging 96, 205–222. https://doi.org/10.1016/j.neurobiolaging.2020.09.010

Madden, D.J., Parks, E.L., Tallman, C.W., Boylan, M.A., Hoagey, D.A., Cocjin, S.B., Packard, L.E., Johnson, M.A., Chou, Y., Potter, G.G., Chen, N., Siciliano, R.E., Monge, Z.A., Honig, J.A., Diaz, M.T., 2017. Sources of disconnection in neurocognitive aging: cerebral white-matter integrity, resting-state functional connectivity, and white-matter hyperintensity volume. Neurobiology of Aging 54, 199–213. https://doi.org/10.1016/j.neurobiolaging.2017.01.027

Marques, P.C.G., Soares, J.M.M., Magalhães, R.J. da S., Santos, N.C., Sousa, N.J.C., 2015. Macro- and micro-structural white matter differences correlate with cognitive performance in healthy aging. Brain Imaging and Behavior 10, 168–181. https://doi.org/10.1007/s11682-015-9378-4

McGinnis, S.M., Brickhouse, M., Pascual, B., Dickerson, B.C., 2011. Age-Related Changes in the Thickness of Cortical Zones in Humans. Brain Topography 24, 279–291. https://doi.org/10.1007/s10548-011-0198-6

Meunier, D., Stamatakis, E.A., Tyler, L.K., 2014. Age-related functional reorganization, structural changes, and preserved cognition. Neurobiology of Aging 35, 42–54. https://doi.org/10.1016/j.neurobiolaging.2013.07.003

Montembeault, M., Joubert, S., Doyon, J., Carrier, J., Gagnon, J.-F., Monchi, O., Lungu, O., Belleville, S., Brambati, S.M., 2012. The impact of aging on gray matter structural covariance networks. NeuroImage 63, 754–759. https://doi.org/10.1016/j.neuroimage.2012.06.052

O'Sullivan, M., Jones, D.K., Summers, P.E., Morris, R.G., Williams, S.C.R., Markus, H.S., 2001. Evidence for cortical "disconnection" as a mechanism of age-related cognitive decline. Neurology 57, 632–638. https://doi.org/10.1212/WNL.57.4.632

Otte, W.M., van Diessen, E., Paul, S., Ramaswamy, R., Subramanyam Rallabandi, V.P., Stam, C.J., Roy, P.K., 2015. Aging alterations in whole-brain networks during adulthood mapped with the minimum spanning tree indices: The interplay of density, connectivity cost and life-time trajectory. NeuroImage 109, 171–189. https://doi.org/10.1016/j.neuroimage.2015.01.011

Park, D.C., Reuter-Lorenz, P., 2009. The Adaptive Brain: Aging and Neurocognitive Scaffolding. Annual Review of Psychology 60, 173–196. https://doi.org/10.1146/annurev.psych.59.103006.093656

Paulo, A.C., Sampaio, A., Santos, N.C., Costa, P.S., Cunha, P., Zihl, J., Cerqueira, J., Palha, J.A., Sousa, N., 2011. Patterns of cognitive performance in healthy ageing in northern portugal: A cross-sectional analysis. PLoS ONE 6, 1–9. https://doi.org/10.1371/journal.pone.0024553

Pierpaoli, C., Basser, P.J., 1996. Toward a quantitative assessment of diffusion anisotropy. Magnetic Resonance in Medicine 36, 893–906. https://doi.org/10.1002/mrm.1910360612

Prins, N.D., Scheltens, P., 2015. White matter hyperintensities, cognitive impairment and dementia: an update. Nature Reviews Neurology 11, 157–165. https://doi.org/10.1038/nrneurol.2015.10

Prins, N.D., van Dijk, E.J., den Heijer, T., Vermeer, S.E., Jolles, J., Koudstaal, P.J., Hofman, A., Breteler, M.M.B., 2005. Cerebral small-vessel disease and decline in information processing speed, executive function and memory. Brain 128, 2034–2041. https://doi.org/10.1093/brain/awh553

Raz, N., 2005. Ageing and the Brain, in: John Wiley & Sons, Ltd (Ed.), Encyclopedia of Life Sciences. John Wiley & Sons, Ltd, Chichester, UK. https://doi.org/10.1038/npg.els.0004063

Raz, N., 1999. Aging of the brain and its impact on cognitive performance: Integration of structural and functional findings. 2nd ed. Mahwah, N: Lawrence Erlbaum Associates; 2.

Raz, N., 1997. Selective aging of the human cerebral cortex observed in vivo: differential vulnerability of the prefrontal gray matter. Cerebral Cortex 7, 268–282. https://doi.org/10.1093/cercor/7.3.268

Raz, N., Lindenberger, U., Rodrigue, K.M., Kennedy, K.M., Head, D., Williamson, A., Dahle, C., Gerstorf, D., Acker, J.D., 2005. Regional Brain Changes in Aging Healthy Adults: General Trends, Individual Differences and Modifiers. Cerebral Cortex 15, 1676–1689. https://doi.org/10.1093/cercor/bhi044

Resnick, S.M., Pham, D.L., Kraut, M.A., Zonderman, A.B., Davatzikos, C., 2003. Longitudinal Magnetic Resonance Imaging Studies of Older Adults: A Shrinking Brain. The Journal of Neuroscience 23, 3295–3301. https://doi.org/10.1523/JNEUROSCI.23-08-03295.2003

Rettmann, M.E., 2005. Cross-sectional and Longitudinal Analyses of Anatomical Sulcal Changes Associated with Aging. Cerebral Cortex 16, 1584–1594. https://doi.org/10.1093/cercor/bhj095

Reuter, N., Genon, S., Kharabian Masouleh, S., Hoffstaedter, F., Liu, X., Kalenscher, T., Eickhoff, S.B., Patil, K.R., 2020. CBPtools: a Python package for regional connectivity-based parcellation. Brain Structure and Function 225, 1261–1275. https://doi.org/10.1007/s00429-020-02046-1

Reuter-Lorenz, P., Mikels, J., 2006. The aging mind and brain: Implications of enduring plasticity for behavioral and cultural change. Lifespan Development and the Brain: The Perspective of Biocultural Co-Constructivism 255–276. https://doi.org/10.1017/CBO9780511499722.014

Reuter-Lorenz, P.A., Cappell, K.A., 2008. Neurocognitive Aging and the Compensation Hypothesis. Current Directions in Psychological Science 17, 177–182. https://doi.org/10.1111/j.1467-8721.2008.00570.x

Reuter-Lorenz, P.A., Lustig, C., 2005. Brain aging: reorganizing discoveries about the aging mind. Current Opinion in Neurobiology 15, 245–251. https://doi.org/10.1016/j.conb.2005.03.016

Reuter-Lorenz, P.A., Park, D.C., 2014. How Does it STAC Up? Revisiting the Scaffolding Theory of Aging and Cognition. Neuropsychology Review 24, 355–370. https://doi.org/10.1007/s11065-014-9270-9

Rubinov, M., Sporns, O., 2010. Complex network measures of brain connectivity: Uses and interpretations. NeuroImage 52, 1059–1069. https://doi.org/10.1016/j.neuroimage.2009.10.003

Sala-Llonch, R., Junqué, C., Arenaza-Urquijo, E.M., Vidal-Piñeiro, D., Valls-Pedret, C., Palacios, E.M., Domènech, S., Salvà, A., Bargalló, N., Bartrés-Faz, D., 2014. Changes in whole-brain functional networks and memory performance in aging. Neurobiology of Aging 35, 2193–2202. https://doi.org/10.1016/j.neurobiolaging.2014.04.007

Salat, D.H., 2011. The Declining Infrastructure of the Aging Brain. Brain Connectivity 1, 279–293. https://doi.org/10.1089/brain.2011.0056

Salat, D.H., 2004. Thinning of the Cerebral Cortex in Aging. Cerebral Cortex 14, 721–730. https://doi.org/10.1093/cercor/bhh032

Salat, D.H., Tuch, D.S., Greve, D.N., van der Kouwe, A.J.W., Hevelone, N.D., Zaleta, A.K., Rosen, B.R., Fischl, B., Corkin, S., Rosas, H.D., Dale, A.M., 2005. Age-related alterations in white matter microstructure measured by diffusion tensor imaging. Neurobiology of Aging 26, 1215–1227. https://doi.org/10.1016/j.neurobiolaging.2004.09.017

Salehi, M., Karbasi, A., Shen, X., Scheinost, D., Constable, R.T., 2018. An exemplar-based approach to individualized parcellation reveals the need for sex specific functional networks. NeuroImage 170, 54–67. https://doi.org/10.1016/j.neuroimage.2017.08.068

Santos, N.C., Costa, P.S., Cunha, P., Portugal-Nunes, C., Amorim, L., Cotter, J., Cerqueira, J.J., Palha, J.A., Sousa, N., 2014. Clinical, physical and lifestyle variables and relationship with cognition and

mood in aging: A cross-sectional analysis of distinct educational groups. Frontiers in Aging Neuroscience 6, 1–15. https://doi.org/10.3389/fnagi.2014.00021

Schacter, D.L., Tulving, E. (Eds.), 1994. Memory systems 1994. MIT Press, Cambridge, Mass.

Sexton, C.E., Walhovd, K.B., Storsve, A.B., Tamnes, C.K., Westlye, L.T., Johansen-Berg, H., Fjell, A.M., 2014. Accelerated Changes in White Matter Microstructure during Aging: A Longitudinal Diffusion Tensor Imaging Study. Journal of Neuroscience 34, 15425–15436. https://doi.org/10.1523/JNEUROSCI.0203-14.2014

Shachter, D.L., Gilbert, D.T., Nock, M.K., Wegner, D.M., 2020. Explicit Memory: Semantic and Episodic, in: Psychology. Worth Publishers.

Shafto, M.A., Tyler, L.K., 2014. Language in the aging brain: The network dynamics of cognitive decline and preservation. Science 346, 583–587. https://doi.org/10.1126/science.1254404

Shaw, M.E., Sachdev, P.S., Anstey, K.J., Cherbuin, N., 2016. Age-related cortical thinning in cognitively healthy individuals in their 60s: the PATH Through Life study. Neurobiology of Aging 39, 202–209. https://doi.org/10.1016/j.neurobiolaging.2015.12.009

Slater, D.A., Melie-Garcia, L., Preisig, M., Kherif, F., Lutti, A., Draganski, B., 2019. Evolution of white matter tract microstructure across the life span. Human Brain Mapping 40, 2252–2268. https://doi.org/10.1002/hbm.24522

Song, S.-K., Sun, S.-W., Ju, W.-K., Lin, S.-J., Cross, A.H., Neufeld, A.H., 2003. Diffusion tensor imaging detects and differentiates axon and myelin degeneration in mouse optic nerve after retinal ischemia. NeuroImage 20, 1714–1722. https://doi.org/10.1016/j.neuroimage.2003.07.005

Song, S.-K., Sun, S.-W., Ramsbottom, M.J., Chang, C., Russell, J., Cross, A.H., 2002. Dysmyelination Revealed through MRI as Increased Radial (but Unchanged Axial) Diffusion of Water. NeuroImage 17, 1429–1436. https://doi.org/10.1006/nimg.2002.1267

Song, S.-K., Yoshino, J., Le, T.Q., Lin, S.-J., Sun, S.-W., Cross, A.H., Armstrong, R.C., 2005. Demyelination increases radial diffusivity in corpus callosum of mouse brain. NeuroImage 26, 132–140. https://doi.org/10.1016/j.neuroimage.2005.01.028

Spreng, R.N., Turner, G.R., 2019. Structure and function of the aging brain., in: The Aging Brain: Functional Adaptation across Adulthood. American Psychological Association, Washington, DC, US, pp. 9–43. https://doi.org/10.1037/0000143-002

Spreng, R.N., Turner, G.R., 2013. Structural Covariance of the Default Network in Healthy and Pathological Aging. Journal of Neuroscience 33, 15226–15234. https://doi.org/10.1523/JNEUROSCI.2261-13.2013

Spreng, R.N., Wojtowicz, M., Grady, C.L., 2010. Reliable differences in brain activity between young and old adults: A quantitative meta-analysis across multiple cognitive domains. Neuroscience & Biobehavioral Reviews 34, 1178–1194. https://doi.org/10.1016/j.neubiorev.2010.01.009

Storsve, A.B., Fjell, A.M., Tamnes, C.K., Westlye, L.T., Overbye, K., Aasland, H.W., Walhovd, K.B., 2014. Differential Longitudinal Changes in Cortical Thickness, Surface Area and Volume across the Adult Life Span: Regions of Accelerating and Decelerating Change. Journal of Neuroscience 34, 8488–8498. https://doi.org/10.1523/JNEUROSCI.0391-14.2014

Sun, S.-W., Liang, H.-F., Cross, A.H., Song, S.-K., 2008. Evolving Wallerian degeneration after transient retinal ischemia in mice characterized by diffusion tensor imaging. NeuroImage 40, 1–10. https://doi.org/10.1016/j.neuroimage.2007.11.049

Sutton, B.P., Ouyang, C., Karampinos, D.C., Miller, G.A., 2009. Current trends and challenges in MRI acquisitions to investigate brain function. International Journal of Psychophysiology 73, 33–42. https://doi.org/10.1016/j.ijpsycho.2008.12.020

Thambisetty, M., Wan, J., Carass, A., An, Y., Prince, J.L., Resnick, S.M., 2010. Longitudinal changes in cortical thickness associated with normal aging. NeuroImage 52, 1215–1223. https://doi.org/10.1016/j.neuroimage.2010.04.258

Toepper, M., 2017. Dissociating Normal Aging from Alzheimer's Disease: A View from Cognitive Neuroscience. Journal of Alzheimer's Disease 57, 331–352. https://doi.org/10.3233/JAD-161099

Tononi, G., Sporns, O., Edelman, G.M., 1994. A measure for brain complexity: relating functional segregation and integration in the nervous system. Proceedings of the National Academy of Sciences 91, 5033–5037. https://doi.org/10.1073/pnas.91.11.5033

Turner, G.R., Spreng, R.N., 2012. Executive functions and neurocognitive aging: dissociable patterns of brain activity. Neurobiology of Aging 33, 826.e1-826.e13. https://doi.org/10.1016/j.neurobiolaging.2011.06.005

United Nations, 2019. World Population Ageing 2019. Economic and Social Affairs, Population Division 1–111.

van den Heuvel, M.P., Sporns, O., 2011. Rich-Club Organization of the Human Connectome. Journal of Neuroscience 31, 15775–15786. https://doi.org/10.1523/JNEUROSCI.3539-11.2011

Vinke, E.J., de Groot, M., Venkatraghavan, V., Klein, S., Niessen, W.J., Ikram, M.A., Vernooij, M.W., 2018. Trajectories of imaging markers in brain aging: the Rotterdam Study. Neurobiology of Aging 71, 32–40. https://doi.org/10.1016/j.neurobiolaging.2018.07.001

Wang, J., Zuo, X., He, Y., Bullmore, E.T., Fornito, A., 2010. Graph-based network analysis of resting-state functional MRI. Neuroscience 4, 1–14. https://doi.org/10.3389/fnsys.2010.00016

Ward, E.V., Berry, C.J., Shanks, D.R., 2013. Age effects on explicit and implicit memory. Frontiers in Psychology 4. https://doi.org/10.3389/fpsyg.2013.00639

Ward, E.V., Berry, C.J., Shanks, D.R., Moller, P.L., Czsiser, E., 2020. Aging Predicts Decline in Explicit and Implicit Memory: A Life-Span Study. Psychological Science 31, 1071–1083. https://doi.org/10.1177/0956797620927648

Wen, W., Zhu, W., He, Y., Kochan, N.A., Reppermund, S., Slavin, M.J., Brodaty, H., Crawford, J., Xia, A., Sachdev, P., 2011. Discrete Neuroanatomical Networks Are Associated with Specific Cognitive Abilities in Old Age. Journal of Neuroscience 31, 1204–1212. https://doi.org/10.1523/JNEUROSCI.4085-10.2011

Westlye, L.T., Walhovd, K.B., Dale, A.M., Bjornerud, A., Due-Tonnessen, P., Engvig, A., Grydeland, H., Tamnes, C.K., Ostby, Y., Fjell, A.M., 2010. Life-Span Changes of the Human Brain White Matter: Diffusion Tensor Imaging (DTI) and Volumetry. Cerebral Cortex 20, 2055–2068. https://doi.org/10.1093/cercor/bhp280

Wiseman, S.J., Booth, T., Ritchie, S.J., Cox, S.R., Muñoz Maniega, S., Valdés Hernández, M. del C., Dickie, D.A., Royle, N.A., Starr, J.M., Deary, I.J., Wardlaw, J.M., Bastin, M.E., 2018. Cognitive abilities, brain white matter hyperintensity volume, and structural network connectivity in older age. Human Brain Mapping 39, 622–632. https://doi.org/10.1002/hbm.23857

Wu, K., Taki, Y., Sato, K., Kinomura, S., Goto, R., Okada, K., Kawashima, R., He, Y., Evans, A.C., Fukuda, H., 2012. Age-related changes in topological organization of structural brain networks in healthy individuals. Human Brain Mapping 33, 552–568. https://doi.org/10.1002/hbm.21232

Yang, Y., Dai, B., Howell, P., Wang, X., Li, K., Lu, C., 2014. White and Grey Matter Changes in the Language Network during Healthy Aging. PLoS ONE 9, e108077. https://doi.org/10.1371/journal.pone.0108077

Yousaf, T., Dervenoulas, G., Politis, M., 2018. Advances in MRI Methodology, in: International Review of Neurobiology. Elsevier, pp. 31–76. https://doi.org/10.1016/bs.irn.2018.08.008

Zalesky, A., Fornito, A., Bullmore, E.T., 2010. Network-based statistic: Identifying differences in brain networks. NeuroImage 53, 1197–1207. https://doi.org/10.1016/j.neuroimage.2010.06.041

Zhao, T., Cao, M., Niu, H., Zuo, X.N., Evans, A., He, Y., Dong, Q., Shu, N., 2015. Age-related changes in the topological organization of the white matter structural connectome across the human lifespan. Human Brain Mapping 36, 3777–3792. https://doi.org/10.1002/hbm.22877

Zimmerman, M.E., Brickman, A.M., Paul, R.H., Grieve, S.M., Tate, D.F., Gunstad, J., Cohen, R.A., Aloia, M.S., Williams, L.M., Clark, C.R., Whitford, T.J., Gordon, E., 2006. The Relationship Between Frontal Gray Matter Volume and Cognition Varies Across the Healthy Adult Lifespan. The American Journal of Geriatric Psychiatry 14, 823–833. https://doi.org/10.1097/01.JGP.0000238502.40963.ac

Zupan, M., 2016. Pathogenesis of Leukoaraiosis: A Review, in: Lenasi, H. (Ed.), Microcirculation Revisited - From Molecules to Clinical Practice. InTech. https://doi.org/10.5772/63655

CHAPTHER II

Ana Coelho, Henrique M. Fernandes, Ricardo Magalhães, Pedro Silva Moreira, Paulo Marques, José M. Soares, Liliana Amorim, Carlos Portugal-Nunes, Teresa Castanho, Nadine Correia Santos, Nuno Sousa (2021)

Signatures of White-matter Microstructure Degradation During Aging and its Association with Cognitive Status

Scientific Reports, doi: 10.1038/s41598-021-83983-7

Signatures of White-matter Microstructure Degradation During Aging and its Association with Cognitive Status

Ana Coelho[1,2,3], Henrique M. Fernandes[4,5], Ricardo Magalhães[1,2,3], Pedro Silva Moreira[1,2,3], Paulo Marques[1,2,3], José M. Soares[1,2,3], Liliana Amorim[1,2,3], Carlos Portugal-Nunes[1,2,3], Teresa Castanho[1,2,3], Nadine Correia Santos[1,2,3], Nuno Sousa[1,2,3]

[1]Life and Health Sciences Research Institute (ICVS), School of Medicine, University of Minho, Braga, Portugal; [2]ICVS/3B's, PT Government Associate Laboratory, Braga/Guimarães, Portugal; [3]Clinical Academic Center – Braga, Braga, Portugal; [4]Center for Music in the Brain (MIB), Aarhus University, Aarhus, Denmark; [5]Department of Psychiatry, University of Oxford, Oxford, UK

1. Abstract

Previous studies have shown an association between cognitive decline and white matter integrity in aging. This led to the formulation of a "disconnection hypothesis" in the aging-brain, which states that the disruption in cortical network communication may explain the cognitive decline during aging. Although some longitudinal studies have already investigated the changes occurring in white matter microstructure, most focused on specific white matter tracts. Our study aims to characterize the longitudinal whole-brain signatures of white matter microstructural change during aging. Furthermore, we assessed the relationship between distinct longitudinal alterations in white matter integrity and cognition. White matter microstructural properties were estimated from diffusion magnetic resonance imaging, and cognitive status characterized from extensive neurocognitive testing. The same individuals were evaluated at two timepoints, with a mean interval time of 52.8 months (SD = 7.24) between first and last assessment. Our results show that age is associated with a decline in cognitive performance and a degradation in white matter integrity. Additionally, significant associations were found between diffusion measures and different cognitive dimensions (memory, executive function and general cognition). Overall, these results suggest that age-related cognitive decline is related to white matter alterations, and thus give support to the "disconnected hypothesis" of the aging brain.

Keywords: diffusion MRI, white matter, tract-based spatial statistics, cognitive performance, aging

2. Introduction

Normal aging is a heterogeneous process characterized by functional (Damoiseaux, 2017; Hakun et al., 2015) and structural alterations (Lockhart and DeCarli, 2014; Soares et al., 2014) at the brain level, along with declines in several cognitive dimensions (Meunier et al., 2014). The "disconnection hypothesis" tries to establish a link between these age-related cognitive and brain changes, postulating that a disruption of communication between cortical regions can lead to a decline in cognitive performance (Andrews-Hanna et al., 2007; Bartzokis, 2004; Fjell et al., 2016a; Madden et al., 2017; O'Sullivan et al., 2001b). One potential source of brain disconnection is white matter (WM) integrity and there is already evidence suggesting this relationship between WM disruption and cognitive decline in "normal" aging (Bennett and Madden, 2014; Marques et al., 2015).

WM integrity can be indirectly measured with diffusion tensor imaging (DTI), which measures the diffusion of water molecules in the brain (Basser et al., 1994; Pierpaoli and Basser, 1996). Tissue integrity can be assessed using different DTI-based measures: fractional anisotropy (FA), mean diffusivity (MD), axial diffusivity (AD) and radial diffusivity (RD). Higher values of FA and lower values of diffusivity (MD, AD and RD) indicate higher tissue integrity (Bennett and Madden, 2014). Previous cross-sectional and longitudinal studies have reported a WM degradation pattern with aging, with the most consistent findings being a decrease in FA and increase in MD with increasing age(de Groot et al., 2015; de Lange et al., 2016; Lebel et al., 2012; Salat et al., 2005; Sexton et al., 2014; Vinke et al., 2018; Westlye et al., 2010). Other studies also report changes in RD and AD, being the observed changes usually more salient for RD than AD (Davis et al., 2009; Madden et al., 2009; Zhang et al., 2010) and the direction of change in AD is still controversial (Burzynska et al., 2010; Sullivan et al., 2010). Since RD is thought to be more sensitive to myelin degeneration, it suggests that age-related WM alterations may be driven by myelination changes (Bennett and Madden, 2014; Davis et al., 2009). Moreover, DTI studies also report an association between WM integrity and cognitive performance within older adults, with larger effect sizes for specific cognitive dimensions, such as executive function and information processing speed (for a review see (Madden et al., 2012)). Additionally, some DTI studies report a mediation effect of WM integrity in the relationship between age and cognitive functions (e.g. associative learning, executive functions, processing speed, episodic memory) (Borghesani et al., 2013; Brickman et al., 2012; Burgmans et al., 2011; Gazes et al., 2016; Li et al., 2018; Samanez-Larkin et al., 2012), which suggests a causal role for WM integrity on age-related differences in cognitive performance.

Most of these studies, however, used a cross-sectional design and the existing longitudinal studies focused on specific WM tracts, despite the evidence for the existence of a global effect alongside the regional effects (Bennett and Madden, 2014; Johnson et al., 2015). Furthermore, a previous study from our lab (Marques et al., 2015) used DTI to assess which WM microstructural properties could discriminate between different profiles of cognitive performance, in a cross-sectional design. In this study, we continue this previous work, using longitudinal data from the same group of individuals. Our main goal was to investigate: i) WM integrity changes along time and ii) associations between WM microstructure alterations and cognition. We hypothesized that aging would trigger a degradation of white-matter integrity and this deterioration will be associated to cognitive decline. To test this, we estimated white-matter microstructural properties of a group of older adults that were followed longitudinally from diffusion MRI. We characterized cognitive status from extensive neurocognitive testing and tested relationships between longitudinal changes in white-matter integrity and cognition.

3. Methods

3.1. Ethics Statement

The present study was conducted in accordance with the principles expressed in the Declaration of Helsinki and was approved by the national ethical committee (Comissão Nacional de Proteção de Dados) and by the local ethics review boards (Hospital de Braga, Braga; Centro Hospitalar do Alto Ave, Guimarães; and Unidade Local de Saúde do Alto Minho, Viana-do-Castelo/Ponte-de-Lima). The study goals and procedures were explained to the participants and all gave informed written consent.

3.2. Participants

The participants included in this study are part of the sample recruited for the SWITCHBOX Consortium project (www.switchbox-online.eu/). These participants were recruited from a larger sample randomly selected from Guimarães and Vizela local area health authority registries, that is representative of the general Portuguese population for age, gender and education (Costa et al., 2013; Santos et al., 2014, 2013). Primary exclusion criteria were inability to understand the informed consent, participant's choice to withdraw from the study, incapacity and/or inability to attend the MRI session, dementia and/or diagnosed neuropsychiatric and/or neurodegenerative disorder and/or cerebrovascular disease (medical records). Mini Mental State Examination (MMSE) scores below the adjusted thresholds for cognitive impairment were also used as exclusion criteria. Following recommendations, the thresholds were

adjusted depending on factors such as age and/or education (Busch and Chapin, 2008; Grigoletto et al., 1999). This resulted in the following adjusted thresholds for cognitive impairment: MMSE score <17 if individual with ≤4 years of formal school education and/or ≥72 years of age, and MMSE score <23 otherwise (follows the MMSE validation study for the Portuguese population) (Guerreiro et al., 1994).

In the first assessment, 100 subjects were contacted for MRI screening. From these, three subjects did not finish the diffusion acquisition and four subjects were excluded after the visual inspection of the MRI scans by a certified neuroradiologist concluded that they had brain lesions/pathology. For the last assessment, all participants from the baseline were contacted to perform the follow-up evaluation but subjects presenting diseases that could affect both cognition and white matter microstructure (e.g., cerebrovascular disease) were excluded. In the end, 55 subjects accepted to be re-evaluated and were able to perform the MRI acquisition protocol, but one did not finish the diffusion acquisition. A total of 51 individuals with diffusion data from both the first and last assessments met all the inclusion criteria for this study.

3.3. Neurocognitive assessment

A team of certified psychologists performed a battery of neurocognitive tests in the two timepoints. This included the following tests validated for the Portuguese population: Stroop color and word test, selective reminding test (SRT) and mini-mental state examination (MMSE). Stroop test was used to evaluate cognitive flexibility and inhibitory control and it was composed of three parameters: words (SW), colors (SC) and words/colors (SWC) evaluated at three parts. In the first part, different words of colors printed in black are presented to the participant which has to read the word (Stroop words). In the second part, the 'XXXX' word is printed in different ink colors and the participant has to name the ink color (Stroop colors). The third and final part corresponds to the interference (Stroop words/colors) component of the test, where the participant is presented with inconsistent association between the word and the ink in which the word is printed (e.g., word "blue" printed in red ink). In this case, the participant has to name the ink color instead of reading the word. SRT was also constituted of three variables: long-term storage (LTS), consistent long-term retrieval (CLTR) and delayed-recall (DR) and assessed verbal learning and memory. MMSE was performed to evaluate general cognition through the assessment of different cognitive domains, such as orientation, word recall, attention and calculation, language and visual-construction abilities. Test scores were transformed to be expressed in the same scale. Since we are dealing with longitudinal data, z-score standardization has some limitations, namely the loss of

information about mean-level changes across time. In order to overcome this issue, we transformed test scores using the proportion of maximum scaling (POMS), according to the formula:

$$POMS = \frac{observed - minimum}{maximum - minimum}$$

The transformed test scores range from 0 (minimum possible value) to 1 (maximum possible value) (Moeller, 2015).

3.4. MRI Data Acquisition

All MRI assessments were performed at Hospital de Braga (Braga, Portugal) on a clinical approved Siemens Magnetom Avanto 1.5T MRI scanner (Siemens Medical Solutions, Erlangen, Germany) with a 12-channel receive-only head-coil. The imaging protocol included several different acquisitions. For the present study, only the Diffusion Weighted Imaging (DWI) acquisition was considered. For this, a spin-echo echo-planar imaging (SE-EPI) sequence was acquired with the following parameters: TR=8800 ms, TE=99 ms, FoV=240x240 mm, acquisition matrix=120x120, 61 2-mm axial slices with no gap, 30 non-collinear gradient direction with b=1000 s mm^{-2}, one b=0 s mm^{-2} and 1 repetition.

All acquisitions were visually inspected by a certified neuroradiologist, before data pre-processing, to ensure that none of the individuals included in this study had brain lesions and/or critical head motion or artifacts that could comprise the quality of the data and reliability of our findings.

3.5. DWI data pre-processing and tensor fitting

All data was pre-processed using FMRIB Diffusion Toolbox (FDT) provided with the FMRIB Software Library (FSL v5.0; https://fsl.fmrib.ox.ac.uk/fsl/). Pre-processing included: correction for motion and eddy current distortions; rotation of gradient vectors accordingly to the affine transformations used to register each volume; extraction and skull stripping of the first b0 volume of each subject; removal of non-brain structures by applying the brain mask created in the previous step to the remaining volumes.

Tensor fitting and scalar maps computation steps were performed with DTIFIT that is part of FDT toolbox. Briefly, DTIFIT fits a diffusion tensor model at each voxel and generates scalar maps of FA and MD, as well as eigenvector and eigenvalues maps. AD scalar map was defined as the principal diffusion eigenvalue and RD as the mean of the second and third eigenvalues.

3.6. Longitudinal Tract-based spatial statistics

Voxel-wise analysis of scalar maps across subjects and timepoints was performed using TBSS procedures (Smith et al., 2006), part of FSL. While this method aims to solve issues of aligning data from multiple subjects, it does not take into account variation from multiple timepoints. Thus, in this study, we implemented a modified TBSS pipeline that improves anatomical longitudinal alignment, as described in (Engvig et al., 2012). First, linear transformations between the b0 images of the first and second timepoints were computed using FLIRT. Then, the b0 images and scalar maps of both timepoints were resampled to a space halfway between the two, that was previously computed with MIDTRANS. Next, a subject-wise mid-space template was created by averaging the two halfway registered FA-maps. These subject's templates were then used in the normal TBSS procedures. Initially, each subject's FA template was slightly eroded, and the end slices were zeroed in order to further remove potential outliers. Next, all FA templates were nonlinearly registered into a 1x1x1 mm standard space. In order to accomplish this particular step, each subject's FA template was nonlinear registered to each other to find the "most representative one" (i.e., the one that requires the least warping to align all images) that served as the study specific target image. Then, the chosen target was affine transformed into Montreal Neurological Institute (MNI) 152 standard space and each subject's FA template was transformed into standard space through the combination of the nonlinear transformation to the study specific target with the affine transformation into MNI space. Next, FA templates of all subjects were averaged, and the resulting image skeletonized and thresholded. Thresholding the mean FA value between 0.2 and 0.3 was found to successfully remove from the skeleton regions encompassing multiple tissue types (Smith et al., 2006). Thus, after visual inspection we thresholded the skeleton image at 0.3. Finally, all scalar maps (FA, AD, MD and RD) from the two time points were projected into this FA skeleton using the same transformation applied to the FA templates.

3.7. Statistical analysis

Statistical analysis of the skeletonized maps of FA, AD, MD and RD was performed in order to discriminate which WM tracts exhibit statistically significant differences. This was accomplished using the permutation methods employed in "randomise", distributed with FSL. We performed a paired sample t-test to investigate age-related trajectories of WM microstructure. Five thousand random permutations were used in the inference of the contrasts of interest. Widespread significant differences were detected with threshold-free cluster enhancement (TFCE), whereas multiple comparisons were corrected using family-

wise error rate (FWE-R) at α=0.05. Clusters showing significant results were labeled according to the Johns Hopkins University ICBM-DTI-81 WM labels atlas (Hua et al., 2008) and dilated with tbss_fill tool (distributed with FSL) for visualization purposes. We also calculated the Dice coefficient between each pair of significant clusters to evaluate the degree of similarity between them. Dice coefficient ranges between 0 and 1, with values of 1 meaning that the two clusters are a perfect match. Subsequently, we investigated the associations between the significant results from this analysis and the scores of neurocognitive tests. To do this, the mean DTI metrics (FA, AD, MD and RD) were extracted from each significant cluster of each contrast of interest and correlation analyses were performed between the mean DTI metric and each cognitive test, for all timepoints. Subjects with missing values in cognitive scores were excluded from the analyses and p-values were corrected for multiple comparisons, using the false discovery rate (FDR) method. The rmcorr R package (https://cran. r-project.org/web/packages/rmcorr/) was used to compute a repeated measures correlation coefficient between each DTI metric and cognitive score. Repeated measures correlation analysis computes the correlation within each individual between two variables measured longitudinally and then estimates the common regression slope, which is the association shared between individuals. This technique takes into account non-independence between observations of repeated measures data and has greater statistical power than the standard Pearson correlation coefficient using averaged data (Bakdash and Marusich, 2017).

Additionally, we calculated the percentage of change between timepoints for each significant cluster of each DTI metric, and for each cognitive test score. The following formula was used:

$$\Delta_{ij} = \frac{M_j - M_i}{|M_i|} \times 100$$

where M_i and M_j are the metric values at timepoint i and j, respectively. We also tested differences between slopes of each significant cluster. For this, we first performed a linear regression for each cluster and then an Analysis of Covariance (ANCOVA) with DTI metric as dependent variable, cluster as the factor and timepoint as the covariate and analyzed the significance of the interaction term. We transformed values to reflect only increases in time, in order to compare slopes independently of the direction.

4. Results

4.1. Sample characteristics

Table 1 shows the demographic characterization of the participants included in this study. In summary, mean age at baseline was 63.5 years (range, 51 – 82 years) and mean interval between evaluations was 52.8 months (range, 45 – 73 months). Interval time was not significantly associated with age at baseline (r = - 0.12, p = 0.41). The sample was balanced for males and females (51% females, 49% males) and they did not differ with respect to interval time ($t(30) = 0.14, p = 0.89$). Mean education level was 5.98 years (range, 0 – 17 years). Regarding neurocognitive test scores, all variables show a decrease along time, with the exception of Stroop words parameter that remains constant (Supplementary Fig. 1). Statistically significant differences were found between timepoints for long-term storage ($t(50) = 3.40, p = 0.003, d = 0.48$), Stroop colors ($t(50) = 4.48, p = 0.0003, d = 0.63$) and MMSE variables ($t(50) = 4.04, p = 0.0006, d = 0.57$).

Table 1. Basic demographic and cognitive characterization of the study's cohort. Statistical results FDR corrected at p<0.05.

	Baseline Mean ± SD (range)	Follow-up Mean ± SD (range)	Test Statistic
N (Females/Males)	51 (26/25)	-	-
Age (years)	63.5 ± 7.41 (51 – 82)	68.0 ± 7.25 (55 – 86)	
Interval (months)	52.8 ± 7.24 (45 – 73)	-	
Education (years)	5.98 ± 3.97 (0 – 17)	-	
LTS	0.53 ± 0.24 (0.069 – 1)	0.43 ± 0.24 (0 – 1)	t(50) = 3.40, p = 0.003**, d = 0.48
CLTR	0.38 ± 0.26 (0 – 1)	0.33 ± 0.25 (0 – 1)	t(50) = 1.86, p = 0.096
DR	0.50 ± 0.27 (0 – 1)	0.45 ± 0.25 (0 – 1)	t(50) = 1.11, p = 0.32
SW	0.55 ± 0.27 (0.013 – 1)	0.55 ± 0.22 (0 – 1)	t(50) = 0.30, p = 0.77
SC	0.63 ± 0.21 (0 – 0.99)	0.53 ± 0.26 (0 – 1)	t(50) = 4.48, p = 0.0003***, d = 0.63
SWC	0.53 ± 0.23 (0 – 1)	0.49 ± 0.24 (0 – 1)	t(50) = 1.98, p = 0.094
MMSE	0.82 ± 0.22 (0 – 1)	0.72 ± 0.23 (0.077 – 1)	t(50) = 4.04, p = 0.0006***, d = 0.57

Abbreviations: LTS, long-term storage; CLTR, consistent long-term retrieval; DR, delayed-recall; SW, Stroop words; SC, Stroop colors; SWC, Stroop words/colors; MMSE, Mini-Mental State Examination.
Significance codes: * p < 0.05, ** p < 0.01, *** p < 0.001

4.2. Age-related trajectories in WM microstructure

Statistical analysis of the skeletonized maps revealed statistically significant differences between timepoints for all DTI metrics (Fig. 1). Significant longitudinal decreases for the FA maps were found in two clusters. One of these clusters (Cluster 1) comprises the body of corpus callosum, and right superior and posterior corona radiata (Supplementary Figure 2A). The other cluster (Cluster 2) includes the genu, body and splenium of corpus callosum, anterior limb of internal capsule, anterior, superior and posterior corona radiata, external capsule and superior longitudinal fasciculus, with most of these tracts located in the left hemisphere (Supplementary Figure 2B). For AD and MD metrics, significant longitudinal increases were found in a large cluster spread throughout the brain. This cluster includes WM tracts such as the genu, body and splenium of corpus callosum, cerebral peduncle, internal capsule, corona radiata, posterior thalamic radiation, sagittal stratum, external capsule, cingulum, fornix, superior longitudinal fasciculus, superior fronto-occipital fasciculus, tapetum and uncinate fasciculus. Regarding RD, two clusters were found, with one of them comprising only the right superior longitudinal fasciculus (Cluster 1) (Supplementary Figure 2C), while the other (Cluster 2) includes the same tracts as the cluster found for AD and MD (Supplementary Figure 2D). A summary of these results, with cluster size, coordinates and corresponding white matter tract of the peak are present in Supplementary Table 1.

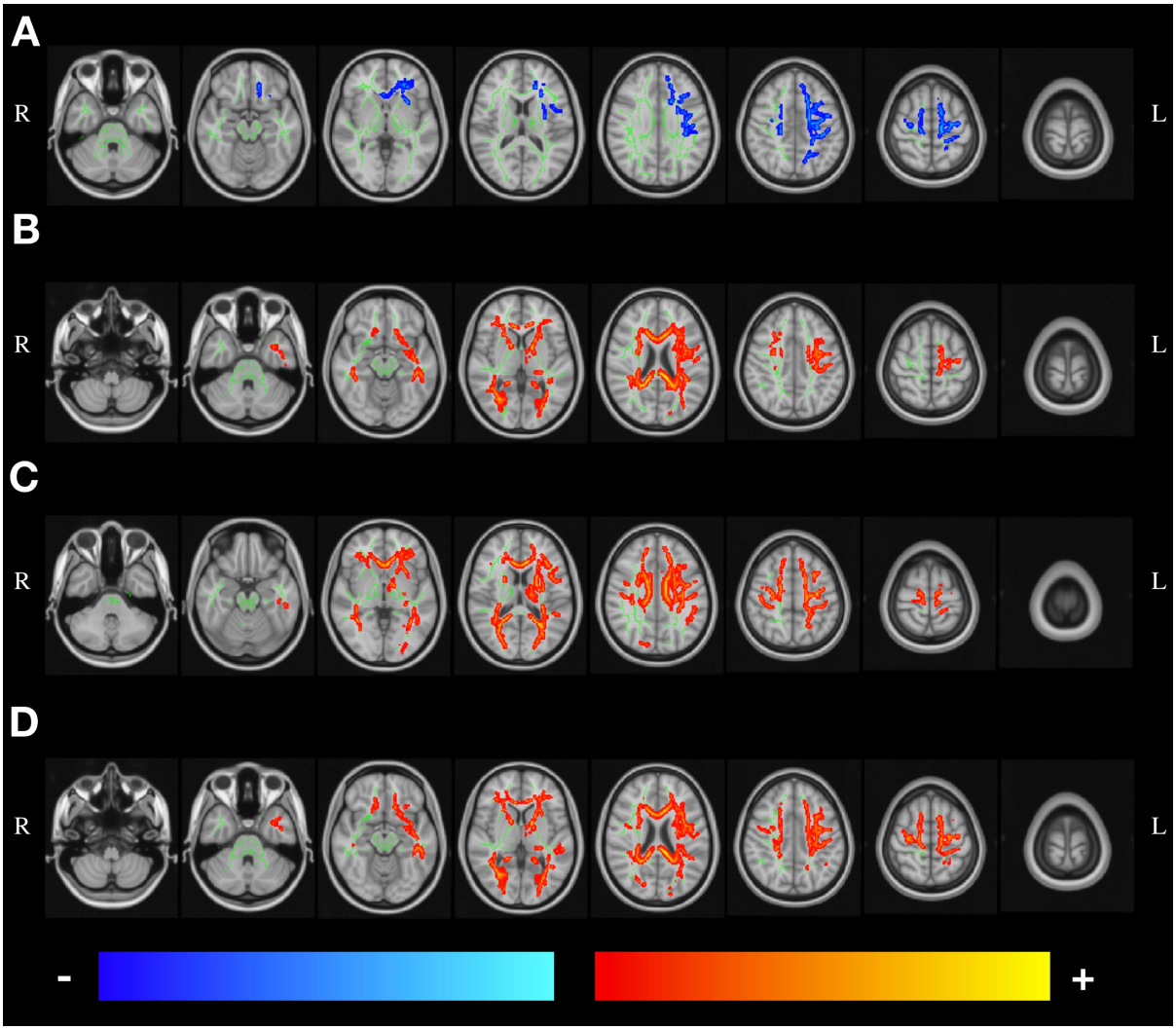

Figure 1. Statistically significant changes along time in a) FA, b) AD, c) RD and d) MD maps. Blue/light-blue gradient indicates decreases along time. Red/yellow gradient indicates increases along time. All results were considered significant at $p<0.05$ (FWE corrected for multiple comparisons). We observe a decrease in FA with a left hemisphere dominant pattern, while the other metrics (AD, RD and MD) exhibit an increase between timepoints with the changes being spread throughout the brain.

Regarding the similarity of the obtained significant clusters, measured with Dice coefficient, we found that FA Cluster 2 and RD Cluster 1 did not overlap with any other cluster. FA Cluster 1 had a small overlap with AD, MD and RD Cluster 2, while FA Cluster 2 had increased similarity with the same clusters. AD, MD and RD Cluster 2 had the highest degrees of similarity between them. A summary of these results is present in Table 2.

Table 2. Dice coefficient between each pair of significant clusters.

Metric	FA Cluster 1	FA Cluster 2	AD Cluster 1	MD Cluster 1	RD Cluster 1	RD Cluster 2
FA Cluster 1	1	-	-	-	-	-
FA Cluster 2	0	1	-	-	-	-
AD Cluster 1	0.001	0.22	1	-	-	-
MD Cluster 1	0.060	0.37	0.76	1	-	-
RD Cluster 1	0	0	0	0	1	-
RD Cluster 2	0.072	0.42	0.63	0.87	0	1

Our analysis of the mean DTI metrics of the significant clusters revealed a linear decrease of FA and a linear increase of AD, MD and RD, from the first to last timepoint (Fig. 2). All slopes were significantly different from zero, with the exception of the first cluster of RD. Table 3 presents the percentages of change between timepoints, the linear regression slopes and the significance of each slope for the different DTI metrics of these significant clusters. We found a significant interaction in the relationship of DTI metric to time for the different clusters ($F(5,600) = 6.35, p < 0.001$), which suggests that there are differences in the slopes. Post-hoc tests with Bonferroni correction revealed that slopes of both FA clusters were significantly different from slopes of the other metrics (AD, RD and MD) (Supplementary Table 2). We can see that slopes of FA clusters are three orders of magnitude higher in comparison to the other metrics, but in terms of percent of change between timepoints, the values are similar for all metrics.

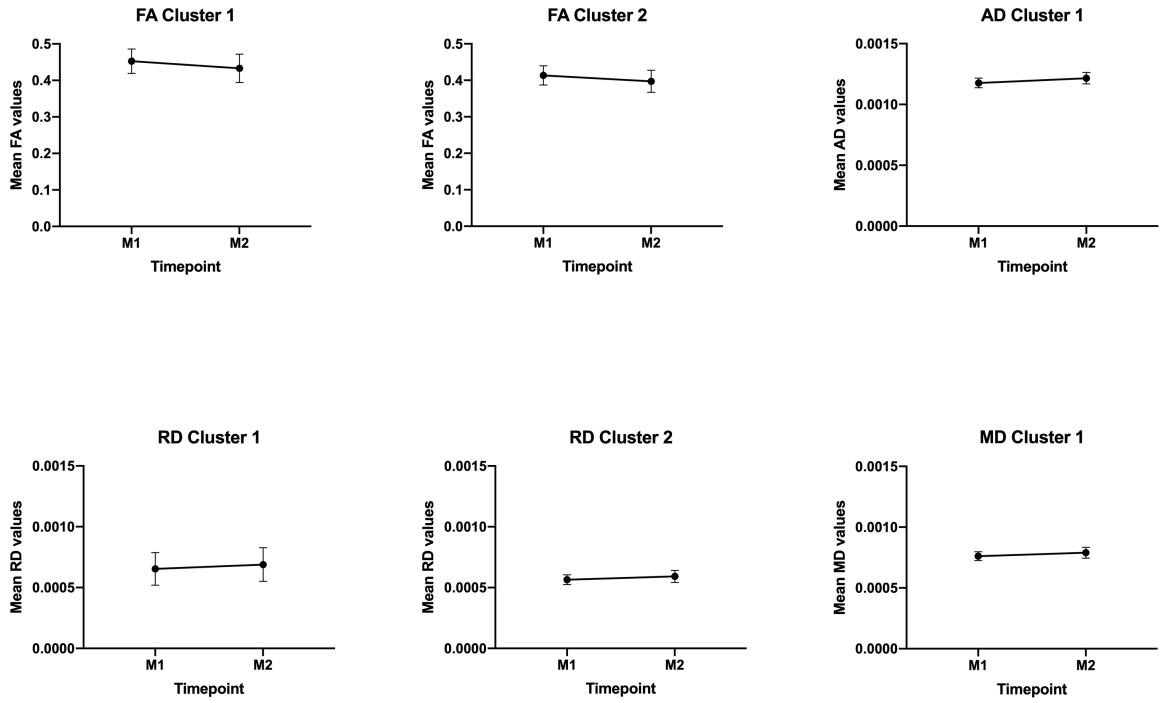

Figure 2. Trajectories of DTI metrics (FA, AD, RD and MD) of each cluster with significant differences between timepoints. The x-axis represents time of assessment and y-axis, the average values of each metric. Error bars represent standard deviation. FA clusters show a decrease along time, while AD, RD and MD clusters exhibit an increase. Overall, these results suggest that aging induces a deterioration of white matter integrity.

Table 3. Percentage of longitudinal changes in DTI metrics, linear regression slopes and significance of slopes of each significant cluster.

Metric	M2 – M1 (%)	Slope	Test Statistic
FA Cluster 1	-4.35	-0.020	F(1,100)=7.62, p=0.007**
FA Cluster 2	-3.94	-0.016	F(1,100)=8.42, p=0.005**
AD Cluster 1	3.30	0.00004	F(1,100)=20.51, p<0.0001***
RD Cluster 1	5.45	0.00004	F(1,100)=1.74, p=0.19
RD Cluster 2	4.78	0.00003	F(1,100)=9.09, p=0.003**
MD Cluster 1	3.69	0.00003	F(1,100)=11.96, p=0.0008***

Abbreviations: FA, fractional anisotropy; AD, axial diffusivity; MD, mean diffusivity; RD, radial diffusivity; M1, timepoint 1; M2, timepoint 2.
Significance codes: * $p < 0.05$, ** $p < 0.01$, *** $p < 0.001$

4.3. Associations with cognition

Significant correlations were found for the different DTI metrics and some of the neurocognitive variables. Specifically, LTS parameter was significantly associated with both FA clusters (FA Cluster 1 – r = 0.33, p = 0.047; FA Cluster 2 - r = 0.39, p = 0.020), AD cluster (r = -0.42, p = 0.010), RD cluster 2 (r = - 0.46, p = 0.005) and MD cluster (r = -0.46, p = 0.005) (Fig. 3). The other parameters of SRT (CLTR and DR) did not display any significant correlation with DTI metrics. Regarding Stroop test, SC was significantly correlated with both FA clusters (FA Cluster 1 – r = 0.51, p = 0.001; FA Cluster 2 – r = 0.45, p = 0.005), AD cluster (r = -0.54, p = 0.001), RD cluster 2 (r = - 52, p = 0.001) and MD cluster (r = -54, p = 0.001), while SWC had significant correlations with FA cluster 1 (r = 0.35, p = 0.04) and the AD cluster (r=-0.35, p = 0.04) (Fig. 4). Finally, MMSE was significantly associated with FA cluster 2 (r = 0.35, p = 0.04) and RD cluster 1 (r = -0.40, p = 0.01) (Fig. 5). Table 4 summarizes results of all correlations performed. Interestingly, the cognitive variables with significant associations have the higher rates of decrease along time, with the exception of CLTR that has the third highest rate of decrease but no significant correlation with any DTI metric (Table 5).

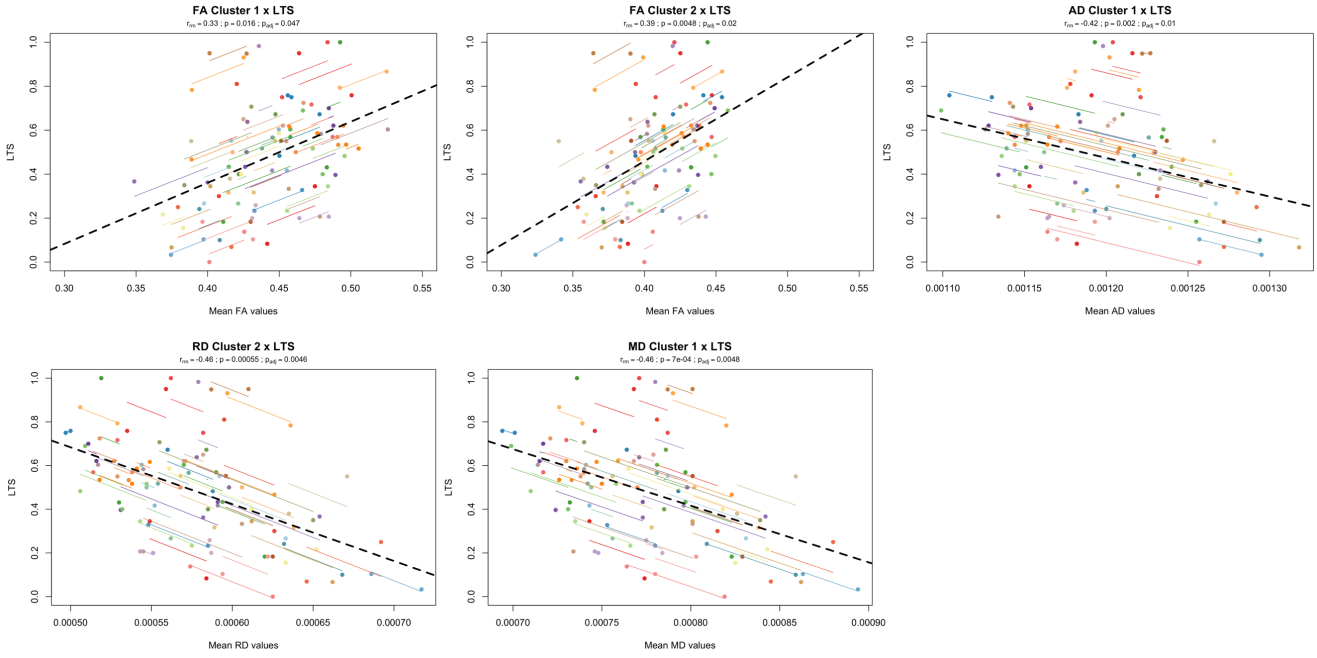

Figure 3. Significant repeated measures correlations between long-term storage (LTS) test score and DTI metrics (FA, AD, RD and MD) of clusters with significant changes between timepoints. The x-axis represents average values of each DTI metric and y-axis, the average values of LTS. Observations from the same individual are represented with the same color, with corresponding lines showing the repeated

measures correlation fit for each subject. Dashed black line represents the overall regression line. All clusters, with the exception of RD cluster 1, were significantly associated with LTS. For FA clusters, we found a positive correlation, meaning that higher FA values are associated with higher LTS scores. For AD, RD and MD clusters, a negative correlation was found, showing that lower AD, RD or MD values are associated with higher LTS scores. Overall, these results suggest that higher WM integrity is associated with higher cognitive performance in the memory domain.

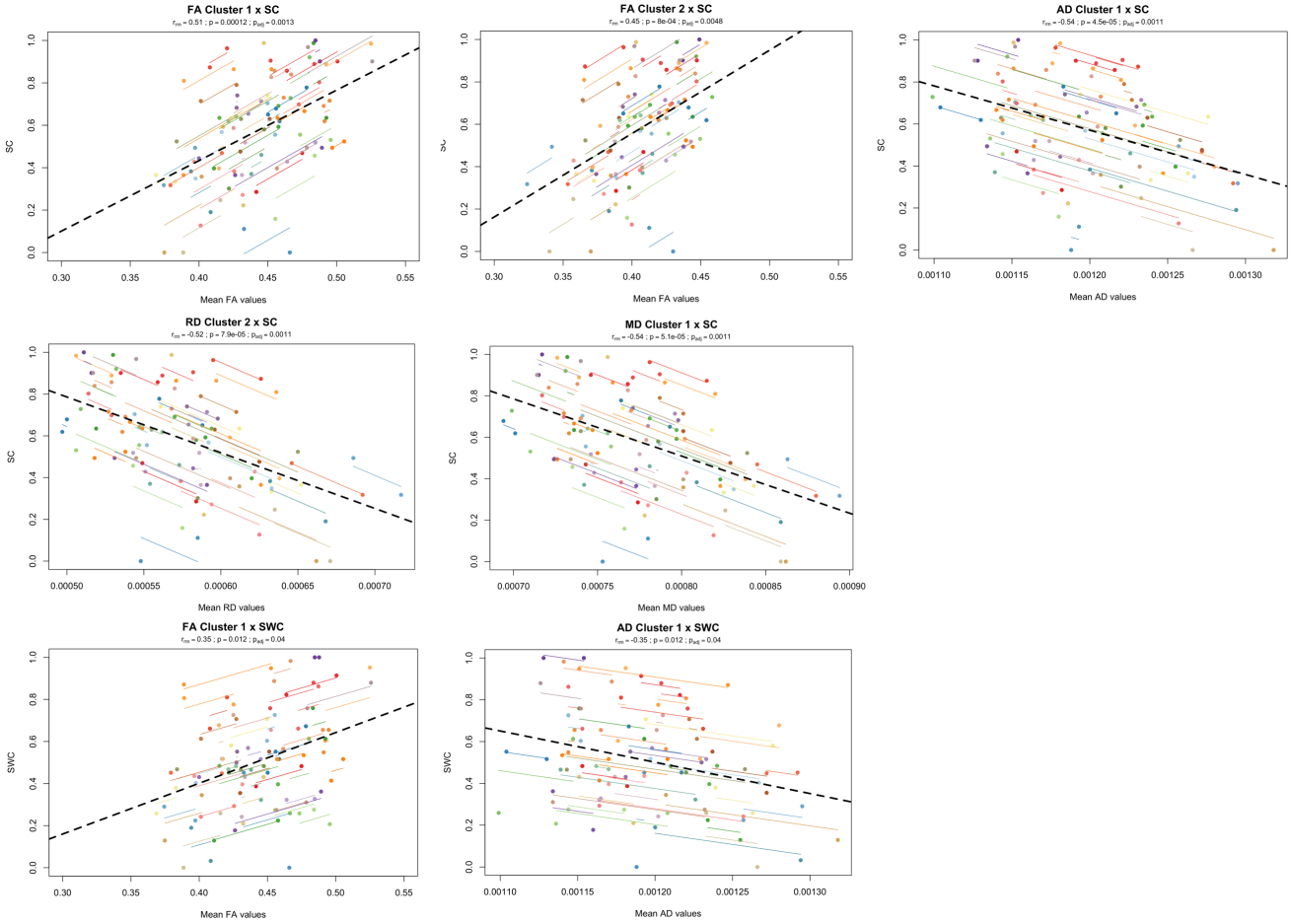

Figure 4. Significant repeated measures correlations between Stroop test variables (Stroop colors – SC, Stroop words/colors – SWC) and DTI metrics (FA, AD, RD and MD) of clusters with significant changes between timepoints. The x-axis represents average values of each DTI metric and y-axis, the average values of SC/SWC. Observations from the same individual are represented with the same color, with corresponding lines showing the repeated measures correlation fit for each subject. Dashed black line represents the overall regression line. All clusters, with the exception of RD cluster 1, were significantly associated with SC. For FA clusters, we found a positive correlation, meaning that higher FA values are associated with higher LTS scores. For AD, RD and MD clusters, a negative correlation was found, showing

that lower AD, RD or MD values are associated with higher SC scores. Regarding SWC, FA cluster 1 was positively correlated and AD was negatively correlated. Overall, these results suggest that higher WM integrity is associated with higher cognitive performance in the executive function domain.

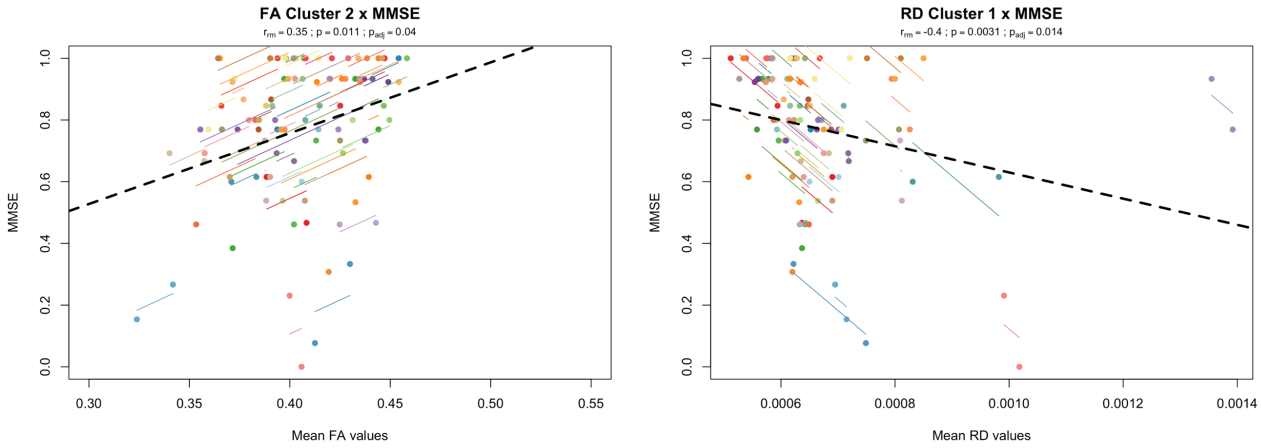

Figure 5. Significant repeated measures correlations between Mini-Mental State Examination (MMSE) and DTI metrics (FA and RD) of clusters with significant changes between timepoints. The x-axis represents average values of each DTI metric and y-axis, the average values of MMSE. Observations from the same individual are represented with the same color, with corresponding lines showing the repeated measures correlation fit for each subject. Dashed black line represents the overall regression line. Only FA cluster 2 and RD cluster 1 were significantly associated with MMSE. FA exhibited a positive correlation, meaning that higher FA values are associated with higher MMSE scores. RD was negatively correlated with MMSE, showing that lower RD values are associated with higher MMSE scores. Overall, these results suggest that higher WM integrity is associated with higher general cognition.

Table 4. Correlations between DTI metrics and scores of cognitive tests at all timepoints (results FDR corrected at p<0.05).

	FA Cluster 1	FA Cluster 2	AD Cluster 1	RD Cluster 1	RD Cluster 2	MD Cluster 1
LTS	**r=0.33* (p=0.047)**	**r=0.39* (p=0.020)**	**r=-0.42* (p=0.010)**	r=-0.31 (p=0.069)	**r=-0.46** (p=0.005)**	**r=-0.46** (p=0.005)**
CLTR	r=0.17 (p=0.32)	r=0.19 (p=0.28)	r=-0.25 (p=0.13)	r=-0.13 (p=0.44)	r=-0.25 (p=0.13)	r=-0.25 (p=0.13)
DR	r=0.079 (p=0.66)	r=0.14 (p=0.40)	r=-0.072 (p=0.68)	r=-0.16 (p=0.35)	r=-0.13 (p=0.44)	r=-0.10 (p=0.55)
SW	r=0.15 (p=0.37)	r=0.017 (p=0.91)	r=0.057 (p=0.72)	r=-0.16 (p=0.36)	r=0.053 (p=0.73)	r=0.063 (p=0.71)
SC	**r=0.51** (p=0.001)**	**r=0.45** (p=0.005)**	**r=-0.54** (p=0.001)**	r=-0.33 (p=0.054)	**r=-0.52** (p=0.001)**	**r=-0.54** (p=0.001)**

SWC	**r=0.35* (p=0.040)**	r=0.28 (p=0.092)	**r=-0.35* (p=0.040)**	r=-0.21 (p=0.23)	r=-0.30 (p=0.083)	r=-0.31 (p=0.066)
MMSE	r=0.26 (p=0.12)	**r=0.35* (p=0.040)**	r=-0.20 (p=0.26)	**r=-0.40* (p=0.014)**	r=-0.28 (p=0.092)	r=-0.25 (p=0.13)

Abbreviations: FA, fractional anisotropy; AD, axial diffusivity; MD, mean diffusivity; RD, radial diffusivity; LTS, long-term storage; CLTR, consistent long-term retrieval; DR, delayed-recall; SW, Stroop words; SC, Stroop colors; SWC, Stroop words/colors; MMSE, Mini-Mental State Examination.
Significance codes: * $p < 0.05$, ** $p < 0.01$, *** $p < 0.001$

Table 5. Percentage of longitudinal changes in neurocognitive test scores.

Metric	M2 – M1 (%)
LTS	-17.8
CLTR	-14.6
DR	-9.48
SW	-0.27
SC	-16.5
SWC	-7.40
MMSE	-11.9

Abbreviations: LTS, long-term storage; CLTR, consistent long-term retrieval; DR, delayed-recall; SW, Stroop words; SC, Stroop colors; SWC, Stroop words/colors; MMSE, Mini-Mental State Examination; M1, timepoint 1; M2, timepoint 2.

5. Discussion

Herein we explore the effect of age on WM microstructure, by combining diffusion magnetic resonance imaging with neurocognitive testing. Our results reveal that aging is characterized by a degradation in white matter integrity and cognitive decline. Furthermore, we found significant associations between diffusion measures and cognitive dimensions of memory, executive function and general cognition. In sum, these findings are in line with the "disconnection" hypothesis of the aging brain, by demonstrating a relationship between white matter integrity deterioration and cognitive decline.

Our analysis of the DTI metrics revealed decreased FA and increased diffusivity (AD, MD and RD) with aging in brain areas where these parameters are statistically different across the 52.8 months of observation, which is consistent with previous longitudinal studies (Sexton et al., 2014; Vinke et al., 2018). While for diffusivity measures, the results were relatively widespread, comprising several WM tracts in both hemispheres, for FA the results were localized. Decreased FA with aging was found in

corpus callosum, left anterior limb of internal capsule, left external capsule, left/right corona radiata and left superior longitudinal fasciculus, which have already been reported in previous longitudinal studies (Hakun et al., 2015; Sexton et al., 2014). This pattern of left-dominant deterioration was already reported in studies with cognitively impaired patients. Specifically, a rightward lateralization of functional connectivity in patients with mild cognitive impairment (MCI) and Alzheimer's Disease (AD) has been reported (Liu et al., 2018), which is possibly due to a compensation mechanism for the loss of cognitive function or because of disease-induced damage in the left hemisphere. Furthermore, Low and colleagues (Low et al., 2019) showed the existence of a higher degree of asymmetry of white matter hyperintensities towards the left hemisphere in AD patients, when compared to MCI and healthy controls, which is associated with poorer global cognition, memory, executive function and language.

Correlation analysis between cognitive scores and age-related WM changes showed significant associations between all diffusion measures (FA, AD, RD and MD), and cognitive variables of memory (LTS) and executive function (SWC). These results may suggest that longitudinal changes in cognition are associated with changes in WM integrity, thus supporting the "disconnection hypothesis". This association has already been extensively reported in the literature, with several studies showing the existence of a clear association between WM integrity deterioration and poorer performance in executive function tasks (Bendlin et al., 2010; Brickman et al., 2012; Cremers et al., 2016; Hedden et al., 2016; Kennedy and Raz, 2009; Sasson et al., 2012; Ystad et al., 2011), with results spanning over different regions in the brain. Particularly, Hedden and colleagues (Hedden et al., 2016) found a mediation effect of WM integrity, along with cortical thickness and glucose metabolism, in age-related differences in executive function. Noticeably, the majority of the studies report larger effect sizes for associations between WM integrity and cognitive dimensions, such as executive function and processing speed, than for memory (Bennett and Madden, 2014; Madden et al., 2012). Still, there is evidence of a relation between WM integrity and memory (Bendlin et al., 2010; Carlesimo et al., 2010; Davis et al., 2009; Gazes et al., 2016; Kennedy and Raz, 2009; Sasson et al., 2012). In our study, the effect sizes for memory and executive function are very similar. We also revealed significant associations between diffusion measures and the color naming parameter (SC) of the Stroop test. Although only the interference parameter (SWC) measures executive function, the other two parameters (SW and SC) are considered measures of processing speed (Jensen, 1965). Previous studies found significant age effects in the SC parameter, which can be the result of a general slowing induced by age (Uttl and Graf, 1997). Uttl and colleagues also found that the age effects on the interference condition was directly related to the performance on the other two conditions. Thus, the longitudinal changes that we observe in the

interference component might be attributed to longitudinal changes in the performance of the color naming task. Regarding general cognition, evaluated through MMSE, significant correlations were found for FA and RD. This result is in accordance with previous literature showing that age effects on WM integrity are often stronger for RD than AD (Davis et al., 2009; Madden et al., 2009; Zhang et al., 2010). Davis and colleagues (Davis et al., 2009), in addition to this, also found that the impact of age-related WM changes in cognitive performance was more prominent for RD than for AD. Additionally, the cognitive variables revealing significant associations with WM integrity presented accentuated declines in subsequent observations, which indicates that steeper declines in cognition are associated with steeper declines in WM integrity along time. Once again, this reinforces the theory that deterioration of WM causes a disruption in the communication between cortical regions, which, in turn, leads to cognitive decline.

One of the limitations of this study was the use of a whole-brain approach to investigate alterations in WM integrity. Although this allowed us to explore the global effect of aging in WM microstructure and its relationship with cognition, it was not possible to examine the contribution of each individual WM tract. Future work may include the analysis of age effects in the integrity of each WM tract and its association with cognitive function. Another limitation is the use of a 1.5T MRI scanner which has lower signal to noise ratio (SNR) when compared to 3T MRI scanners (Lee and Shannon, 2007). Furthermore, the parameters used to acquire the DWI sequence, namely 30 gradients directions and only a single b=0 s mm^{-2} volume, also impact on the resolution diffusion data.

In summary, our findings confirm the existing evidence of a degradation of the WM with aging. We also found significant associations between DTI metrics and the different cognitive dimensions evaluated (memory, executive function and general cognition). This result indicates a relationship between age-related changes in WM microstructural properties and cognitive function, which brings further support to the "disconnection hypothesis". Furthermore, this association between the effects of aging on WM integrity and cognition is only possible with the use of a longitudinal design (Damoiseaux, 2017), such as what we present here. Finally, our findings open new perspectives for future studies to identify the main drivers in WM integrity levels at different levels of cognitive ability. Hence, this could help in the development of new in-vivo brain biomarkers of inter-individual variability in cognitive trajectories.

6. References

Andrews-Hanna, J.R., Snyder, A.Z., Vincent, J.L., Lustig, C., Head, D., Raichle, M.E., Buckner, R.L., 2007. Disruption of Large-Scale Brain Systems in Advanced Aging. Neuron 56, 924–935. https://doi.org/10.1016/j.neuron.2007.10.038

Bakdash, J.Z., Marusich, L.R., 2017. Repeated Measures Correlation. Frontiers in Psychology 8. https://doi.org/10.3389/fpsyg.2017.00456

Bartzokis, G., 2004. Age-related myelin breakdown: a developmental model of cognitive decline and Alzheimer's disease. Neurobiology of Aging 25, 5–18. https://doi.org/10.1016/j.neurobiolaging.2003.03.001

Basser, P.J., Mattiello, J., LeBihan, D., 1994. MR diffusion tensor spectroscopy and imaging. Biophysical Journal 66, 259–267. https://doi.org/10.1016/S0006-3495(94)80775-1

Bendlin, B.B., Fitzgerald, M.E., Ries, M.L., Xu, G., Kastman, E.K., Thiel, B.W., Rowley, H.A., Lazar, M., Alexander, A.L., Johnson, S.C., 2010. White Matter in Aging and Cognition: A Cross-Sectional Study of Microstructure in Adults Aged Eighteen to Eighty-Three. Developmental Neuropsychology 35, 257–277. https://doi.org/10.1080/87565641003696775

Bennett, I.J., Madden, D.J., 2014. Disconnected aging: Cerebral white matter integrity and age-related differences in cognition. Neuroscience 276, 187–205. https://doi.org/10.1016/j.neuroscience.2013.11.026

Borghesani, P.R., Madhyastha, T.M., Aylward, E.H., Reiter, M.A., Swarny, B.R., Warner Schaie, K., Willis, S.L., 2013. The association between higher order abilities, processing speed, and age are variably mediated by white matter integrity during typical aging. Neuropsychologia 51, 1435–1444. https://doi.org/10.1016/j.neuropsychologia.2013.03.005

Brickman, A.M., Meier, I.B., Korgaonkar, M.S., Provenzano, F.A., Grieve, S.M., Siedlecki, K.L., Wasserman, B.T., Williams, L.M., Zimmerman, M.E., 2012. Testing the white matter retrogenesis hypothesis of cognitive aging. Neurobiology of Aging 33, 1699–1715. https://doi.org/10.1016/j.neurobiolaging.2011.06.001

Burgmans, S., Gronenschild, E.H.B.M., Fandakova, Y., Shing, Y.L., van Boxtel, M.P.J., Vuurman, E.F.P.M., Uylings, H.B.M., Jolles, J., Raz, N., 2011. Age differences in speed of processing are partially mediated by differences in axonal integrity. NeuroImage 55, 1287–1297. https://doi.org/10.1016/j.neuroimage.2011.01.002

Burzynska, A.Z., Preuschhof, C., Backman, L., Nyberg, L., Li, S.C., Lindenberger, U., Heekeren, H.R., 2010. Age-related differences in white matter microstructure: Region-specific patterns of diffusivity. NeuroImage 49, 2104–2112. https://doi.org/10.1016/j.neuroimage.2009.09.041

Busch, R.M., Chapin, J.S., 2008. Review of Normative Data For Common Screening Measures Used to Evaluate Cognitive Functioning in Elderly Individuals. The Clinical Neuropsychologist 22, 620–650. https://doi.org/10.1080/13854040701448793

Carlesimo, G.A., Cherubini, A., Caltagirone, C., Spalletta, G., 2010. Hippocampal mean diffusivity and memory in healthy elderly individuals: A cross-sectional study. Neurology 74, 194–200. https://doi.org/10.1212/WNL.0b013e3181cb3e39

Costa, P.S., Santos, N.C., Cunha, P., Palha, J.A., Sousa, N., 2013. The Use of Bayesian Latent Class Cluster Models to Classify Patterns of Cognitive Performance in Healthy Ageing. PLoS ONE 8. https://doi.org/10.1371/journal.pone.0071940

Cremers, L.G.M., de Groot, M., Hofman, A., Krestin, G.P., van der Lugt, A., Niessen, W.J., Vernooij, M.W., Ikram, M.A., 2016. Altered tract-specific white matter microstructure is related to poorer cognitive performance: The Rotterdam Study. Neurobiology of Aging 39, 108–117. https://doi.org/10.1016/j.neurobiolaging.2015.11.021

Damoiseaux, J.S., 2017. Effects of aging on functional and structural brain connectivity. NeuroImage 1–9. https://doi.org/10.1016/j.neuroimage.2017.01.077

Davis, S.W., Dennis, N.A., Buchler, N.G., White, L.E., Madden, D.J., Cabeza, R., 2009. Assessing the effects of age on long white matter tracts using diffusion tensor tractography. NeuroImage 46, 530–541. https://doi.org/10.1016/j.neuroimage.2009.01.068

de Groot, M., Ikram, M.A., Akoudad, S., Krestin, G.P., Hofman, A., van der Lugt, A., Niessen, W.J., Vernooij, M.W., 2015. Tract-specific white matter degeneration in aging: The Rotterdam Study. Alzheimer's & Dementia 11, 321–330. https://doi.org/10.1016/j.jalz.2014.06.011

de Lange, A.-M.G., Bråthen, A.C.S., Grydeland, H., Sexton, C., Johansen-Berg, H., Andersson, J.L.R., Rohani, D.A., Nyberg, L., Fjell, A.M., Walhovd, K.B., 2016. White matter integrity as a marker for cognitive plasticity in aging. Neurobiology of Aging 47, 74–82. https://doi.org/10.1016/j.neurobiolaging.2016.07.007

Engvig, A., Fjell, A.M., Westlye, L.T., Moberget, T., Sundseth, Ø., Larsen, V.A., Walhovd, K.B., 2012. Memory training impacts short-term changes in aging white matter: A Longitudinal Diffusion Tensor Imaging Study. Human Brain Mapping 33, 2390–2406. https://doi.org/10.1002/hbm.21370

Fjell, A.M., Sneve, M.H., Grydeland, H., Storsve, A.B., Walhovd, K.B., 2016. The Disconnected Brain and Executive Function Decline in Aging. Cerebral Cortex bhw082. https://doi.org/10.1093/cercor/bhw082

Gazes, Y., Bowman, F.D., Razlighi, Q.R., O'Shea, D., Stern, Y., Habeck, C., 2016. White matter tract covariance patterns predict age-declining cognitive abilities. NeuroImage 125, 53–60. https://doi.org/10.1016/j.neuroimage.2015.10.016

Grigoletto, F., Zappala, G., Anderson, D.W., Lebowitz, B.D., 1999. Norms for the Mini-Mental State Examination in a healthy population. Neurology 53, 315–315. https://doi.org/10.1212/WNL.53.2.315

Guerreiro, M., Silva, A.P., Botelho, M.A., Leitão, O., Castro-Caldas, A., Garcia, C., 1994. Adaptação à população portuguesa da tradução do Mini Mental State Examination (MMSE). Revista Portuguesa de Neurologia 1, 9–10.

Hakun, J.G., Zhu, Z., Brown, C.A., Johnson, N.F., Gold, B.T., 2015. Longitudinal alterations to brain function, structure, and cognitive performance in healthy older adults: A fMRI-DTI study. Neuropsychologia 71, 225–235. https://doi.org/10.1016/j.neuropsychologia.2015.04.008

Hedden, T., Schultz, A.P., Rieckmann, A., Mormino, E.C., Johnson, K.A., Sperling, R.A., Buckner, R.L., 2016. Multiple Brain Markers are Linked to Age-Related Variation in Cognition. Cerebral Cortex 26, 1388–1400. https://doi.org/10.1093/cercor/bhu238

Hua, K., Zhang, J., Wakana, S., Jiang, H., Li, X., Reich, D.S., Calabresi, P.A., Pekar, J.J., van Zijl, P.C.M., Mori, S., 2008. Tract probability maps in stereotaxic spaces: Analyses of white matter anatomy and tract-specific quantification. NeuroImage 39, 336–347. https://doi.org/10.1016/j.neuroimage.2007.07.053

Jensen, A.R., 1965. Scoring the Stroop test. Acta Psychologica 24, 398–408. https://doi.org/10.1016/0001-6918(65)90024-7

Johnson, M.A., Diaz, M.T., Madden, D.J., 2015. Global versus tract-specific components of cerebral white matter integrity: relation to adult age and perceptual-motor speed. Brain Structure and Function 220, 2705–2720. https://doi.org/10.1007/s00429-014-0822-9

Kennedy, K.M., Raz, N., 2009. Aging white matter and cognition: Differential effects of regional variations in diffusion properties on memory, executive functions, and speed. Neuropsychologia 47, 916–927. https://doi.org/10.1016/j.neuropsychologia.2009.01.001

Lebel, C., Gee, M., Camicioli, R., Wieler, M., Martin, W., Beaulieu, C., 2012. Diffusion tensor imaging of white matter tract evolution over the lifespan. NeuroImage 60, 340–352. https://doi.org/10.1016/j.neuroimage.2011.11.094

Lee, J.W.K., Shannon, S.P., 2007. 3 Tesla Magnetic Resonance Imaging (MRI)—Is it Ready for Prime Time Clinical Applications? Canadian Journal of Medical Radiation Technology 38, 37–50. https://doi.org/10.1016/S0820-5930(09)60258-9

Li, P., Tsapanou, A., Qolamreza, R.R., Gazes, Y., 2018. White matter integrity mediates decline in age-related inhibitory control. Behavioural Brain Research 339, 249–254. https://doi.org/10.1016/j.bbr.2017.11.005

Liu, H., Zhang, L., Xi, Q., Zhao, X., Wang, F., Wang, X., Men, W., Lin, Q., 2018. Changes in Brain Lateralization in Patients with Mild Cognitive Impairment and Alzheimer's Disease: A Resting-State Functional Magnetic Resonance Study from Alzheimer's Disease Neuroimaging Initiative. Frontiers in Neurology 9. https://doi.org/10.3389/fneur.2018.00003

Lockhart, S.N., DeCarli, C., 2014. Structural Imaging Measures of Brain Aging. Neuropsychology Review 24, 271–289. https://doi.org/10.1007/s11065-014-9268-3

Low, A., Ng, K.P., Chander, R.J., Wong, B., Kandiah, N., 2019. Association of Asymmetrical White Matter Hyperintensities and Apolipoprotein E4 on Cognitive Impairment. Journal of Alzheimer's Disease 70, 953–964. https://doi.org/10.3233/JAD-190159

Madden, D.J., Bennett, I.J., Burzynska, A., Potter, G.G., kuei Chen, N., Song, A.W., 2012. Diffusion tensor imaging of cerebral white matter integrity in cognitive aging. Biochimica et Biophysica Acta - Molecular Basis of Disease 1822, 386–400. https://doi.org/10.1016/j.bbadis.2011.08.003

Madden, D.J., Parks, E.L., Tallman, C.W., Boylan, M.A., Hoagey, D.A., Cocjin, S.B., Packard, L.E., Johnson, M.A., Chou, Y., Potter, G.G., Chen, N., Siciliano, R.E., Monge, Z.A., Honig, J.A., Diaz, M.T., 2017. Sources of disconnection in neurocognitive aging: cerebral white-matter integrity, resting-state functional connectivity, and white-matter hyperintensity volume. Neurobiology of Aging 54, 199–213. https://doi.org/10.1016/j.neurobiolaging.2017.01.027

Madden, D.J., Spaniol, J., Costello, M.C., Bucur, B., White, L.E., Cabeza, R., Davis, S.W., Dennis, N.A., Provenzale, J.M., Huettel, S.A., 2009. Cerebral White Matter Integrity Mediates Adult Age Differences in Cognitive Performance. Journal of Cognitive Neuroscience 21, 289–302. https://doi.org/10.1162/jocn.2009.21047

Marques, P.C.G., Soares, J.M.M., Magalhães, R.J. da S., Santos, N.C., Sousa, N.J.C., 2015. Macro- and micro-structural white matter differences correlate with cognitive performance in healthy aging. Brain Imaging and Behavior 10, 168–181. https://doi.org/10.1007/s11682-015-9378-4

Meunier, D., Stamatakis, E.A., Tyler, L.K., 2014. Age-related functional reorganization, structural changes, and preserved cognition. Neurobiology of Aging 35, 42–54. https://doi.org/10.1016/j.neurobiolaging.2013.07.003

Moeller, J., 2015. A word on standardization in longitudinal studies: don't. Frontiers in Psychology 6. https://doi.org/10.3389/fpsyg.2015.01389

O'Sullivan, M., Jones, D.K., Summers, P.E., Morris, R.G., Williams, S.C.R., Markus, H.S., 2001. Evidence for cortical "disconnection" as a mechanism of age-related cognitive decline. Neurology 57, 632–638. https://doi.org/10.1212/WNL.57.4.632

Pierpaoli, C., Basser, P.J., 1996. Toward a quantitative assessment of diffusion anisotropy. Magnetic Resonance in Medicine 36, 893–906. https://doi.org/10.1002/mrm.1910360612

Salat, D.H., Tuch, D.S., Greve, D.N., van der Kouwe, A.J.W., Hevelone, N.D., Zaleta, A.K., Rosen, B.R., Fischl, B., Corkin, S., Rosas, H.D., Dale, A.M., 2005. Age-related alterations in white matter microstructure measured by diffusion tensor imaging. Neurobiology of Aging 26, 1215–1227. https://doi.org/10.1016/j.neurobiolaging.2004.09.017

Samanez-Larkin, G.R., Levens, S.M., Perry, L.M., Dougherty, R.F., Knutson, B., 2012. Frontostriatal White Matter Integrity Mediates Adult Age Differences in Probabilistic Reward Learning. Journal of Neuroscience 32, 5333–5337. https://doi.org/10.1523/JNEUROSCI.5756-11.2012

Santos, N.C., Costa, P.S., Cunha, P., Cotter, J., Sampaio, A., Zihl, J., Almeida, O.F.X., Cerqueira, J.J., Palha, J.A., Sousa, N., 2013. Mood is a key determinant of cognitive performance in community-dwelling older adults: A cross-sectional analysis. Age 35, 1983–1993. https://doi.org/10.1007/s11357-012-9482-y

Santos, N.C., Costa, P.S., Cunha, P., Portugal-Nunes, C., Amorim, L., Cotter, J., Cerqueira, J.J., Palha, J.A., Sousa, N., 2014. Clinical, physical and lifestyle variables and relationship with cognition and mood in aging: A cross-sectional analysis of distinct educational groups. Frontiers in Aging Neuroscience 6, 1–15. https://doi.org/10.3389/fnagi.2014.00021

Sasson, E., Doniger, G.M., Pasternak, O., Tarrasch, R., Assaf, Y., 2012. Structural correlates of cognitive domains in normal aging with diffusion tensor imaging. Brain Structure and Function 217, 503–515. https://doi.org/10.1007/s00429-011-0344-7

Sexton, C.E., Walhovd, K.B., Storsve, A.B., Tamnes, C.K., Westlye, L.T., Johansen-Berg, H., Fjell, A.M., 2014. Accelerated Changes in White Matter Microstructure during Aging: A Longitudinal Diffusion Tensor Imaging Study. Journal of Neuroscience 34, 15425–15436. https://doi.org/10.1523/JNEUROSCI.0203-14.2014

Smith, S.M., Jenkinson, M., Johansen-Berg, H., Rueckert, D., Nichols, T.E., Mackay, C.E., Watkins, K.E., Ciccarelli, O., Cader, M.Z., Matthews, P.M., Behrens, T.E.J., 2006. Tract-based spatial statistics: Voxelwise analysis of multi-subject diffusion data. NeuroImage 31, 1487–1505. https://doi.org/10.1016/j.neuroimage.2006.02.024

Soares, J.M., Marques, P., Magalhães, R., Santos, N.C., Sousa, N., 2014. Brain structure across the lifespan: the influence of stress and mood. Frontiers in Aging Neuroscience 6. https://doi.org/10.3389/fnagi.2014.00330

Sullivan, E.V., Zahr, N.M., Rohlfing, T., Pfefferbaum, A., 2010. Fiber tracking functionally distinct components of the internal capsule. Neuropsychologia 48, 4155–4163. https://doi.org/10.1016/j.neuropsychologia.2010.10.023

Uttl, B., Graf, P., 1997. Color-Word Stroop test performance across the adult life span. Journal of Clinical and Experimental Neuropsychology 19, 405–420. https://doi.org/10.1080/01688639708403869

Vinke, E.J., de Groot, M., Venkatraghavan, V., Klein, S., Niessen, W.J., Ikram, M.A., Vernooij, M.W., 2018. Trajectories of imaging markers in brain aging: the Rotterdam Study. Neurobiology of Aging 71, 32–40. https://doi.org/10.1016/j.neurobiolaging.2018.07.001

Westlye, L.T., Walhovd, K.B., Dale, A.M., Bjornerud, A., Due-Tonnessen, P., Engvig, A., Grydeland, H., Tamnes, C.K., Ostby, Y., Fjell, A.M., 2010. Life-Span Changes of the Human Brain White Matter: Diffusion Tensor Imaging (DTI) and Volumetry. Cerebral Cortex 20, 2055–2068. https://doi.org/10.1093/cercor/bhp280

Ystad, M., Hodneland, E., Adolfsdottir, S., Haász, J., Lundervold, A.J., Eichele, T., Lundervold, A., 2011. Cortico-striatal connectivity and cognition in normal aging: A combined DTI and resting state fMRI study. NeuroImage 55, 24–31. https://doi.org/10.1016/j.neuroimage.2010.11.016

Zhang, Y., Du, A.-T., Hayasaka, S., Jahng, G., Hlavin, J., Zhan, W., Weiner, Michael.W., Schuff, N., 2010. Patterns of age-related water diffusion changes in human brain by concordance and discordance analysis. Neurobiology of Aging 31, 1991–2001. https://doi.org/10.1016/j.neurobiolaging.2008.10.009

7. Supplementary Material

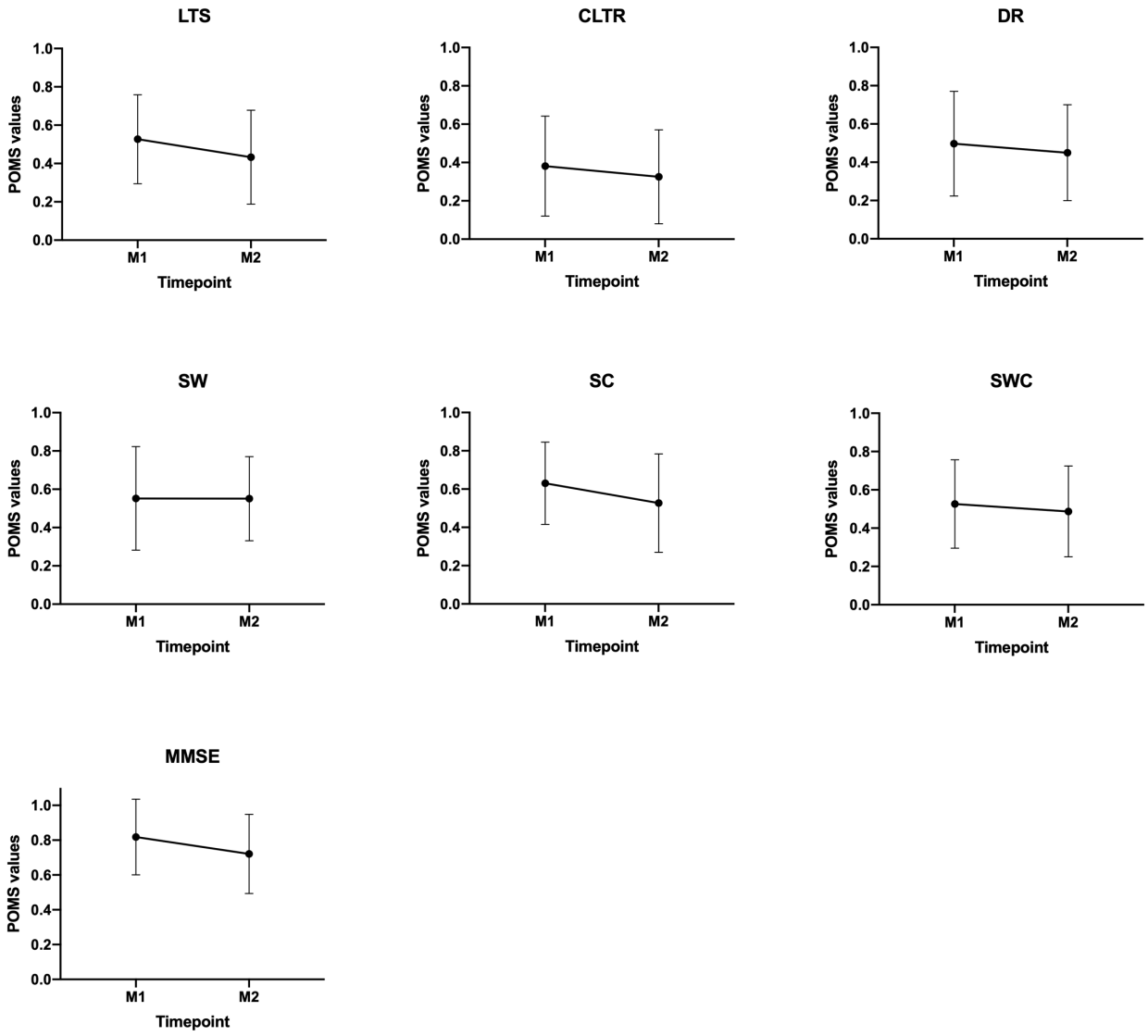

Figure S1. Trajectories of cognitive test scores for memory (LTS, CLTR, DR), executive function (SW, SC, SWC) and general cognition (MMSE) along time. The x-axis represents time of assessment and y-axis, the average values of each test. Error bars represent standard deviation. All cognitive test scores exhibit a decrease between timepoints, with the exception of SW that remains practically constant.

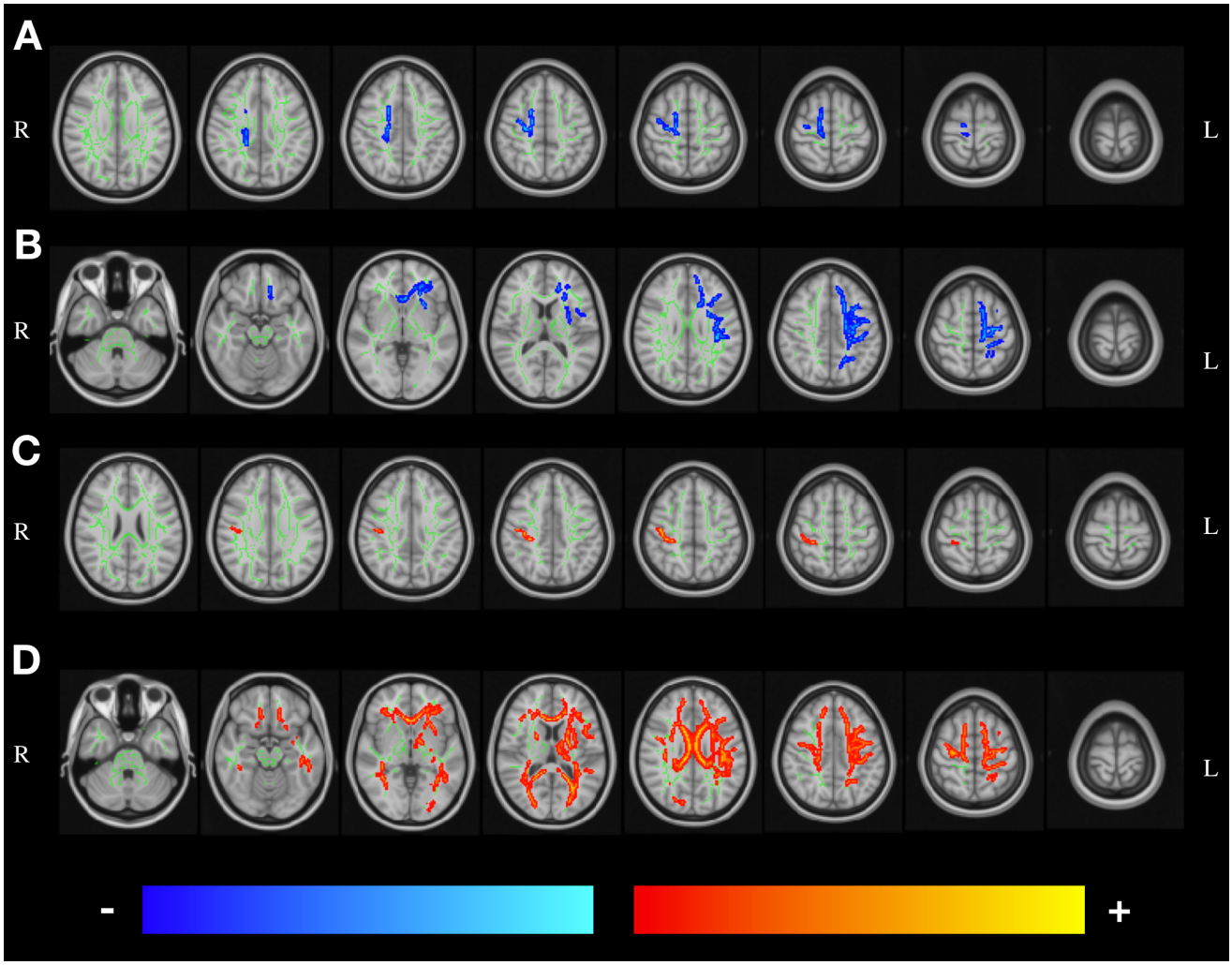

Figure S2. Statistically significant changes along time in a) FA Cluster 1, b) FA Cluster 2, c) RD Cluster 1 and d) RD Cluster 2. Blue/light-blue gradient indicates decreases along time. Red/yellow gradient indicate increases along time. All results were considered significant at $p<0.05$ (FWE corrected for multiple comparisons).

Table S1. Clusters presenting significant results between timepoints.

Metric	White Matter Tract	Cluster Size (Number of Voxels)	Peak Coordinates in mm (x, y, z)	Peak Value (1-p)
FA	Right Posterior corona radiata	1335	19, -29, 35	0.984
	Left Superior corona radiata	9813	-18, -23, 36	0.999
AD	Unclassified	28881	-12, 23, -14	1
RD	Unclassified	533	43, -21, 51	0.973
	Unclassified	35144	-41, -25, -20	1
MD	Unclassified	35502	-41, -25, -20	1

Abbreviations: FA, fractional anisotropy; AD, axial diffusivity; MD, mean diffusivity; RD, radial diffusivity.

Table S2. Pairwise comparisons between slopes of the different significant clusters of each DTI metric (results Bonferroni corrected at p<0.05).

Contrast	Test Statistic
FA Cluster 1 – FA Cluster 2	t(600) = 0.65, p=1
FA Cluster 1 – AD Cluster 1	**t(600) = 3.75, p=0.003****
FA Cluster 1 – RD Cluster 1	**t(600) = 3.75, p=0.003****
FA Cluster 1 – RD Cluster 2	**t(600) = 3.75, p=0.003****
FA Cluster 1 – MD Cluster 1	**t(600) = 3.75, p=0.003****
FA Cluster 2 – AD Cluster 1	**t(600) = 3.10, p=0.03***
FA Cluster 2 – RD Cluster 1	**t(600) = 3.10, p=0.03***
FA Cluster 2 – RD Cluster 2	**t(600) = 3.10, p=0.03***
FA Cluster 2 – MD Cluster 1	**t(600) = 3.10, p=0.03***
AD Cluster 1 – RD Cluster 1	t(600) = 0.001, p=1
AD Cluster 1 – RD Cluster 2	t(600) = 0.002, p=1
AD Cluster 1 – MD Cluster 1	t(600) = 0.002, p=1
RD Cluster 1 – RD Cluster 2	t(600) = 0.002, p=1
RD Cluster 1 – MD Cluster 1	t(600) = 0.001, p=1
RD Cluster 2 – MD Cluster 1	t(600) = -0.0002 , p=1

Abbreviations: FA, fractional anisotropy; AD, axial diffusivity; MD, mean diffusivity; RD, radial diffusivity.
Significance codes: * p < 0.05, ** p < 0.01, *** p < 0.001

CHAPTHER III

Ana Coelho, Henrique M. Fernandes, Ricardo Magalhães, Pedro Silva Moreira, Paulo Marques, José M. Soares, Liliana Amorim, Carlos Portugal-Nunes, Teresa Castanho, Nadine Correia Santos, Nuno Sousa (2021)

Reorganization of brain structural networks in aging: a longitudinal study

Journal of Neuroscience Research, doi: 10.1002/jnr.24795

Reorganization of brain structural networks in aging: a longitudinal study

Ana Coelho[1,2,3], Henrique M. Fernandes[4,5], Ricardo Magalhães[1,2,3], Pedro Silva Moreira[1,2,3], Paulo Marques[1,2,3], José M. Soares[1,2,3], Liliana Amorim[1,2,3], Carlos Portugal-Nunes[1,2,3], Teresa Castanho[1,2,3], Nadine Correia Santos[1,2,3], Nuno Sousa[1,2,3]

[1]Life and Health Sciences Research Institute (ICVS), School of Medicine, University of Minho, Braga, Portugal; [2]ICVS/3B's, PT Government Associate Laboratory, Braga/Guimarães, Portugal; [3]Clinical Academic Center – Braga, Braga, Portugal; [4]Center for Music in the Brain (MIB), Aarhus University, Aarhus, Denmark; [5]Department of Psychiatry, University of Oxford, Oxford, UK

1. Abstract

Normal aging is characterized by structural and functional changes in the brain contributing to cognitive decline. Structural connectivity describes the anatomical backbone linking distinct functional subunits of the brain and disruption of this communication is thought to be one of the potential contributors for the age-related deterioration observed in cognition. Several studies already explored brain network's reorganization during aging, but most focused on average connectivity of the whole-brain or in specific networks, such as the resting state networks. Here, we aimed to characterize longitudinal changes of white matter structural brain networks, through the identification of sub-networks with significantly altered connectivity along time. Then, we tested associations between longitudinal changes in network connectivity and cognition. We also assessed longitudinal changes in topological properties of the networks. For this, older adults were evaluated at two timepoints, with a mean interval time of 52.8 months (SD = 7.24). White matter structural networks were derived from diffusion magnetic resonance imaging, and cognitive status from neurocognitive testing. Our results show age-related changes in brain structural connectivity, characterized by both decreases and increases in connectivity weight. Interestingly, decreases occur in intra-hemispheric connections formed mainly by association fibers, while increases occur mostly in inter-hemispheric connections and involve association, commissural and projection fibers, supporting the last-in-first-out hypothesis. Regarding topology, two hubs were lost, alongside with a decrease in connector-hub inter-modular connectivity, reflecting reduced integration. Simultaneously, there was an increase in the number of provincial hubs, suggesting increased

segregation. Overall, these results confirm that aging triggers a reorganization of the brain structural network.

Keywords: diffusion MRI, white matter, aging, cognitive performance, network

2. Statement of Significance

Normal aging is characterized by structural and functional alterations in the brain contributing to cognitive decline, with structural connectivity being the anatomical backbone for the communication between different functional subunits. Previous studies have suggested that the disruption of this communication contributes to the age-related deterioration observed in cognition, but most have focused on average connectivity of the whole-brain or in specific networks, such as the resting-state networks. Here, using a longitudinal design, we show that aging induces a reorganization of the brain structural network, that is characterized by connectivity decreases in intra-hemispheric connections and increases in inter-hemispheric connections, alongside with a reduction in integration and an increase in segregation. Structural connectivity decreases were mainly due to loss of association fibers, an observation which is consistent with the last-in-first-out hypothesis.

3. Introduction

Human brain undergoes structural and functional changes during aging, even in the absence of disease (Damoiseaux, 2017; Grady, 2012; Hakun et al., 2015; Lockhart and DeCarli, 2014; Soares et al., 2014). According to the "disconnected brain" theory, originally proposed by Geschwind in 1965 (Geschwind, 1965a, 1965b), these alterations are thought to account for the cognitive decline that is observed during normal aging (Andrews-Hanna et al., 2007; Bartzokis, 2004; Fjell et al., 2016a; Madden et al., 2017; O'Sullivan et al., 2001). Since cognitive functions rely on the communication between distinct functional subunits that are anatomically connected (Bressler and Menon, 2010; Bullmore and Sporns, 2009; Craddock et al., 2013; Park and Friston, 2013; van den Heuvel and Hulshoff Pol, 2010), the disruption of this communication (measured either as changes in structural or functional connectivity between different brain regions) in aging could be one of the potential sources of cognitive decline (Antonenko and Flöel, 2013; Salat, 2011; Zimmermann et al., 2016).

Network analysis has emerged as a tool to characterize brain's structural and functional organization (Bullmore and Sporns, 2009). In this context, brain is conceptualized as a complex network of inter-

connected regions, and thus it can be modeled as a graph, with nodes defined as brain regions and edges as the structural/functional connections between regions. Graph theory analysis allows the extraction of quantifiable topological properties of networks that can clarify the organization and function of the brain network (Rubinov and Sporns, 2010). Functional networks can be constructed from resting-state functional MRI (rs-fMRI), where functional connectivity (FC) reflects the temporal coherence in the blood oxygen level dependent (BOLD) signal across brain regions (Damoiseaux, 2017). On the other hand, structural networks can be built from structural MRI, where the structural connectivity (SC) measure is the structural covariance of gray matter volumes or cortical thickness (Bassett et al., 2008). Another option for determining SC is to use diffusion MRI which allows the estimation of white matter (WM) pathways, and in this case the SC measure will be the number of streamlines or the probability of connection between brain regions (Damoiseaux, 2017). Previous studies have revealed a number of non-trivial properties of the human functional and structural networks, such as small-worldness, modular architecture, hubs and cores, rich club structure, among others (Bullmore and Sporns, 2009; van den Heuvel and Sporns, 2011; Wang et al., 2010).

Normal aging induces a reorganization of brain's structural and functional networks, characterized as reduced global and local efficiency (Gong et al., 2009; Wu et al., 2012; Zhao et al., 2015), increased shortest path length and clustering coefficient (Otte et al., 2015; Sala-Llonch et al., 2014), reduced rich club organization (Zhao et al., 2015), modularity architecture reorganization (Betzel et al., 2014; Wu et al., 2012), and also a decrease in long-range connections accompanied by simultaneous increase in short-range connections (Andrews-Hanna et al., 2007; Cao et al., 2014; Sala-Llonch et al., 2014; Wu et al., 2012). Recent studies have emphasized the role of brain network connectivity in cognitive performance in aging. Associations between network connectivity changes and multiple cognitive domains, such as, visuospatial reasoning, information processing speed, crystallized ability, executive function and memory have been reported (Bernard et al., 2015; Fjell et al., 2016a, 2016b; Persson et al., 2014; Wen et al., 2011; Wiseman et al., 2018). Nevertheless, most of these studies focus on graph theory metrics that reflect the topological organization of brain networks or in the connectivity weight of the whole-brain or of specific networks, such as resting-state networks. In this study, in addition to explore longitudinal changes of topological properties of brain structural networks during normal aging, we also inspect the existence of sub-networks that present significant age-related alterations in connectivity weight. To our knowledge, this is the first study to explore the presence of these sub-networks in aging. We hypothesized that aging will induce a reorganization of the brain structural network, characterized by disrupted connectivity in specific sub-networks, consistent with the findings of previous longitudinal

diffusion MRI studies which demonstrated alterations in diffusion tensor imaging (DTI) based measures as a function of age (Sexton et al., 2014; Vinke et al., 2018). Furthermore, we hypothesized that changes in brain structural connectivity would affect differently distinct WM tracts, consistent with the last-in-first-out hypothesis which posits that brain regions that reach full maturation later are more vulnerable to age-related atrophy (Raz, 1999) and this was already observed for WM tracts (Bender et al., 2016; Slater et al., 2019). Brain network reorganization will also be characterized by changes in topological features, as it has already been reported in some cross-sectional studies (Betzel et al., 2014; Gong et al., 2009; Otte et al., 2015; Zhao et al., 2015), but to date no longitudinal study using diffusion MRI has explored changes in brain structural network topology. To test this, we construct structural connectomes for a group of older adults who were followed longitudinally, with a mean time interval of 52.8 months (SD = 7.24). We characterized longitudinal topological alterations in structural connectivity using advanced structural connectomics analysis. Furthermore, we tested associations between longitudinal changes in network connectivity and cognition.

4. Methods

4.1. Ethics Statements

The present study was conducted in accordance with the principles expressed in the Declaration of Helsinki and was approved by local and national ethics committees. The study goals and tests were explained to the participants and all gave informed written consent.

4.2. Participants

The participants included in this study are part of a larger sample recruited for the SWITCHBOX Consortium project (www.switchbox-online.eu/), and are representative of the general Portuguese population with respect to age, gender and education (Costa et al., 2013; Santos et al., 2014, 2013). Primary exclusion criteria were inability to understand the informed consent, participant choice to withdraw from the study, incapacity and/or inability to attend MRI sessions, dementia and/or diagnosed neuropsychiatric and/or neurodegenerative disorder (from medical records). Mini Mental State Examination (MMSE) scores below the adjusted thresholds for cognitive impairment were also used as exclusion criteria. The adjusted thresholds were the following: MMSE score <17 if individual with ≤4 years of formal school education and/or ≥72 years of age, and MMSE score <23 otherwise (follows the MMSE validation study for the Portuguese population) (Guerreiro et al., 1994). These exclusion criteria were

applied at both evaluations. Subjects were evaluated at two timepoints, with a mean interval time between first and last assessments of 52.8 months (SD = 7.24). At each evaluation, participants underwent an imaging session and a battery of neurocognitive/neuropsychological tests.

In the first assessment, 100 subjects were contacted for MRI screening. From these, one subject did not finish the diffusion acquisition and four subjects had brain lesions/pathology. In the last assessment, 55 subjects accepted to participate and underwent MRI acquisition protocol, but one did not finish the diffusion acquisition. A total of 51 individuals with data from both the first and last evaluations met all the inclusion criteria for this study.

4.3. Neurocognitive Assessment

A team of certified psychologists performed an identical battery of neurocognitive tests at both timepoints. This included the following tests previously validated for the Portuguese population: Stroop color and word test, selective reminding test (SRT) and mini-mental state examination (MMSE). A previous report from our group examined the longitudinal measurement invariance of this set of cognitive tests (Moreira et al., 2018). Using confirmatory factor analysis, we observed that a two-factor solution encompassing (1) a general cognition and executive functioning dimension (EXEC) and (2) a memory dimension (MEM) was reliable over time. The MEM factor was comprised of long-term storage (LTS), consistent long-term retrieval (CLTR) and delayed-recall (DR) variables assessed with SRT. The EXEC factor was composed of the variables MMSE and Stroop parameters: words, colors and words/colors. We obtained evidence of partial strong invariance which indicates an equivalence of the factorial structure and factor loadings for all the items, as well as of the intercepts of most items comprising this factorial solution. Thus, we estimated factor scores for each of these dimensions, based on the estimates for the model with strictest measurement invariance. The analytical pipeline was based on a maximum likelihood mean- and variance- adjusted (MLMV) implemented with MPlus. The mean factor scores for the two dimensions were extracted for each participant.

4.4. MRI Data Acquisition

All imaging sessions were performed at Hospital de Braga (Braga, Portugal) on a clinical approved Siemens Magnetom Avanto 1.5T MRI scanner (Siemens Medical Solutions, Erlangen, Germany) with a 12-channel receive-only head-coil. The imaging protocol included several different acquisitions. For the present study, only the Diffusion Weighted Imaging (DWI) acquisition was considered. For this, a spin-

echo echo-planar imaging (SE-EPI) sequence was acquired with the following parameters: TR=8800 ms, TE=99 ms, FoV=240x240 mm, acquisition matrix=120x120, 61 2-mm axial slices with no gap, 30 non-collinear gradient direction with b=1000 s mm-2, one b=0 s mm-2 and 1 repetition.

All acquisitions were visually inspected by a certified neuroradiologist, before any pre-processing step, in order to ensure that none of the individuals had brain lesions and/or critical head motion or artifacts that could affect the quality of data.

4.5. MRI Data pre-processing

Data was pre-processed using FMRIB Diffusion Toolbox (FDT) provided with the FMRIB Software Library (FSL v5.0; https://fsl.fmrib.ox.ac.uk/fsl/). First, DWI images were corrected for motion and eddy current distortions, followed by rotation of gradient vectors according to the affine transformations used to register each volume. Then, the first b0 volume of each subject was extracted and skull stripped, which generated a brain mask that was applied to the remaining volumes in order to remove non-brain structures. Finally, local modelling of diffusion parameters was performed using *bedpostx* algorithm which employs Markov Chain Monte Carlo sampling to build up probability distributions of the diffusion parameters at each voxel, thereby allowing modelling of crossing fibers (Behrens et al., 2007). In addition, we also extracted the levels of head-motion in a diffusion scan, using FSL tools, for all subjects at both timepoints. We then sought to determine if these values were associated with age (Supplementary Figure 1) or if they were different between timepoints (Supplementary Figure 2). Since there was no significant correlation with age neither differences in head motion levels between assessments, we thus concluded that there was no need to account for this variable in subsequent statistical analyses.

4.6. Network construction

Network nodes were defined as the 90 regions of the Automated Anatomical Labeling (AAL) template. These regions were normalized to each subject native diffusion space. This was done by applying the inverted affine transformation from diffusion space to MNI space. Probabilistic tractography was used to estimate connections between nodes (i.e., edges). This was accomplished using *probtrackx2* algorithm from FDT toolbox. 5000 streamlines were sampled from each voxel in the seed mask. This resulted in a structural connectivity (SC) matrix, for each subject, representing the number of streamlines leaving each seed mask and reaching any of the other regions. This matrix was normalized by first dividing each line by the waytotal value (i.e., the total number of generated tracts not rejected by inclusion/exclusion mask

criteria) and then dividing by the maximum SC value of each individual, in order to have connectivity values between [0, 1]. Each element of this matrix, P_{ij}, represents the connectivity probability between region *i* and region *j*. Since tractography is dependent on seeding location, the connectivity probability from *i* to *j* is not necessarily equal to that from *j* to *i*. Still, these two probabilities are highly correlated across the brain for all participants. Thus, we defined the undirected connectivity probability as the average of these two probabilities, P_{ij} and P_{ji}, which originated an undirected connectivity matrix. At the end of this process, a 90 x 90 symmetric connectivity matrix for each subject was obtained. A threshold set to 1% of the strongest connection was then applied to each subject's SC matrix, in order to remove spurious connections. An additional threshold was applied, based on a consistency-based thresholding technique. This method measures the consistency of edge weights across subjects and retains the most consistent ones, with the goal of reducing the false-positives in group-averaged connectivity matrices (for a description of the method see (Roberts et al., 2017)). It was proven to preserve more long-distance connections, than the traditional weight-based thresholding, which often removes such connections since, in general, they represent weak edges. In this work, we applied consistency-based thresholding at 30% density (the same density used in (Roberts et al., 2017)) and then we performed a validation of the method by analyzing the connections that were removed. Specifically, we analyzed the connections that were removed in each individual after applying the threshold, both the number of connections removed (Supplementary Figure 3) and the strength of these connections (Supplementary Figure 4). Furthermore, the consistency-based threshold method generates a group consistency mask that is then applied to each subject's SC matrix, in order to retain only the most consistent connections. Thus, we also analyzed the connections that were present in this group consistency mask but were not present in all subjects SC matrices. Once again, we evaluated the number of connections that were not present in all subjects (Supplementary Figure 5) and their strength (Supplementary Figure 6). We can observe that, in each subject, a small percentage of connections is removed (Supplementary Figure 3) and they represent mostly weak connections (Supplementary Figure 4). Also, for each subject, the connections from group consistency mask that are not present in its SC matrix do not represent more than 50% of all group consistency links (Supplementary Figure 5) and once again, the majority of these edges are characterized by low connection strength (Supplementary Figure 6). Together, these results support the use of this threshold technique to remove spurious connections.

Given that our sample covers a 30-year age range and the rate of white matter change is known not to be homogeneous across age (Sexton et al., 2014; Westlye et al., 2010), we performed an additional

analysis to evaluate the potential impacts of both age and sex on our estimations of SC. To perform this, we analyzed the levels of intra- and inter-timepoint consistency in the resulting signatures of individual SC, i.e., how consistent are the patterns of estimated SC across all subjects in a timepoint, as well as between timepoints. To do this, we used the following two strategies for evaluating timepoint consistency (TC) in SC:

TC-I: Intra-timepoint consistency measured as the Pearson's correlation between each subject's SC and timepoint mean SC (considering upper diagonal matrix elements). The resulting r values were z-transformed (Fisher-Z transformation) before averaging and converting (inverse of Fisher-Z) the resultant timepoint consistency back to r scale. This value represents the within-timepoint consistency, i.e., for each timepoint, how well all subjects' SC correlate with the timepoint's average SC.

TC-II: Intra-timepoint consistency measured as the distribution of Pearson's correlations between all possible pairs of subjects in a timepoint. The resulting distribution of all pairwise (pairs of subjects) SC comparisons is represented as a histogram. This indicates how well SCs in a timepoint correlate with each other. Inter-timepoint consistency was also assessed by considering all subjects as part of the same timepoint.

4.7. Graph Theoretical Analysis

Brain networks can be described in terms of its topological organization, using graph theory measures. Brain Connectivity Toolbox (https://sites.google.com/site/bctnet/) was used to extract these metrics. The following local and global measures were computed:

Degree. The degree of a node k_i, in a binary undirected network, is the number of links connecting node i with the other $j = 1 \dots N - 1$ nodes:

$$k_i = \sum_{j \neq 1} A_{ij}$$

where A is the adjacency matrix.

The mean degree of an undirected network is the average of all node degrees:

$$\langle k \rangle = \frac{1}{N}\sum_{i=1}^{N} k_i$$

Connection Density. The connection density of a network is the proportion of the actual number of edges in the network relative to the total possible number of connections. For an undirected network with N nodes without self-connections, the total number of possible connections is given by $N(N-1)/2$. Thus, the connection density, κ , of an undirected network can be measured as:

$$\kappa = \frac{2E}{N(N-1)}$$

where E is the total number of edges in the adjacency matrix.

Global Efficiency. Global efficiency is a measure of integration that reveals how efficiently information can be exchanged between nodes. It is defined by the mean of the inverse shortest path length, l_{ij} , between each pair of nodes:

$$E_{glob} = \frac{1}{N(N-1)}\sum_{i \neq j} \frac{1}{l_{ij}}$$

Nodal Efficiency. Nodal efficiency measures how well a node is integrated within the network via its shortest paths, i.e., how well a given node connects to all other nodes in the network. It is defined as the mean of the inverse shortest path length, l_{ij}, between a given node and all other nodes in the network:

$$E_{nodal}(j) = \frac{1}{(N-1)}\sum_{i} \frac{1}{l_{ij}}$$

Local Efficiency. Local efficiency reflects globally how information is exchanged within the neighborhood of a given node. It is defined as the average nodal efficiency:

$$E_{local} = \frac{1}{N}\sum_{i} E_{nodal}(i)$$

Characteristic Path Length. The characteristic path length, L, is the mean shortest path length between all possible pairs of nodes in a network. The shortest path between nodes i and j is equal to the minimum number of connections or the minimum cost needed to connect nodes i and j, where connection cost is defined as the inverse of connection weight. So, the characteristic path length is defined as:

$$L = \frac{1}{N}\sum_{i} l_i = \frac{1}{N(N-1)}\sum_{i \neq j} l_{ij}$$

where l_i is the average shortest path length from node i to all other nodes in the network and l_{ij} is the shortest path length from node j to node i.

Clustering Coefficient. The clustering coefficient is measured as the fraction of closed triangles that are connected to node i, relative to the total number of possible closed triangles between i's neighbors. It is a measure of local interconnectivity in a network and is calculated as follows:

$$Cl = \frac{1}{N}\sum_{i \in N} \frac{2t_i}{k_i(k_i - 1)}$$

where k_i is the degree of node i and t_i is the number of closed triangles attached to i.

Small-World index. Networks with high clustering and low average shortest path length are considered small-world networks. This is quantified by the index σ, that is a ratio of the normalized clustering coefficient and shortest path length. The normalization of these measures is done by dividing their empirical value by the average measure of an ensemble of randomized networks that preserves the degree distribution of the original network. When $\sigma > 1$, the network is considered to present small-world properties.

$$\sigma = \frac{Cl/\langle Cl_{rand}\rangle}{L/\langle L_{rand}\rangle}$$

where $\langle Cl_{rand}\rangle$ is the average clustering coefficient of the randomized networks and $\langle L_{rand}\rangle$ is the average shortest path length of the randomized networks. In this work, we generated an ensemble of 100 randomized networks.

In addition, the following topological features were also assessed.

Modularity. Modularity quantifies the degree to which nodes of a network may aggregate into densely connected non-overlapping modules or communities (Fornito et al., 2016). Nodes within a community are more strongly connected with each other than with nodes outside this community. Thus, the optimal community structure will be the partition of the network that maximizes intra-module connectivity and minimizes inter-module connectivity. The index of modularity, Q, is given by the difference between the empirical degree of intra-module connectivity and the degree expected by chance (Fornito et al., 2016). The optimal community structure can be found by searching for the partition that maximizes Q. One popular algorithm used to find the optimal partition is the Louvain algorithm and, shortly, this is how it works: first, it starts with all nodes in a distinct module, then it chooses a node at random and merges it with the module that produces the largest gain in Q, these steps are repeated until no additional gains in Q are possible (Blondel et al., 2008). Given that at each iteration, nodes are chosen randomly, running the algorithm multiple times can lead to different solutions. Also, another limitation is the so-called degeneracy problem, that can cause the existence of large number of different solutions, since there is not a clear global maximum of Q (Good et al., 2010). To circumvent this problem, we ran the Louvain algorithm 10000 times and selected the partition having the higher number of occurrences in the set of 10000 partitions, i.e., the partition that was more consistent. To compare the optimal community structures found at each timepoint, we defined a similarity metric. For each module in a partition, we found the module in the other partition that was more similar to this one (by finding the maximum of the number of shared regions divided by the total number of regions in the two modules). The similarity metric was then calculated as the mean of the maximum values for each module. Values close to 1 indicate higher similarity between the partitions.

Additionally, we characterized the overlap between each module of the optimal partition and resting-state networks (RSN). For this, we calculated a matrix where each entry represents the percentage of intersection between all anatomical regions in a module and a given RSN, normalized by the total intersected volume between all regions of the anatomical atlas and each of the RSNs. The anatomical atlas used was the AAL as it was also used to construct the SC matrices, and the RSN atlas used was the parcellation into 7 RSNs from (Yeo et al., 2011).

Hubs. Hubs can be defined as nodes with high regional efficiency (E_{nodal}) (Achard and Bullmore, 2007). Specifically, for each node, if the normalized E_{nodal} (divided by the mean E_{nodal} of all nodes) is larger than the normalized mean E_{nodal} of all nodes of the network plus one standard deviation (SD), the node is considered a hub (Lo et al., 2010).

Furthermore, we analyzed the topological roles of nodes in the communication within and between modules. This allowed the classification of nodes into provincial and connector hubs. The definition of these roles is described below.

Provincial Hubs are nodes with high within-module degree z-score (greater than the mean plus SD of all nodes) and low participation coefficient (PC $\leq$ 0.3). Positive values of within-module degree z-score indicate high (above the average) intra-module connectivity, and thus higher values of this measure suggest that the node plays a central role in intra-modular communication. Participation coefficient (PC) compares the number of connections of a node with other nodes in different modules, to the total number of connections to other nodes in the same module. Values close to one indicate that the edges of a node are distributed uniformly across modules while a value of zero means that all edges of a nodes are limited to its own module. Thus, provincial hubs are characterized by comprising most of their connections within their own module (Fornito et al., 2016).

Connector Hubs were also defined as nodes with high within-module degree z-score and high participation coefficient (PC > 0.3). This means they have many connections with other modules, and thus play a key role in inter-modular communication (Fornito et al., 2016).

4.8. Statistical analysis

Statistical comparison of the SC matrices between first and last assessments, at the edge level, was performed by applying a paired sample t-test with SC as the dependent variable and time of evaluation as independent variable. The obtained SC networks are comprised of 90 nodes, yielding a total number of possible edges of 4005 (90*89/2). Testing the hypothesis of interest at the edge level, therefore poses a multiple comparisons problem. In order to increase the statistical power of the analysis, we used the network-based statistics (NBS) procedure implemented in the NBS toolbox (https://sites.google.com/site/bctnet/comparison/nbs). This is a non-parametric statistical method that allows the identification of significantly different sub-networks, while controlling for the family-wise error rate (FWER) (Zalesky et al., 2010). First, it independently tests the hypotheses at every connection in the network and threshold the ones exceeding a user defined primary threshold, then it identifies sub-networks constituted by interconnected edges that survived the primary threshold. The significance of these sub-networks is then calculated by comparing their sizes to the distribution of the size of sub-networks obtained through random permutations of the original hypothesis. It is important to note that the primary threshold only affects the sensitivity of the method and thus, FWER is assured independently

of this threshold. In this study, the primary threshold was set to F = 17.0, which was the maximum threshold that detected a unique significant connected component having more than two connections (Supplementary Figure 8). Longitudinal changes in structural connectivity detected with NBS are represented by significantly connected components at a corrected level of $p < 0.05$ FWE corrected.

Additionally, we extracted, for each subject, the mean connectivity values of the significant component resulting from the NBS approach. We analyzed these values separately for the connections with increases in connectivity between timepoints, the connections with decreases and both types of connections. We then examined, for these three types, the values of mean connectivity of all connections, intra-left, intra-right and inter-hemispheric connections. Moreover, we tested potential associations between the connectivity values of these networks and cognitive scores of MEM and EXEC. The rmcorr R package (https://cran. r-project.org/web/packages/rmcorr/) was used to compute a repeated measures correlation coefficient between each sub-network and cognitive score. This coefficient, unlike simple correlation, does not violate independence assumptions nor requires averaging the data and thus is suitable to use with repeated measures data (Bakdash and Marusich, 2017). The p-values of all correlations were corrected for multiple comparisons, using the false discovery rate (FDR) method.

The comparison of graph measures between timepoints was performed using paired sample t-tests and p-values were corrected for multiple comparisons, using the FDR method. In addition, we analyzed, for each timepoint, the network fingerprints of inter-modular (global and connector-hub-driven) and intra-modular connectivity. The same method of analysis as described in (Fernandes et al., 2019), was applied in this work. In summary, modular connectivity strength was defined as the degree (total number of connections) of all nodes constituting a module. To quantify this connectivity at both timepoints, a reference scheme of community structure was chosen based on the mean score of community-structure goodness-of-fit. Then, matrices of inter-modular and intra-modular connectivity were created for both timepoints.

4.9. White matter tracts analysis

After identifying sub-networks with significant longitudinal changes, using the NBS approach described before, we performed an additional analysis designed to identify the white matter tracts that are responsible for connecting the brain regions comprising the identified sub-networks. For this, we used streamline density maps obtained with probabilistic tractography. These maps represent the number of streamlines reaching each voxel and one map is generated for each seed region. So, we first normalized

the streamline density maps of each subject to the MNI space using the affine transformation computed previously, and then applied a threshold of 1% of the maximum number of streamlines to remove spurious connections (same threshold as applied to construct the SC matrices). Next, we extracted WM tract masks from the JHU white-matter tractography atlas (Hua et al., 2008; Wakana et al., 2007) and computed the mean intensity (i.e. mean number of streamlines) of the overlapping region between each of these WM tracts and the streamline density map of each region. We repeated the process for each subject and each timepoint, then we grouped all this information in two matrices (one for each timepoint) that represent the mean intensity values of the overlap between each seed region and each WM tract averaged across subjects. Then, we applied a threshold of 5% of the maximum value to each matrix. Finally, we calculated the proportion of change between timepoints by computing the difference between the matrices of the last and first timepoints and then dividing by the matrix of the first timepoint. To identify WM tracts connecting a pair of regions, we inspected the proportion of change matrix and we selected WM tracts that had, for both brain regions, negative or positive values if that connection represented an SC decrease or an SC increase, respectively. In case regions shared multiple WM tracts, we chose the tract with the highest mean intensity value at both timepoints. When there wasn't any common tract, we also chose based on the mean intensity values at both timepoints instead of the proportion of change.

5. Results

5.1. Sample Characterization

Table 1 shows the demographic characterization of the participants included in this study. In summary, mean age at baseline was 63.5 years (range, 51 – 82 years) and mean interval between evaluations was 52.8 months (range, 45 – 73 months). Interval time was not significantly associated with age at baseline ($r = -0.12$, $p = 0.41$). The sample was balanced for sex (51% females, 49% males) and they did not differ with respect to interval time ($t(30) = 0.14, p = 0.89$). Mean education level was 5.98 years (range, 0 – 17 years). Regarding memory, at baseline, the mean factor score was 0.24 (range, -1.51 – 2.23) and at follow-up it was lower, with a mean value of 0.063 (range, -1.64 – 2.67). EXEC scores also decreased between assessments, with a mean value of 0.20 (range, -2.46 – 1.72) at baseline and 0.098 (range, -1.90 – 2.05) at follow-up.

Table 1. Basic demographic characterization of the study's cohort.

	Mean ± SD (range)
N (Females/Males)	51 (26/25)
Age at baseline (years)	63.5 ± 7.41 (51 - 82)
Age at follow-up (years)	68.0 ± 7.25 (55 - 86)
Interval (months)	52.8 ± 7.24 (45 - 73)
Education (years)	5.98 ± 3.97 (0 - 17)
F-MEM at baseline	0.24 ± 0.98 (-1.51 – 2.23)
F-EXEC at baseline	0.20 ± 1.01 (-2.46 – 1.72)
F-MEM at follow-up	0.063 ± 1.00 (-1.64 – 2.67)
F-EXEC at follow-up	0.098 ± 0.99 (-1.90 – 2.05)

Abbreviations: F-MEM, Mean Factor Scores for the memory composite dimension; F- EXEC, Mean Factor Scores for the general cognition and executive function composite dimension

5.2. Timepoint Consistency

High levels of intra- and inter-timepoint consistency were found for both timepoints in the estimation of whole-brain SC (Supplementary Figure 7). We thus concluded that potential bias due to age and/or sex did not have a significant impact on the estimation of SC so that the inclusion of additional confounds for these variables in the statistical analysis was not necessary.

5.3. Structural Connectivity Longitudinal Changes

From first to last timepoint there were significant changes in structural connectivity in a brain sub-network ($p < .001$), comprising 16 connections, where 9 correspond to decreases and 7 to increases in structural connectivity between timepoints (Fig. 1). Analyzing the individual connections of this network, we observe that the connections with longitudinal decreases in connectivity are composed by 3 intra-left, 5 intra-right and 1 inter-hemispheric connections. On the other hand, the connections with increasing connectivity are constituted by 2 intra-left and 5 inter-hemispheric connections. The summary of the connections is present in Table 2.

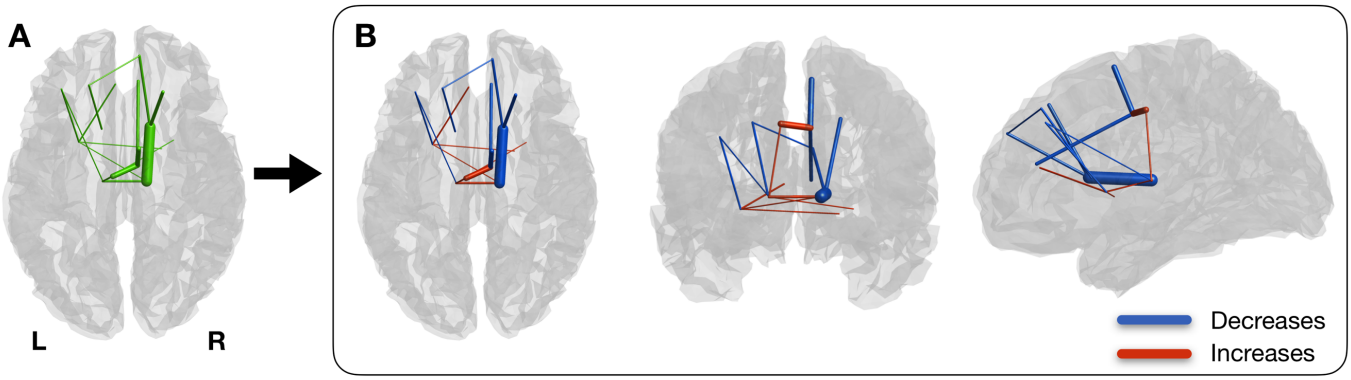

Figure 1. Significant changes in structural connectivity between timepoints. A) Binarized version of the connected component of significantly altered structural connectivity. B) Weighted version of A), with edge thickness representing the amplitude of differences. Blue represents decreases in connectivity strength between timepoints and red represents increases. Connections with decreases are mostly intra-hemispheric, while most of the increases are composed of intra-hemispheric connections. Both increases and decreases are mainly composed by links between subcortical and frontal regions.

Table 2. Description of the connections comprising the connected component of significant structural connectivity differences between timepoints ($p < .001$).

Area 1		Area 2		Difference	Intra-Left	Intra-Right	Inter-Hemispheric
N	Name	N	Name				
			Increases				
77	Thalamus L	74	Putamen R	0.008	0	0	1
78	Thalamus R	73	Putamen L	0.009	0	0	1
76	Pallidum R	73	Putamen L	0.009	0	0	1
77	Thalamus L	33	Cingulum Mid L	0.013	1	0	0
73	Putamen L	31	Cingulum Ant L	0.013	1	0	0
78	Thalamus R	77	Thalamus L	0.019	0	0	1
34	Cingulum Mid R	33	Cingulum Mid L	0.044	0	0	1
			Decreases				
78	Thalamus R	72	Caudate R	-0.088	0	1	0
34	Cingulum Mid R	20	Supp Motor Area R	-0.040	0	1	0
72	Caudate R	4	Frontal Sup R	-0.028	0	1	0

34	Cingulum Mid R	32	Cingulum Ant R	-0.026	0	1	0
72	Caudate R	24	Frontal Sup Medial R	-0.022	0	1	0
71	Caudate L	3	Frontal Sup L	-0.016	1	0	0
73	Putamen L	7	Frontal Mid L	-0.014	1	0	0
24	Frontal Sup Medial R	3	Frontal Sup L	-0.011	0	0	1
77	Thalamus L	7	Frontal Mid L	-0.010	1	0	0

Next, we examined the mean connectivity values of the significant sub-network (Fig. 2). In the network with all connections, we observe an overall decrease in connectivity. When examining the three types of connections (intra-left, intra-right and inter-hemispheric) we see that connections within the same hemisphere exhibit a decrease between the two timepoints, with a more pronounced decrease for the right hemisphere, while inter-hemispheric connections show an increase along time. In the network of increases, inter-hemispheric connections are the major contributors for this increase, while intra-hemispheric connections have lower connectivity values. In the network of decreases, most of the decrease in connectivity is due to connections within the right hemisphere, while intra-left and inter-hemispheric connections present lower connectivity values. Rates of change for the different sub-networks are reported in Table 3.

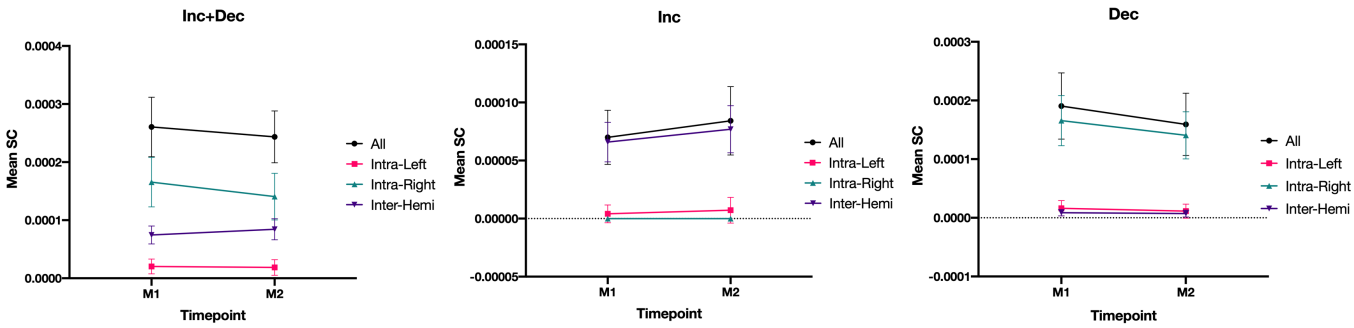

Figure 2. Mean connectivity values of the significant connected component. (A) all the connections; (B) connections with increases in connectivity along time; (C) connections with decreases in connectivity. For each plot, we present the connectivity values for all connections (black), intra-left (red), intra-right (green) and inter-hemispheric (purple) connections. Intra-hemispheric connections exhibit a decrease along time, while inter-hemispheric links show an increase. Most of the decreases in SC are due to connections within the right hemisphere.

Table 3. Percentage of longitudinal changes in the mean connectivity of the significant connected component. Percentages are given for all the connections comprising the connected component, only the connections with increases in connectivity and connections with decreases.

Network	All connections	Intra-Left	Intra-Right	Inter-Hemispheric
All Connections	-6.53	-8.70	-15.07	13.04
Increases	20.35	76.54	0	16.86
Decreases	-16.40	-30.10	-15.07	-15.9

Regarding associations between mean connectivity values and cognition, only the correlation between the network with increases and EXEC was significant, although it did not survive the multiple comparisons correction (Supplementary Table 1). In order to verify if the multiple comparisons correction was too conservative, we calculated the bootstrap confidence interval of the correlation coefficient using 10000 draws. We obtained the following result: r=0.31, 95% CI [-0.40, -0.18]. Thus, we estimate with 95% confidence that the true correlation coefficient between the network with increases and EXEC is between -0.40 and -0.18. Analyzing this association, we see that higher values of SC in this network are related to lower values of EXEC (Supplementary Figure 9).

5.4. White matter tracts analysis

Figures 3 and 4 present the proportion of change between timepoints in the mean number of streamlines encompassed by the volume of overlap between each WM tract and seed region of the sub-network with decreases (Fig. 3) and the sub-network with increases (Fig. 4). The values of the mean number of streamlines for each timepoint are displayed in Supplementary Figures 10 and 11. For the regions of the sub-network with decreases, connections were composed of association (anterior thalamic radiation, uncinate fasciculus, superior longitudinal fasciculus, cingulate gyrus part of cingulum bundle) and commissural fibers (forceps minor). While for the sub-network of increases, connections were attributed to all types of fibers, namely, association (inferior fronto-occipital fasciculus, cingulate gyrus part of cingulum bundle), commissural (forceps minor) and projection fibers (corticospinal tract). There was one special case in the network of increases that were the connections involving the left middle cingulate cortex. This region had only decreases in the mean number of streamlines, so we chose the WM tract with the highest value in both timepoints that was the left cingulate gyrus part of the cingulum.

Information of which WM tract connects each pair of regions along with mean number of streamlines values is summarized in Table 4.

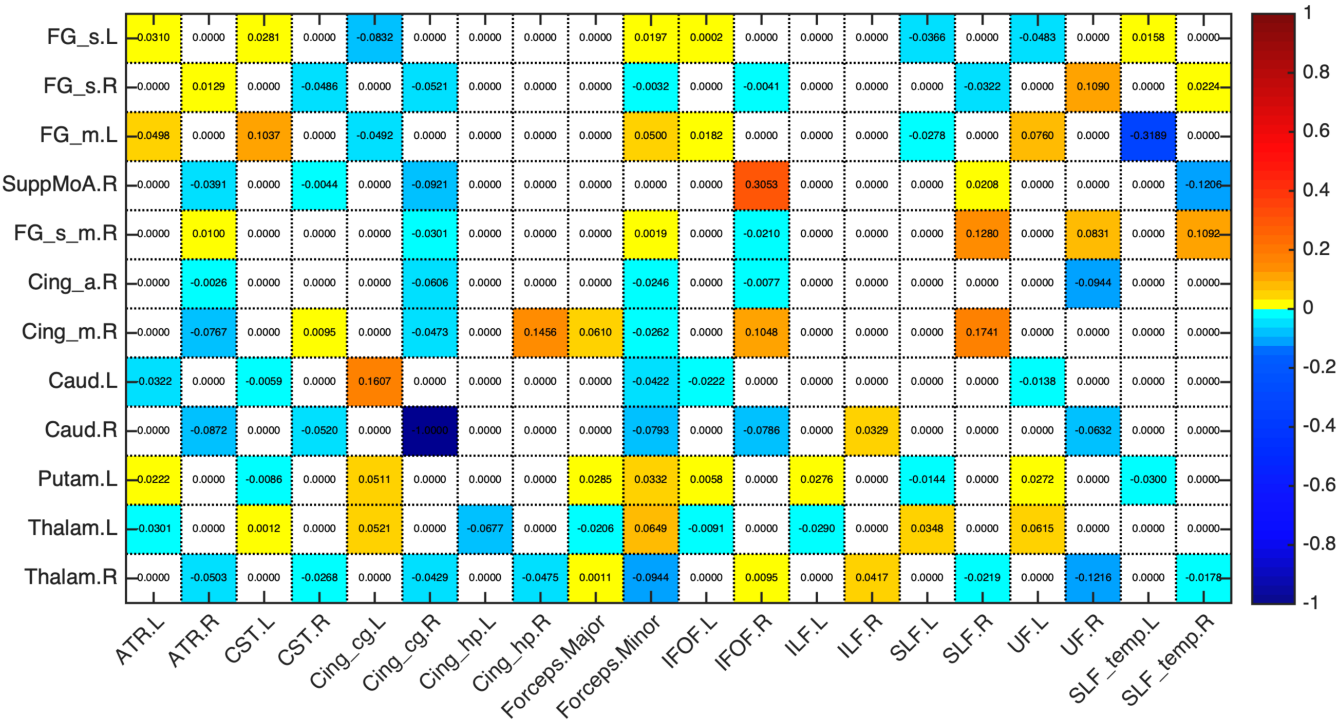

Figure 3. Proportion of change between timepoints in the mean number of streamlines of the overlap between each seed region of the sub-network with decreases in structural connectivity and WM tract. Seed regions are presented in rows and white matter tracts in columns. For most of the connections, we found a common WM tract and the majority were association fibers.

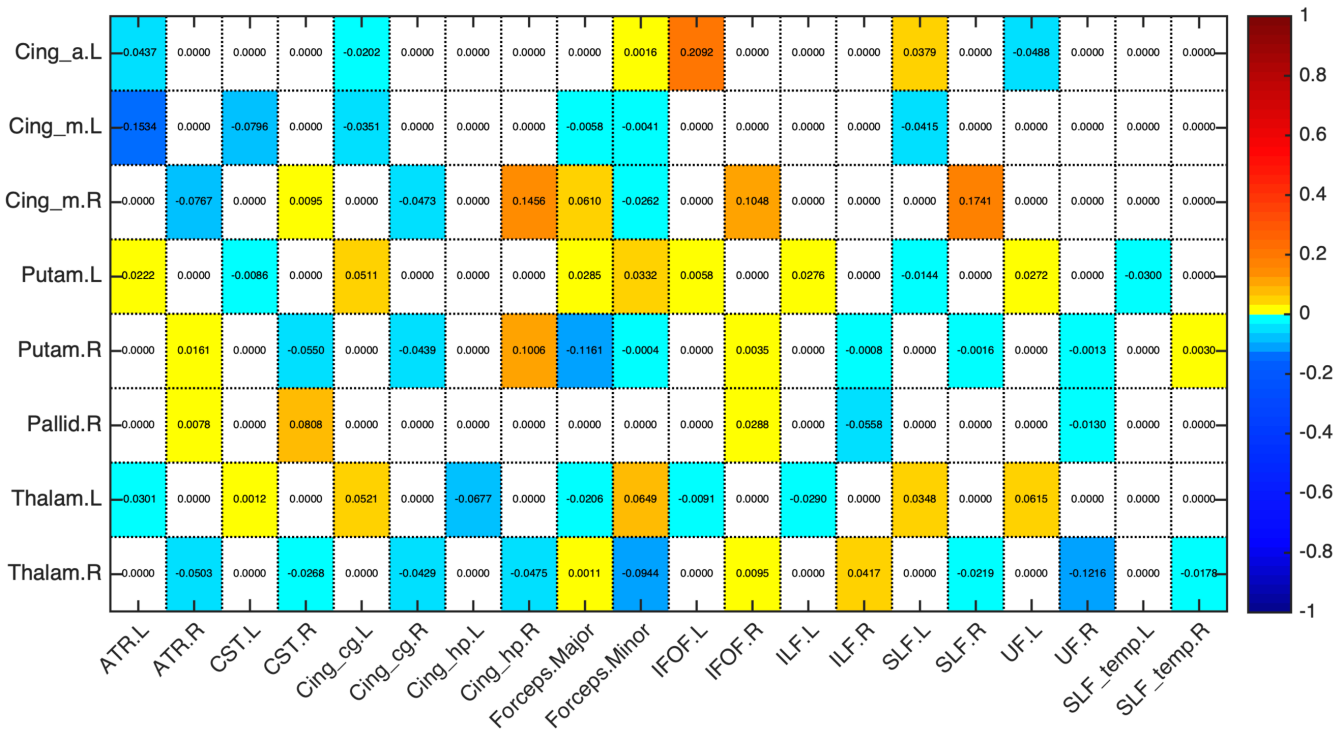

Figure 4. Proportion of change between timepoints in the mean number of streamlines of the overlap between each seed region of the sub-network with increases in structural connectivity and WM tract. Seed regions are presented in rows and white matter tracts in columns. There were more than a single WM tract connecting the regions, probably due to the fact that almost all the connections were inter-hemispheric.

Table 4. WM tracts connecting each pair of regions of the significant sub-networks with structural connectivity differences between timepoints.

Area 1		Area 2		WM Tract
N	Name	N	Name	
		Increases		
77	Thalamus L	74	Putamen R	CST L; IFOF R
78	Thalamus R	73	Putamen L	IFOF R; IFOF L
76	Pallidum R	73	Putamen L	IFOF R; IFOF L
77	Thalamus L	33	Cingulum Mid L	CST L; CGC L
73	Putamen L	31	Cingulum Ant L	IFOF L; FMI
78	Thalamus R	77	Thalamus L	IFOF R; CST L

34	Cingulum Mid R	33	Cingulum Mid L	CST R; CST L
			Decreases	
78	Thalamus R	72	Caudate R	ATR R
34	Cingulum Mid R	20	Supp Motor Area R	CGC R
72	Caudate R	4	Frontal Sup R	FMI
34	Cingulum Mid R	32	Cingulum Ant R	CGC R
72	Caudate R	24	Frontal Sup Medial R	CGC R
71	Caudate L	3	Frontal Sup L	UF L
73	Putamen L	7	Frontal Mid L	SLF L
24	Frontal Sup Medial R	3	Frontal Sup L	CGC R; CGC L
77	Thalamus L	7	Frontal Mid L	ATR L; SLF L

Abbreviations: ATR, anterior thalamic radiation; IFOF, inferior fronto-occipital fasciculus; SLF, superior longitudinal fasciculus; UF, uncinate fasciculus; FMI, forceps minor; CGC, cingulate gyrus part of cingulum; CST, corticospinal tract.

5.5. Topological Organization Longitudinal Changes

5.5.1. Graph Theory Metrics

Characteristic path length decreased significantly from the first to the second timepoint ($t_{(50)} = 3.45$, $p = .009$, $d = 0.29$). Regarding the other graph measures (node degree, connection density, global efficiency, local efficiency, clustering coefficient and small-world index) no statistically significant differences were found (see Supplementary Table 2).

5.5.2. Hubs

Network hubs were defined as regions with high normalized nodal efficiency. In the first assessment, 13 regions were identified as hubs (Fig. 5-6, Table 5). In timepoint 2, two hubs were lost in comparison to timepoint 1, that were left inferior parietal and left fusiform gyrus.

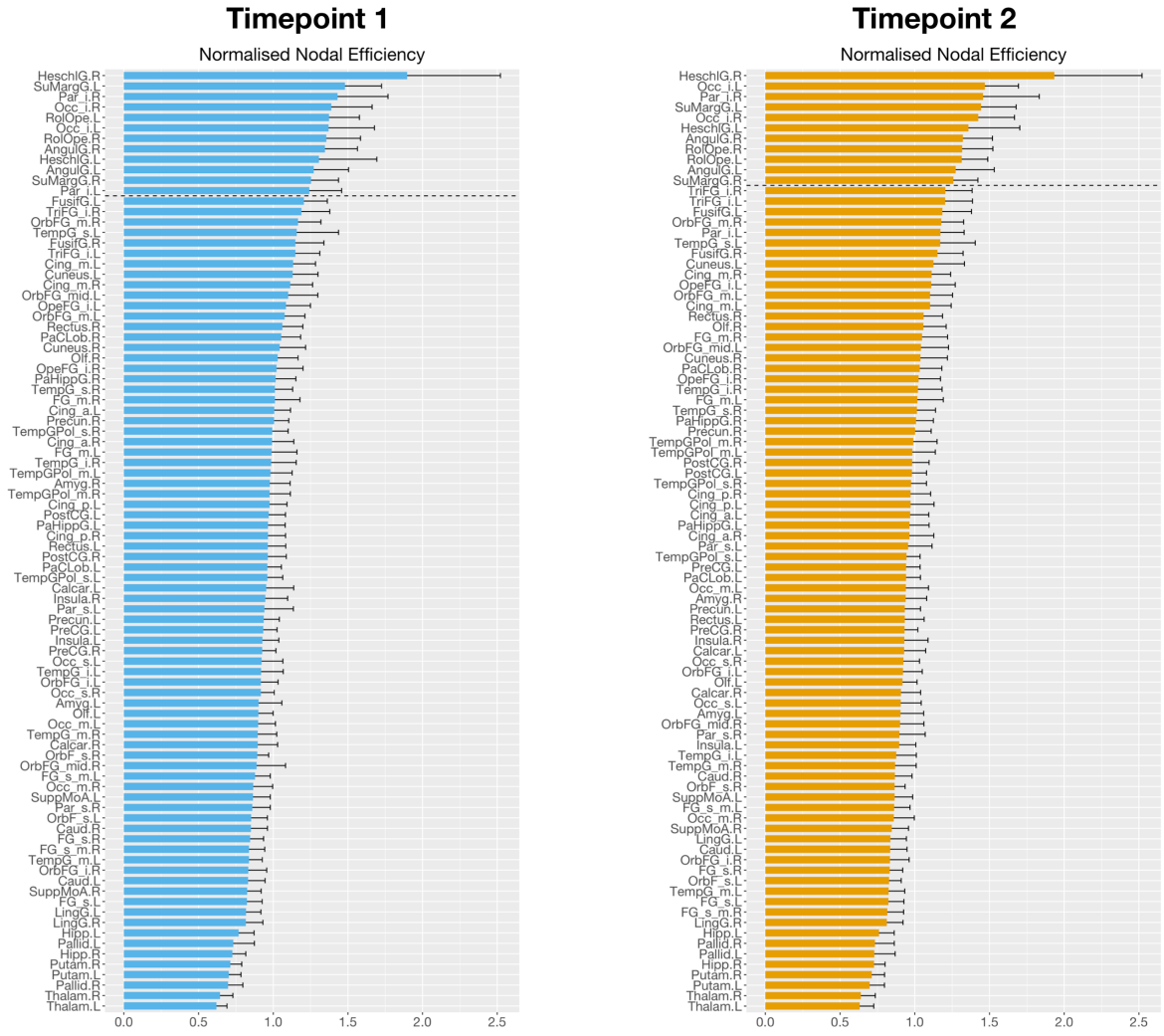

Figure 5. Global hubs identified in the two timepoints as measured by the normalized nodal efficiency. Here, we observe the plot of the normalized nodal efficiency for all the 90 AAL regions, sorted in descending order of efficiency values, for timepoint 1 (left) and timepoint 2 (right). We observe a reorganization of brain structural networks in aging, characterized by the loss of two hubs (left inferior parietal cortex and left fusiform gyrus).

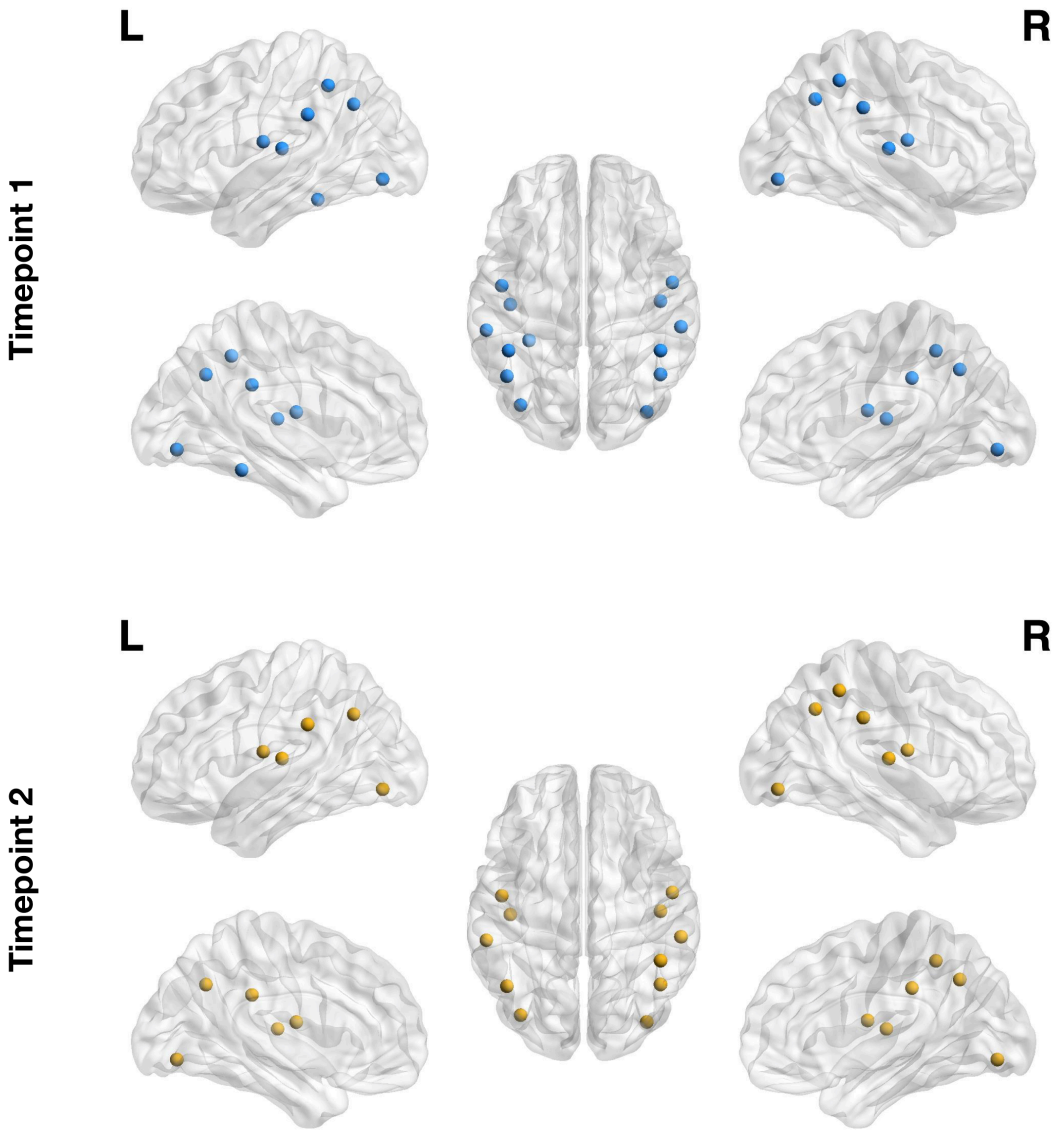

Figure 6. Global hubs identified in the two timepoints as measured by the normalized nodal efficiency. Here, we represent in the brain the identified hubs for timepoint 1 (top row) and timepoint 2 (bottom row). We observe a reorganization of brain structural networks in aging, characterized by the loss of two hubs (left inferior parietal cortex and left fusiform gyrus).

Table 5. Hubs of the brain for the two timepoints, according to three classification methods used. Global hubs are sorted by nodal efficiency, and provincial and connector hubs are sorted by modularity degree z-score.

Global Hubs		Provincial Hubs		Connector Hubs	
M1	M2	M1	M2	M1	M2
Heschl R	Heschl R	Frontal Sup Orb L	Rolandic Operculum R	Cingulum Mid R	Occipital Mid L
SupraMarginal L	Occipital Inf L	ParaHippocampal R	ParaHippocampal R	Postcentral Gyrus L	Putamen R
Parietal Inf R	Parietal Inf R	Insula R	Temporal Inf L	Caudate L	Postcentral Gyrus R
Occipital Inf R	SupraMarginal L	Parietal Inf L	Rectus R	Putamen L	Putamen L
Rolandic Operculum L	Occipital Inf R	Rolandic Operculum L	Parietal Inf R	Putamen R	
Occipital Inf L	Heschl L	Rectus L	Frontal Med Orb R		
Rolandic Operculum R	Angular R	Fusiform L	Caudate R		
Angular R	Rolandic Operculum R	Fusiform R	Fusiform L		
Heschl L	Rolandic Operculum L		Fusiform R		
Angular L	Angular L		Insula L		
SupraMarginal R	SupraMarginal R				
Parietal Inf L					
Fusiform L					

Abbreviations: M1, Timepoint 1; M2, Timepoint 2.

In the case of the provincial hubs, which play a central role in intra-modular communication, eight hubs were detected at timepoint 1 and ten at timepoint 2. Only the right parahippocampal and bilateral fusiform gyrus were detected at both timepoints (Table 5).

Connector hubs represent a central role in inter-modular communication. At timepoint 1, five regions were identified as connector hubs, while at timepoint 2 only four regions were detected (Table 5). Left and right putamen were common to both timepoints.

5.5.3. Modularity

The optimal modularity structure had six modules at both timepoints, and the two arrangements had a similarity of 0.80. Modules 4, 5 and 6 were common to both partitions. Module 3 changed from a leftward

lateralization at timepoint 1 to a rightward lateralization at timepoint 2, which caused slight differences in the arrangement of the frontal regions of modules 1 and 2 (Fig. 7A). Details of the regions belonging to each module are given in Supplementary Table 3. Furthermore, analyzing the connectivity profile of the connector hubs (Fig. 7B), we observe distinct patterns at the two timepoints. Even regions that were classified as connector hubs at both timepoints (left and right putamen), have different profiles of connectivity.

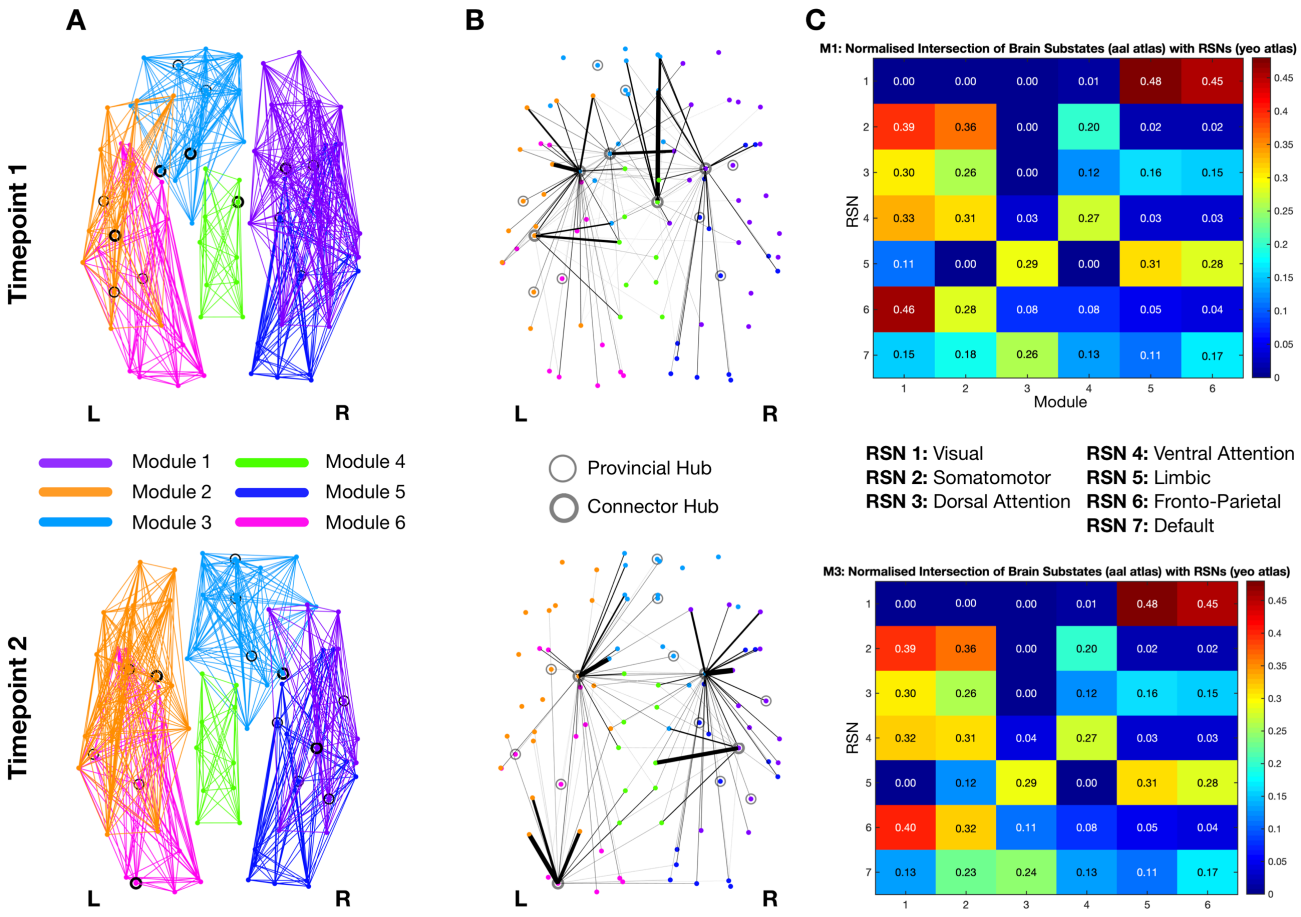

Figure 7. Modularity structure (A), connector-hub connectivity (B) and matrices of RSNs overlap (C) at timepoint 1 (top row) and timepoint 2 (bottom row). Filled circles represent connector hubs and unfilled circles represent provincial hubs. Although very similar modular arrangements were found at both timepoints (A, B), the undirected structural connectivity profile for the connector hubs was different (C). These differences are probably due to the loss of two connector hubs from first to last timepoint, namely left caudate and right midcingulate cortex, while left middle occipital gyrus was identified as a connector hub only in the last timepoint. Giving the role of connector hubs in inter-modular communication, the

reduction in their number between timepoints reflects a decrease in integration of brain structural networks in aging.

Regarding the overlap between modules and RSNs, despite their differences in the arrangement, the percentage of overlap has only very subtle differences in the first three modules. Module 1 has the highest overlap with both fronto-parietal and somatomotor networks, with slightly higher overlap with fronto-parietal network at timepoint 1. Module 2 again overlaps with fronto-parietal (higher value at timepoint 2) and somatomotor, but also with the ventral attention network, and module 3 overlaps with limbic and default mode networks with higher value for the limbic network at both timepoints. In relation to the last three modules, module 4 overlaps with limbic and somatomotor networks, and modules 5 and 6 with visual and limbic networks. The matrices with the values of overlap at both timepoints are represented in Figure 7C.

5.5.4. Fingerprints of Modular Connectivity

The reference scheme chosen to analyze fingerprints of modular connectivity was the community structure of timepoint 2. Significant alterations in connector-hub driven inter-modular connectivity were found (Fig. 8). From timepoint 1 to timepoint 2, a decrease of around 19% of overall connectivity is found. Focusing on the specific connections that contribute to this decrease, at timepoint 1, we observe increased connectivity from module 2 (left hemisphere; frontal and parietal regions, insula, supramarginal, angular, putamen, pallidum, thalamus and superior temporal gyrus) to module 4 (bilateral supplementary motor area, middle and posterior cingulate cortex, precuneus and paracentral lobule) as well as from module 3 (frontal regions most on the right hemisphere, bilateral anterior cingulate cortex, caudate, right putamen, right pallidum and right thalamus) to modules 2, 4 and 6 (left hemisphere; occipital and temporal regions, hippocampus, parahippocampal, amygdala, calcarine, cuneus, lingual and fusiform gyrus). Of notice, at timepoint 1 there are two connector hubs that belong to module 2 (left postcentral gyrus and left putamen) and also two connector hubs in module 3 (left caudate and right putamen), while at timepoint 2 there is only one connector hub in each of these modules (left putamen in module 2 and right putamen in module 3). Furthermore, modules 1 and 6, at timepoint 1, have no connectivity with any other modules, and the same happens with module 4 in timepoint 2 and module 5 at both timepoints. This is because there is a lack of connector hubs belonging to any of these modules, at the referred timepoints. No differences were found for intra-modular and inter-modular connectivity.

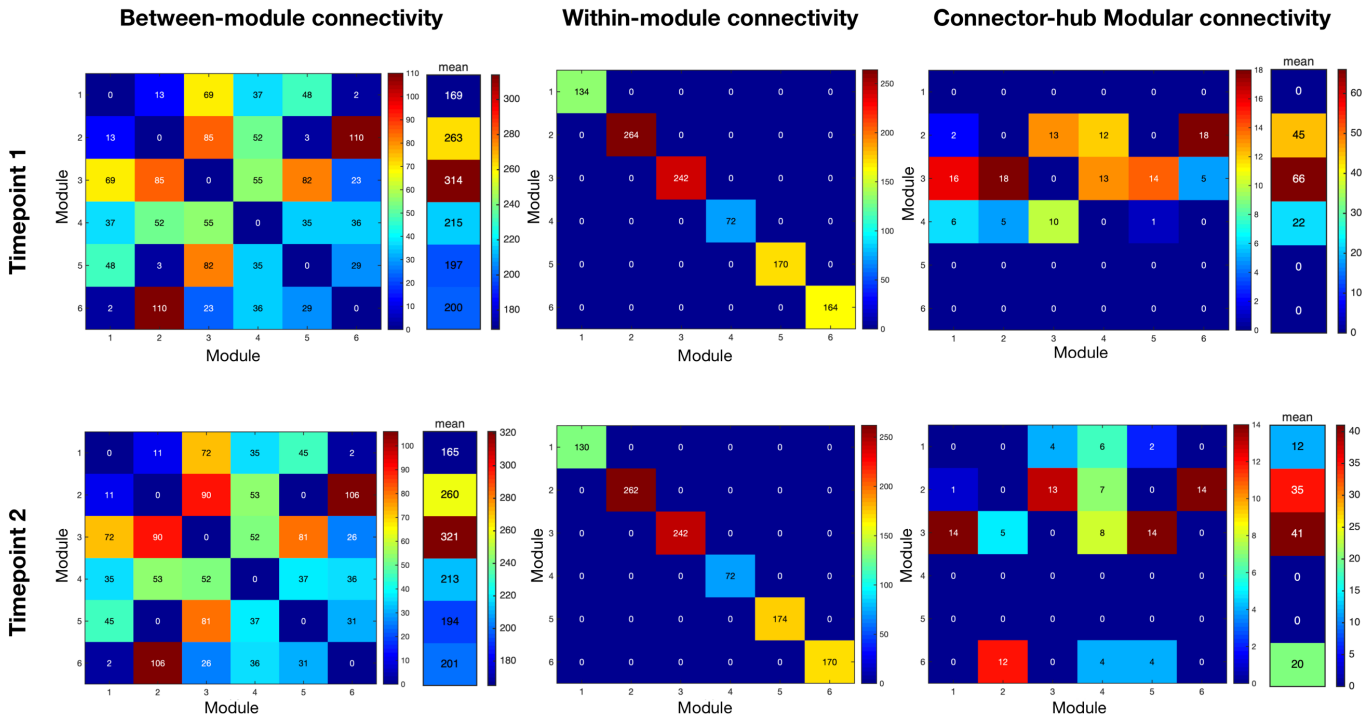

Figure 8. Fingerprints of modular connectivity at timepoint 1 (top row) and timepoint 2 (bottom row). Left column represents the inter-modular connectivity, middle column the intra-module connectivity and right column the connector-hub driven inter-modular connectivity. Modular connectivity strength is quantified as the total number of connections (degree) of all nodes forming a module. Community structure of timepoint 2 was selected as the reference scheme, since it had higher group goodness-of-fit. We observe different patterns only in connector-hub driven inter-modular connectivity. Overall, there was a decrease of around 19% in this connectivity between timepoints, which is probably due to the loss of one connector hub. This results again suggests a decrease in integration of brain SC during aging.

6. Discussion

In this study, we explored the longitudinal changes in the topological organization of brain structural networks in normal aging, using diffusion magnetic resonance imaging. Our results revealed both decreases and increases in white matter structural connectivity along time. Interestingly, the sub-network with decreasing connectivity is composed mainly of intra-hemispheric connections, while inter-hemispheric connections are in majority in the sub-network of increases. Both networks are mainly comprised by connections between subcortical and frontal regions. This differential pattern of changes in different types of connections could be explained by the last-in-first-out hypothesis, which claims that

regions developing later are more prone to age-related decline (Raz, 1999). In terms of white matter tracts, association fibers, that connect different regions within a hemisphere, have a later peak of maturation when compared to commissural fibers that connect regions between the two hemispheres (Hermoye et al., 2006). According to this hypothesis it is expected that association fibers will undergo a steeper decline in comparison to commissural fibers, which was already demonstrated in studies of white matter microstructural properties indirectly estimated from DTI-based metrics (Bender et al., 2016; Brickman et al., 2012; Davis et al., 2009; Slater et al., 2019). Our results are in line with these findings, since intra-hemispheric links decline along aging, while inter-hemispheric links appear to be maintained and even enhanced. This enhance in connectivity between hemispheres along aging, has been reported in recent functional studies. One such study found stronger functional connectivity between bilateral frontoparietal control network that was associated with better cognition in the visuospatial domain (Jiang et al., 2020). Moreover, there are also reports of increased bilateral frontal activation in episodic memory retrieval tasks, for high-performing older adults (Cabeza et al., 2002). Another study found that higher cognitive status in healthy older adults was associated with higher between-network and inter-hemispheric functional connectivity (Sullivan et al., 2019). Our findings add to this evidence by demonstrating that this increase in bilateral connectivity also occurs in structural connectivity. In terms of white matter structural connectivity, there are few reports showing age-related increases. Of those, Lee and colleagues (Lee et al., 2015) found age-related increases between the prefrontal cortex and temporal regions, and between occipital and posterior brain regions. In our study, we found age-related increases between frontal and subcortical regions.

Our analysis of the WM tracts involved in the connections of each sub-network further supports the last-in-first-out hypothesis. The sub-network with decreases in SC was mainly composed of association fibers, with only one commissural fiber (forceps minor). While the sub-network with increases in SC, although it also included association fibers, was comprised by many commissural and projection fibers. It should be noted that connections with increasing connectivity are mainly inter-hemispheric, so it is very probable that the corpus callosum is involved in all these connections. Association fibers are the latest to develop in comparison to commissural and projection fibers and previous studies have reported more pronounced decline of DTI-based metrics for association fibers, which may possibly indicate a steepest decline in WM integrity (Bender et al., 2016; Benitez et al., 2018; Bennett and Madden, 2014; Cox et al., 2016; de Groot et al., 2015). Our results conform with these findings by demonstrating that disruption in WM structural connectivity occurs primarily in association fibers.

Furthermore, we analyzed the association between the mean connectivity of these sub-networks and cognitive scores of memory (MEM) and global cognition and executive function (EXEC). We found a trend in the correlation between the sub-network of increases and EXEC. Specifically, higher SC values were associated with lower EXEC scores. Previous studies reported that age-related functional connectivity increase was associated with poorer cognitive performance (Chen et al., 2019; Nashiro et al., 2017). Our finding is in line with the dedifferentiation hypothesis of the aging brain, which suggests that age is accompanied by a loss of specificity in the neural response to cognitive tasks (Chan et al., 2014; Dennis and Cabeza, 2011; Geerligs et al., 2015, 2014; Goh, 2011; Park et al., 2004). Our result on structural connectivity might suggest that the increase in SC is necessary to recruit additional areas in order to try to compensate for the cognitive decline these older adults are experiencing. Although we still see a decline in cognitive performance, this increase in SC is probably critical for the older adults to be able to perform cognitive tasks. Further research will be needed to confirm that this association reflects a compensatory mechanism.

Analysis of the topological features of brain white matter structural networks revealed some, although few, longitudinal alterations. No significant differences were found in most of the analyzed graph metrics, namely, node degree, connection density, global and local efficiency. Although some studies report age-related declines in some of these metrics, others present null results. Regarding global efficiency, (Wen et al., 2011; Zhao et al., 2015) report reduced global efficiency in advanced ages, whereas (Gong et al., 2009) found no significant age effect on this metric. Thus, the existence of controversial results might explain the lack of significant results in our study. Moreover, the limited sample size used in this study is a limitation which may have contributed to the lack of significant alterations in these measures. Characteristic path length was the only metric found to be significantly different between timepoints, having lower values in the last timepoint. This finding means that the average shortest path length between all possible pairs of nodes in the network was lower in the last assessment and thus, globally, the communication between different regions was more efficient. This result is not in accordance with earlier studies which reported increases in characteristic path length (Fischer et al., 2014; Zhu et al., 2012), but it should be noted that the effect size for this significant difference was rather small ($d = 0.29$) and this metric is inversely related to global efficiency, in which we found no significant differences.

In nodal efficiency, differences were found between assessments, with the loss of two hubs (left inferior parietal and left fusiform gyrus) from the first to last timepoint. Left inferior parietal cortex (IPC) is known to be associated with language processing, namely reading, phonology and semantic processing (Amici

et al., 2006; Gorno-Tempini et al., 2004; Graves et al., 2010; Price and Mechelli, 2005; Turkeltaub and Branch Coslett, 2010; Vigneau et al., 2006). Additionally, it also plays a significant role in episodic memory (Wagner et al., 2005), attention (Corbetta and Shulman, 2002; Fan et al., 2005), action and salience processing (Behrmann et al., 2004; Caspers et al., 2010; Iacoboni, 2005), and social cognition (Bzdok et al., 2016). It is also an important node of the default mode network (DMN) (Greicius et al., 2003). Previous aging studies have found age-related changes in the functional connectivity (FC) of this region and an association between these changes and cognitive decline in different domains, specifically, executive function (Lou et al., 2019; Zhao et al., 2020), semantic knowledge (Hoffman and Morcom, 2018), inhibitory control (Hu et al., 2018) and memory (Huo et al., 2018; Lamichhane et al., 2018). In line with our results, there is evidence of the loss of hub role for left IPC in aging, which was demonstrated using cortical thickness covariance networks (Carey et al., 2019). Regarding fusiform gyrus, this region is involved in object recognition (Grill-Spector et al., 2001), face perception (Kanwisher et al., 1997), including haptic and visual identification of faces (Kitada et al., 2009), reading (Cohen et al., 2000; Wandell et al., 2007) and memory (Wagner et al., 1999). Functional studies of aging using face recognition tasks have demonstrated a relationship between patterns of activation in the fusiform gyrus and age-related declines in face recognition or perception (Dennis et al., 2008; Lee et al., 2011; Wright et al., 2008). There is also evidence of age-related atrophy of the fusiform gyrus (Hogstrom et al., 2013; Shah et al., 2020). Supporting our results, previous studies found the loss of hub role for the left fusiform characterized by reduced betweenness centrality in cortical networks of regional gray matter volumes (Li et al., 2018).

Concerning modularity structure, we found very similar modular arrangements at both timepoints, with only some differences in frontal regions. Regarding fingerprints of modular connectivity, longitudinal differences were found in connector-hub driven inter-modular connectivity. Overall, there was a decrease of around 19% in this connectivity from timepoint 1 to timepoint 2, which could be the result of the loss of one connector hub. This decrease suggests a reduction of integration of brain structural networks during aging, since connector hubs play an important role in inter-modular communication (characterized by high participation coefficient) and thus, there is less communication between different functional modules of the brain. There is already evidence suggesting a decrease in integration and increase in segregation of brain functional networks during the aging process (Sala-Llonch et al., 2014).

Between assessments, two regions lost their connector hub role, namely left caudate and right midcingulate cortex, while left middle occipital gyrus was identified as a connector hub only at the last

timepoint. Both left caudate and right midcingulate cortex were part of the identified sub-network with decreases in connectivity between timepoints. Thus, this decrease in the anatomical connections between either left caudate or right midcingulate cortex and other regions of the brain would be expected to isolate these two regions and could explain the loss of these two nodes as connector hubs. Caudate is associated with different aspects of cognition, including motor and action planning, decision-making (particularly, goal-directed behavior), motivation and reward processing (Bick et al., 2019; Grahn et al., 2008; Tartaro, 2019; Wilson, 2018). Previous studies exploring age-related changes in the caudate have shown associations with different cognitive domains, such as episodic memory (Fjell et al., 2016b; Rieckmann et al., 2018), instrumental learning (Perosa et al., 2020), cognitive flexibility (Verstynen et al., 2012) and reward processing (Bowen et al., 2020; Dhingra et al., 2020). Interestingly, (Esteves et al., 2018) reported that older adults had overall longitudinal rightward lateralization of the caudate volume and subjects with extreme increase in this rightward asymmetry had increased Stroop interference scores (i.e. a measure of cognitive flexibility) but decreased scores of general cognition. Our results provide additional support to this, by showing that the left caudate also loses its role of integrating different regions of the brain. Midcingulate cortex is associated with motor control (from self-initiated movements to reflexive motor activity), and also with the response to acute nociceptive stimuli, fear and pain (Hoffstaedter et al., 2015; Vogt, 2016). A previous study found age-related reductions in FC between dorsal anterior insula and midcingulate cortex, which are part of the dorsal salience sub-network and these changes were found to be a mediator of age-related declines in executive function (Touroutoglou et al., 2018). Another study elucidated the role of midcingulate cortex in motor functions. Specifically, this region is involved in a network associated with intentional movement initiation and it was found to present decreased FC with anterior cingulate motor area in aging, and there was also a decrease of gray matter volume with age (Hoffstaedter et al., 2015). These previous studies suggesting decreased connectivity and atrophy of this region with aging could explain the loss of connector hub status of the midcingulate cortex in our results.

At the last timepoint, left middle occipital gyrus emerged as a connector hub. This region is associated with visual information processing and communication (Anurova et al., 2015; Teng et al., 2018; Wandell et al., 2007), and also plays a role in the perception of facial emotion as well as in category-selective attention modulating unconscious face/tool processing (Tu et al., 2013). Previous studies found age-related differences in the patterns of activation of the middle occipital gyrus during visual tasks (Berghuis et al., 2019; Piefke et al., 2012). Additionally, in a study of autobiographical memory retrieval, increases in activation of middle occipital gyrus in older adults were found during episodic memory retrieval, which could reflect a compensatory mechanism due to impairment of vivid visual imagery, or higher use of

visuospatial processing during episodic memory retrieval (Donix et al., 2010). This compensatory increase in activation of middle occipital gyrus might explain its appearance as a connector hub at the last timepoint.

Lastly, there was an increase of detected provincial hubs along time, which may reflect higher segregation/specialization of structural networks. These hubs are characterized by having most of their connections within their own module and thus play a key role in intra-modular communication. The additional regions detected at timepoint 2 were right caudate and left inferior temporal gyrus. As described before, caudate was found to have a rightward asymmetry in aging, what may explain the gain of provincial hub status along time. Inferior temporal gyrus is associated with semantic processing, particularly the selection and controlled retrieval of information from memory (Thompson-Schill, 2003), and it has also been involved in intelligence and executive function (Jung and Haier, 2007). Some studies report relative preservation of cortical thickness of this region until later in life (Fjell et al., 2009; Lee et al., 2018), and this can be related to the preservation of semantic memory also observed in aging (Gold et al., 2009). Our results also support the maintenance of this region along aging as it was characterized as an important hub of the brain network in the last timepoint.

This study has some limitations, particularly the low sample size and the period between evaluations. This could explain why there were almost no differences in graph theory metrics, and thus an extended period of evaluation and a larger sample could allow to observe differences in these measures. Another limitation is the use of a 1.5T MRI scanner which has lower signal to noise ratio (SNR) when compared to 3T MRI scanners (Lee and Shannon, 2007). Future studies will benefit from using a 3T scanner, which will allow to obtain high-quality images. While these limitations may have had some influence on the obtained results (changes in network connectivity, hubs and modularity structure), we believe these effects were minimal since the same protocol (same scanner, acquisition parameters and data processing pipeline) was used at both evaluations.

In summary, our findings bring further support of the existing evidence of the reorganization of brain structural networks during aging. Specifically, we found decreases in intra-hemispheric connectivity and increases in inter-hemispheric connectivity. Association fibers were primarily responsible for the decreases in white matter structural connectivity and their functional loss is consistent with the last-in-first-out hypothesis. Additionally, we found a trend for an association between cognition and a sub-network with increasing connectivity, exhibiting lower general cognition and executive functioning scores for higher

SC values, possibly suggesting some form of a compensatory mechanism. Regarding topological features of brain networks, we found evidence suggesting reduced integration, characterized by a decrease in connector-hub driven inter-modular connectivity, and increased segregation, portrayed as an increase in the number of detected provincial hubs, of brain structural networks in aging. Taken together, these findings elucidate the changes occurring in the brain during aging, in terms of communication between the hemispheres and between specialized modules. This can help identify brain regions responsible for this disruption, that could be targeted as biomarkers to prevent cognitive decline in aging.

7. References

Achard, S., Bullmore, E., 2007. Efficiency and cost of economical brain functional networks. PLoS Computational Biology 3, 174–183. https://doi.org/10.1371/journal.pcbi.0030017

Amici, S., Gorno-Tempini, M.L., Ogar, J.M., Dronkers, N.F., Miller, B.L., 2006. An Overview on Primary Progressive Aphasia and Its Variants. Behavioural Neurology 17, 77–87. https://doi.org/10.1155/2006/260734

Andrews-Hanna, J.R., Snyder, A.Z., Vincent, J.L., Lustig, C., Head, D., Raichle, M.E., Buckner, R.L., 2007. Disruption of Large-Scale Brain Systems in Advanced Aging. Neuron 56, 924–935. https://doi.org/10.1016/j.neuron.2007.10.038.Disruption

Antonenko, D., Flöel, A., 2013. Healthy aging by staying selectively connected: A mini-review. Gerontology 60, 3–9. https://doi.org/10.1159/000354376

Anurova, I., Renier, L.A., De Volder, A.G., Carlson, S., Rauschecker, J.P., 2015. Relationship Between Cortical Thickness and Functional Activation in the Early Blind. Cerebral Cortex 25, 2035–2048. https://doi.org/10.1093/cercor/bhu009

Bakdash, J.Z., Marusich, L.R., 2017. Repeated Measures Correlation. Frontiers in Psychology 8. https://doi.org/10.3389/fpsyg.2017.00456

Bartzokis, G., 2004. Age-related myelin breakdown: a developmental model of cognitive decline and Alzheimer's disease. Neurobiology of Aging 25, 5–18. https://doi.org/10.1016/j.neurobiolaging.2003.03.001

Bassett, D.S., Bullmore, E., Verchinski, B.A., Mattay, V.S., Weinberger, D.R., Meyer-Lindenberg, A., 2008. Hierarchical Organization of Human Cortical Networks in Health and Schizophrenia. Journal of Neuroscience 28, 9239–9248. https://doi.org/10.1523/JNEUROSCI.1929-08.2008

Behrens, T.E.J., Berg, H.J., Jbabdi, S., Rushworth, M.F.S., Woolrich, M.W., 2007. Probabilistic diffusion tractography with multiple fibre orientations: What can we gain? NeuroImage 34, 144–155. https://doi.org/10.1016/j.neuroimage.2006.09.018

Behrmann, M., Geng, J.J., Shomstein, S., 2004. Parietal cortex and attention. Current Opinion in Neurobiology 14, 212–217. https://doi.org/10.1016/j.conb.2004.03.012

Bender, A.R., Völkle, M.C., Raz, N., 2016. Differential aging of cerebral white matter in middle-aged and older adults: A seven-year follow-up. NeuroImage 125, 74–83. https://doi.org/10.1016/j.neuroimage.2015.10.030

Benitez, A., Jensen, J.H., Falangola, M.F., Nietert, P.J., Helpern, J.A., 2018. Modeling white matter tract integrity in aging with diffusional kurtosis imaging. Neurobiology of Aging 70, 265–275. https://doi.org/10.1016/j.neurobiolaging.2018.07.006

Bennett, I.J., Madden, D.J., 2014. Disconnected aging: Cerebral white matter integrity and age-related differences in cognition. Neuroscience 276, 187–205. https://doi.org/10.1016/j.neuroscience.2013.11.026

Berghuis, K.M.M., Fagioli, S., Maurits, N.M., Zijdewind, I., Marsman, J.B.C., Hortobágyi, T., Koch, G., Bozzali, M., 2019. Age-related changes in brain deactivation but not in activation after motor learning. NeuroImage 186, 358–368. https://doi.org/10.1016/j.neuroimage.2018.11.010

Bernard, C., Dilharreguy, B., Helmer, C., Chanraud, S., Amieva, H., Dartigues, J.-F., Allard, M., Catheline, G., 2015. PCC characteristics at rest in 10-year memory decliners. Neurobiology of Aging 36, 2812–2820. https://doi.org/10.1016/j.neurobiolaging.2015.07.002

Betzel, R.F., Byrge, L., He, Y., Goñi, J., Zuo, X.N., Sporns, O., 2014. Changes in structural and functional connectivity among resting-state networks across the human lifespan. NeuroImage 102, 345–357. https://doi.org/10.1016/j.neuroimage.2014.07.067

Bick, S.K., Patel, S.R., Katnani, H.A., Peled, N., Widge, A., 2019. Caudate stimulation enhances learning. Brain 142, 8.

Blondel, V.D., Guillaume, J.-L., Lambiotte, R., Lefebvre, E., 2008. Fast unfolding of communities in large networks. Journal of Statistical Mechanics: Theory and Experiment 2008, P10008. https://doi.org/10.1088/1742-5468/2008/10/p10008

Bowen, H.J., Ford, J.H., Grady, C.L., Spaniol, J., 2020. Frontostriatal functional connectivity supports reward-enhanced memory in older adults. Neurobiology of Aging 90, 1–12. https://doi.org/10.1016/j.neurobiolaging.2020.02.013

Bressler, S.L., Menon, V., 2010. Large-scale brain networks in cognition: emerging methods and principles. Trends in Cognitive Sciences 14, 277–290. https://doi.org/10.1016/j.tics.2010.04.004

Brickman, A.M., Meier, I.B., Korgaonkar, M.S., Provenzano, F.A., Grieve, S.M., Siedlecki, K.L., Wasserman, B.T., Williams, L.M., Zimmerman, M.E., 2012. Testing the white matter retrogenesis hypothesis of cognitive aging. Neurobiology of Aging 33, 1699–1715. https://doi.org/10.1016/j.neurobiolaging.2011.06.001

Bullmore, E.T., Sporns, O., 2009. Complex brain networks: graph theoretical analysis of structural and functional systems. Nature reviews. Neuroscience 10, 186–198. https://doi.org/10.1038/nrn2575

Bzdok, D., Hartwigsen, G., Reid, A., Laird, A.R., Fox, P.T., Eickhoff, S.B., 2016. Left inferior parietal lobe engagement in social cognition and language. Neuroscience & Biobehavioral Reviews 68, 319–334. https://doi.org/10.1016/j.neubiorev.2016.02.024

Cabeza, R., Anderson, N.D., Locantore, J.K., McIntosh, A.R., 2002. Aging Gracefully: Compensatory Brain Activity in High-Performing Older Adults. NeuroImage 17, 1394–1402. https://doi.org/10.1006/nimg.2002.1280

Cao, M., Wang, J.H., Dai, Z.J., Cao, X.Y., Jiang, L.L., Fan, F.M., Song, X.W., Xia, M.R., Shu, N., Dong, Q., Milham, M.P., Castellanos, F.X., Zuo, X.N., He, Y., 2014. Topological organization of the human brain functional connectome across the lifespan. Developmental Cognitive Neuroscience 7, 76–93. https://doi.org/10.1016/j.dcn.2013.11.004

Carey, D., Nolan, H., Kenny, R.A., Meaney, J., 2019. Cortical covariance networks in ageing: Cross-sectional data from the Irish Longitudinal Study on Ageing (TILDA). Neuropsychologia 122, 51–61. https://doi.org/10.1016/j.neuropsychologia.2018.11.013

Caspers, S., Zilles, K., Laird, A.R., Eickhoff, S.B., 2010. ALE meta-analysis of action observation and imitation in the human brain. NeuroImage 50, 1148–1167. https://doi.org/10.1016/j.neuroimage.2009.12.112

Chan, M.Y., Park, D.C., Savalia, N.K., Petersen, S.E., Wig, G.S., 2014. Decreased segregation of brain systems across the healthy adult lifespan. Proceedings of the National Academy of Sciences 111, E4997–E5006. https://doi.org/10.1073/pnas.1415122111

Chen, X., Huang, L., Ye, Q., Yang, D., Qin, R., Luo, C., Li, M., Zhang, B., Xu, Y., 2019. Disrupted functional and structural connectivity within default mode network contribute to WMH-related cognitive impairment. NeuroImage: Clinical 24, 102088. https://doi.org/10.1016/j.nicl.2019.102088

Cohen, L., Dehaene, S., Naccache, L., Lehericy, S., Henaff, M.-A., Michel, F., 2000. The visual word form area. Brain 123, 17.

Corbetta, M., Shulman, G.L., 2002. Control of goal-directed and stimulus-driven attention in the brain. Nature Reviews Neuroscience 3, 201–215. https://doi.org/10.1038/nrn755

Costa, P.S., Santos, N.C., Cunha, P., Palha, J.A., Sousa, N., 2013. The Use of Bayesian Latent Class Cluster Models to Classify Patterns of Cognitive Performance in Healthy Ageing. PLoS ONE 8. https://doi.org/10.1371/journal.pone.0071940

Cox, S.R., Ritchie, S.J., Tucker-Drob, E.M., Liewald, D.C., Hagenaars, S.P., Davies, G., Wardlaw, J.M., Gale, C.R., Bastin, M.E., Deary, I.J., 2016. Ageing and brain white matter structure in 3,513 UK Biobank participants. Nature Communications 7. https://doi.org/10.1038/ncomms13629

Craddock, R.C., Jbabdi, S., Yan, C.-G., Vogelstein, J.T., Castellanos, F.X., Di Martino, A., Kelly, C., Heberlein, K., Colcombe, S., Milham, M.P., 2013. Imaging human connectomes at the macroscale. Nature Methods 10, 524–539. https://doi.org/10.1038/nmeth.2482

Damoiseaux, J.S., 2017. Effects of aging on functional and structural brain connectivity. NeuroImage 1–9. https://doi.org/10.1016/j.neuroimage.2017.01.077

Davis, S.W., Dennis, N.A., Buchler, N.G., White, L.E., Madden, D.J., Cabeza, R., 2009. Assessing the effects of age on long white matter tracts using diffusion tensor tractography. NeuroImage 46, 530–541. https://doi.org/10.1016/j.neuroimage.2009.01.068

de Groot, M., Ikram, M.A., Akoudad, S., Krestin, G.P., Hofman, A., van der Lugt, A., Niessen, W.J., Vernooij, M.W., 2015. Tract-specific white matter degeneration in aging: The Rotterdam Study. Alzheimer's & Dementia 11, 321–330. https://doi.org/10.1016/j.jalz.2014.06.011

Dennis, N.A., Cabeza, R., 2011. Age-related dedifferentiation of learning systems: an fMRI study of implicit and explicit learning. Neurobiology of Aging 32, 2318.e17-2318.e30. https://doi.org/10.1016/j.neurobiolaging.2010.04.004

Dennis, N.A., Hayes, S.M., Prince, S.E., Madden, D.J., Huettel, S.A., Cabeza, R., 2008. Effects of aging on the neural correlates of successful item and source memory encoding. Journal of Experimental Psychology: Learning, Memory, and Cognition 34, 791–808. https://doi.org/10.1037/0278-7393.34.4.791

Dhingra, I., Zhang, S., Zhornitsky, S., Le, T.M., Wang, W., Chao, H.H., Levy, I., Li, C.-S.R., 2020. The effects of age on reward magnitude processing in the monetary incentive delay task. NeuroImage 207, 116368. https://doi.org/10.1016/j.neuroimage.2019.116368

Donix, M., Poettrich, K., Weiss, P.H., Werner, A., von Kummer, R., Fink, G.R., Holthoff, V.A., 2010. Age-Dependent Differences in the Neural Mechanisms Supporting Long-Term Declarative Memories. Archives of Clinical Neuropsychology 25, 383–395. https://doi.org/10.1093/arclin/acq037

Esteves, M., Moreira, P.S., Marques, P., Castanho, T.C., Magalhães, R., Amorim, L., Portugal-Nunes, C., Soares, J.M., Coelho, A., Almeida, A., Santos, N.C., Sousa, N., Leite-Almeida, H., 2018. Asymmetrical subcortical plasticity entails cognitive progression in older individuals. Aging Cell 18, e12857. https://doi.org/10.1111/acel.12857

Fan, J., Mccandliss, B., Fossella, J., Flombaum, J., Posner, M., 2005. The activation of attentional networks. NeuroImage 26, 471–479. https://doi.org/10.1016/j.neuroimage.2005.02.004

Fernandes, H.M., Cabral, J., van Hartevelt, T.J., Lord, L.-D., Gleesborg, C., Møller, A., Deco, G., Whybrow, P.C., Petrovic, P., James, A.C., Kringelbach, M.L., 2019. Disrupted brain structural connectivity in Pediatric Bipolar Disorder with psychosis. Scientific Reports 9. https://doi.org/10.1038/s41598-019-50093-4

Fischer, F.U., Wolf, D., Scheurich, A., Fellgiebel, A., 2014. Association of structural global brain network properties with intelligence in normal aging. PLoS ONE 9. https://doi.org/10.1371/journal.pone.0086258

Fjell, A.M., Sneve, M.H., Grydeland, H., Storsve, A.B., Walhovd, K.B., 2017. The Disconnected Brain and Executive Function Decline in Aging. Cerebral cortex (New York, N.Y. : 1991) 27, 2303–2317. https://doi.org/10.1093/cercor/bhw082

Fjell, A.M., Sneve, M.H., Storsve, A.B., Grydeland, H., Yendiki, A., Walhovd, K.B., 2016. Brain Events Underlying Episodic Memory Changes in Aging: A Longitudinal Investigation of Structural and Functional Connectivity. Cerebral Cortex 26, 1272–1286. https://doi.org/10.1093/cercor/bhv102

Fjell, A.M., Westlye, L.T., Amlien, I., Espeseth, T., Reinvang, I., Raz, N., Agartz, I., Salat, D.H., Greve, D.N., Fischl, B., Dale, A.M., Walhovd, K.B., 2009. High Consistency of Regional Cortical Thinning in Aging across Multiple Samples. Cerebral Cortex 19, 2001–2012. https://doi.org/10.1093/cercor/bhn232

Fornito, A., Zalesky, A., Bullmore, E.T., 2016. Fundamentals of Brain Network Analysis. Academic Press, San Diego.

Geerligs, L., Maurits, N.M., Renken, R.J., Lorist, M.M., 2014. Reduced specificity of functional connectivity in the aging brain during task performance: Functional Connectivity in the Aging Brain. Human Brain Mapping 35, 319–330. https://doi.org/10.1002/hbm.22175

Geerligs, L., Renken, R.J., Saliasi, E., Maurits, N.M., Lorist, M.M., 2015. A Brain-Wide Study of Age-Related Changes in Functional Connectivity. Cerebral Cortex 25, 1987–1999. https://doi.org/10.1093/cercor/bhu012

Geschwind, N., 1965a. Disconnexion syndromes in animal and man. Part I. Brain 88, 237–294.

Geschwind, N., 1965b. Disconnexion syndromes in animal and man. Part II. Brain 88, 585–644.

Goh, J.O.S., 2011. Functional Dedifferentiation and Altered Connectivity in Older Adults: Neural Accounts of Cognitive Aging. Aging and Disease 2, 19.

Gold, B.T., Andersen, A.H., Jicha, G.A., Smith, C.D., 2009. Aging Influences the Neural Correlates of Lexical Decision but Not Automatic Semantic Priming. Cerebral Cortex 19, 2671–2679. https://doi.org/10.1093/cercor/bhp018

Gong, G., Rosa-Neto, P., Carbonell, F., Chen, Z.J., He, Y., Evans, A.C., 2009. Age- and Gender-Related Differences in the Cortical Anatomical Network. Journal of Neuroscience 29, 15684–15693. https://doi.org/10.1523/JNEUROSCI.2308-09.2009

Good, B.H., de Montjoye, Y.-A., Clauset, A., 2010. Performance of modularity maximization in practical contexts. Phys. Rev. E 81, 046106. https://doi.org/10.1103/PhysRevE.81.046106

Gorno-Tempini, M.L., Dronkers, N.F., Rankin, K.P., Ogar, J.M., Phengrasamy, L., Rosen, H.J., Johnson, J.K., Weiner, M.W., Miller, B.L., 2004. Cognition and anatomy in three variants of primary progressive aphasia. Annals of Neurology 55, 335–346. https://doi.org/10.1002/ana.10825

Grady, C., 2012. The cognitive neuroscience of ageing. Nature Reviews Neuroscience 13, 491–505. https://doi.org/10.1038/nrn3256

Grahn, J.A., Parkinson, J.A., Owen, A.M., 2008. The cognitive functions of the caudate nucleus. Progress in Neurobiology 15.

Graves, W.W., Desai, R., Humphries, C., Seidenberg, M.S., Binder, J.R., 2010. Neural Systems for Reading Aloud: A Multiparametric Approach. Cerebral Cortex 20, 1799–1815. https://doi.org/10.1093/cercor/bhp245

Greicius, M.D., Krasnow, B., Reiss, A.L., Menon, V., 2003. Functional connectivity in the resting brain: A network analysis of the default mode hypothesis. Proceedings of the National Academy of Sciences 100, 253–258. https://doi.org/10.1073/pnas.0135058100

Grill-Spector, K., Kourtzi, Z., Kanwisher, N., 2001. The lateral occipital complex and its role in object recognition. Vision Research 41, 1409–1422. https://doi.org/10.1016/S0042-6989(01)00073-6

Guerreiro, M., Silva, A.P., Botelho, M.A., Leitão, O., Castro-Caldas, A., Garcia, C., 1994. Adaptação à população portuguesa da tradução do Mini Mental State Examination (MMSE). Revista Portuguesa de Neurologia 1, 9–10.

Hakun, J.G., Zhu, Z., Brown, C.A., Johnson, N.F., Gold, B.T., 2015. Longitudinal alterations to brain function, structure, and cognitive performance in healthy older adults: A fMRI-DTI study. Neuropsychologia 71, 225–235. https://doi.org/10.1016/j.neuropsychologia.2015.04.008

Hermoye, L., Saint-Martin, C., Cosnard, G., Lee, S.-K., Kim, J., Nassogne, M.-C., Menten, R., Clapuyt, P., Donohue, P.K., Hua, K., Wakana, S., Jiang, H., van Zijl, P.C.M., Mori, S., 2006. Pediatric diffusion tensor imaging: Normal database and observation of the white matter maturation in early childhood. NeuroImage 29, 493–504. https://doi.org/10.1016/j.neuroimage.2005.08.017

Hoffman, P., Morcom, A.M., 2018. Age-related changes in the neural networks supporting semantic cognition: A meta-analysis of 47 functional neuroimaging studies. Neuroscience & Biobehavioral Reviews 84, 134–150. https://doi.org/10.1016/j.neubiorev.2017.11.010

Hoffstaedter, F., Grefkes, C., Roski, C., Caspers, S., Zilles, K., Eickhoff, S.B., 2015. Age-related decrease of functional connectivity additional to gray matter atrophy in a network for movement initiation. Brain Structure and Function 220, 999–1012. https://doi.org/10.1007/s00429-013-0696-2

Hogstrom, L.J., Westlye, L.T., Walhovd, K.B., Fjell, A.M., 2013. The Structure of the Cerebral Cortex Across Adult Life: Age-Related Patterns of Surface Area, Thickness, and Gyrification. Cerebral Cortex 23, 2521–2530. https://doi.org/10.1093/cercor/bhs231

Hu, S., Ide, J.S., Chao, H.H., Castagna, B., Fischer, K.A., Zhang, S., Li, C.R., 2018. Structural and functional cerebral bases of diminished inhibitory control during healthy aging. Human Brain Mapping 39, 5085–5096. https://doi.org/10.1002/hbm.24347

Hua, K., Zhang, J., Wakana, S., Jiang, H., Li, X., Reich, D.S., Calabresi, P.A., Pekar, J.J., van Zijl, P.C.M., Mori, S., 2008. Tract probability maps in stereotaxic spaces: Analyses of white matter anatomy and tract-specific quantification. NeuroImage 39, 336–347. https://doi.org/10.1016/j.neuroimage.2007.07.053

Huo, L., Li, R., Wang, P., Zheng, Z., Li, J., 2018. The Default Mode Network Supports Episodic Memory in Cognitively Unimpaired Elderly Individuals: Different Contributions to Immediate Recall and Delayed Recall. Frontiers in Aging Neuroscience 10. https://doi.org/10.3389/fnagi.2018.00006

Iacoboni, M., 2005. Neural mechanisms of imitation. Current Opinion in Neurobiology 15, 632–637. https://doi.org/10.1016/j.conb.2005.10.010

Jiang, J., Liu, T., Crawford, J.D., Kochan, N.A., Brodaty, H., Sachdev, P.S., Wen, W., 2020. Stronger bilateral functional connectivity of the frontoparietal control network in near-centenarians and centenarians without dementia. NeuroImage 215, 116855. https://doi.org/10.1016/j.neuroimage.2020.116855

Jung, R.E., Haier, R.J., 2007. The Parieto-Frontal Integration Theory (P-FIT) of intelligence: Converging neuroimaging evidence. Behavioral and Brain Sciences 30, 135–154. https://doi.org/10.1017/S0140525X07001185

Kanwisher, N., McDermott, J., Chun, M.M., 1997. The Fusiform Face Area: A Module in Human Extrastriate Cortex Specialized for Face Perception. The Journal of Neuroscience 17, 10.

Kitada, R., Johnsrude, I.S., Kochiyama, T., Lederman, S.J., 2009. Functional Specialization and Convergence in the Occipito-temporal Cortex Supporting Haptic and Visual Identification of Human Faces and Body Parts: An fMRI Study. Journal of Cognitive Neuroscience 21, 2027–2045. https://doi.org/10.1162/jocn.2009.21115

Lamichhane, B., McDaniel, M.A., Waldum, E.R., Braver, T.S., 2018. Age-related changes in neural mechanisms of prospective memory. Cognitive, Affective, & Behavioral Neuroscience 18, 982–999. https://doi.org/10.3758/s13415-018-0617-1

Lee, A., Ratnarajah, N., Tuan, T.A., Chen, S.H.A., Qiu, A., 2015. Adaptation of brain functional and structural networks in aging. PLoS ONE 10, 1–16. https://doi.org/10.1371/journal.pone.0123462

Lee, J.S., Kim, S., Yoo, H., Park, S., Jang, Y.K., Kim, H.J., Kim, K.W., Kim, Y., Jang, H., Park, K.-C., Yaffe, K., Yang, J.-J., Lee, J.-M., Na, D.L., Seo, S.W., 2018. Trajectories of Physiological Brain Aging and Related Factors in People Aged from 20 to over-80. Journal of Alzheimer's Disease 65, 1237–1246. https://doi.org/10.3233/JAD-170537

Lee, J.W.K., Shannon, S.P., 2007. 3 Tesla Magnetic Resonance Imaging (MRI)—Is it Ready for Prime Time Clinical Applications? Canadian Journal of Medical Radiation Technology 38, 37–50. https://doi.org/10.1016/S0820-5930(09)60258-9

Lee, Y., Grady, C.L., Habak, C., Wilson, H.R., Moscovitch, M., 2011. Face Processing Changes in Normal Aging Revealed by fMRI Adaptation. Journal of Cognitive Neuroscience 23, 3433–3447. https://doi.org/10.1162/jocn_a_00026

Li, W., Yang, C., Shi, F., Wang, Q., Wu, S., Lu, W., Li, S., Nie, Y., Zhang, X., 2018. Alterations in Normal Aging Revealed by Cortical Brain Network Constructed Using IBASPM. Brain Topography 31, 577–590. https://doi.org/10.1007/s10548-018-0642-y

Lo, C.-Y., Wang, P.-N., Chou, K.-H., Wang, J., He, Y., Lin, C.-P., 2010. Diffusion Tensor Tractography Reveals Abnormal Topological Organization in Structural Cortical Networks in Alzheimer's Disease. Journal of Neuroscience 30, 16876–16885. https://doi.org/10.1523/JNEUROSCI.4136-10.2010

Lockhart, S.N., DeCarli, C., 2014. Structural Imaging Measures of Brain Aging. Neuropsychology Review 24, 271–289. https://doi.org/10.1007/s11065-014-9268-3

Lou, W., Wang, D., Wong, A., Chu, W.C.W., Mok, V.C.T., Shi, L., 2019. Frequency-specific age-related decreased brain network diversity in cognitively healthy elderly: A whole-brain data-driven analysis. Human Brain Mapping 40, 340–351. https://doi.org/10.1002/hbm.24376

Madden, D.J., Parks, E.L., Tallman, C.W., Boylan, M.A., Hoagey, D.A., Cocjin, S.B., Packard, L.E., Johnson, M.A., Chou, Y., Potter, G.G., Chen, N., Siciliano, R.E., Monge, Z.A., Honig, J.A., Diaz, M.T., 2017. Sources of disconnection in neurocognitive aging: cerebral white-matter integrity, resting-state functional connectivity, and white-matter hyperintensity volume. Neurobiology of Aging 54, 199–213. https://doi.org/10.1016/j.neurobiolaging.2017.01.027

Moreira, P.S., Santos, N., Castanho, T., Amorim, L., Portugal-Nunes, C., Sousa, N., Costa, P., 2018. Longitudinal measurement invariance of memory performance and executive functioning in healthy aging. PLOS ONE 13, e0204012. https://doi.org/10.1371/journal.pone.0204012

Nashiro, K., Sakaki, M., Braskie, M.N., Mather, M., 2017. Resting-state networks associated with cognitive processing show more age-related decline than those associated with emotional processing. Neurobiology of Aging 54, 152–162. https://doi.org/10.1016/j.neurobiolaging.2017.03.003

O'Sullivan, M., Jones, D.K., Summers, P.E., Morris, R.G., Williams, S.C.R., Markus, H.S., 2001. Evidence for cortical "disconnection" as a mechanism of age-related cognitive decline. Neurology 57, 632–638. https://doi.org/10.1212/WNL.57.4.632

Otte, W.M., van Diessen, E., Paul, S., Ramaswamy, R., Subramanyam Rallabandi, V.P., Stam, C.J., Roy, P.K., 2015. Aging alterations in whole-brain networks during adulthood mapped with the minimum spanning tree indices: The interplay of density, connectivity cost and life-time trajectory. NeuroImage 109, 171–189. https://doi.org/10.1016/j.neuroimage.2015.01.011

Park, D.C., Polk, T.A., Park, R., Minear, M., Savage, A., Smith, M.R., 2004. Aging reduces neural specialization in ventral visual cortex. Proceedings of the National Academy of Sciences 101, 13091–13095.

Park, H.-J., Friston, K., 2013. Structural and Functional Brain Networks: From Connections to Cognition. Science 342, 1238411–1238411. https://doi.org/10.1126/science.1238411

Perosa, V., de Boer, L., Ziegler, G., Apostolova, I., Buchert, R., Metzger, C., Amthauer, H., Guitart-Masip, M., Düzel, E., Betts, M.J., 2020. The Role of the Striatum in Learning to Orthogonalize Action and Valence: A Combined PET and 7 T MRI Aging Study. Cerebral Cortex. https://doi.org/10.1093/cercor/bhz313

Persson, J., Pudas, S., Nilsson, L.-G., Nyberg, L., 2014. Longitudinal assessment of default-mode brain function in aging. Neurobiology of Aging 35, 2107–2117. https://doi.org/10.1016/j.neurobiolaging.2014.03.012

Piefke, M., Onur, Ö.A., Fink, G.R., 2012. Aging-related changes of neural mechanisms underlying visual-spatial working memory. Neurobiology of Aging 33, 1284–1297. https://doi.org/10.1016/j.neurobiolaging.2010.10.014

Price, C.J., Mechelli, A., 2005. Reading and reading disturbance. Current Opinion in Neurobiology 15, 231–238. https://doi.org/10.1016/j.conb.2005.03.003

Raz, N., 1999. Aging of the brain and its impact on cognitive performance: Integration of structural and functional findings. 2nd ed. Mahwah, N: Lawrence Erlbaum Associates; 2.

Rieckmann, A., Johnson, K.A., Sperling, R.A., Buckner, R.L., Hedden, T., 2018. Dedifferentiation of caudate functional connectivity and striatal dopamine transporter density predict memory change in normal aging. Proceedings of the National Academy of Sciences 115, 10160–10165. https://doi.org/10.1073/pnas.1804641115

Roberts, J.A., Perry, A., Roberts, G., Mitchell, P.B., Breakspear, M., 2017. Consistency-based thresholding of the human connectome. NeuroImage 145, 118–129. https://doi.org/10.1016/j.neuroimage.2016.09.053

Rubinov, M., Sporns, O., 2010. Complex network measures of brain connectivity: Uses and interpretations. NeuroImage 52, 1059–1069. https://doi.org/10.1016/j.neuroimage.2009.10.003

Sala-Llonch, R., Junqué, C., Arenaza-Urquijo, E.M., Vidal-Piñeiro, D., Valls-Pedret, C., Palacios, E.M., Domènech, S., Salvà, A., Bargalló, N., Bartrés-Faz, D., 2014. Changes in whole-brain functional networks and memory performance in aging. Neurobiology of Aging 35, 2193–2202. https://doi.org/10.1016/j.neurobiolaging.2014.04.007

Salat, D.H., 2011. The Declining Infrastructure of the Aging Brain. Brain Connectivity 1, 279–293. https://doi.org/10.1089/brain.2011.0056

Santos, N.C., Costa, P.S., Cunha, P., Cotter, J., Sampaio, A., Zihl, J., Almeida, O.F.X., Cerqueira, J.J., Palha, J.A., Sousa, N., 2013. Mood is a key determinant of cognitive performance in community-dwelling older adults: A cross-sectional analysis. Age 35, 1983–1993. https://doi.org/10.1007/s11357-012-9482-y

Santos, N.C., Costa, P.S., Cunha, P., Portugal-Nunes, C., Amorim, L., Cotter, J., Cerqueira, J.J., Palha, J.A., Sousa, N., 2014. Clinical, physical and lifestyle variables and relationship with cognition and mood in aging: A cross-sectional analysis of distinct educational groups. Frontiers in Aging Neuroscience 6, 1–15. https://doi.org/10.3389/fnagi.2014.00021

Sexton, C.E., Walhovd, K.B., Storsve, A.B., Tamnes, C.K., Westlye, L.T., Johansen-Berg, H., Fjell, A.M., 2014. Accelerated Changes in White Matter Microstructure during Aging: A Longitudinal Diffusion

Tensor Imaging Study. Journal of Neuroscience 34, 15425–15436. https://doi.org/10.1523/JNEUROSCI.0203-14.2014

Shah, M., Kurth, F., Luders, E., 2020. The impact of aging on the subregions of the fusiform gyrus in healthy older adults. Journal of Neuroscience Research. https://doi.org/10.1002/jnr.24586

Slater, D.A., Melie-Garcia, L., Preisig, M., Kherif, F., Lutti, A., Draganski, B., 2019. Evolution of white matter tract microstructure across the life span. Human Brain Mapping 40, 2252–2268. https://doi.org/10.1002/hbm.24522

Soares, J.M., Marques, P., Magalhães, R., Santos, N.C., Sousa, N., 2014. Brain structure across the lifespan: the influence of stress and mood. Frontiers in Aging Neuroscience 6. https://doi.org/10.3389/fnagi.2014.00330

Sullivan, M.D., Anderson, J.A.E., Turner, G.R., Spreng, R.N., 2019. Intrinsic neurocognitive network connectivity differences between normal aging and mild cognitive impairment are associated with cognitive status and age. Neurobiology of Aging 73, 219–228. https://doi.org/10.1016/j.neurobiolaging.2018.10.001

Tartaro, A., 2019. Altered Cingulate Cortex Functional Connectivity in Normal Aging and Mild Cognitive Impairment. Frontiers in Neuroscience 13, 15.

Teng, C., Zhou, J., Ma, H., Tan, Y., Wu, X., Guan, C., Qiao, H., Li, J., Zhong, Y., Wang, C., Zhang, N., 2018. Abnormal resting state activity of left middle occipital gyrus and its functional connectivity in female patients with major depressive disorder. BMC Psychiatry 18. https://doi.org/10.1186/s12888-018-1955-9

Thompson-Schill, S.L., 2003. Neuroimaging studies of semantic memory: inferring "how" from "where." Neuropsychologia 41, 280–292. https://doi.org/10.1016/S0028-3932(02)00161-6

Touroutoglou, A., Zhang, J., Andreano, J.M., Dickerson, B.C., Barrett, L.F., 2018. Dissociable Effects of Aging on Salience Subnetwork Connectivity Mediate Age-Related Changes in Executive Function and Affect. Frontiers in Aging Neuroscience 10. https://doi.org/10.3389/fnagi.2018.00410

Tu, S., Qiu, J., Martens, U., Zhang, Q., 2013. Category-selective attention modulates unconscious processes in the middle occipital gyrus. Consciousness and Cognition 22, 479–485. https://doi.org/10.1016/j.concog.2013.02.007

Turkeltaub, P.E., Branch Coslett, H., 2010. Localization of sublexical speech perception components. Brain and Language 114, 1–15. https://doi.org/10.1016/j.bandl.2010.03.008

van den Heuvel, M.P., Hulshoff Pol, H.E., 2010. Exploring the brain network: A review on resting-state fMRI functional connectivity. European Neuropsychopharmacology 20, 519–534. https://doi.org/10.1016/j.euroneuro.2010.03.008

van den Heuvel, M.P., Sporns, O., 2011. Rich-Club Organization of the Human Connectome. Journal of Neuroscience 31, 15775–15786. https://doi.org/10.1523/JNEUROSCI.3539-11.2011

Verstynen, T.D., Lynch, B., Miller, D.L., Voss, M.W., Prakash, R.S., Chaddock, L., Basak, C., Szabo, A., Olson, E.A., Wojcicki, T.R., Fanning, J., Gothe, N.P., McAuley, E., Kramer, A.F., Erickson, K.I., 2012. Caudate Nucleus Volume Mediates the Link between Cardiorespiratory Fitness and Cognitive Flexibility in Older Adults. Journal of Aging Research 2012, 1–11. https://doi.org/10.1155/2012/939285

Vigneau, M., Beaucousin, V., Hervé, P.Y., Duffau, H., Crivello, F., Houdé, O., Mazoyer, B., Tzourio-Mazoyer, N., 2006. Meta-analyzing left hemisphere language areas: Phonology, semantics, and sentence processing. NeuroImage 30, 1414–1432. https://doi.org/10.1016/j.neuroimage.2005.11.002

Vinke, E.J., de Groot, M., Venkatraghavan, V., Klein, S., Niessen, W.J., Ikram, M.A., Vernooij, M.W., 2018. Trajectories of imaging markers in brain aging: the Rotterdam Study. Neurobiology of Aging 71, 32–40. https://doi.org/10.1016/j.neurobiolaging.2018.07.001

Vogt, B.A., 2016. Midcingulate cortex: Structure, connections, homologies, functions and diseases. Journal of Chemical Neuroanatomy 74, 28–46. https://doi.org/10.1016/j.jchemneu.2016.01.010

Wagner, A.D., Koutstaal, W., Schacter, D.L., 1999. When encoding yields remembering: insights from event-related neuroimaging. Philosophical Transactions of the Royal Society of London. Series B: Biological Sciences 354, 1307–1324. https://doi.org/10.1098/rstb.1999.0481

Wagner, A.D., Shannon, B.J., Kahn, I., Buckner, R.L., 2005. Parietal lobe contributions to episodic memory retrieval. Trends in Cognitive Sciences 9, 445–453. https://doi.org/10.1016/j.tics.2005.07.001

Wakana, S., Caprihan, A., Panzenboeck, M.M., Fallon, J.H., Perry, M., Gollub, R.L., Hua, K., Zhang, J., Jiang, H., Dubey, P., Blitz, A., van Zijl, P., Mori, S., 2007. Reproducibility of quantitative tractography methods applied to cerebral white matter. NeuroImage 36, 630–644. https://doi.org/10.1016/j.neuroimage.2007.02.049

Wandell, B.A., Dumoulin, S.O., Brewer, A.A., 2007. Visual Field Maps in Human Cortex. Neuron 56, 366–383. https://doi.org/10.1016/j.neuron.2007.10.012

Wang, J., Zuo, X., He, Y., Bullmore, E.T., Fornito, A., 2010. Graph-based network analysis of resting-state functional MRI. Neuroscience 4, 1–14. https://doi.org/10.3389/fnsys.2010.00016

Wen, W., Zhu, W., He, Y., Kochan, N.A., Reppermund, S., Slavin, M.J., Brodaty, H., Crawford, J., Xia, A., Sachdev, P., 2011. Discrete Neuroanatomical Networks Are Associated with Specific Cognitive Abilities in Old Age. Journal of Neuroscience 31, 1204–1212. https://doi.org/10.1523/JNEUROSCI.4085-10.2011

Westlye, L.T., Walhovd, K.B., Dale, A.M., Bjornerud, A., Due-Tonnessen, P., Engvig, A., Grydeland, H., Tamnes, C.K., Ostby, Y., Fjell, A.M., 2010. Life-Span Changes of the Human Brain White Matter: Diffusion Tensor Imaging (DTI) and Volumetry. Cerebral Cortex 20, 2055–2068. https://doi.org/10.1093/cercor/bhp280

Wilson, R.P., 2018. The Neural Substrate of Reward Anticipation in Health: A Meta-Analysis of fMRI Findings in the Monetary Incentive Delay Task. Neuropsychol Rev 11.

Wiseman, S.J., Booth, T., Ritchie, S.J., Cox, S.R., Muñoz Maniega, S., Valdés Hernández, M. del C., Dickie, D.A., Royle, N.A., Starr, J.M., Deary, I.J., Wardlaw, J.M., Bastin, M.E., 2018. Cognitive abilities, brain white matter hyperintensity volume, and structural network connectivity in older age. Human Brain Mapping 39, 622–632. https://doi.org/10.1002/hbm.23857

Wright, C.I., Negreira, A., Gold, A.L., Britton, J.C., Williams, D., Feldman Barrett, L., 2008. Neural correlates of novelty and face–age effects in young and elderly adults. NeuroImage 42, 956–968. https://doi.org/10.1016/j.neuroimage.2008.05.015

Wu, K., Taki, Y., Sato, K., Kinomura, S., Goto, R., Okada, K., Kawashima, R., He, Y., Evans, A.C., Fukuda, H., 2012. Age-related changes in topological organization of structural brain networks in healthy individuals. Human Brain Mapping 33, 552–568. https://doi.org/10.1002/hbm.21232

Yeo, B.T.T., Krienen, F.M., Sepulcre, J., Sabuncu, M.R., Lashkari, D., Hollinshead, M., Roffman, J.L., Smoller, J.W., Zöllei, L., Polimeni, J.R., Fischl, B., Liu, H., Buckner, R.L., 2011. The organization of the human cerebral cortex estimated by intrinsic functional connectivity. Journal of Neurophysiology 106, 1125–1165. https://doi.org/10.1152/jn.00338.2011

Zalesky, A., Fornito, A., Bullmore, E.T., 2010. Network-based statistic: Identifying differences in brain networks. NeuroImage 53, 1197–1207. https://doi.org/10.1016/j.neuroimage.2010.06.041

Zhao, J., Manza, P., Wiers, C., Song, H., Zhuang, P., Gu, J., Shi, Y., Wang, G.-J., He, D., 2020. Age-Related Decreases in Interhemispheric Resting-State Functional Connectivity and Their Relationship With Executive Function. Frontiers in Aging Neuroscience 12. https://doi.org/10.3389/fnagi.2020.00020

Zhao, T., Cao, M., Niu, H., Zuo, X.N., Evans, A., He, Y., Dong, Q., Shu, N., 2015. Age-related changes in the topological organization of the white matter structural connectome across the human lifespan. Human Brain Mapping 36, 3777–3792. https://doi.org/10.1002/hbm.22877

Zhu, W., Wen, W., He, Y., Xia, A., Anstey, K.J., Sachdev, P., 2012. Changing topological patterns in normal aging using large-scale structural networks. Neurobiology of Aging 33, 899–913. https://doi.org/10.1016/j.neurobiolaging.2010.06.022

Zimmermann, J., Ritter, P., Shen, K., Rothmeier, S., Schirner, M., McIntosh, A.R., 2016. Structural architecture supports functional organization in the human aging brain at a regionwise and network level. Human Brain Mapping 37, 2645–2661. https://doi.org/10.1002/hbm.23200

8. Supplementary Material

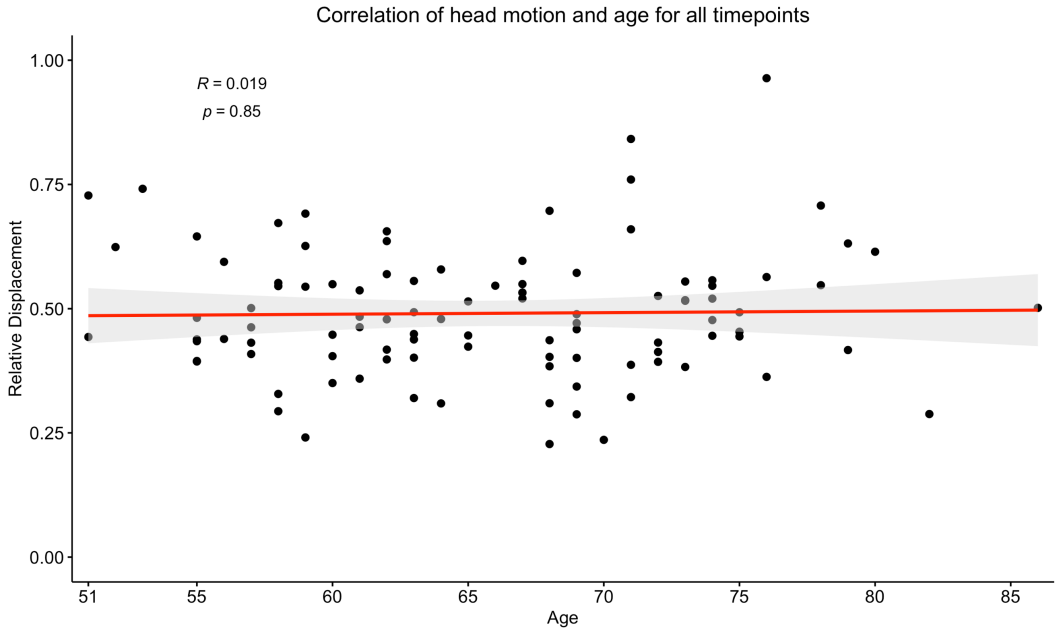

Figure S1. Correlation between head-motion relative displacement values and age for all subjects and both timepoints. Head-motion displacement values were extracted using FSL tools and averaged across all volumes acquired for one subject. Correlation is not significant (r = 0.019, p = 0.85) meaning that age is not associated with head-motion.

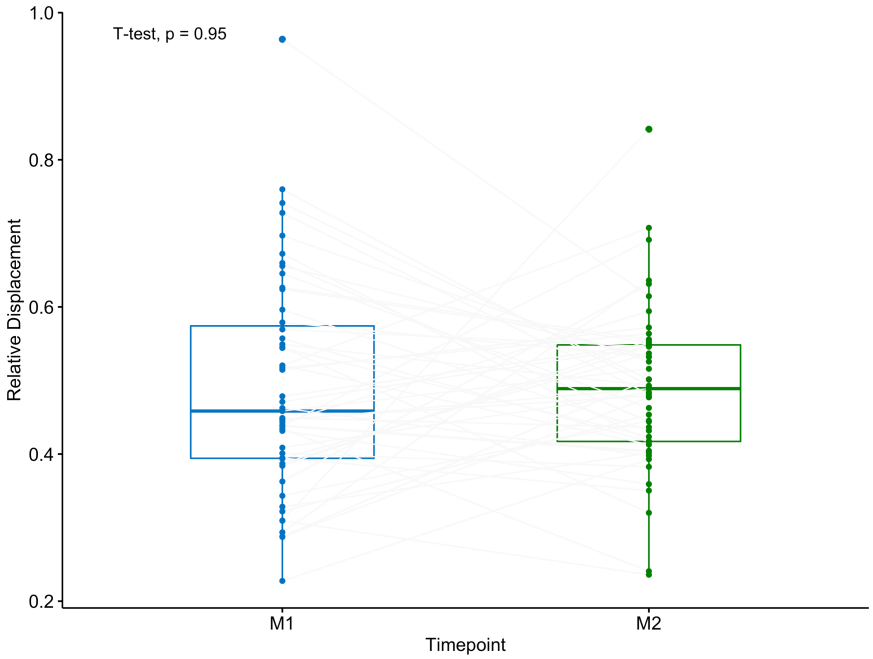

Figure S2. Comparison of head-motion relative displacement values between timepoints. A paired t-test was performed, and it was not significant (p = 0.95) meaning that head-motion values did not differ between timepoints.

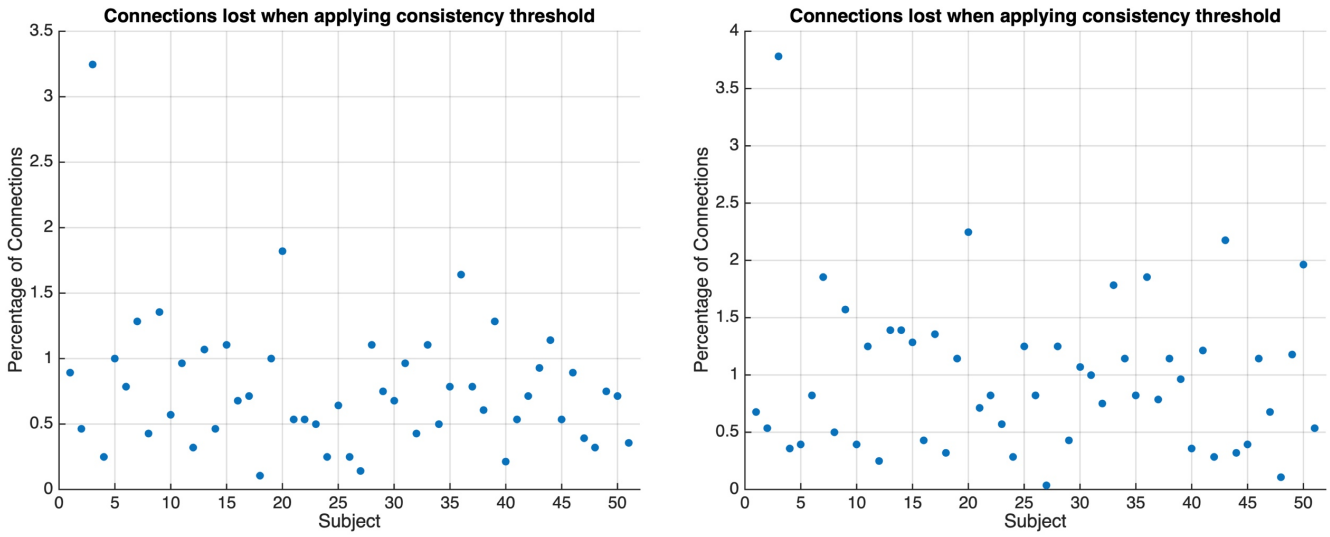

Figure S3. Percentage of connections lost in each subject when applying consistency-based thresholding. Percentage is calculated as the proportion of connections removed in the subject SC matrix relative to the total number of connections removed in the group consistency mask. Plot on the left illustrates results for timepoint 1 and on the right, results for timepoint 2.

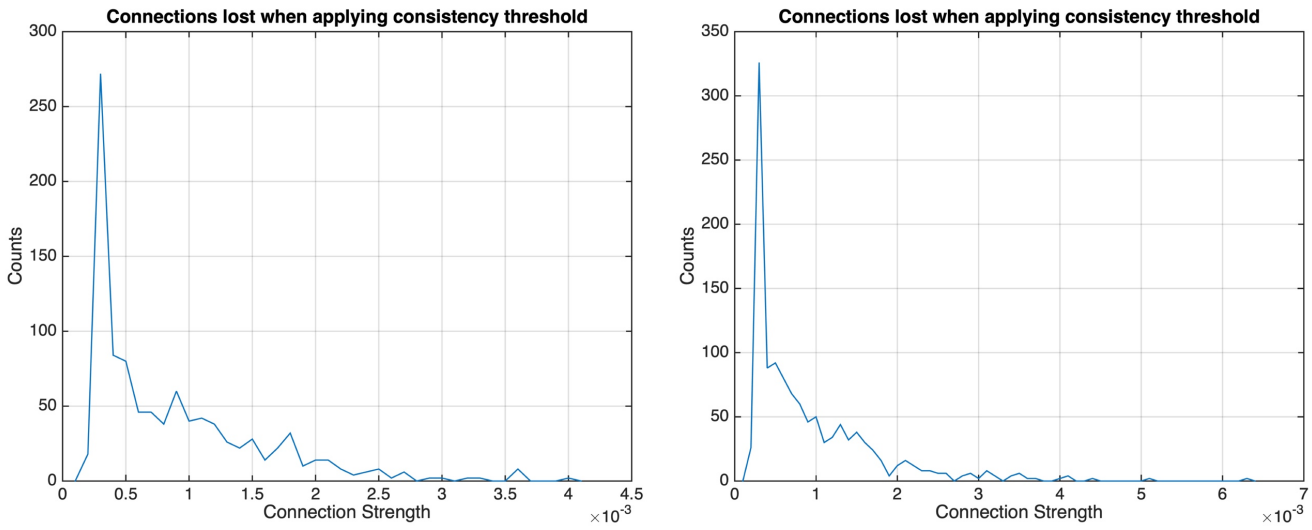

Figure S4. Frequency distribution for the connection strength of the links removed when applying consistency-based thresholding. Plot on the left illustrates results for timepoint 1 and on the right, results for timepoint 3.

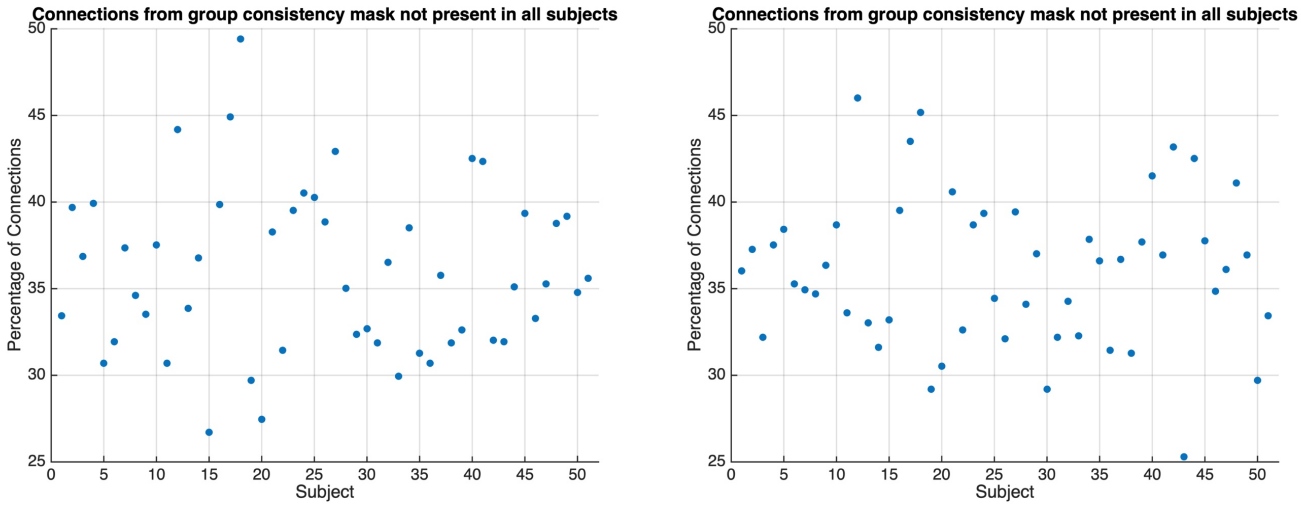

Figure S5. Percentage of connections that were present in the group consistency mask but were not present in all subjects' SC matrices. Percentage is calculated as the proportion of connections not present in the subject SC matrix relative to the total number of connections in the group consistency mask. Plot on the left illustrates results for timepoint 1 and on the right, results for timepoint 2.

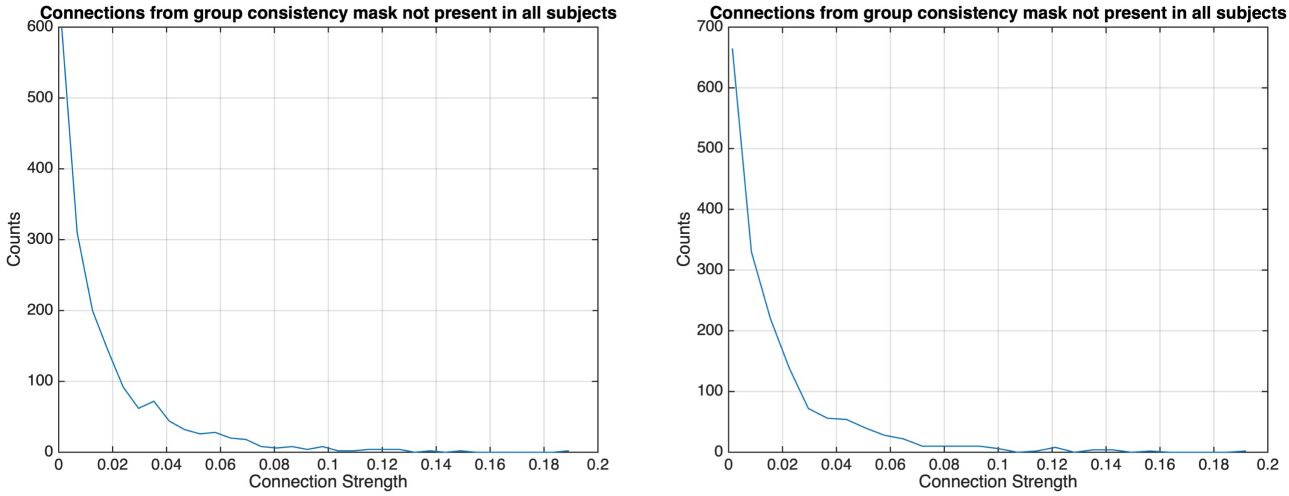

Figure S6. Frequency distribution for the connection strength of the links from the group consistency mask not present in all subjects, when applying consistency-based thresholding. Plot on the left illustrates results for timepoint 1 and on the right, results for timepoint 3.

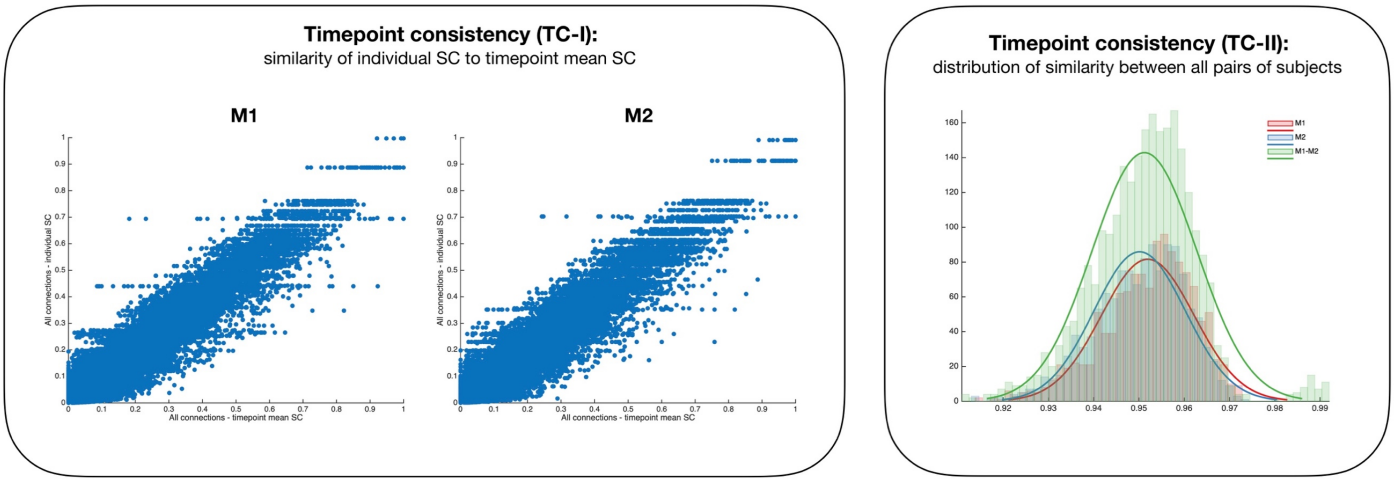

Figure S7. Consistent signatures of SC for M1 and M2 timepoints. Left panel shows intra-timepoint consistency measured as the association between individual SC signatures and timepoint average SC and we can observe that the two timepoints reveal a very high level of intra-timepoint consistency (M1: 97.6%; M2: 97.5%). Right panel shows the degree of association between the signatures of SC for all pairs of subjects in the same timepoint. Once again, we notice a high level of timepoint consistency in SC (100% and 99.8% of all pairwise combinations in M1 and M2 timepoints respectively have a correlation higher than r=0.9137, with number of occurrences peaking at approximately r=0.96 for both timepoints). The overlap between the distributions of intra-timepoint consistency of both timepoints is additionally confirmed by the inter-timepoint consistency distribution (M1-M2: peak at approximately r=0.95). Taken

together, these results suggest that, at a global level, the patterns of SC are highly consistent within and between timepoints, and thus potential differences due to age and sex do not have a significant impact on the estimation of SC patterns.

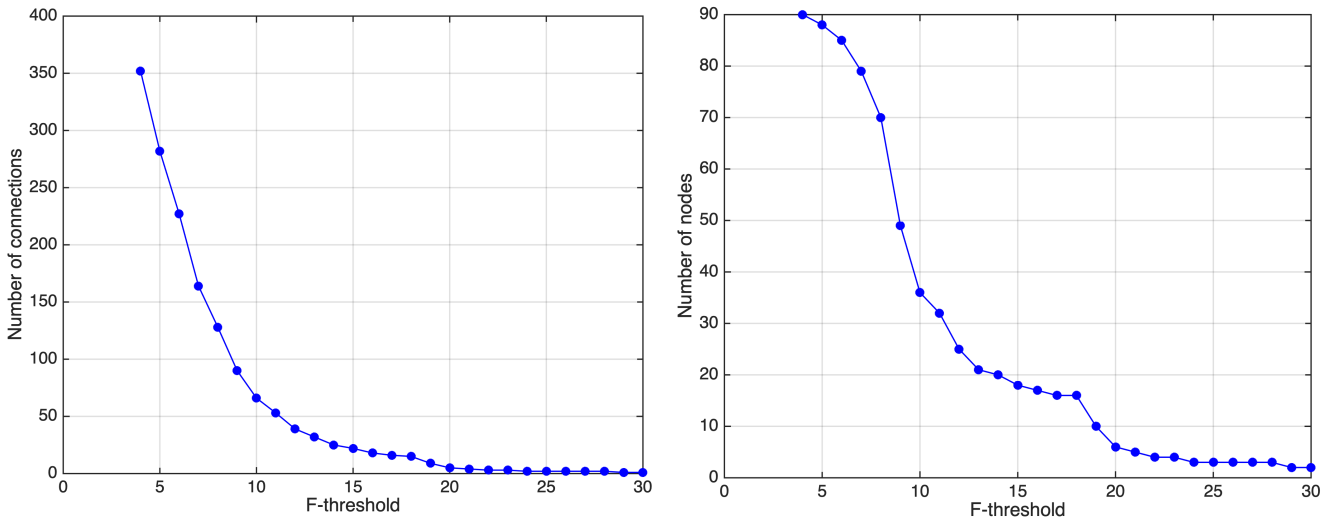

Figure S8. Relationship between F-threshold and number of connections/nodes, that detected a significant component. The F-threshold used in this study (17.0) was selected based on the maximal F-threshold that detected a single component with more than two connections. This generated an NBS component with 19% nodes of the network and 16 links.

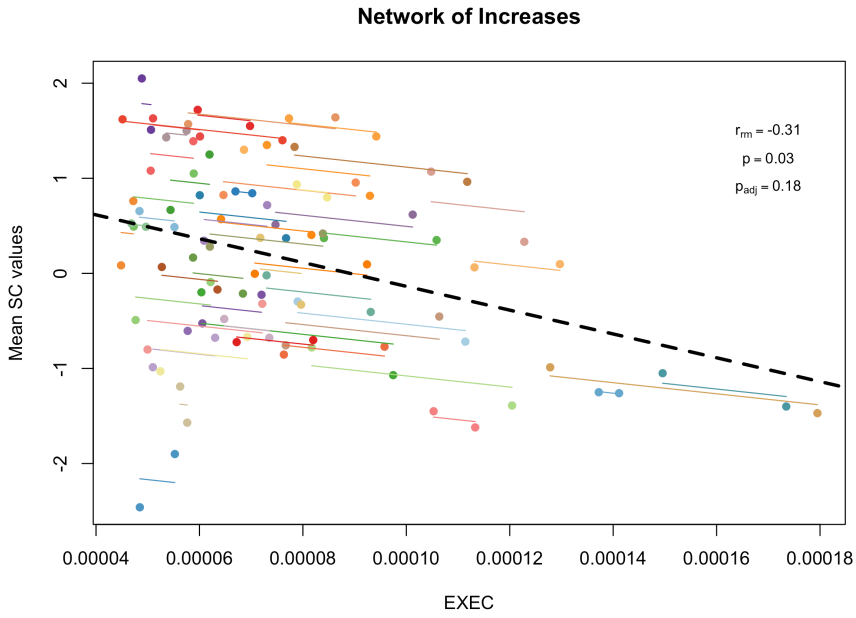

Figure S9. Repeated measures correlation between mean SC values of the network with increases and mean factor scores of general cognition and executive function.

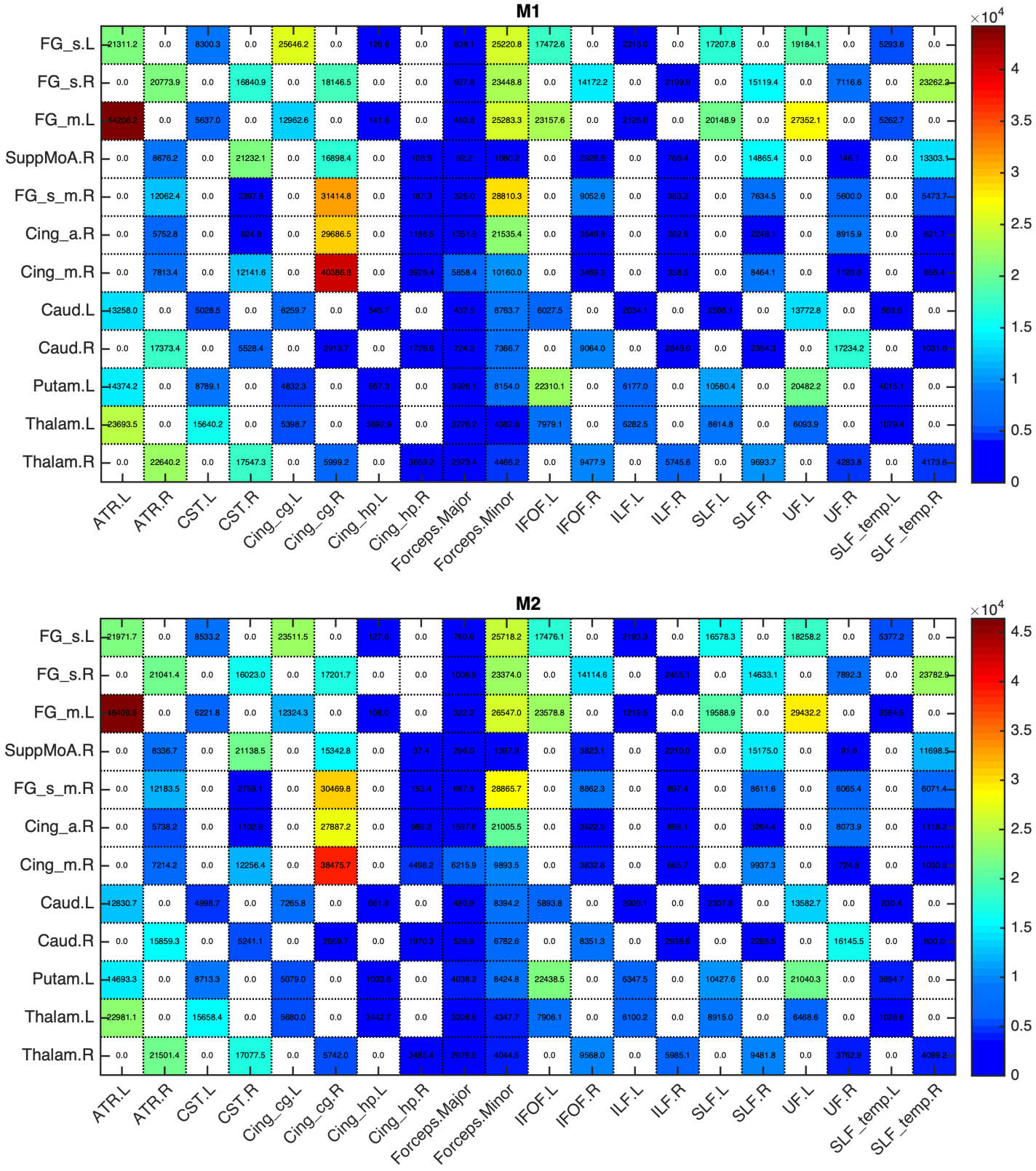

Figure S10. Values of the mean number of streamlines for seed regions of the sub-network with decreases in structural connectivity. Top row shows values for timepoint M1 and bottom row shows values for timepoint M2. Seed regions are presented in rows and white matter tracts in columns.

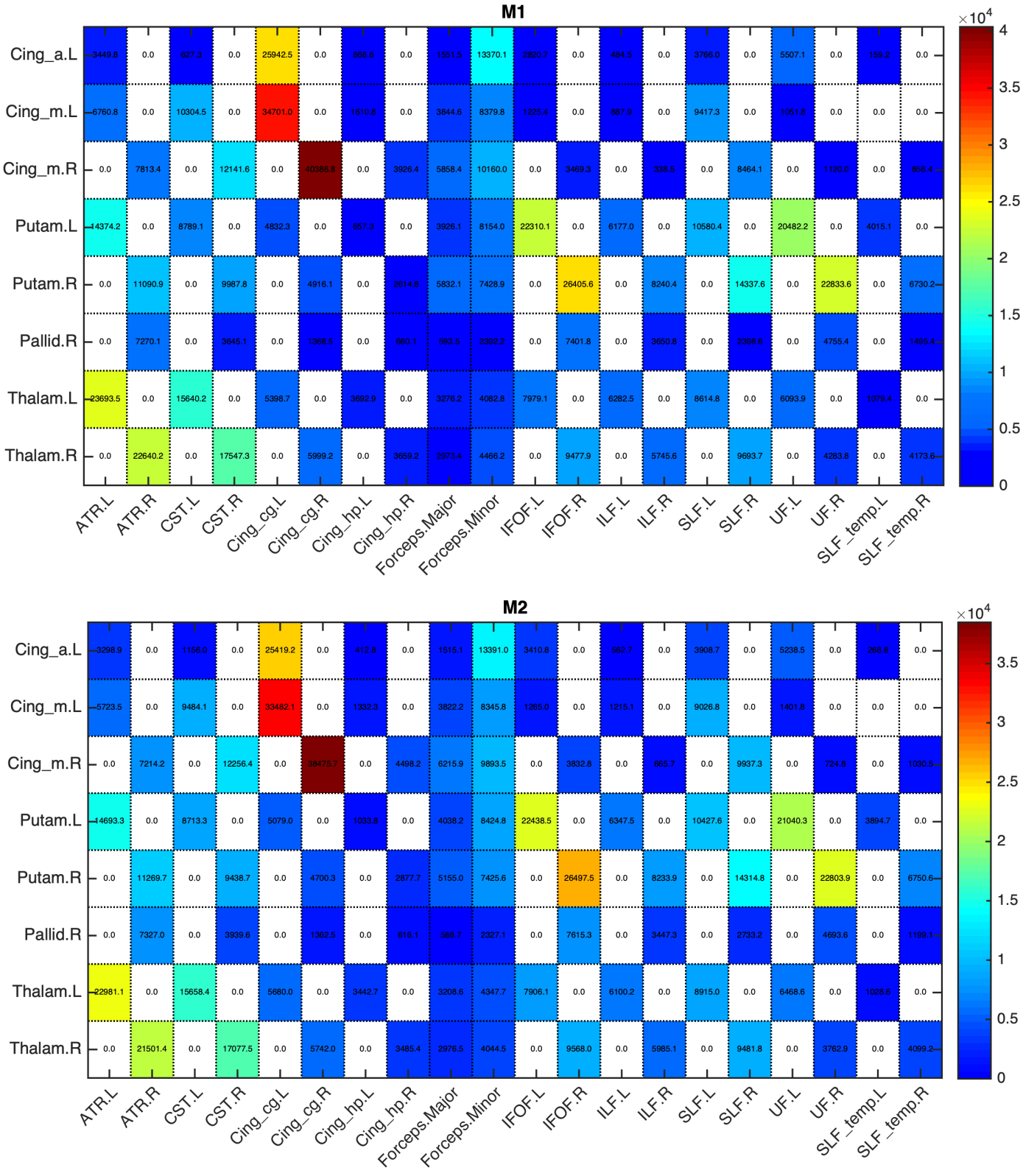

Figure S11. Values of the mean number of streamlines for seed regions of the sub-network with increases in structural connectivity. Top row shows values for timepoint M1 and bottom row shows values for timepoint M2. Seed regions are presented in rows and white matter tracts in columns.

Table S1. Correlations between mean SC values of sub-networks and cognitive composite dimensions (MEM and EXEC).

	MEM			EXEC		
	r_{rm}	p-value	p-value (FDR corrected)	r_{rm}	p-value	p-value (FDR corrected)
All Connections	-0.055	0.70	0.70	-0.11	0.46	0.70
Increases	-0.27	0.062	0.19	-0.31	0.030	0.18
Decreases	0.087	0.55	0.70	0.066	0.65	0.70

Abbreviations: r_{rm}, repeated measures correlation coefficient

Table S2. Timepoint differences in graph theory metrics (results FDR corrected at p < 0.05).

Network Metric	Timepoint 1		Timepoint 2		t-test	
	mean	SD	mean	SD	t-stat	p-value
Mean Connectivity	0.013	0.001	0.013	0.001	-0.17	0.90
Degree	1541	114	1539	104	0.082	0.90
Connection Density	0.19	0.014	0.19	0.013	0.14	0.90
Global Efficiency	0.11	0.006	0.11	0.007	-0.36	0.90
Local Efficiency	0.11	0.005	0.11	0.006	-1.23	0.90
Clustering Coefficient [a]	3.25	0.24	3.24	0.23	0.44	0.90
Characteristic Path Length [a]	1.46	0.026	1.45	0.029	3.45	**0.009****
Small-World Index	2.22	0.16	2.23	0.15	-0.13	0.90

[a] divided by 100 random networks; * p < .05, ** p < .01, *** p < .001

Table S3. Brain regions belonging to the different modules of each timepoint's modularity community structure.

Timepoint 1	
Module	Area
1	Precentral R
	Frontal Sup R
	Frontal Sup Orb R
	Frontal Mid R
	Frontal Mid Orb R
	Frontal Inf Oper R
	Frontal Inf Tri R
	Frontal Inf Orb R
	Rolandic Oper R
	Insula R
	Postcentral R
	Parietal Sup R
	Parietal Inf R
	SupraMarginal R
	Angular R
	Caudate R
	Putamen R
	Pallidum R
	Thalamus R
	Heschl R
	Temporal Sup R
2	Precentral L
	Frontal Sup L
	Frontal Mid L
	Frontal Inf Oper L
	Frontal Inf Tri L
	Rolandic Oper L
	Insula L
	Postcentral L

Timepoint 2	
Module	Area
1	Precentral L
	Frontal Sup L
	Frontal Sup Orb L
	Frontal Mid L
	Frontal Mid Orb L
	Frontal Inf Oper L
	Frontal Inf Tri L
	Frontal Inf Orb L
	Rolandic Oper L
	Insula L
	Postcentral L
	Parietal Sup L
	Parietal Inf L
	SupraMarginal L
	Angular L
	Putamen L
	Pallidum L
	Thalamus L
	Heschl L
	Temporal Sup L
2	Hippocampus L
	ParaHippocampal L
	Amygdala L
	Calcarine L
	Cuneus L
	Lingual L
	Occipital Sup L
	Occipital Mid L
	Occipital Inf L

	Parietal Sup L
	Parietal Inf L
	SupraMarginal L
	Angular L
	Heschl L
	Temporal Sup L
3	Frontal Sup Orb L
	Frontal Mid Orb L
	Frontal Inf Orb L
	Olfactory L
	Olfactory R
	Frontal Sup Medial L
	Frontal Sup Medial R
	Frontal Med Orb L
	Frontal Med Orb R
	Rectus L
	Rectus R
	Cingulum Ant L
	Cingulum Ant R
	Caudate L
	Putamen L
	Pallidum L
	Thalamus L
4	Supp Motor Area L
	Supp Motor Area R
	Cingulum Mid L
	Cingulum Mid R
	Cingulum Post L
	Cingulum Post R
	Precuneus L
	Precuneus R
	Paracentral Lobule L
	Paracentral Lobule R
5	Hippocampus R
	Fusiform L
	Temporal Pole Sup L
	Temporal Mid L
	Temporal Pole Mid L
	Temporal Inf L
3	Supp Motor Area L
	Supp Motor Area R
	Cingulum Mid L
	Cingulum Mid R
	Cingulum Post L
	Cingulum Post R
	Precuneus L
	Precuneus R
	Paracentral Lobule L
	Paracentral Lobule R
4	Precentral R
	Frontal Sup R
	Frontal Mid R
	Frontal Inf Oper R
	Frontal Inf Tri R
	Rolandic Oper R
	Insula R
	Postcentral R
	Parietal Sup R
	Parietal Inf R
	SupraMarginal R
	Angular R
	Heschl R
	Temporal Sup R
5	Frontal Sup Orb R
	Frontal Mid Orb R
	Frontal Inf Orb R
	Olfactory L
	Olfactory R

	ParaHippocampal R		Frontal Sup Medial L
	Amygdala R		Frontal Sup Medial R
	Calcarine R		Frontal Med Orb L
	Cuneus R		Frontal Med Orb R
	Lingual R		Rectus L
	Occipital Sup R		Rectus R
	Occipital Mid R		Cingulum Ant L
	Occipital Inf R		Cingulum Ant R
	Fusiform R		Caudate L
	Temporal Pole Sup R		Caudate R
	Temporal Mid R		Putamen R
	Temporal Pole Mid R		Pallidum R
	Temporal Inf R		Thalamus R
6	Hippocampus L	6	Hippocampus R
	ParaHippocampal L		ParaHippocampal R
	Amygdala L		Amygdala R
	Calcarine L		Calcarine R
	Cuneus L		Cuneus R
	Lingual L		Lingual R
	Occipital Sup L		Occipital Sup R
	Occipital Mid L		Occipital Mid R
	Occipital Inf L		Occipital Inf R
	Fusiform L		Fusiform R
	Temporal Pole Sup L		Temporal Pole Sup R
	Temporal Mid L		Temporal Mid R
	Temporal Pole Mid L		Temporal Pole Mid R
	Temporal Inf L		Temporal Inf R

CHAPTHER IV

Ana Coelho, Ricardo Magalhães, Pedro Silva Moreira, Liliana Amorim, Carlos Portugal-Nunes, Teresa Castanho, Nadine Correia Santos, Nuno Sousa, Henrique M. Fernandes (2021)

A novel method for estimating connectivity-based parcellation of the human brain from diffusion MRI: application to an aging cohort

Manuscript under review in Human Brain Mapping

A novel method for estimating connectivity-based parcellation of the human brain from diffusion MRI: application to an aging cohort

Ana Coelho[1,2,3], Ricardo Magalhães[1,2,3], Pedro Silva Moreira[1,2,3], Liliana Amorim[1,2,3], Carlos Portugal-Nunes[1,2,3], Teresa Castanho[1,2,3], Nadine Correia Santos[1,2,3], Nuno Sousa[1,2,3#,] Henrique M. Fernandes[4,5#]

[1]Life and Health Sciences Research Institute (ICVS), School of Medicine, University of Minho, Braga, Portugal; [2]ICVS/3B's, PT Government Associate Laboratory, Braga/Guimarães, Portugal; [3]Clinical Academic Center – Braga, Braga, Portugal; [4]Center for Music in the Brain (MIB), Aarhus University, Aarhus, Denmark; [5]Department of Psychiatry, University of Oxford, Oxford, UK

[#] Corresponding authors and equal contribution

1. Abstract

Connectivity-based parcellation (CBP) methods have gained popularity in neuroimaging research and lead to a high heterogeneity of developed methods. This technique is used to group voxels with similar connectivity profiles to form homogeneous parcels based on structural or functional patterns of brain connectivity. It is commonly used to define highly homogenous and biologically meaningful nodes; the basic foundation for brain network fingerprinting. To date there is no standard method for CBP and its application to study the aging brain is very scarce. In this study, we aimed to 1) create a novel CBP method from diffusion MRI data and 2) use the generated parcellation to characterize the signatures of longitudinal brain network alteration underlying aging, both in terms of structural connectivity and topological properties. For this purpose, we constructed whole-brain connectivity maps from diffusion tensor imaging data of older adults, for two timepoints (interval time: mean = 52.8; SD = 7.24 months). State-of-the-art clustering techniques were implemented and tested to identify the best performing technique. Furthermore, we developed a new metric (connectivity homogeneity fingerprint - CHF) to evaluate the final CBP. Our results show that the developed method was successful in generating highly homogeneous parcels, as described by the significantly larger CHF score of the final parcellation, when compared to the original anatomical parcellation. Additionally, we demonstrated that the developed

parcellation provides a robust anatomical framework to assess longitudinal changes in the aging brain. We found that aging was predominantly characterized by a reorganization of the brain's structural network which involves the decrease of intra-hemispheric and increase of inter-hemispheric structural. connectivity. These findings are consistent with previous literature, particularly with the "last-in, first-out" hypothesis. Moreover, our results revealed a rearrangement in the topological roles of brain network nodes. Overall, this study proposes a new methodology to perform and evaluate CBP of the human brain with high accuracy and robustness. Hence, the method here proposed can open new avenues to advance our understanding of brain connectivity in health and disease.

Keywords: diffusion MRI, structural connectivity, brain parcellation, network neuroscience, clustering, pattern recognition, aging, humans

2. Introduction

Human brain organization is ruled by two main functional principles: integration and segregation. Functional integration is characterized by long-range connections and functional segregation through local differentiation (Tononi et al., 1994). Each functionally specialized brain region might be described by a different set of connections, so the two concepts of functional integration and segregation are not mutually exclusive, but instead they are closely entangled (Eickhoff et al., 2018, 2015). This view inspired the development of a new family of methods in neuroimaging research known as connectivity-based parcellation (CBP) (Eickhoff et al., 2015). CBP exploits the heterogeneity of connections within a brain region and divides it according to its voxels' connectivity profiles (Eickhoff et al., 2015; Reuter et al., 2020). After estimating the connectivity profiles (i.e., connection strengths between a seed voxel and a set of target voxels) of each voxel inside a region, voxels with similar connectivity profiles are grouped together. This is usually performed using clustering algorithms (e.g., k-means clustering, hierarchical clustering, spectral clustering) and results in subregions which represent homogeneous units with regard to the measured connectivity. Connectivity between voxels can be defined as functional connectivity which is estimated from resting-state functional Magnetic Resonance Imaging (rs-fMRI), structural connectivity which is derived from diffusion weighted imaging (DWI), or task-dependent functional connectivity which is computed from meta-analytic connectivity modeling (MACM).

Network analysis tools allow the characterization of brain's structural and functional organization through quantifiable topological properties, based on the concept that the brain is a complex network of interconnected regions (Bullmore and Sporns, 2009). In this sense, the brain network is modeled as a

graph composed of nodes and edges. While edges, defined as either functional or structural connectivity, were already subject of many studies in recent years, nodes are most of the time defined arbitrarily (Tittgemeyer et al., 2018). The most common approach is to use a pre-existing parcellation that divides the brain into different regions based in local properties, such as cytoarchitecture (Brodmann, 1909), myelo-architecture (Vogt, 1919) or receptor-architecture (Zilles et al., 2002). Early efforts to define brain nodes using these local criteria usually required post-mortem tissues or invasive studies and were extremely time consuming (Gao et al., 2018). As an alternative, local properties can be estimated using measurements derived from MRI, such as myelin density maps, but these will only reflect an indirect measure since these properties are not directly observable through MRI (Eickhoff et al., 2018). Furthermore, and although these parcellations define nodes with a biological meaning, they might not adequately reflect brain organization and inter-individual variability, as connectivity also plays a role in brain differentiation (Arslan et al., 2018; Eickhoff et al., 2015). In contrast, nodes generated with CBP present high homogeneity and functional coherence and distinct connectivity patterns between them, making them suitable for network analysis (Arslan et al., 2018).

First studies performing CBP segmented only a single region of the brain. Examples include the thalamus (Behrens et al., 2003), medial frontal cortex (Johansen-Berg et al., 2004) and Broca's area (Anwander et al., 2007). With the advent of new computational tools, whole-brain approaches are becoming popular, yielding a great heterogeneity of methods (Eickhoff et al., 2018). However, to date a robust and standard method to perform whole-brain CBP is still missing. Moreover, the application of CBP methods to study the aging brain is very scarce and limited to specific brain regions (Fritz et al., 2019). Herein we propose a new method to create a CBP of the human brain using diffusion MRI data. For this, we implemented and tested different state-of-the-art clustering techniques and selected the best performing according to different criteria (Silhouette scores and consistency of clusters' sizes). Additionally, we developed a new metric (connectivity homogeneity fingerprint - CHF) to evaluate the final CBP and prove its possibly advantage over the original parcellation. This metric reflects if the voxels inside a region establish more homogeneous connections (i.e., if they are connected to the same parts of the brain) or more heterogeneous connections (i.e., if they are connected to different parts of the brain) and thus it demonstrates if the main goal of CBP was accomplished. We hypothesized that the generated CBP would present higher values of CHF in comparison to the original partition. Moreover, with the developed CBP we characterized longitudinal changes in topological features of white matter structural connectivity networks during normal aging. To the best of our knowledge, this is the first study applying CBP methods to study age-related longitudinal changes in the whole brain.

3. Methods

3.1. Ethics Statement

The present study was conducted in accordance with the principles expressed in the Declaration of Helsinki and was approved by the national ethical committee (Comissão Nacional de Proteção de Dados) and by the local ethics review boards (Hospital de Braga, Braga; Centro Hospitalar do Alto Ave, Guimarães and Unidade Local de Saúde do Alto Minho, Viana do Castelo/Ponte de Lima). The study goals and procedures were explained to the participants and all gave informed written consent.

3.2. Participants

The participants included in this study are part of a larger sample recruited for the SWITCHBOX Consortium project (www.switchbox-online.eu/), and are representative of the general Portuguese population with respect to age, gender and education (Costa et al., 2013; Santos et al., 2014, 2013). Primary exclusion criteria were inability to understand the informed consent, participant choice to withdraw from the study, incapacity and/or inability to attend MRI sessions, dementia and/or diagnosed neuropsychiatric and/or neurodegenerative disorder (from medical records). Mini Mental State Examination (MMSE) scores below the adjusted thresholds for cognitive impairment were also used as exclusion criteria. The adjusted thresholds were the following: MMSE score <17 if individual with ≤4 years of formal school education and/or ≥72 years of age, and MMSE score <23 otherwise (follows the MMSE validation study for the Portuguese population) (Guerreiro et al., 1994). These exclusion criteria were applied at both evaluations. Subjects were evaluated at two timepoints, with a mean interval time between first and last assessments of 52.8 months (SD = 7.24). At each evaluation, participants underwent an imaging session and a battery of neurocognitive/neuropsychological tests.

In the first assessment, 100 subjects were contacted for MRI screening. In the last assessment, 55 subjects accepted to participate and underwent MRI acquisition protocol, but one did not finish the diffusion acquisition. From these, one subject did not finish the diffusion acquisition and four subjects had brain lesions/pathology. A total of 51 individuals with data from both the first and last evaluations met all the inclusion criteria for this study.

3.3. MRI Data Acquisition

All MRI assessments were performed at Hospital de Braga (Braga, Portugal) on a clinical approved Siemens Magnetom Avanto 1.5T MRI scanner (Siemens Medical Solutions, Erlangen, Germany) with a 12-channel receive-only head-coil. The imaging protocol included several different acquisitions. For the present study, two types of acquisition were considered: Diffusion Weighted Imaging (DWI) and structural scans. For the DWI acquisition a spin-echo echo-planar imaging (SE-EPI) sequence was acquired with the following parameters: TR=8800 ms, TE=99 ms, FoV=240x240 mm, acquisition matrix=120x120, 61 2-mm axial slices with no gap, 30 non-collinear gradient direction with b=1000 s mm^{-2}, one b=0 s mm^{-2} and 1 repetition. For the structural acquisition, a T1-weighted magnetization prepared rapid gradient echo (MPRAGE) sequence was acquired with the following parameters: 176 sagittal slices, TR/TE = 2730/3.48 ms, FA = 7°, slice thickness = 1 mm, slice gap = 0 mm, voxel size = 1x1 mm^2, FoV = 256 mm.

All acquisitions were visually inspected by a certified neuroradiologist, before any pre-processing step, in order to ensure that none of the individuals had brain lesions and/or critical head motion or artifacts that could affect the quality of the data and reliability of our findings.

3.4. MRI Data pre-processing

DWI data was pre-processed using FMRIB Diffusion Toolbox (FDT) provided with the FMRIB Software Library (FSL v5.0; https://fsl.fmrib.ox.ac.uk/fsl/). Pre-processing included: correction for motion and eddy current distortions; rotation of gradient vectors accordingly to the affine transformations used to register each volume; extraction and skull stripping of the first b0 volume that created a mask which was then applied to remove non-brain structures of the remaining volumes; local modelling of diffusion parameters using *bedpostx* algorithm that runs Markov Chain Monte Carlo sampling to build up probability distributions of the diffusion parameters at each voxel and allows modelling of crossing fibers (Behrens et al., 2007).

Structural data was processed using the standard semi-automatic workflow implemented in FreeSurfer toolkit version 6.0 (http://surfer.nmr.mgh.harvard.edu/). In summary, the entire pipeline involves 31 processing steps which include the spatial normalization to Talairach standard space, skull stripping, intensity normalization, tessellation of gray matter (GM)-white matter (WM) boundary, and cortical, subcortical, and WM segmentation. This pipeline has been validated against manual segmentations (Fischl et al., 2002) and is considered reliable across sessions, scanner platforms,

updates and field strengths (Jovicich et al., 2009). It has suffered several improvements throughout the years and details of the procedures are described in several publications (Desikan et al., 2006; Destrieux et al., 2010; Fischl et al., 2002). For the present study the cortical segmentation according to the Desikan-Killiany-Tourville (DKT40) template (Klein et al., 2017) and the subcortical segmentation according to the Buckner (Buckner40) template (Fischl et al., 2002) were considered.

3.5. Voxel-wise Structural Connectivity Network Construction

Probabilistic tractography was used to estimate connections between brain voxels. The 76 regions of the DKT40 and Buckner40 templates obtained with FreeSurfer were used as seed masks. These masks were first converted to the volumetric space of FSL using in-house scripts, and then normalized to each subject native diffusion space by applying the affine transformation from diffusion space to structural space. Then, probabilistic tractography was run using *probtrackx2* algorithm from FDT toolbox. 5000 streamlines were sampled from each voxel in the seed mask. This allowed to obtain the structural connectivity (SC) profiles of each voxel, by counting the number of streamlines that reached any voxel belonging to any seed mask. Tractography was performed only for data of the first assessment.

3.6. Connectivity-based Parcellation

After running probabilistic tractography, each region was subdivided based on its voxels' connectivity patterns and the results of all subjects were merged in a group-wise parcellation. The multiple steps performed are described below and an outline of the method can be seen in Figure 1.

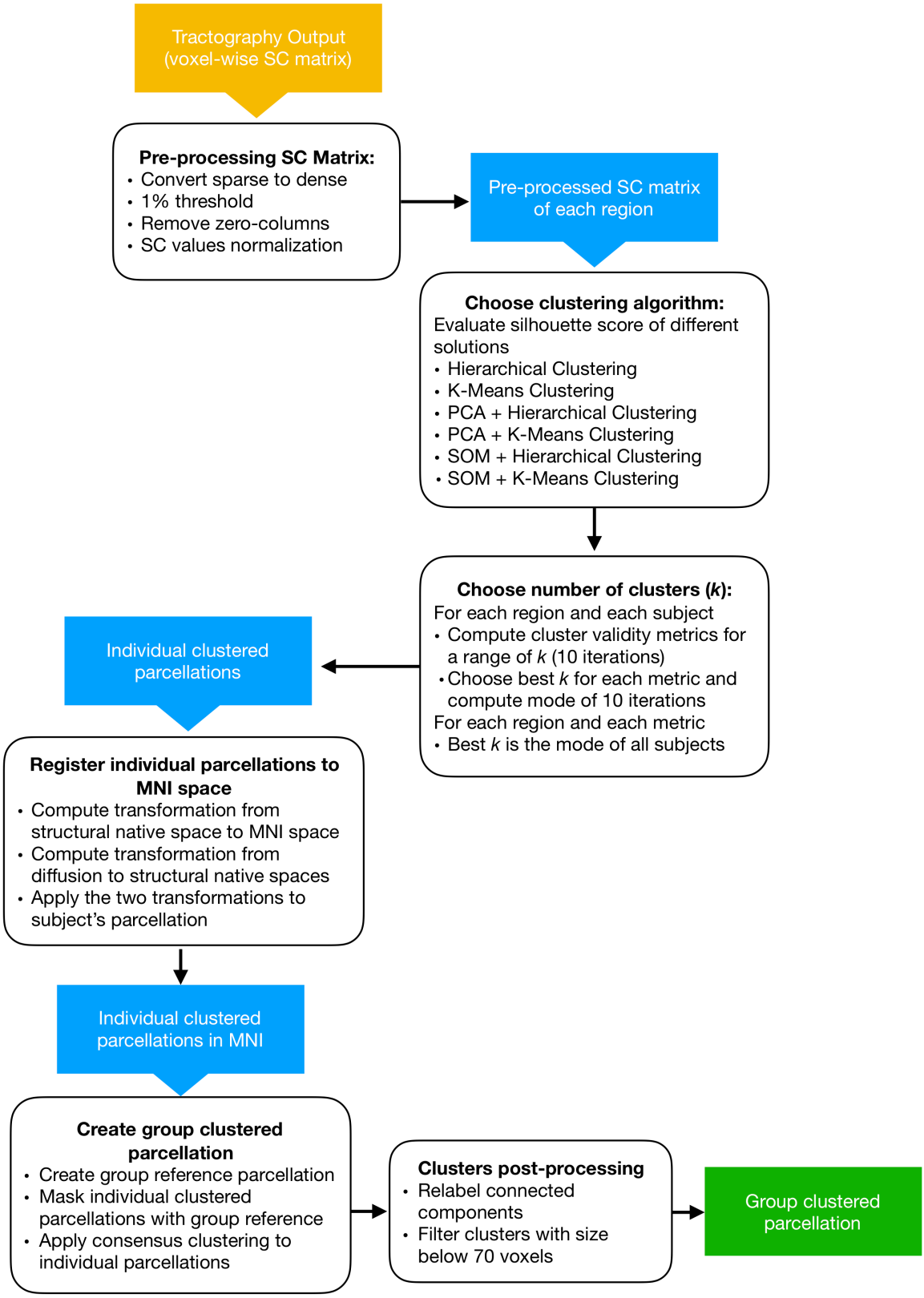

Figure 1. Overview of the workflow employed for the CBP method. Yellow boxes represent the initial input, blue boxes represent intermediate outputs and green boxes the final output.

3.6.1. Pre-processing structural connectivity data

The output of probabilistic tractography was a sparse voxel-wise SC matrix for each region, which contains the connectivity values between each voxel of the seed mask and the voxels in all 76 masks (including the mask used as seed). These matrices were pre-processed before applying the clustering algorithm to group voxels with similar connectivity patterns. Firstly, we performed sparse to dense format conversion, which resulted in a matrix per region with each row representing a voxel of the seed mask and each column the voxels of all 76 masks. Secondly, a threshold of 1% of the strongest connection was applied to each matrix to remove spurious connections resulting from the probabilistic nature of tractography. After this, the columns of each matrix containing only null elements were removed, given that these represent brain voxels with no connections to seed mask voxels, and thus do not add valuable information for the clustering step. Finally, the connectivity values of each matrix were normalized by applying the Box-Cox transformation. Different options for normalization of connectivity values were tested, namely log, cubic and Box-Cox transform, and the latter was selected since it gave the best approximation of a normal distribution (Supplementary Figure 1).

3.6.2. Choice of Clustering Algorithm

Several different clustering algorithms can be used to group voxels according to their connectivity profiles. Here, we applied two of the most common used clustering algorithms in CBP: *k*-means and hierarchical clustering. After clustering was performed, we evaluated the performance of the two algorithms on our dataset to identify the best method for our CBP pipeline. This was done by calculating the silhouette coefficient of the clustering results for each method and selecting the one that scored highest. Silhouette coefficient is an internal cluster validation metric that is used when the ground truth labels are not known, and its value is higher when the clusters are dense and well separated (Rousseeuw, 1987). Furthermore, since the total number of voxels in all brain regions can go up to 200000 and we are considering connectivity between voxels, our data is high-dimensional which can undermine the performance of the clustering algorithm. This is known as the curse of dimensionality as termed by Richard Bellman (Bellman, 1957) and dimensionality reduction techniques can help overcome this issue. As such, we used the silhouette coefficient to evaluate the performance of the two clustering algorithms in conjunction with a dimensionality reduction applied prior to the clustering. Two methods were used, namely Principal Component Analysis (PCA) and Self-Organizing Maps (SOM). PCA is a linear technique which reduces a large set of variables to a smaller set, known as principal components (PC), while preserving as much of

the data's variance as possible (Bishop, 2006). Here, we selected the PCs that preserved 95% of the variance. SOMs are unsupervised learning neural networks that are trained to produce a low-dimensional representation of the data while preserving the topology of the input space and were inspired by the topographical organization of the sensory cortex of the mammalian brain (Kohonen, 1990, 1982). This method has already been applied to perform CBP of functional data (Mishra et al., 2014).

3.6.3. Determination of optimal clustering solution

After choosing the clustering algorithm, we applied it to each subject and each region for a range of different number of clusters, $k = [2:6]$. For each k value, we estimated multiple internal cluster validation metrics. Specifically, we computed the Silhouette, Davies-Bouldin and Calinski-Harabasz metrics, which are often used when the ground truth labels are unknown. To circumvent the random initialization associated with clustering algorithms, we run 10 iterations of this procedure for each subject and region. For each run we selected the best k according to each metric and computed the mode of all these k (i.e., we choose the most frequent k in the 10 iterations run for each metric), which resulted in a k for each subject and region for the three metrics. Following this, we computed the mode of the k per region, over all subjects, to obtain a single k value per region and metric. Finally, we computed the clustering solution for each subject and region according to the selected k of each region and metric. By combining all the clustered regions of a subject, we obtained the individual clustered parcellations. Since we selected different k values based on each of three metrics, this step resulted in three individual parcellation solutions per subject.

3.6.4. Register individual parcellations to standard space

After obtaining the individual clustered parcellations, they were normalized to the Montreal Neurological Institute (MNI) space so that we could combine them to generate the group-level parcellation. The normalization to the MNI space was performed using Advanced Normalization Tools (ANTs) software package, available at http://stnava.github.io/ANTs/. First, the transformation from native structural space to MNI space was computed, which was composed by an affine and a non-linear transform. Then, once again an affine and non-linear transform were concatenated to create the transformation from diffusion to structural native spaces. Finally, the two transformations (diffusion to structural, structural to MNI) were sequentially applied to normalize the subjects' individual clustered parcellations to the MNI space.

3.6.5. Group-wise clustered parcellation

Group-wise parcellation was obtained by combining all individuals clustered parcellations through a consensus clustering algorithm. This algorithm is used to aggregate multiple partitions of the same dataset (either coming from different clustering algorithms, different runs of the same algorithm, different samples of data) into a single partition (Vega-Pons and Ruiz-Shulcloper, 2011). We used the package Cluster Ensembles available at: https://pypi.org/project/Cluster_Ensembles/. This package combines three approximation algorithms to solve the problem of maximizing the average similarity between partitions and the one with the best performance is selected (Giecold et al., 2016; Strehl, 2002).

First, we created a group reference parcellation, since our initial parcellation (DKT40 and Buckner40) was obtained for each individual as a result of FreeSurfer's segmentation. For this, we normalized each individual parcellation from structural native space to the MNI space using ANTs, as described before. Then, for each voxel we attributed a label that was the mode of all subjects. Finally, we applied a threshold of 20% of the total number of subjects in order to remove voxels that were only present in few subjects. After obtaining the group reference parcellation, we masked each individual clustered parcellation using this reference and then applied consensus clustering to each region. In the end, we combined all regions to create a group clustered parcellation of the whole brain.

3.6.6. Clusters postprocessing

Since the clustering algorithm can generate spatially disjoint clusters, we forced these to be spatially contiguous by relabeling connected components. Thus, each connected component in a region was assigned to a different cluster. This means that for some regions the final number of clusters was higher than the chosen k.

Finally, clusters with a size under 300 voxels were removed by merging them with its neighborhood. The size of 300 voxels was chosen after evaluating the clusters' sizes of the group parcellation registered to each individual's native diffusion space. Since subjects' diffusion space had lower resolution (2x2x2 mm) when compared to the resolution of the group parcellation (1x1x1 mm), the clusters' sizes registered in the native diffusion space had less voxels. We opted for selecting the threshold level leading to a minimum cluster size higher than 5 voxels in the subjects' diffusion space (Supplementary Figure 2).

3.7. Connectivity Homogeneity Fingerprint

We developed a metric to evaluate parcellation homogeneity and thus compare the accuracy of different parcellations in terms of regional connectivity fingerprint homogeneity – connectivity homogeneity fingerprint (CHF). This metric reflects homogeneity level of the structural connectivity fingerprint of all voxels in a region (i.e., the magnitude of overlap between the structural connectivity fingerprint of all voxels contained a region). Higher values mean that a region contains a larger pool of voxels with homogeneous connectivity profiles to the rest of the brain. It is calculated using the voxel-wise SC matrix of each region with the following steps: (1) the matrix is binarized; (2) the sum of each column is computed and divided by the size of the region, which results in a vector; (3) the CHF is equal to the average of the vector.

Since the main goal of CBP is to group voxels with similar connectivity patterns, we evaluated the CHF of the original and the final parcellation to verify if our CBP method resulted in a parcellation with higher CHF. To do this, we performed probabilistic tractography with the obtained group parcellation. First, the group parcellation was registered to each individual's diffusion space with ANTs, by applying sequentially the transformation from MNI space to native structural space (composed by an affine and a non-linear transform) and the transformation from structural to diffusion native spaces (composed by an affine and a non-linear transform). Gray matter and white matter masks, estimated with FreeSurfer for each individual, were applied to the group parcellation to exclude voxels outside these regions (e.g., voxels belonging to cerebrospinal fluid (CSF)). Then, probabilistic tractography was run using the group parcellation clusters as seed masks (5000 streamlines were sampled from each voxel in the seed mask). This allowed to obtain the voxel-wise SC matrix for each cluster (i.e., SC between each voxel of the cluster and the voxels of all clusters in the parcellation) and then we calculated the CHF of each cluster for all subjects. The CHF of the original parcellation was computed with the voxel-wise SC matrices that were used as the input of CBP. Statistical comparison of the CHF between each developed parcellation and the original parcellation was performed using independent samples t-tests and p values were corrected for multiple comparisons, using the false discovery rate (FDR) method.

3.8. Selection of group parcellation and network construction

After evaluating the CHF of the group parcellations estimated with each cluster validity metric (i.e., Silhouette, Davies-Bouldin, Calinski-Harabasz), we selected one group parcellation to assess longitudinal changes in the topological properties of white matter structural connectivity networks. To do this, we

repeated the steps described in the previous section for the second timepoint dataset, with the selected partition (registration of group parcellation to individual's diffusion space, probabilistic tractography and calculation of CHF).

Then, we created the SC network matrices, for each subject and timepoint, by performing probabilistic tractography using the clusters of the selected group parcellation as seed masks. This resulted in a SC matrix, for each subject, representing the number of streamlines leaving each seed mask and reaching any of the other regions. This matrix was normalized by dividing each line by the waytotal value (i.e., the total number of generated tracts not rejected by inclusion/exclusion mask criteria). We further divided the matrix by its maximum value, in order to have connectivity values between [0, 1]. Since tractography is dependent on seeding location, the connectivity probability from *i* to *j* is not necessarily equal to that from *j* to *i*. Still, these two probabilities are highly correlated across the brain for all participants. Thus, we defined the undirected connectivity probability as the average of these two probabilities, P_{ij} and P_{ji}, which originated an undirected connectivity matrix. Next, a consistency-based threshold at 30% density was applied, which retains the most consistent connections across subjects with the aim of reducing the false-positive in group-average connectivity matrices (Roberts et al., 2017). Subsequently, we tested different strategies to account for connectivity between clusters of the same region: 1) set intra-cluster connectivity to 0 and normalize regional connectivity values by the maximum; 2) set intra-cluster connectivity to 1 and normalize regional connectivity values by the maximum (excluding the intra-cluster connectivity) and 3) use the original intra-cluster connectivity values. Supplementary Figure 3 shows the example for one subject of the connections surviving each of these strategies. We opted to use the original intra-cluster connectivity values as the other two strategies seem to include more connections which could lead to the inclusion of false-positive connections. Finally, a threshold set to 1% of the strongest connection was applied to each SC matrix, in order to remove spurious connections.

3.9. Graph Theoretical Analysis

Brain networks can be described in terms of its topological organization, using graph theory measures. Brain Connectivity Toolbox (https://sites.google.com/site/bctnet/) was used to extract these metrics. The structural connectivity networks built with the selected group parcellation were used. The following topological features were evaluated for both timepoints.

Modularity. Modularity quantifies the degree to which nodes of a network may aggregate into densely connected non-overlapping modules or communities (Fornito et al., 2016). Nodes within a community

are more strongly connected with each other than with nodes outside this community. Thus, the optimal community structure will be the partition of the network that maximizes intra-module connectivity and minimizes inter-module connectivity. The index of modularity, Q, is given by the difference between the empirical degree of intra-module connectivity and the degree expected by chance (Fornito et al., 2016). The optimal community structure can be found by searching for the partition that maximizes Q. One popular algorithm used to find the optimal partition is the Louvain algorithm and, shortly, this is how it works: first, it starts with all nodes in a distinct module, then it chooses a node at random and merges it with the module that produces the largest gain in Q, these steps are repeated until no additional gains in Q are possible (Blondel et al., 2008). Given that at each iteration, nodes are chosen randomly, running the algorithm multiple times can lead to different solutions. Also, another limitation is the so-called degeneracy problem, that can cause the existence of large number of different solutions, since there is not a clear global maximum of Q (Good et al., 2010). To circumvent this problem, we ran the Louvain algorithm 10000 times and selected the partition having the higher number of occurrences in the set of 10000 partitions, i.e., the partition that was more consistent. To compare the optimal community structures found at each timepoint, we defined a similarity metric. For each module in a partition, we found the module in the other partition that was more similar to this one (by finding the maximum of the number of shared regions divided by the total number of regions in the two modules). The similarity metric was then calculated as the mean of the maximum values for each module. Values close to 1 indicate higher similarity between the partitions.

Hubs. Hubs can be defined as nodes with high regional efficiency (E_{nodal}) (Achard and Bullmore, 2007). This measure reflects how well a node is integrated within the network via its shortest paths and is defined as the mean of the inverse shortest path length, l_{ij}, between a given node and all other nodes in the network:

$$E_{nodal}(j) = \frac{1}{(N-1)} \sum_{i} \frac{1}{l_{ij}}$$

If the normalized E_{nodal} (divided by the mean E_{nodal} of all nodes) is larger than the normalized mean E_{nodal} of all nodes of the network plus one standard deviation (SD), the node is considered a hub (Lo et al., 2010).

Furthermore, we analyzed the topological roles of nodes in the communication within and between modules. This allowed the classification of nodes into provincial and connector hubs. The definition of these roles is described below.

Provincial Hubs are nodes with high within-module degree z-score (greater than the mean plus SD of all nodes) and low participation coefficient (PC $\leq$ 0.3). Positive values of within-module degree z-score indicate high (above the average) intra-module connectivity, and thus higher values of this measure suggest that the node plays a central role in intra-modular communication. Participation coefficient (PC) compares the number of connections of a node with other nodes in different modules, to the total number of connections to other nodes in the same module. Values close to one indicate that the edges of a node are distributed uniformly across modules while a value of zero means that all edges of a nodes are limited to its own module. Thus, provincial hubs are characterized by comprising most of their connections within their own module (Fornito et al., 2016).

Connector Hubs were also defined as nodes with high within-module degree z-score and high participation coefficient (PC > 0.3). This means they have many connections with other modules, and thus play a key role in inter-modular communication (Fornito et al., 2016).

3.10. Fingerprints of modular connectivity

We also analyzed, for each timepoint, the network fingerprints of inter-modular (global and connector-hub-driven) and intra-modular connectivity. The same method of analysis as described in (Fernandes et al., 2019), was applied in this work. In summary, modular connectivity strength was defined as the degree (total number of connections) of all nodes constituting a module. To quantify this connectivity at both timepoints, a reference scheme of community structure was chosen based on the mean score of community-structure goodness-of-fit. Subsequently, matrices of inter-modular and intra-modular connectivity were created for both timepoints.

3.11. Statistical analysis

Statistical comparison of the SC matrices between first and last assessments, at the edge level, was performed by applying a paired sample t-test with SC as the dependent variable and time of evaluation as independent variable. The obtained SC networks are comprised of 170 nodes, yielding a total number of possible edges of 14365 (170*169/2). Testing the hypothesis of interest at the edge level, therefore

poses a multiple comparisons problem. In order to increase the statistical power of the analysis, we used the network-based statistics (NBS) procedure implemented in the NBS toolbox (https://sites.google.com/site/bctnet/comparison/nbs). This is a non-parametric statistical method that allows the identification of significantly different sub-networks, while controlling for the family-wise error rate (FWER) (Zalesky et al., 2010). First, it independently tests the hypotheses at every connection in the network and threshold the ones exceeding a user defined primary threshold, then it identifies sub-networks constituted by interconnected edges that survived the primary threshold. The significance of these sub-networks is then calculated by comparing their sizes to the distribution of the size of sub-networks obtained through random permutations of the original hypothesis. It is important to note that the primary threshold only affects the sensitivity of the method and thus, FWER is assured independently of this threshold. In this study, the primary threshold was set to F = 7.0, which was the maximum threshold that detected a unique significant connected component having more than two connections (Supplementary Figure 4). Longitudinal changes in structural connectivity detected with NBS are represented by significantly connected components at a corrected level of $p < 0.05$ FWE corrected.

4. Results

4.1. Sample Characterization

Table 1 shows the demographic characterization of the participants included in this study. In summary, mean age at baseline was 63.5 years (range, 51 – 82 years) and mean interval between evaluations was 52.8 months (range, 45 – 73 months). Interval time was not significantly associated with age at baseline ($r = -0.12$, $p = 0.41$). The sample was balanced for sex (51% females, 49% males) and they did not differ with respect to interval time ($t(30) = 0.14, p = 0.89$). Mean education level was 5.98 years (range, 0 – 17 years).

Table 1. Basic demographic characterization of the study's cohort.

	Mean ± SD (range)
N (Females/Males)	51 (26/25)
Age at baseline (years)	63.5 ± 7.41 (51 - 82)
Age at follow-up (years)	68.0 ± 7.25 (55 - 86)
Interval (months)	52.8 ± 7.24 (45 - 73)
Education (years)	5.98 ± 3.97 (0 - 17)

4.2. Clustering algorithm

The analysis of the silhouette scores of different clustering algorithms revealed that the best solution was the *k*-means algorithm in conjunction with SOM for dimensionality reduction. Figure 2 represents the silhouette coefficient scores of the different solutions for one brain region. This solution in addition to result in higher silhouette scores also originated clusters more balanced in terms of size.

Figure 2. Example of silhouette scores of one brain region for different clustering algorithms (hierarchical and *k*-means clustering) and different clustering algorithms in conjunction with different data dimensionality reduction techniques (PCA and SOM). Different clustering solutions (2 to 6 clusters) were tested. SOM + *k*-means clustering is the solution with the highest values of silhouette coefficient and with more balanced cluster sizes.

4.3. Optimal clustering solution

Table 2 presents the optimal number of clusters for each brain region according to each cluster validity metric (Silhouette, Davies-Bouldin and Calinski-Harabasz). For the Silhouette coefficient, most of regions were partitioned in two clusters, with the exception of right entorhinal cortex, left and right caudate, right amygdala and left and right acumbens area which were subdivided in six clusters. Davies-Bouldin score also subdivided almost all brain regions in two clusters, with the exception of right transverse temporal, left and right acumbens area that were subdivided in six clusters and right amygdala which was partitioned in three clusters. According to the Calinski-Harabasz coefficient, all brain regions were split in six clusters.

Table 2. Optimal number of clusters for each brain region according to each clustering validity metric.

	Silhouette		Davies-Bouldin		Calinski-Harabasz	
ROI Name	n_{left}	n_{right}	n_{left}	n_{right}	n_{left}	n_{right}
Caudal Anterior Cingulate	2	2	2	2	6	6
Caudal Middle Frontal	2	2	2	2	6	6
Cuneus	2	2	2	2	6	6
Entorhinal	2	6	2	2	6	6
Fusiform	2	2	2	2	6	6
Inferior Parietal	2	2	2	2	6	6
Inferior Temporal	2	2	2	2	6	6
Isthmus Cingulate	2	2	2	2	6	6
Lateral Occipital	2	2	2	2	6	6
Lateral Orbitofrontal	2	2	2	2	6	6
Lingual	2	2	2	2	6	6
Medial Orbitofrontal	2	2	2	2	6	6
Middle Temporal	2	2	2	2	6	6
Parahippocampal	2	2	2	2	6	6
Paracentral	2	2	2	2	6	6
Pars Opercularis	2	2	2	2	6	6
Pars Orbitalis	2	2	2	2	6	6
Pars Triangularis	2	2	2	2	6	6
Pericalcarine	2	2	2	2	6	6
Postcentral	2	2	2	2	6	6
Posterior Cingulate	2	2	2	2	6	6
Precentral	2	2	2	2	6	6
Precuneus	2	2	2	2	6	6
Rostral Anterior Cingulate	2	2	2	2	6	6
Rostral Middle Frontal	2	2	2	2	6	6
Superior Frontal	2	2	2	2	6	6
Superior Parietal	2	2	2	2	6	6
Superior Temporal	2	2	2	2	6	6
Supramarginal	2	2	2	2	6	6
Transverse Temporal	2	2	2	6	6	6

Insula	2	2	2	2	6	6
Thalamus Proper	2	2	2	2	6	6
Caudate	6	6	2	2	6	6
Putamen	2	2	2	2	6	6
Pallidum	2	2	2	2	6	6
Hippocampus	2	2	2	2	6	6
Amygdala	2	6	2	3	6	6
Accumbens Area	6	6	6	6	6	6

The final group clustered parcellations according to each metric are represented in Figure 3. Silhouette coefficients generated a group partition with 170 clusters, Davies-Bouldin a group parcellation with 163 clusters and Calinski-Harabasz produced a group partition with 472 clusters.

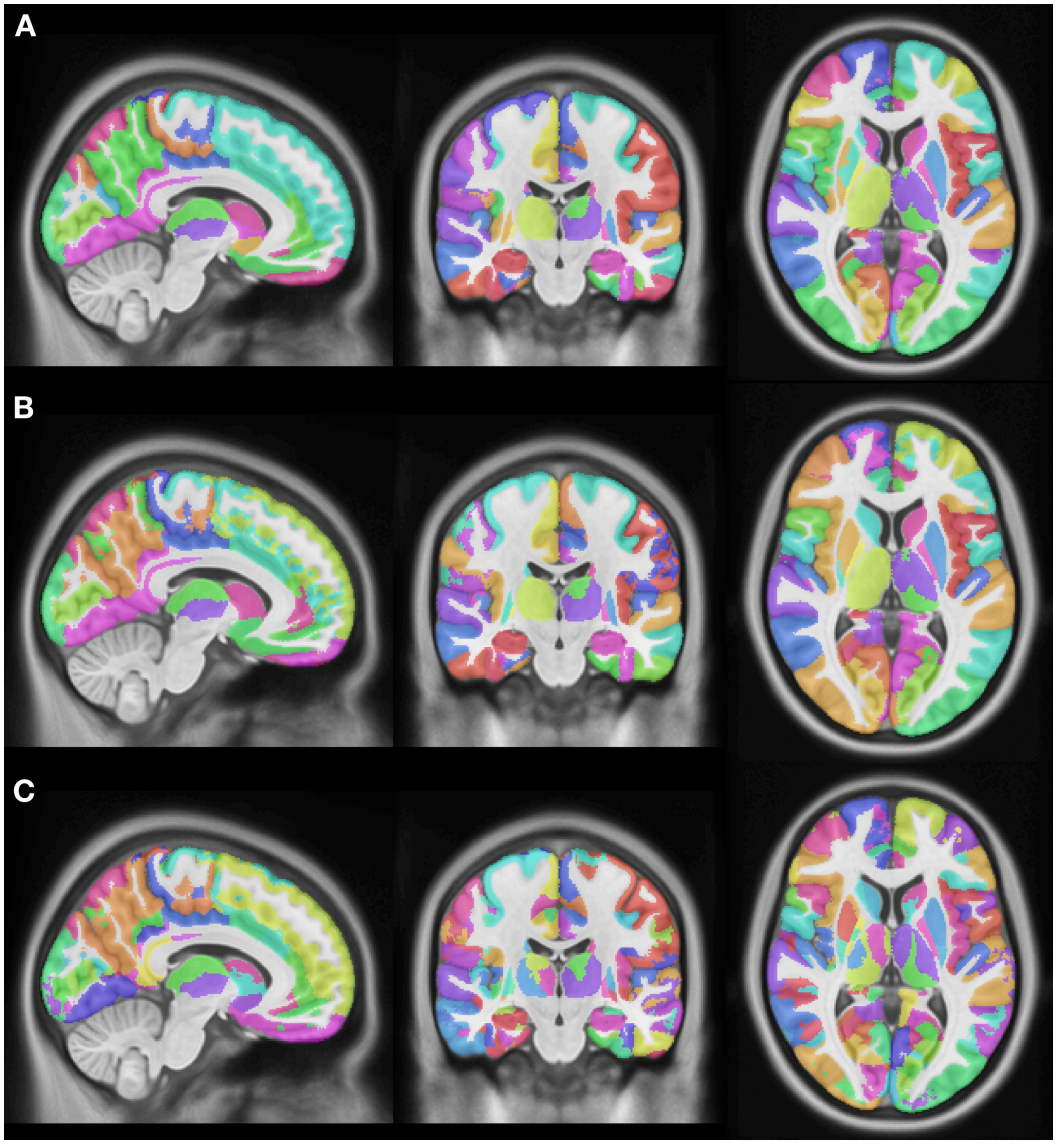

Figure 3. Final group parcellations for the different validity metrics: A) silhouette, B) Davies-Bouldin, C) Calinski-Harabasz. Parcellations are displayed in MNI standard space.

4.4. Connectivity Homogeneity Fingerprint

The three group parcellations present higher values of CHF in comparison to the initial parcellation (DKT40 + Buckner40) (Fig. 4). The parcellations produced from Silhouette and Davies-Bouldin coefficients exhibit similar values of CHF (Silhouette - $M = 0.057, SD = 0.031$); Davies-Bouldin – $M = 0.052, SD = 0.038$); the one originating from Calinski-Harabasz has the highest value ($M = 0.10, SD = 0.035$). The initial partition displays the lowest value ($M = 0.020, SD = 0.020$). Statistical comparison of CHF values revealed that the three parcellations had statistically significant higher CHF values in comparison to the original parcellation (Silhouette – $t_{(127.8)} = 8.86, p < 0.001, d = 1.44$; Davies-Bouldin – $t_{(114.2)} = 6.65, p < 0.001, d = 1.08$; Calisnki-Harabasz – $t_{(119.3)} = 17.4, p < 0.001, d = 2.82$).

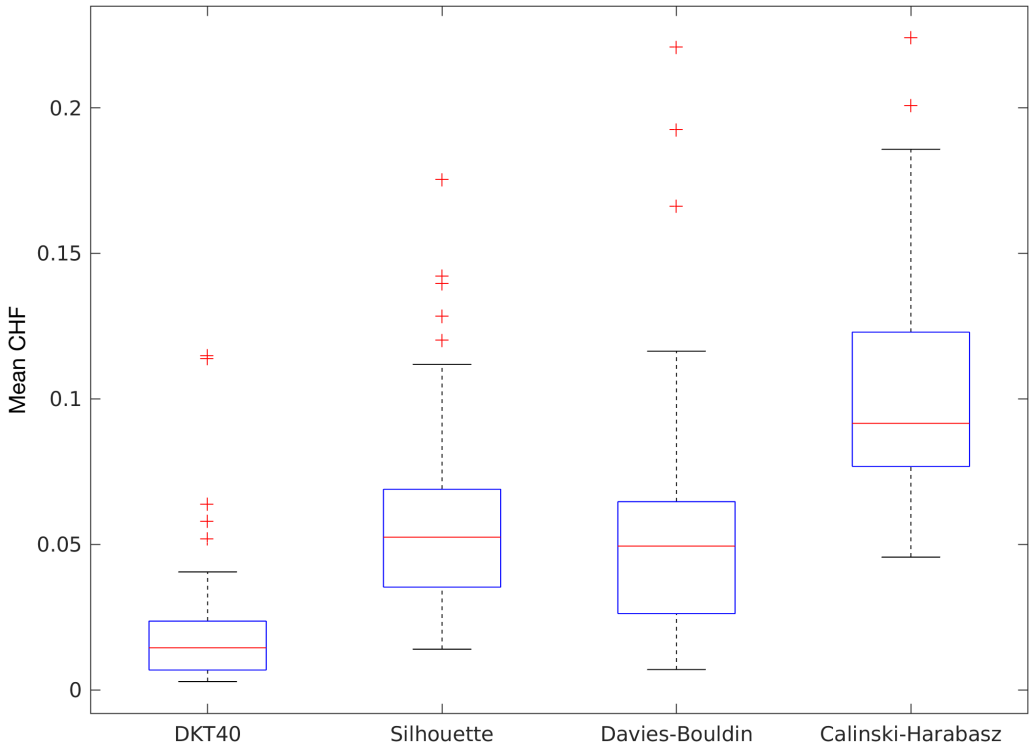

Figure 4. Mean connectivity homogeneity fingerprint (CHF) scores of the different group parcellations for all subjects. The three solutions resulted in parcellations with higher CHF in comparison to the original partition. Calinski-Harabasz parcellation had the highest homogeneity values but also the highest number of clusters.

We selected the estimated group parcellation based on the Silhouette score to assess longitudinal changes in white matter structural connectivity. The Calinski-Harabasz parcellation has a very high number of clusters, which may in part explain its high value of CHF, but this increased granularity may not be beneficial and can make subsequent analyses computationally expensive. Furthermore, the Davies-Bouldin partition had some regions that were clustered in a pattern that may not be biologically plausible (checkerboard pattern, Supplementary Figure 5). Thus, we selected the Silhouette parcellation which does not present these limitations and still has higher CHF in comparison to the initial parcellation. Details of the label and coordinates of the regions belonging to this parcellation are given in Supplementary Table 1.

In addition, in the second timepoint, the values of CHF for the Silhouette parcellation are very similar when compared to the first timepoint ($M = 0.060, SD = 0.032$, Fig. 5).

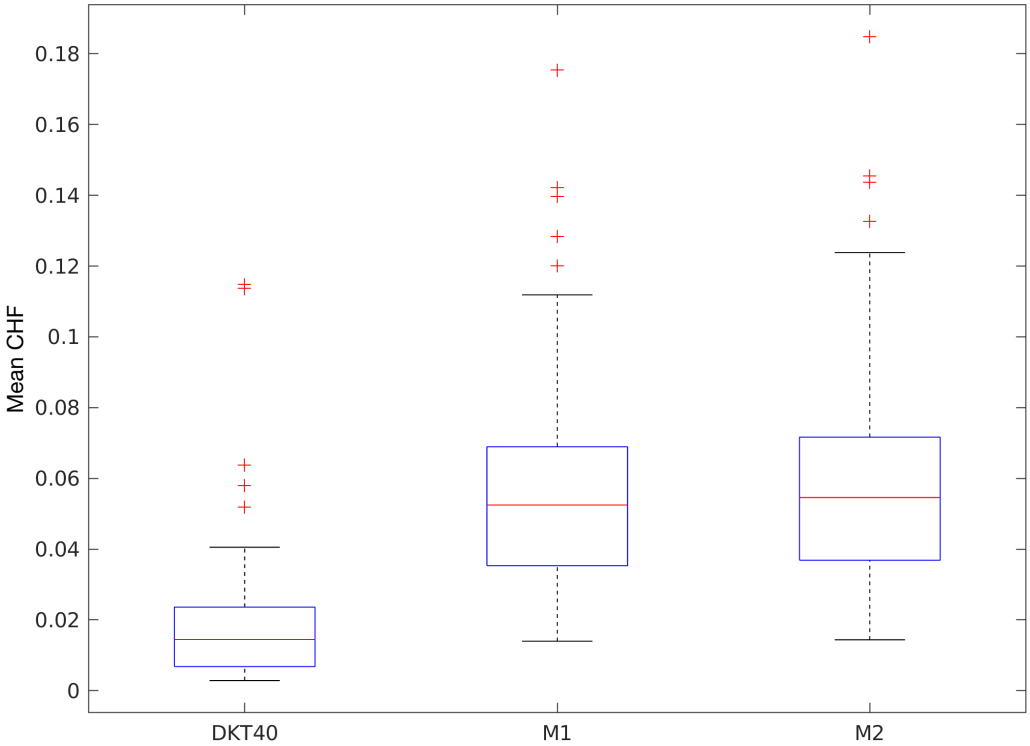

Figure 5. Mean CHF values for the two timepoints and the initial parcellation. At both timepoints, the homogeneity is higher in comparison to the original partition.

4.5. Longitudinal Changes in Brain Structural Connectivity

Using the Silhouette parcellation, we found significant changes in structural connectivity between timepoints in a brain sub-network ($p < 0.001$), comprising 122 connections, from which 52 correspond to decreases and 70 to increases in structural connectivity (Fig. 6). When analyzing the individual connections of this sub-network, we concluded that the connections with longitudinal decreases in connectivity are represented by 19 intra-left, 24 intra-right and 9 inter-hemispheric connections. The connections with longitudinal increases in connectivity are composed by 16 intra-left, 22 intra-right and 32 inter-hemispheric connections. The summary of the connections is present in Table 3.

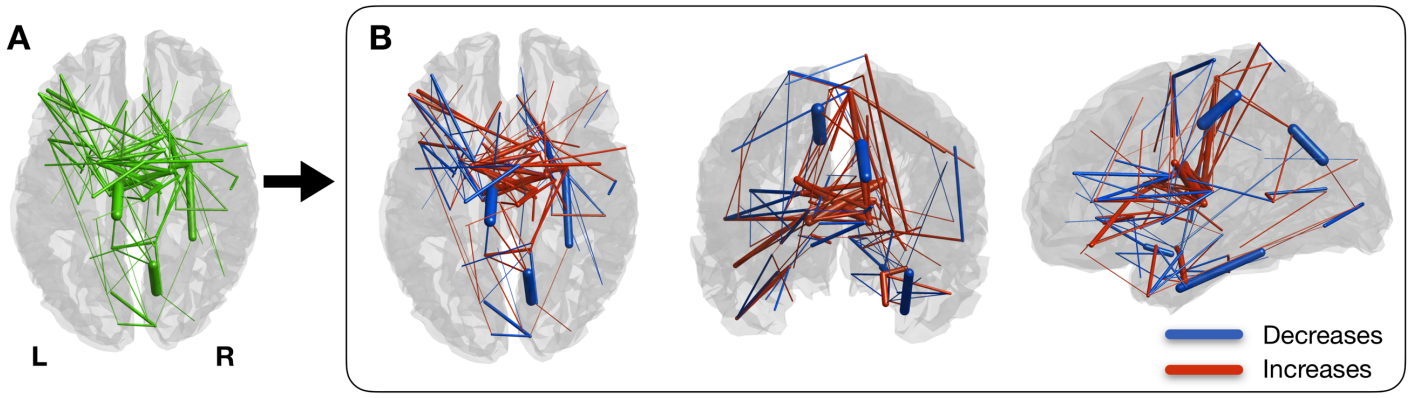

Figure 6. Significant changes in structural connectivity between timepoints. A) Binarized version of the connected component of significantly altered structural connectivity. B) Weighted version of A), with edge thickness representing the amplitude of differences. Blue represents decreases in connectivity strength between timepoints and red represents increases. Connections with decreases are mostly intra-hemispheric, while most of the increases are composed of intra-hemispheric connections.

Table 3. Description of the connections comprising the connected component of significant structural connectivity differences between timepoints ($p < .001$).

Area 1		Area 2		Difference	Intra-Left	Intra-Right	Inter-Hemispheric
N	Name	N	Name				
			Increases				
68	Left Thalamus Proper 2	99	Right Caudate 4	0.035	0	0	1
71	Left Caudate 3	102	Right Thalamus Proper 1	0.033	0	0	1
85	Right Amygdala 2	160	Right Entorhinal 1	0.029	0	1	0

102	Right Thalamus Proper 1	140	Right Paracentral 2	0.027	0	1	0
70	Left Caudate 2	101	Right Caudate 6	0.026	0	0	1
85	Right Amygdala 2	89	Right Amygdala 6	0.024	0	1	0
70	Left Caudate 2	99	Right Caudate 4	0.023	0	0	1
34	Left Pars Orbitalis 1	73	Left Caudate 5	0.022	1	0	0
70	Left Caudate 2	96	Right Caudate 1	0.022	0	0	1
71	Left Caudate 3	103	Right Thalamus Proper 2	0.018	0	0	1
37	Left Pars Triangularis 2	73	Left Caudate 5	0.018	1	0	0
115	Right Superior Frontal 2	123	Right Precentral 1	0.017	0	1	0
20	Left Lateral Orbitofrontal 2	26	Left Middle Temporal 2	0.016	1	0	0
73	Left Caudate 5	96	Right Caudate 1	0.016	0	0	1
67	Left Thalamus Proper 1	99	Right Caudate 4	0.015	0	0	1
15	Left Isthmus Cingulate 1	153	Right Isthmus Cingulate 2	0.015	0	0	1
49	Left Rostral Anterior Cingulate 1	72	Left Caudate 4	0.015	1	0	0
92	Right Pallidum 1	140	Right Paracentral 2	0.013	0	1	0
68	Left Thalamus Proper 2	96	Right Caudate 1	0.013	0	0	1
69	Left Caudate 1	102	Right Thalamus Proper 1	0.013	0	0	1
95	Right Putamen 2	130	Right Postcentral 3	0.013	0	1	0
73	Left Caudate 5	102	Right Thalamus Proper 1	0.012	0	0	1
142	Right Parahippocampal 2	154	Right Inferior Temporal 1	0.011	0	1	0
102	Right Thalamus Proper 1	139	Right Paracentral 1	0.011	0	1	0
67	Left Thalamus Proper 1	101	Right Caudate 6	0.011	0	0	1
94	Right Putamen 1	120	Right Rostral Anterior Cingulate 2	0.011	0	1	0
94	Right Putamen 1	111	Right Superior Temporal 2	0.011	0	1	0
90	Right Hippocampus 1	96	Right Caudate 1	0.010	0	1	0
44	Left Posterior Cingulate 2	140	Right Paracentral 2	0.010	0	0	1
115	Right Superior Frontal 2	124	Right Precentral 2	0.009	0	1	0
67	Left Thalamus Proper 1	96	Right Caudate 1	0.009	0	0	1
92	Right Pallidum 1	121	Right Precuneus 1	0.009	0	1	0
83	Right Accumbens Area 1	105	Right Insula 2	0.009	0	1	0
97	Right Caudate 2	99	Right Caudate 4	0.009	0	1	0
15	Left Isthmus Cingulate 1	122	Right Precuneus 2	0.008	0	0	1
30	Left Paracentral 1	122	Right Precuneus 2	0.008	0	0	1
70	Left Caudate 2	97	Right Caudate 2	0.007	0	0	1
71	Left Caudate 3	115	Right Superior Frontal 2	0.007	0	0	1
34	Left Pars Orbitalis 1	68	Left Thalamus Proper 2	0.007	1	0	0
54	Left Superior Frontal 1	71	Left Caudate 3	0.007	1	0	0
31	Left Paracentral 2	121	Right Precuneus 1	0.007	0	0	1
70	Left Caudate 2	140	Right Paracentral 2	0.006	0	0	1
161	Right Entorhinal 2	164	Right Entorhinal 5	0.006	0	1	0
3	Left Caudal Middle Frontal 1	32	Left Pars Opercularis 1	0.006	1	0	0
15	Left Isthmus Cingulate 1	165	Right Cuneus 1	0.006	0	0	1
7	Left Entorhinal 1	78	Left Hippocampus 1	0.006	1	0	0

31	Left Paracentral 2	122	Right Precuneus 2	0.006	0	0	1
69	Left Caudate 1	140	Right Paracentral 2	0.006	0	0	1
74	Left Putamen 1	101	Right Caudate 6	0.005	0	0	1
35	Left Pars Orbitalis 2	73	Left Caudate 5	0.005	1	0	0
73	Left Caudate 5	103	Right Thalamus Proper 2	0.005	0	0	1
29	Left Parahippocampal 2	38	Left Pericalcarine 1	0.005	1	0	0
74	Left Putamen 1	115	Right Superior Frontal 2	0.005	0	0	1
4	Left Caudal Middle Frontal 2	37	Left Pars Triangularis 2	0.005	1	0	0
40	Left Postcentral 1	140	Right Paracentral 2	0.005	0	0	1
101	Right Caudate 6	149	Right Lateral Orbitofrontal 2	0.005	0	1	0
67	Left Thalamus Proper 1	97	Right Caudate 2	0.004	0	0	1
76	Left Pallidum 1	116	Right Superior Frontal 3	0.004	0	0	1
26	Left Middle Temporal 2	39	Left Pericalcarine 2	0.004	1	0	0
102	Right Thalamus Proper 1	136	Right Pars Orbitalis 2	0.004	0	1	0
151	Right Lateral Occipital 2	166	Right Cuneus 2	0.004	0	1	0
101	Right Caudate 6	134	Right Pars Triangularis 2	0.004	0	1	0
31	Left Paracentral 2	67	Left Thalamus Proper 1	0.004	1	0	0
19	Left Lateral Orbitofrontal 1	26	Left Middle Temporal 2	0.003	1	0	0
131	Right Pericalcarine 1	158	Right Fusiform 1	0.003	0	1	0
95	Right Putamen 2	115	Right Superior Frontal 2	0.003	0	1	0
21	Left Lingual 1	28	Left Parahippocampal 1	0.003	1	0	0
77	Left Pallidum 2	98	Right Caudate 3	0.002	0	0	1
73	Left Caudate 5	78	Left Hippocampus 1	0.002	1	0	0
1	Left Caudal Anterior Cingulate 1	126	Right Posterior Cingulate 1	0.002	0	0	1
			Decreases				
67	Left Thalamus Proper 1	77	Left Pallidum 2	-0.002	1	0	0
88	Right Amygdala 5	155	Right Inferior Parietal 1	-0.002	0	1	0
63	Left Transverse Temporal 1	75	Left Putamen 2	-0.003	1	0	0
16	Left Isthmus Cingulate 2	165	Right Cuneus 1	-0.003	0	0	1
88	Right Amygdala 5	98	Right Caudate 3	-0.003	0	1	0
54	Left Superior Frontal 1	94	Right Putamen 1	-0.003	0	0	1
84	Right Amygdala 1	102	Right Thalamus Proper 1	-0.003	0	1	0
134	Right Pars Triangularis 2	167	Right Caudal Middle Frontal 1	-0.003	0	1	0
98	Right Caudate 3	114	Right Superior Frontal 1	-0.003	0	1	0
83	Right Accumbens Area 1	92	Right Pallidum 1	-0.004	0	1	0
54	Left Superior Frontal 1	99	Right Caudate 4	-0.004	0	0	1
38	Left Pericalcarine 1	153	Right Isthmus Cingulate 2	-0.004	0	0	1
154	Right Inferior Temporal 1	161	Right Entorhinal 2	-0.004	0	1	0
89	Right Amygdala 6	155	Right Inferior Parietal 1	-0.004	0	1	0
159	Right Fusiform 2	160	Right Entorhinal 1	-0.004	0	1	0
35	Left Pars Orbitalis 2	53	Left Rostral Middle Frontal 3	-0.004	1	0	0
45	Left Precentral 1	75	Left Putamen 2	-0.004	1	0	0
126	Right Posterior Cingulate 1	152	Right Isthmus Cingulate 1	-0.004	0	1	0

89	Right Amygdala 6	120	Right Rostral Anterior Cingulate 2	-0.004	0	1	0
3	Left Caudal Middle Frontal 1	45	Left Precentral 1	-0.005	1	0	0
30	Left Paracentral 1	70	Left Caudate 2	-0.005	1	0	0
83	Right Accumbens Area 1	119	Right Rostral Anterior Cingulate 1	-0.005	0	1	0
146	Right Medial Orbitofrontal 2	161	Right Entorhinal 2	-0.005	0	1	0
58	Left Superior Temporal 1	72	Left Caudate 4	-0.006	1	0	0
71	Left Caudate 3	74	Left Putamen 1	-0.006	1	0	0
49	Left Rostral Anterior Cingulate 1	77	Left Pallidum 2	-0.007	1	0	0
56	Left Superior Parietal 1	130	Right Postcentral 3	-0.007	0	0	1
98	Right Caudate 3	120	Right Rostral Anterior Cingulate 2	-0.007	0	1	0
86	Right Amygdala 3	146	Right Medial Orbitofrontal 2	-0.008	0	1	0
53	Left Rostral Middle Frontal 3	76	Left Pallidum 1	-0.008	1	0	0
142	Right Parahippocampal 2	161	Right Entorhinal 2	-0.008	0	1	0
84	Right Amygdala 1	154	Right Inferior Temporal 1	-0.008	0	1	0
26	Left Middle Temporal 2	78	Left Hippocampus 1	-0.009	1	0	0
85	Right Amygdala 2	92	Right Pallidum 1	-0.009	0	1	0
8	Left Entorhinal 2	20	Left Lateral Orbitofrontal 2	-0.009	1	0	0
1	Left Caudal Anterior Cingulate 1	15	Left Isthmus Cingulate 1	-0.009	1	0	0
46	Left Precentral 2	115	Right Superior Frontal 2	-0.009	0	0	1
39	Left Pericalcarine 2	131	Right Pericalcarine 1	-0.011	0	0	1
37	Left Pars Triangularis 2	67	Left Thalamus Proper 1	-0.012	1	0	0
120	Right Rostral Anterior Cingulate 2	148	Right Lateral Orbitofrontal 1	-0.013	0	1	0
111	Right Superior Temporal 2	129	Right Postcentral 2	-0.013	0	1	0
26	Left Middle Temporal 2	81	Left Amygdala 2	-0.014	1	0	0
67	Left Thalamus Proper 1	75	Left Putamen 2	-0.014	1	0	0
132	Right Pericalcarine 2	153	Right Isthmus Cingulate 2	-0.014	0	1	0
37	Left Pars Triangularis 2	70	Left Caudate 2	-0.014	1	0	0
53	Left Rostral Middle Frontal 3	70	Left Caudate 2	-0.015	1	0	0
21	Left Lingual 1	131	Right Pericalcarine 1	-0.017	0	0	1
45	Left Precentral 1	115	Right Superior Frontal 2	-0.018	0	0	1
86	Right Amygdala 3	148	Right Lateral Orbitofrontal 1	-0.029	0	1	0
158	Right Fusiform 1	163	Right Entorhinal 4	-0.041	0	1	0
122	Right Precuneus 2	166	Right Cuneus 2	-0.052	0	1	0
30	Left Paracentral 1	43	Left Posterior Cingulate 1	-0.057	1	0	0

4.6. Longitudinal analysis of topological properties

4.6.1. Modularity

The optimal modularity structure had eight modules at both timepoints, and the two configurations had a similarity of 0.55. The arrangement of the modules has some differences between timepoints (Fig 7).

Particularly, module 1 at timepoint 2 includes some occipital regions that are not included in the first timepoint, module 4 changes from left to right hemisphere, module 5 comprises frontal regions at timepoint 2 that are not present at timepoint 1, module 6 loses occipital regions between timepoints, module 7 shifts from frontal to occipital regions and module 8 also loses some frontal regions. Details of the regions belonging to each module are given in Supplementary Table 2. Regarding the connector hubs' connectivity profiles, we observe differences between evaluations, with a higher number of connections in the posterior regions of the brain at timepoint 2 (Fig. 7).

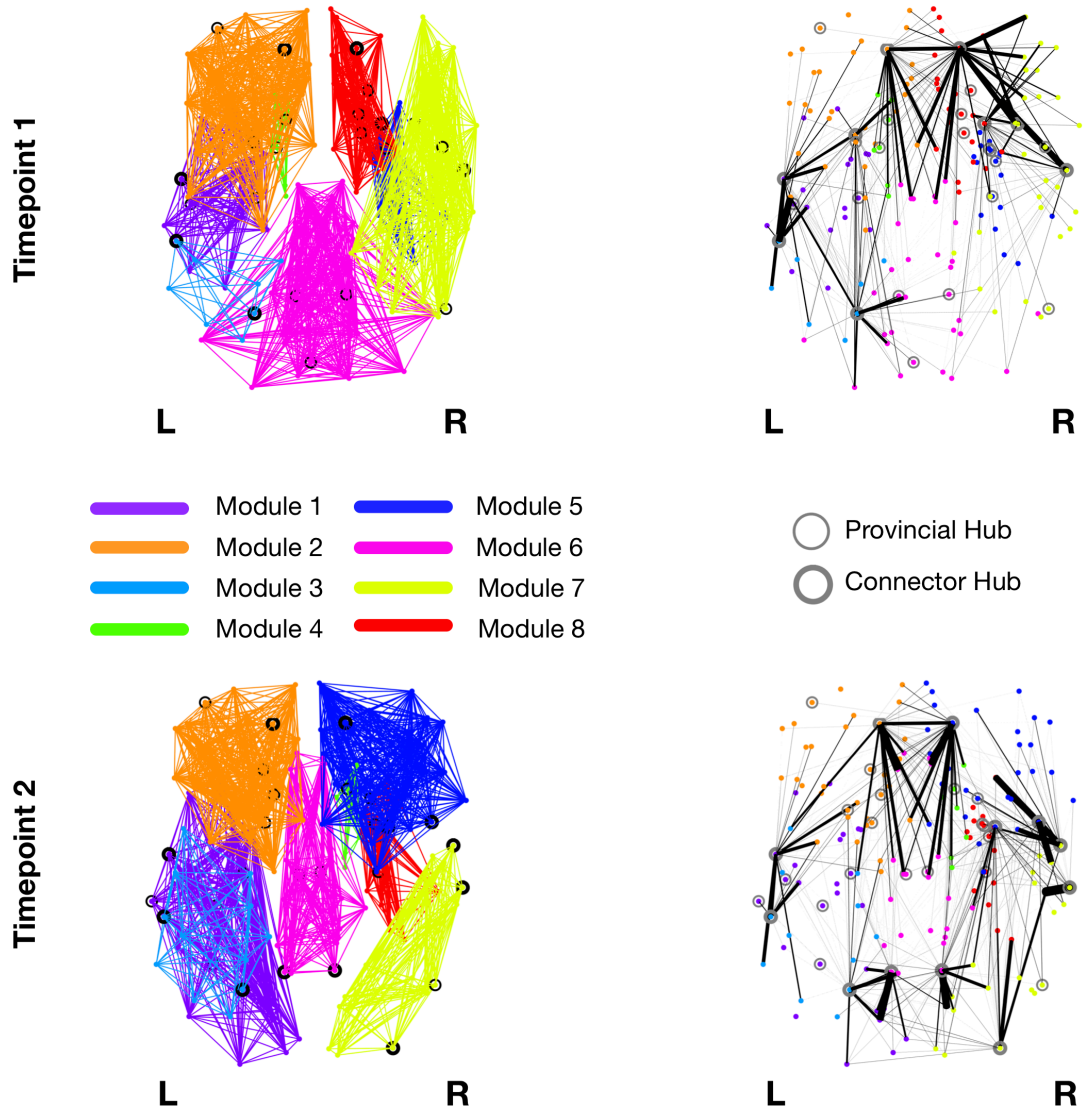

Figure 7. Modularity structure (A) and connector-hub connectivity (B) at timepoint 1 (top row) and timepoint 2 (bottom row). Filled circles represent connector hubs and unfilled circles represent provincial hubs. The same number of modules was found at both timepoints but there were evident differences in modular arrangements (A, B) and in the undirected structural connectivity profile for the connector hubs (C). These differences are probably due to the higher number of connector hubs at the last timepoint.

Giving the role of connector hubs in inter-modular communication, the increase in their number between timepoints reflects an increase in integration of brain structural networks in aging.

4.6.2. Hubs

Global hubs were defined as regions with high normalized nodal efficiency. In the first timepoint, 19 regions were identified as hubs, while at timepoint 2, two additional regions were classified as hubs, namely left lateral occipital 1 (nomenclature of anatomical parcels is done according to: [hemisphere region subdivision]) and left transverse temporal 1 (Table 4, Fig. 8).

Table 4. Global hubs of the brain for the two timepoints. Hubs are sorted by nodal efficiency.

Global Hubs	
M1	M2
Left Rostral Middle Frontal 1	Left Rostral Middle Frontal 1
Left Rostral Middle Frontal 2	Left Rostral Middle Frontal 2
Right Amygdala 2	Right Lateral Occipital 1
Right Lateral Occipital 1	Left Caudate 1
Left Caudate 1	Right Inferior Parietal 2
Right Caudate 1	Right Amygdala 2
Right Middle Temporal 2	Right Middle Temporal 2
Right Inferior Parietal 2	Left Caudal Middle Frontal 1
Right Caudate 6	Left Middle Temporal 2
Left Caudal Middle Frontal 1	Right Caudate 5
Left Supramarginal 2	Right Caudal Middle Frontal 1
Right Rostral Middle Frontal 2	Right Caudate 1
Right Caudal Middle Frontal 1	Right Rostral Middle Frontal 2
Right Caudate 5	Right Amygdala 1
Left Middle Temporal 2	Left Supramarginal 2
Right Amygdala 3	Right Amygdala 3
Right Amygdala 1	Right Caudate 6
Left Middle Temporal 3	Left Transverse Temporal 1
Right Fusiform 1	Left Lateral Occipital 1
	Left Middle Temporal 3
	Right Fusiform 1

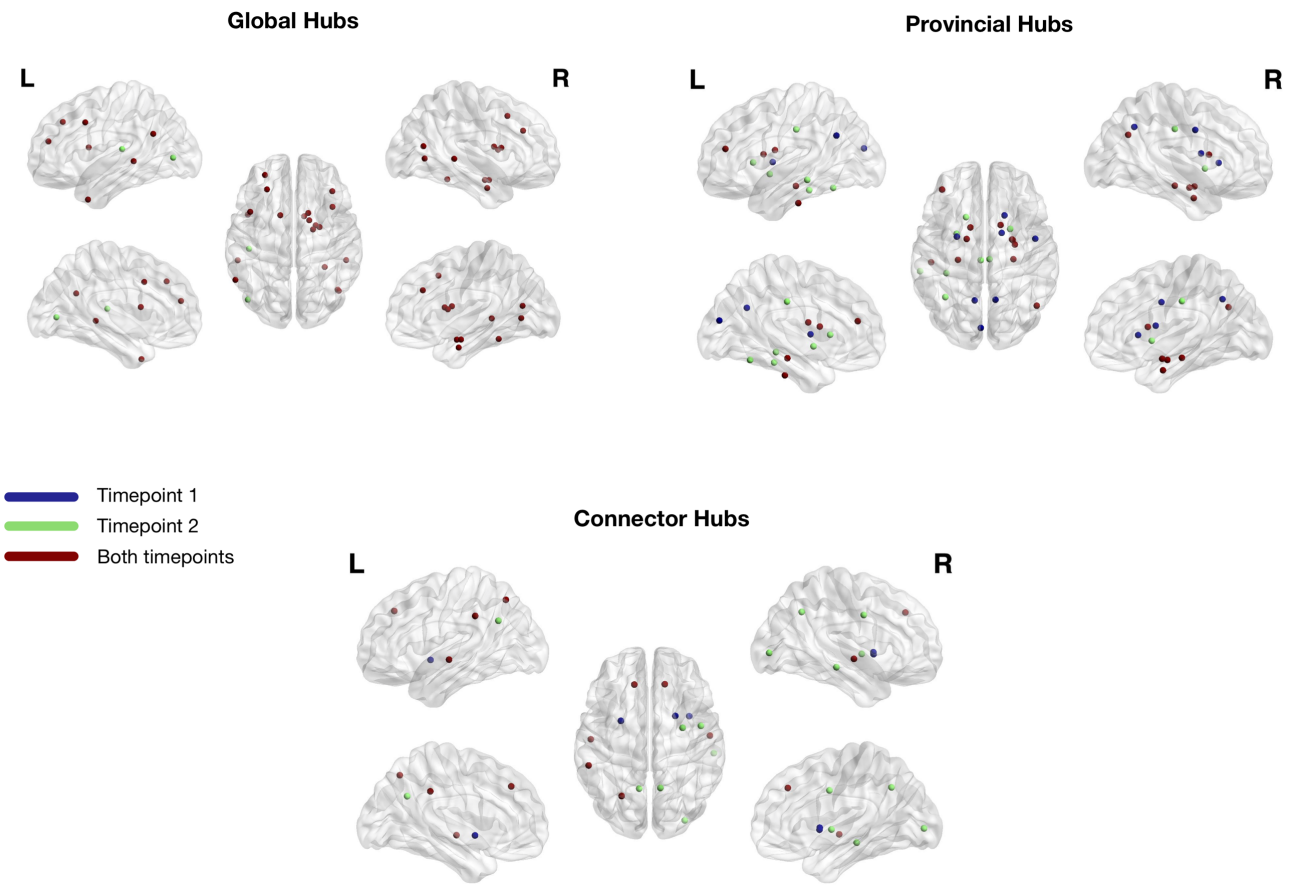

Figure 8. Hubs (global, provincial and connector) identified in the two timepoints. Blue represents hubs only identified at timepoint 1, green represents hubs only identified at timepoint 2 and red represents hubs identified at both timepoints. We observe an increase in all type of hubs (global, provincial and connector) between timepoints. Furthermore, some hubs change their role between timepoints (from provincial to connector – left precuneus 2, right precuneus 2 and right precentral 1; and from connector to provincial – left putamen 2 and right putamen 1).

Regarding provincial hubs, which play a key role in intra-modular communication, 18 hubs were detected at the first timepoint and 19 at the last timepoint (Table 5). Left cuneus 2, left precuneus 2, left putamen 1, right caudate 1, right caudate 2, right precuneus 2 and right precentral 1 were only detected at timepoint 1, while left fusiform 1, left fusiform 2, left middle temporal 1, left posterior cingulate 2, left caudate 5, left putamen 2, right putamen 1 and right posterior cingulate 2 were only detected at timepoint 2. The rest of the regions were common to both timepoints (Fig. 8).

Table 5. Provincial and connector hubs for the two timepoints. Hubs are sorted by modularity degree z-score.

Provincial Hubs		Connector Hubs	
M1	M2	M1	M2
Right Precuneus 2	Right Putamen 1	Left Superior Frontal 2	Right Superior Frontal 3
Right Precentral 1	Right Inferior Parietal 1	Right Superior Temporal 2	Left Superior Frontal 2
Right Caudate 6	Right Posterior Cingulate 2	Right Superior Frontal 3	Left Supramarginal 1
Left Precuneus 2	Right Caudate 6	Left Superior Temporal 2	Left Superior Temporal 2
Left Rostral Middle Frontal 3	Left Rostral Middle Frontal 3	Left Putamen 2	Right Precuneus 2
Right Hippocampus 2	Right Hippocampus 2	Left Superior Parietal 2	Left Superior Parietal 2
Right Inferior Parietal 1	Right Amygdala 1	Right Putamen 1	Right Superior Temporal 2
Right Amygdala 5	Left Posterior Cingulate 2	Right Insula 2	Right Lateral Occipital 2
Right Amygdala 1	Right Amygdala 5	Left Supramarginal 1	Right Precentral 1
Left Hippocampus 2	Left Putamen 2		Right Middle Temporal 1
Left Cuneus 2	Left Hippocampus 2		Right Putamen 2
Right Amygdala 4	Right Amygdala 4		Left Precuneus 2
Left Putamen 1	Left Fusiform 2		
Left Inferior Temporal 2	Left Caudate 1		
Left Caudate 1	Left Inferior Temporal 2		
Right Caudate 1	Left Caudate 2		
Left Caudate 2	Left Caudate 5		
Right Caudate 2	Left Fusiform 1		
	Left Middle Temporal 1		

In the case of connector hubs, which have a central role in inter-modular communication, 9 hubs were detected at timepoint 1 and 12 at timepoint 2 (Table 5).

Left putamen 2, right putamen 1 and right insula 2 were only detected at timepoint 1, while left precuneus 2, right putamen 2, right precuneus 2, right precentral 1, right middle temporal 1 and right lateral occipital 2 was only detected at timepoint 2 (Fig. 8).

Interestingly, left putamen 2 and right putamen 2 lost their connector hub status between timepoints but they were identified as provincial hubs at timepoint 2. In the opposite direction, right left precuneus 2, right precuneus 2 and right precentral 1 lost its provincial hub status and were identified as a connector hub at timepoint 2. Furthermore, left caudate 1, right amygdala 1, right caudate 1 and right caudate 6 were identified as global and provincial hubs at both timepoints.

4.6.3. Fingerprints of Modular Connectivity

The reference scheme chosen to analyze fingerprints of modular connectivity was the community structure of timepoint 2. Connector-hub-driven inter-modular connectivity had significant alterations between timepoints (Fig. 9). Overall, there was an increase of around 33% in modular connectivity strength in the second timepoint. Specifically, we found increased connectivity from module 7 (right hemisphere; temporal, parietal and occipital regions) to modules 1 (left hemisphere; entorhinal, hippocampus, amygdala, parahippocampal, temporal and occipital regions), 5 (right hemisphere; accumbens area, pallidum, putamen, caudate, insula, cingulate and frontal regions) and 8 (right hemisphere; amygdala, hippocampus, parahippocampal, entorhinal, fusiform and temporal regions). Also, module 6 (bilateral cingulate cortex regions, bilateral paracentral, bilateral precuneus and right postcentral) had no connectivity with any other module at timepoint 1, but at timepoint 2 there was connectivity between module 6 and the other modules. Connectivity between module 2 (left hemisphere; caudate, putamen, pallidum, accumbens area, thalamus, insula, rostral anterior cingulate and frontal regions) and module 1 and 3 (left hemisphere; inferior and superior parietal, postcentral, precentral and supramarginal) decreased between timepoints. Of notice, at timepoint 1, module 2 had two connector hubs (left superior frontal 2 and left putamen 2), module 6 had none and module 7 had one (right superior temporal 2), while at timepoint 2, module 2 had one connector hub (left superior frontal 2), module 6 had two (left precuneus 2 and right precuneus 2), and module 7 had three (right superior temporal 2, right middle temporal 1 and right lateral occipital 2). Modules 4 and 8 had no connector hubs at both timepoints. No differences were found for intra-modular and inter-modular connectivity.

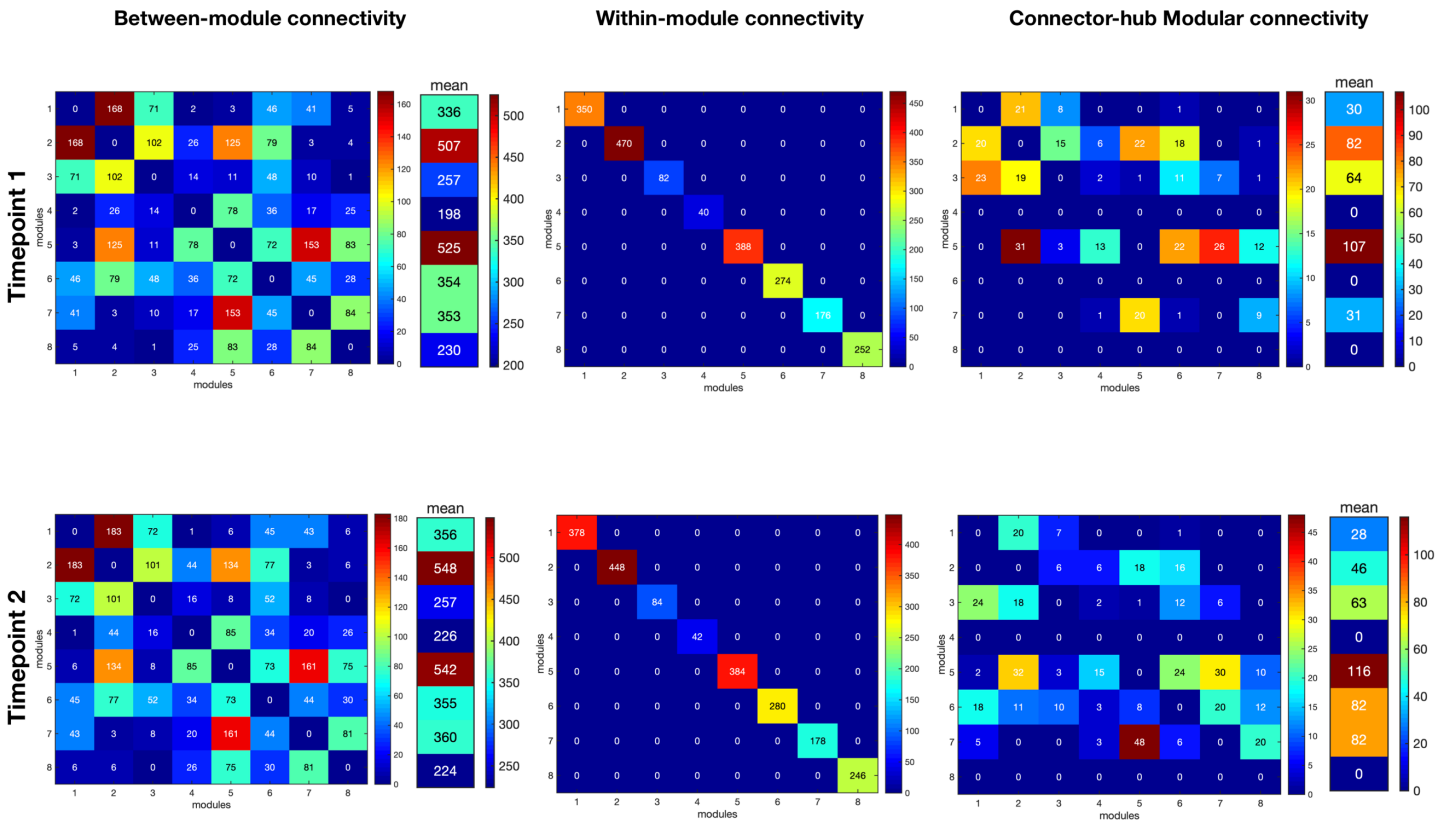

Figure 9. Fingerprints of modular connectivity at timepoint 1 (top row) and timepoint 2 (bottom row). Left column represents the inter-modular connectivity, middle column the intra-module connectivity and right column the connector-hub driven inter-modular connectivity. Modular connectivity strength is quantified as the total number of connections (degree) of all nodes forming a module. Community structure of timepoint 2 was selected as the reference scheme, since it had higher group goodness-of-fit. We observe different patterns only in connector-hub driven inter-modular connectivity. Overall, there was an increase of around 33% in this connectivity between timepoints, which is probably due to the increase in the number of connector hub. This results again suggests an increase in integration of brain SC during aging.

5. Discussion

In this study, we developed a new CBP method, based on diffusion MRI data. We evaluated different clustering algorithms in conjunction with different dimensionality reduction techniques and chose the best performing method. *K*-means clustering combined with Self-Organizing Maps was the selected method due to its higher silhouette coefficient and resulting clusters with more evenly distributed sizes. Previous

studies have used *k*-means clustering, making it the most popular clustering algorithm amongst CBP works, so its appropriateness for CBP has already been validated (Abivardi and Bach, 2017; Anwander et al., 2007; Bach et al., 2011; Klein et al., 2007; Reuter et al., 2020). We also demonstrated that SOMs are a suitable method for dimensionality reduction that can be applied prior to clustering. To date, this technique has only been used in one study performing CBP of functional data (Mishra et al., 2014). Here we show evidence that pre-clustering dimensionality reduction with SOM presents a valid and recommended solution for CBP methods which preserves the topographic organization of the input data (Kohonen, 1990, 1982).

Moreover, we developed a new metric to evaluate the estimated CBP, specifically, to verify if the goal of grouping voxels with similar connectivity profiles was successfully accomplished – connectivity homogeneity fingerprint. This novel metric takes into account the connections of each voxel inside a region, with higher values representing a region with more homogeneous signatures of structural connectivity across all of its voxels (i.e., most of the region's voxels are connected to the same brain regions). So far, many techniques to evaluate the quality of a parcellation have been proposed. Yet, choosing the most suitable evaluation method is a challenging task due to the lack of a ground truth. The existing methods either evaluate the reproducibility (i.e., the alignment between different parcellations from different subjects or different acquisitions of the same subject), quality of clustering solutions (i.e., the similarity of voxels grouped in the same cluster), agreement with cytoarchitecture, task fMRI activation and myelination or impact on network analysis (Arslan et al., 2018). One of the metrics developed to evaluate the quality of clustering solutions is the functional homogeneity; the average Pearson's correlation coefficient between the connectivity fingerprints of each pair of voxels inside a cluster (Chong et al., 2017; Kong et al., 2018; Schaefer et al., 2018). The metric we propose here (CHF) does not consider the connectivity weights directly which can lead to lower homogeneity values, even if a pair of voxels is connected to the same brain regions but with different connectivity strengths. Thus, the CHF reflects a more adequate measure of regional homogeneity, which evaluates the strength or consistency level of a region's connectivity fingerprint to the rest of the brain, thus representing a more complete and robust approach to evaluating a parcellation. Furthermore, the previous existing homogeneity measure was designed specifically for functional data, thus limiting its extension to structural data. Our results from CHF analysis validate the CBP method developed here, since all the parcellations exhibit higher homogeneity values in comparison to the original partition. Moreover, when one of the generated parcellations was applied to the data of a different timepoint (for the same cohort), the homogeneity values were very similar to the baseline, which demonstrates its appropriateness for longitudinal analysis.

Regarding longitudinal changes in structural connectivity, our results revealed a significant sub-network with both decreases and increases in WM structural connectivity along time. Increases in connectivity were mainly composed by inter-hemispheric connections, while decreases occurred mostly in intra-hemispheric connections. These results are in accordance with the "last-in, first-out" hypothesis, which states that regions developing later are more prone to age-related decline (Raz, 1999). This theory has been supported by DTI studies investigating white matter microstructural properties, which report steepest declines for association fibers (i.e., fibers connecting regions of the same hemisphere) in comparison to commissural fibers (i.e., fibers crossing hemispheres).

The longitudinal analysis of topological features of brain WM structural networks also revealed some alterations. Concerning nodal efficiency and the topological roles of nodes (provincial and connector), there was an increase in the number of hubs (global, provincial and connector) from the first to last timepoint. Interestingly, left caudate 1, right amygdala 1, and right caudate 6 were consistently identified as both global and provincial hubs in all timepoints. The caudate nuclei are involved in different cognitive dimensions, such as, motor and action planning, decision making, motivation and reward processing (Bick et al., 2019; Grahn et al., 2008; Tartaro, 2019; Wilson, 2018). Previous studies found significant atrophy of the caudate along aging (Hoffstaedter et al., 2015; Raz et al., 2003). Interestingly, we identified as hubs two clusters in the right caudate and only one in the left caudate and there is one study reporting a longitudinal rightward lateralization of the caudate volume in older adults (Esteves et al., 2018). The amygdala has been associated with emotion processing of both fearful and rewarding stimuli. It is also known to modulate memory and attention for emotional stimuli and to be involved in positive affect and motivation (Gallagher and Chiba, 1996; Janak and Tye, 2015; Mather, 2016; Sah et al., 2003; Salzman and Fusi, 2010). Past studies report relative preservation of both structure and function of the amygdala in normal aging (Good et al., 2001; Mather, 2016; Nashiro et al., 2012). Alongside with this, emotional processing also appears to be spared in aging (Nashiro et al., 2012). Our results align with these findings, since the amygdala maintains its importance in the brain structural network along time, both in terms of nodal efficiency and intra-modular communication.

Two clusters (left putamen 2 and right putamen 1) lost their role as connector hubs and were identified as provincial hubs. This means that the participation coefficient of these clusters was lower and thus they established more connections with regions belonging to the same module than with regions outside their own module and lost their importance in integrating different regions of the brain. The putamina are involved in different cognitive functions, such as, reinforcement learning and motor control, language and

processing of sensory and motor aspects of pain (Haber, 2016; Starr et al., 2011; Viñas-Guasch and Wu, 2017). Studies investigating age effects on this region described significant atrophy (Fjell and Walhovd, 2010; Jäncke et al., 2015; Raz et al., 2003) and also microstructural damage (Cherubini et al., 2009) of these subcortical nuclei, which might explain why the putamen lost its connector hub role in the brain structural network. On the opposite direction, right precuneus 2 and right precentral 1 changed from provincial to connector hubs. Precuneus plays an important role in multiple higher-order cognitive functions, such as, visuo-spatial imagery, episodic memory retrieval, self-processing and consciousness (Cavanna and Trimble, 2006). Some aging studies report a relative preservation of precuneus' cortical thickness in comparison to other regions (Fjell et al., 2009; Lee et al., 2018). In line with our findings, Gong and colleagues (Gong et al., 2009) found that the precuneus was consistently identified as a hub independent of age in white matter structural networks. Precentral gyrus is known to be involved in motor performance (Picard, 2003; Porro et al., 1996; Ribas, 2010; Yousry, 1997) but some studies also report a role of this region in emotion processing (de Gelder et al., 2004; Hajcak et al., 2007; Hardee et al., 2017; Mazzola et al., 2013; Saarimäki et al., 2016). Although aging studies report significant atrophy of this region (Salat, 2004; Thambisetty et al., 2010), one recent fMRI study using graph theory analysis described increased degree centrality (i.e., a measure of the importance of the node in the network) of precentral gyrus in both cognitively normal older adults and subjects with mild cognitive impairment (MCI) despite existing volume declines (Behfar et al., 2020). Furthermore, Behfar and colleagues showed that the increased degree centrality was correlated with better scores of cognitive performance in the MCI group, which might represent a compensatory mechanism. Our results align with these findings, since the precentral gyrus increased its importance in the network along time, by moving from having a role only in intra-modular communication to have the function of establishing communication with different modules of the brain and thus being important for functional integration.

Concerning modularity structure, the same number of modules was identified at the two timepoints but some differences in the modules' configuration were found. In terms of fingerprints of modular connectivity, there was a longitudinal increase in connector-hub driven inter-modular connectivity, which could be driven by the increase in the number of detected connector hubs at timepoint 2. This result suggests an increase of brain structural networks' integration during aging. Some past fMRI studies report increased integration along aging (Cao et al., 2014; He et al., 2020). However, a recent study exploring white matter structural connectivity report decreased integration with normal aging (Puxeddu et al., 2020). Our result could be attributed to the higher resolution of our parcellation, which may have allowed the identification of additional connector hubs, that at lower resolutions would not be identified.

This study has some limitations, namely the use of a 1.5T MRI scanner. While we recognize that this limitation may inevitably influence to some extent our results (changes in network connectivity, hubs and modularity structure), we believe that its effects are minimized by the fact that we compared two evaluations/timepoints sharing the same neuroimaging acquisition and preprocessing protocol (same scanner, acquisition parameters and data processing pipeline).

In summary, we present a new method to create a CBP of the human brain based on white matter structural connectivity data has accomplished the main goal of grouping voxels with similar connectivity profiles. Additionally, we propose a new metric (connectivity homogeneity fingerprint) to evaluate the quality of a parcellation by computing the consistency level of regional connectivity fingerprints, with potential for application to other types of neuroimaging data. Furthermore, we applied the derived parcellation to explore longitudinal changes in structural networks of an aging cohort and found signatures of brain's reorganization along aging. Particularly, we found decreases in intra-hemispheric connectivity and increases in inter-hemispheric connectivity, which supports the "last-in, first-out" hypothesis and a rearrangement in the topological roles of the nodes in the network. We also found evidence of increased integration, which was not observed in previous studies, but it can be explained by the higher resolution of our parcellation which allowed the identification of more connector hubs. Taken together, our study proposes a novel and robust solution for performing and evaluating CBP of the human brain. With potential for application to any whole-brain DTI-based cohort, here we show its potential appropriateness and potential by characterizing the longitudinal changes of the structural connectome in aging, which were highly consistency with the existing literature.

6. References

Abivardi, A., Bach, D.R., 2017. Deconstructing white matter connectivity of human amygdala nuclei with thalamus and cortex subdivisions in vivo: Structural Amygdala-Thalamus and Amygdala-Cortex Connectivity. Human Brain Mapping 38, 3927–3940. https://doi.org/10.1002/hbm.23639

Achard, S., Bullmore, E., 2007. Efficiency and cost of economical brain functional networks. PLoS Computational Biology 3, 174–183. https://doi.org/10.1371/journal.pcbi.0030017

Anwander, A., Tittgemeyer, M., von Cramon, D., Friederici, A., Knosche, T., 2006. Connectivity-Based Parcellation of Broca's Area. Cerebral Cortex 17, 816–825. https://doi.org/10.1093/cercor/bhk034

Arslan, S., Ktena, S.I., Makropoulos, A., Robinson, E.C., Rueckert, D., Parisot, S., 2018. Human brain mapping: A systematic comparison of parcellation methods for the human cerebral cortex. NeuroImage 170, 5–30. https://doi.org/10.1016/j.neuroimage.2017.04.014

Bach, D.R., Behrens, T.E., Garrido, L., Weiskopf, N., Dolan, R.J., 2011. Deep and Superficial Amygdala Nuclei Projections Revealed In Vivo by Probabilistic Tractography. Journal of Neuroscience 31, 618–623. https://doi.org/10.1523/JNEUROSCI.2744-10.2011

Behfar, Q., Behfar, S.K., von Reutern, B., Richter, N., Dronse, J., Fassbender, R., Fink, G.R., Onur, O.A., 2020. Graph Theory Analysis Reveals Resting-State Compensatory Mechanisms in Healthy Aging and Prodromal Alzheimer's Disease. Frontiers in Aging Neuroscience 12. https://doi.org/10.3389/fnagi.2020.576627

Behrens, T.E.J., Berg, H.J., Jbabdi, S., Rushworth, M.F.S., Woolrich, M.W., 2007. Probabilistic diffusion tractography with multiple fibre orientations: What can we gain? NeuroImage 34, 144–155. https://doi.org/10.1016/j.neuroimage.2006.09.018

Behrens, T.E.J., Johansen-Berg, H., Woolrich, M.W., Smith, S.M., Wheeler-Kingshott, C.A.M., Boulby, P.A., Barker, G.J., Sillery, E.L., Sheehan, K., Ciccarelli, O., Thompson, A.J., Brady, J.M., Matthews, P.M., 2003. Non-invasive mapping of connections between human thalamus and cortex using diffusion imaging. NATURE NEUROSCIENCE 6, 8.

Bellman, R., 1957. Dynamic Programming, Rand Corporation research study. Princeton University Press.

Bick, S.K., Patel, S.R., Katnani, H.A., Peled, N., Widge, A., 2019. Caudate stimulation enhances learning. Brain 142, 8.

Bishop, C.M., 2006. Pattern recognition and machine learning, Information science and statistics. Springer, New York.

Blondel, V.D., Guillaume, J.-L., Lambiotte, R., Lefebvre, E., 2008. Fast unfolding of communities in large networks. Journal of Statistical Mechanics: Theory and Experiment 2008, P10008. https://doi.org/10.1088/1742-5468/2008/10/p10008

Brodmann, K., 1909. Vergleichende Lokalisationslehre der Grosshirnrinde in ihren Prinzipien dargestellt auf Grund des Zellenbaues von Dr. K. Brodmann ... J.A. Barth.

Bullmore, E.T., Sporns, O., 2009. Complex brain networks: graph theoretical analysis of structural and functional systems. Nature reviews. Neuroscience 10, 186–198. https://doi.org/10.1038/nrn2575

Cao, M., Wang, J.H., Dai, Z.J., Cao, X.Y., Jiang, L.L., Fan, F.M., Song, X.W., Xia, M.R., Shu, N., Dong, Q., Milham, M.P., Castellanos, F.X., Zuo, X.N., He, Y., 2014. Topological organization of the human brain functional connectome across the lifespan. Developmental Cognitive Neuroscience 7, 76–93. https://doi.org/10.1016/j.dcn.2013.11.004

Cavanna, A.E., Trimble, M.R., 2006. The precuneus: a review of its functional anatomy and behavioural correlates. Brain 129, 564–583. https://doi.org/10.1093/brain/awl004

Cera, N., Esposito, R., Cieri, F., Tartaro, A., 2019. Altered Cingulate Cortex Functional Connectivity in Normal Aging and Mild Cognitive Impairment. Frontiers in Neuroscience 13. https://doi.org/10.3389/fnins.2019.00857

Cherubini, A., Péran, P., Caltagirone, C., Sabatini, U., Spalletta, G., 2009. Aging of subcortical nuclei: Microstructural, mineralization and atrophy modifications measured in vivo using MRI. NeuroImage 48, 29–36. https://doi.org/10.1016/j.neuroimage.2009.06.035

Chong, M., Bhushan, C., Joshi, A.A., Choi, S., Haldar, J.P., Shattuck, D.W., Spreng, R.N., Leahy, R.M., 2017. Individual parcellation of resting fMRI with a group functional connectivity prior. NeuroImage 156, 87–100. https://doi.org/10.1016/j.neuroimage.2017.04.054

Costa, P.S., Santos, N.C., Cunha, P., Palha, J.A., Sousa, N., 2013. The Use of Bayesian Latent Class Cluster Models to Classify Patterns of Cognitive Performance in Healthy Ageing. PLoS ONE 8. https://doi.org/10.1371/journal.pone.0071940

de Gelder, B., Snyder, J., Greve, D., Gerard, G., Hadjikhani, N., 2004. Fear fosters flight: A mechanism for fear contagion when perceiving emotion expressed by a whole body. Proceedings of the National Academy of Sciences 101, 16701–16706. https://doi.org/10.1073/pnas.0407042101

Desikan, R.S., Ségonne, F., Fischl, B., Quinn, B.T., Dickerson, B.C., Blacker, D., Buckner, R.L., Dale, A.M., Maguire, R.P., Hyman, B.T., Albert, M.S., Killiany, R.J., 2006. An automated labeling system for subdividing the human cerebral cortex on MRI scans into gyral based regions of interest. NeuroImage 31, 968–980. https://doi.org/10.1016/j.neuroimage.2006.01.021

Destrieux, C., Fischl, B., Dale, A., Halgren, E., 2010. Automatic parcellation of human cortical gyri and sulci using standard anatomical nomenclature. NeuroImage 53, 1–15. https://doi.org/10.1016/j.neuroimage.2010.06.010

Eickhoff, S.B., Thirion, B., Varoquaux, G., Bzdok, D., 2015. Connectivity-based parcellation: Critique and implications. Human Brain Mapping 36, 4771–4792. https://doi.org/10.1002/hbm.22933

Eickhoff, S.B., Yeo, B.T.T., Genon, S., 2018. Imaging-based parcellations of the human brain. Nature Reviews Neuroscience 19, 672–686. https://doi.org/10.1038/s41583-018-0071-7

Esteves, M., Moreira, P.S., Marques, P., Castanho, T.C., Magalhães, R., Amorim, L., Portugal-Nunes, C., Soares, J.M., Coelho, A., Almeida, A., Santos, N.C., Sousa, N., Leite-Almeida, H., 2018. Asymmetrical subcortical plasticity entails cognitive progression in older individuals. Aging Cell 18, e12857. https://doi.org/10.1111/acel.12857

Fernandes, H.M., Cabral, J., van Hartevelt, T.J., Lord, L.-D., Gleesborg, C., Møller, A., Deco, G., Whybrow, P.C., Petrovic, P., James, A.C., Kringelbach, M.L., 2019. Disrupted brain structural connectivity in Pediatric Bipolar Disorder with psychosis. Scientific Reports 9. https://doi.org/10.1038/s41598-019-50093-4

Fischl, B., Salat, D.H., Busa, E., Albert, M., Dieterich, M., Haselgrove, C., van der Kouwe, A., Killiany, R., Kennedy, D., Klaveness, S., Montillo, A., Makris, N., Rosen, B., Dale, A.M., 2002. Whole Brain Segmentation. Neuron 33, 341–355. https://doi.org/10.1016/S0896-6273(02)00569-X

Fjell, A.M., Walhovd, K.B., 2010. Structural Brain Changes in Aging: Courses, Causes and Cognitive Consequences. Reviews in the Neurosciences 21. https://doi.org/10.1515/REVNEURO.2010.21.3.187

Fjell, A.M., Westlye, L.T., Amlien, I., Espeseth, T., Reinvang, I., Raz, N., Agartz, I., Salat, D.H., Greve, D.N., Fischl, B., Dale, A.M., Walhovd, K.B., 2009. High Consistency of Regional Cortical Thinning in Aging across Multiple Samples. Cerebral Cortex 19, 2001–2012. https://doi.org/10.1093/cercor/bhn232

Fornito, A., Zalesky, A., Bullmore, E.T., 2016. Fundamentals of Brain Network Analysis. Academic Press, San Diego.

Fritz, H.J., Ray, N., Dyrba, M., Sorg, C., Teipel, S., Grothe, M.J., 2019. The corticotopic organization of the human basal forebrain as revealed by regionally selective functional connectivity profiles. Human Brain Mapping 40, 868–878. https://doi.org/10.1002/hbm.24417

Gallagher, M., Chiba, A.A., 1996. The amygdala and emotion. Current Opinion in Neurobiology 6, 221–227. https://doi.org/10.1016/S0959-4388(96)80076-6

Gao, Y., Schilling, K.G., Stepniewska, I., Plassard, A.J., Choe, A.S., Li, X., Landman, B.A., Anderson, A.W., 2018. Tests of cortical parcellation based on white matter connectivity using diffusion tensor imaging. NeuroImage 170, 321–331. https://doi.org/10.1016/j.neuroimage.2017.02.048

Giecold, G., Marco, E., Trippa, L., Yuan, G.-C., n.d. Robust Lineage Reconstruction from High-Dimensional Single-Cell Data 22.

Gong, G., Rosa-Neto, P., Carbonell, F., Chen, Z.J., He, Y., Evans, A.C., 2009. Age- and Gender-Related Differences in the Cortical Anatomical Network. Journal of Neuroscience 29, 15684–15693. https://doi.org/10.1523/JNEUROSCI.2308-09.2009

Good, B.H., de Montjoye, Y.-A., Clauset, A., 2010. Performance of modularity maximization in practical contexts. Phys. Rev. E 81, 046106. https://doi.org/10.1103/PhysRevE.81.046106

Good, C.D., Johnsrude, I.S., Ashburner, J., Henson, R.N.A., Friston, K.J., Frackowiak, R.S.J., 2001. A Voxel-Based Morphometric Study of Ageing in 465 Normal Adult Human Brains. NeuroImage 14, 21–36. https://doi.org/10.1006/nimg.2001.0786

Grahn, J.A., Parkinson, J.A., Owen, A.M., 2008. The cognitive functions of the caudate nucleus. Progress in Neurobiology 15.

Guerreiro, M., Silva, A.P., Botelho, M.A., Leitão, O., Castro-Caldas, A., Garcia, C., 1994. Adaptação à população portuguesa da tradução do Mini Mental State Examination (MMSE). Revista Portuguesa de Neurologia 1, 9–10.

Haber, S.N., 2016. Corticostriatal circuitry. Dialogues in Clinical Neuroscience 18, 15.

Hajcak, G., Molnar, C., George, M.S., Bolger, K., Koola, J., Nahas, Z., 2007. Emotion facilitates action: A transcranial magnetic stimulation study of motor cortex excitability during picture viewing. Psychophysiology 44, 91–97. https://doi.org/10.1111/j.1469-8986.2006.00487.x

Hardee, J.E., Cope, L.M., Munier, E.C., Welsh, R.C., Zucker, R.A., Heitzeg, M.M., 2017. Sex differences in the development of emotion circuitry in adolescents at risk for substance abuse: a longitudinal fMRI study. Social Cognitive and Affective Neuroscience 12, 965–975. https://doi.org/10.1093/scan/nsx021

He, L., Wang, X., Zhuang, K., Qiu, J., 2020. Decreased Dynamic Segregation but Increased Dynamic Integration of the Resting-state Functional Networks During Normal Aging. Neuroscience 437, 54–63. https://doi.org/10.1016/j.neuroscience.2020.04.030

Hoffstaedter, F., Grefkes, C., Roski, C., Caspers, S., Zilles, K., Eickhoff, S.B., 2015. Age-related decrease of functional connectivity additional to gray matter atrophy in a network for movement initiation. Brain Structure and Function 220, 999–1012. https://doi.org/10.1007/s00429-013-0696-2

Janak, P.H., Tye, K.M., 2015. From circuits to behaviour in the amygdala. Nature 517, 284–292. https://doi.org/10.1038/nature14188

Jäncke, L., Mérillat, S., Liem, F., Hänggi, J., 2015. Brain size, sex, and the aging brain: Brain Size, Sex, and Aging. Hum. Brain Mapp. 36, 150–169. https://doi.org/10.1002/hbm.22619

Johansen-Berg, H., Behrens, T.E.J., Robson, M.D., Drobnjak, I., Rushworth, M.F.S., Brady, J.M., Smith, S.M., Higham, D.J., Matthews, P.M., 2004. Changes in connectivity profiles define functionally distinct regions in human medial frontal cortex. Proceedings of the National Academy of Sciences 101, 13335–13340. https://doi.org/10.1073/pnas.0403743101

Jovicich, J., Czanner, S., Han, X., Salat, D., van der Kouwe, A., Quinn, B., Pacheco, J., Albert, M., Killiany, R., Blacker, D., 2009. MRI-derived measurements of human subcortical, ventricular and intracranial brain volumes: Reliability effects of scan sessions, acquisition sequences, data analyses, scanner upgrade, scanner vendors and field strengths. NeuroImage 46, 177–192. https://doi.org/10.1016/j.neuroimage.2009.02.010

Klein, A., Ghosh, S.S., Bao, F.S., Giard, J., Häme, Y., Stavsky, E., Lee, N., Rossa, B., Reuter, M., Chaibub Neto, E., Keshavan, A., 2017. Mindboggling morphometry of human brains. PLoS Comput Biol 13, e1005350. https://doi.org/10.1371/journal.pcbi.1005350

Klein, J.C., Behrens, T.E.J., Robson, M.D., Mackay, C.E., Higham, D.J., Johansen-Berg, H., 2007. Connectivity-based parcellation of human cortex using diffusion MRI: Establishing reproducibility, validity and observer independence in BA 44/45 and SMA/pre-SMA. NeuroImage 34, 204–211. https://doi.org/10.1016/j.neuroimage.2006.08.022

Kohonen, T., 1990. The Self-Organizing Map. Proceedings of the IEEE 78, 1464–1480.

Kohonen, T., 1982. Self-organized formation of topologically correct feature maps. Biological Cybernetics 43, 59–69. https://doi.org/10.1007/BF00337288

Kong, R., Li, J., Orban, C., Sabuncu, M.R., Liu, H., Schaefer, A., Sun, N., Zuo, X.-N., Holmes, A.J., Eickhoff, S.B., Yeo, B.T.T., 2018. Spatial Topography of Individual-Specific Cortical Networks Predicts Human Cognition, Personality, and Emotion 19.

Lee, J.S., Kim, S., Yoo, H., Park, S., Jang, Y.K., Kim, H.J., Kim, K.W., Kim, Y., Jang, H., Park, K.-C., Yaffe, K., Yang, J.-J., Lee, J.-M., Na, D.L., Seo, S.W., 2018. Trajectories of Physiological Brain Aging and Related Factors in People Aged from 20 to over-80. Journal of Alzheimer's Disease 65, 1237–1246. https://doi.org/10.3233/JAD-170537

Lo, C.-Y., Wang, P.-N., Chou, K.-H., Wang, J., He, Y., Lin, C.-P., 2010. Diffusion Tensor Tractography Reveals Abnormal Topological Organization in Structural Cortical Networks in Alzheimer's Disease. Journal of Neuroscience 30, 16876–16885. https://doi.org/10.1523/JNEUROSCI.4136-10.2010

Mather, M., 2016. The Affective Neuroscience of Aging. Annual Review of Psychology 67, 213–238. https://doi.org/10.1146/annurev-psych-122414-033540

Mazzola, V., Vuilleumier, P., Latorre, V., Petito, A., Gallese, V., Popolizio, T., Arciero, G., Bondolfi, G., 2013. Effects of Emotional Contexts on Cerebello-Thalamo-Cortical Activity during Action Observation. PLoS ONE 8, e75912. https://doi.org/10.1371/journal.pone.0075912

Mishra, A., Rogers, B.P., Chen, L.M., Gore, J.C., 2014. Functional connectivity-based parcellation of amygdala using self-organized mapping: A data driven approach. Human Brain Mapping 35, 1247–1260. https://doi.org/10.1002/hbm.22249

Nashiro, K., Sakaki, M., Mather, M., 2012. Age Differences in Brain Activity during Emotion Processing: Reflections of Age-Related Decline or Increased Emotion Regulation? Gerontology 58, 156–163. https://doi.org/10.1159/000328465

Picard, N., 2003. Activation of the Supplementary Motor Area (SMA) during Performance of Visually Guided Movements. Cerebral Cortex 13, 977–986. https://doi.org/10.1093/cercor/13.9.977

Porro, C.A., Francescato, M.P., Cettolo, V., Diamond, M.E., Baraldi, P., Zuiani, C., Bazzocchi, M., di Prampero, P.E., 1996. Primary Motor and Sensory Cortex Activation during Motor Performance and Motor Imagery: A Functional Magnetic Resonance Imaging Study. The Journal of Neuroscience 16, 7688–7698. https://doi.org/10.1523/JNEUROSCI.16-23-07688.1996

Puxeddu, M.G., Faskowitz, J., Betzel, R.F., Petti, M., Astolfi, L., Sporns, O., 2020. The modular organization of brain cortical connectivity across the human lifespan. NeuroImage 218, 116974. https://doi.org/10.1016/j.neuroimage.2020.116974

Raz, N., 1999. Aging of the brain and its impact on cognitive performance: Integration of structural and functional findings. 2nd ed. Mahwah, N: Lawrence Erlbaum Associates; 2.

Raz, N., Rodrigue, K.M., Kennedy, K.M., Head, D., Gunning-Dixon, F., Acker, J.D., 2003. Differential Aging of the Human Striatum: Longitudinal Evidence 9.

Reuter, N., Genon, S., Kharabian Masouleh, S., Hoffstaedter, F., Liu, X., Kalenscher, T., Eickhoff, S.B., Patil, K.R., 2020. CBPtools: a Python package for regional connectivity-based parcellation. Brain Structure and Function 225, 1261–1275. https://doi.org/10.1007/s00429-020-02046-1

Ribas, G.C., 2010. The cerebral sulci and gyri. Neurosurgical Focus 28, E2. https://doi.org/10.3171/2009.11.FOCUS09245

Roberts, J.A., Perry, A., Roberts, G., Mitchell, P.B., Breakspear, M., 2017. Consistency-based thresholding of the human connectome. NeuroImage 145, 118–129. https://doi.org/10.1016/j.neuroimage.2016.09.053

Rousseeuw, P.J., 1987. Silhouettes: A graphical aid to the interpretation and validation of cluster analysis. Journal of Computational and Applied Mathematics 20, 53–65. https://doi.org/10.1016/0377-0427(87)90125-7

Saarimäki, H., Gotsopoulos, A., Jääskeläinen, I.P., Lampinen, J., Vuilleumier, P., Hari, R., Sams, M., Nummenmaa, L., 2016. Discrete Neural Signatures of Basic Emotions. Cerebral Cortex 26, 2563–2573. https://doi.org/10.1093/cercor/bhv086

Sah, P., Faber, E.S.L., Lopez De Armentia, M., Power, J., 2003. The Amygdaloid Complex: Anatomy and Physiology. Physiological Reviews 83, 803–834. https://doi.org/10.1152/physrev.00002.2003

Salat, D.H., 2004. Thinning of the Cerebral Cortex in Aging. Cerebral Cortex 14, 721–730. https://doi.org/10.1093/cercor/bhh032

Salzman, C.D., Fusi, S., 2010. Emotion, Cognition, and Mental State Representation in Amygdala and Prefrontal Cortex. Annual Review of Neuroscience 33, 173–202. https://doi.org/10.1146/annurev.neuro.051508.135256

Santos, N.C., Costa, P.S., Cunha, P., Cotter, J., Sampaio, A., Zihl, J., Almeida, O.F.X., Cerqueira, J.J., Palha, J.A., Sousa, N., 2013. Mood is a key determinant of cognitive performance in community-dwelling older adults: A cross-sectional analysis. Age 35, 1983–1993. https://doi.org/10.1007/s11357-012-9482-y

Santos, N.C., Costa, P.S., Cunha, P., Portugal-Nunes, C., Amorim, L., Cotter, J., Cerqueira, J.J., Palha, J.A., Sousa, N., 2014. Clinical, physical and lifestyle variables and relationship with cognition and mood in aging: A cross-sectional analysis of distinct educational groups. Frontiers in Aging Neuroscience 6, 1–15. https://doi.org/10.3389/fnagi.2014.00021

Schaefer, A., Kong, R., Gordon, E.M., Laumann, T.O., Zuo, X.-N., Holmes, A.J., Eickhoff, S.B., Yeo, B.T.T., 2018. Local-Global Parcellation of the Human Cerebral Cortex from Intrinsic Functional Connectivity MRI. Cerebral Cortex 28, 3095–3114. https://doi.org/10.1093/cercor/bhx179

Starr, C.J., Sawaki, L., Wittenberg, G.F., Burdette, J.H., Oshiro, Y., Quevedo, A.S., McHaffie, J.G., Coghill, R.C., 2011. The contribution of the putamen to sensory aspects of pain: insights from structural connectivity and brain lesions. Brain 134, 1987–2004. https://doi.org/10.1093/brain/awr117

Strehl, A., Ghosh, J., 2002. Cluster Ensembles – A Knowledge Reuse Framework for Combining Multiple Partitions. Journal of Machine Learning Research 3, 583–617.

Thambisetty, M., Wan, J., Carass, A., An, Y., Prince, J.L., Resnick, S.M., 2010. Longitudinal changes in cortical thickness associated with normal aging. NeuroImage 52, 1215–1223. https://doi.org/10.1016/j.neuroimage.2010.04.258

Tittgemeyer, M., Rigoux, L., Knösche, T.R., 2018. Cortical parcellation based on structural connectivity: A case for generative models. NeuroImage 173, 592–603. https://doi.org/10.1016/j.neuroimage.2018.01.077

Tononi, G., Sporns, O., Edelman, G.M., 1994. A measure for brain complexity: relating functional segregation and integration in the nervous system. Proceedings of the National Academy of Sciences 91, 5033–5037. https://doi.org/10.1073/pnas.91.11.5033

Vega-Pons, S., Ruiz-Shulcloper, J., 2011. A Survey of Clustering Ensemble Algorithms. Int. J. Patt. Recogn. Artif. Intell. 25, 337–372. https://doi.org/10.1142/S0218001411008683

Viñas-Guasch, N., Wu, Y.J., 2017. The role of the putamen in language: a meta-analytic connectivity modeling study. Brain Struct Funct 222, 3991–4004. https://doi.org/10.1007/s00429-017-1450-y

Vogt, C., 1919. Allgemeinere ergebnisse unserer hirnforschung. J Psychol Neurol (Leipz) 25, 279–461.

Wilson, R.P., Colizzi, M., Bossong, M.G., Allen, P., Kempton, M., MTAC, Bhattacharyya, S., 2018. The Neural Substrate of Reward Anticipation in Health: A Meta-Analysis of fMRI Findings in the Monetary Incentive Delay Task. Neuropsychology Review 28, 496–506. https://doi.org/10.1007/s11065-018-9385-5

Yousry, T., 1997. Localization of the motor hand area to a knob on the precentral gyrus. A new landmark. Brain 120, 141–157. https://doi.org/10.1093/brain/120.1.141

Zalesky, A., Fornito, A., Bullmore, E.T., 2010. Network-based statistic: Identifying differences in brain networks. NeuroImage 53, 1197–1207. https://doi.org/10.1016/j.neuroimage.2010.06.041

Zilles, K., Palomero-Gallagher, N., Grefkes, C., Scheperjans, F., Boy, C., Amunts, K., Schleicher, A., 2002. Architectonics of the human cerebral cortex and transmitter receptor fingerprints: reconciling functional neuroanatomy and neurochemistry. European Neuropsychopharmacology 12, 587–599. https://doi.org/10.1016/S0924-977X(02)00108-6

7. Supplementary Material

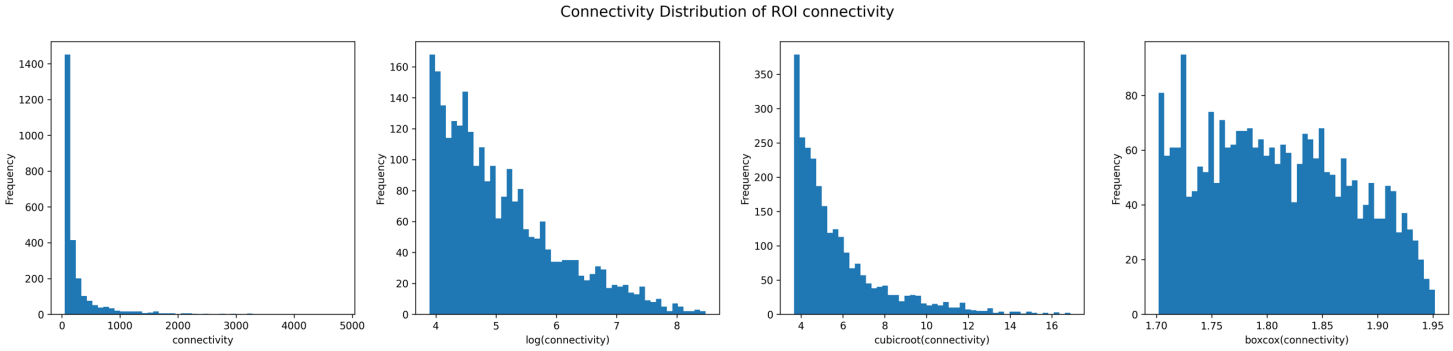

Figure S1. Example of the distribution of structural connectivity values for a region and the different transforms applied to normalize values. The BoxCox transform is the one achieving a distribution more approximated to a normal distribution.

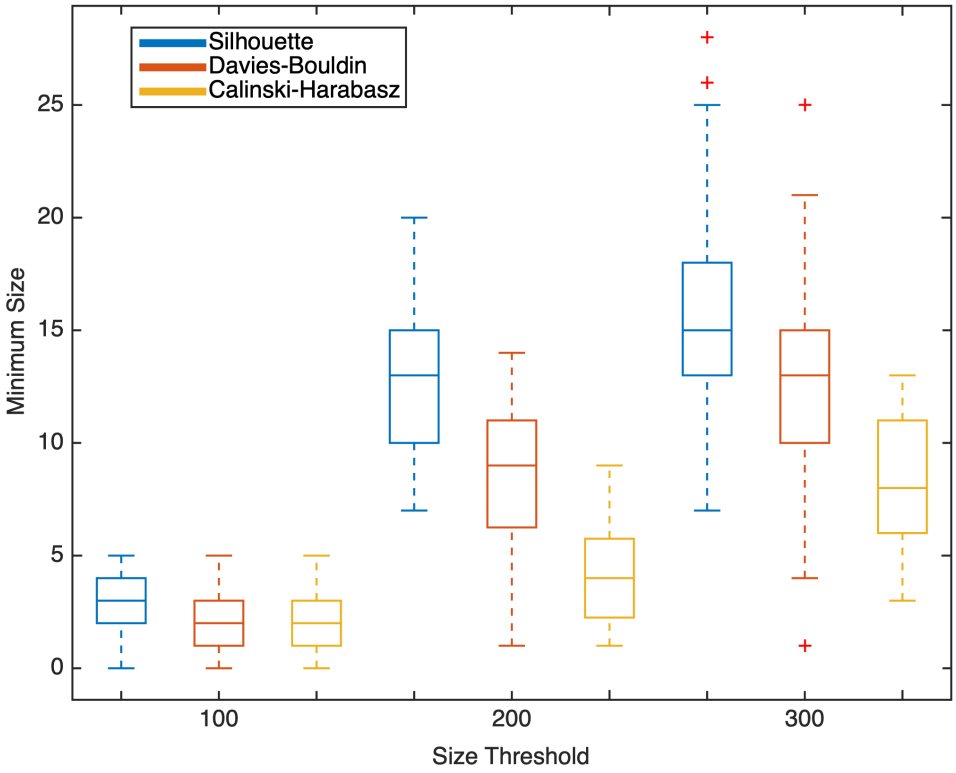

Figure S2. Plot with the minimum cluster size of all subjects for each threshold and each metric. The threshold of 300 voxels gives a minimum cluster size above 5 voxels for all metrics.

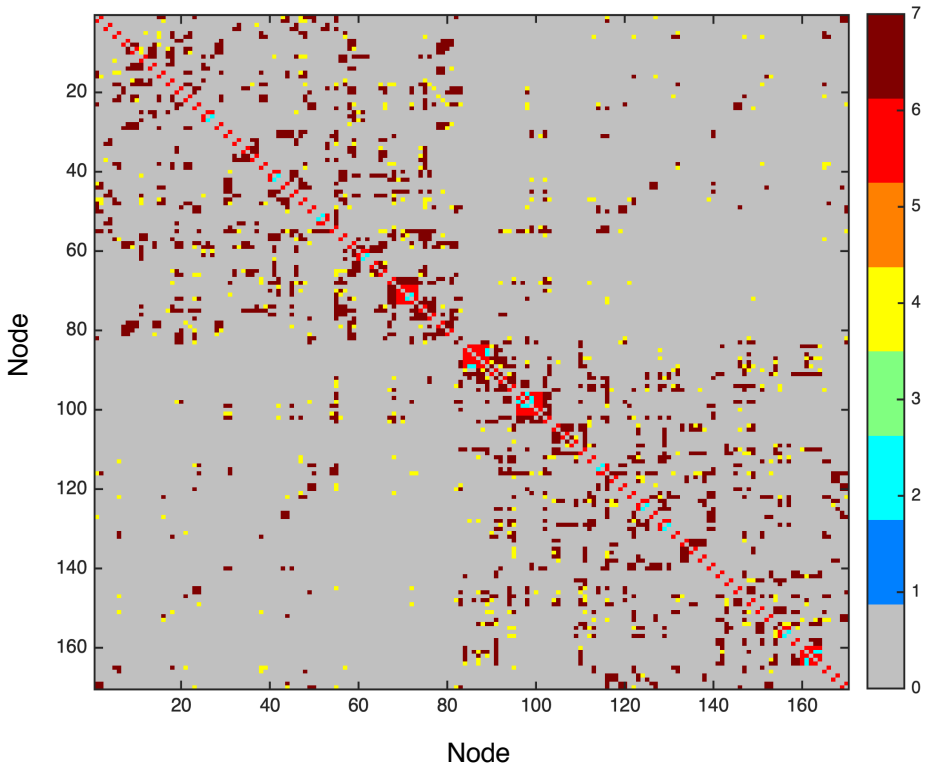

Figure S3. Structural connections surviving the different methods accounting for intra-cluster connectivity. 1 represents connections with intra-cluster connectivity set to 0; 2 represents connections with intra-cluster connectivity set to 1; 3 represents connections with original intra-cluster connectivity values; 4 represents connections common to intra-cluster connectivity set to 0 and 1; 5 represents connections common to intra-cluster connectivity set to 0 and original values; 6 represents connections common to intra-cluster connectivity set to 1 and original values; 7 represents connections common to the three strategies.

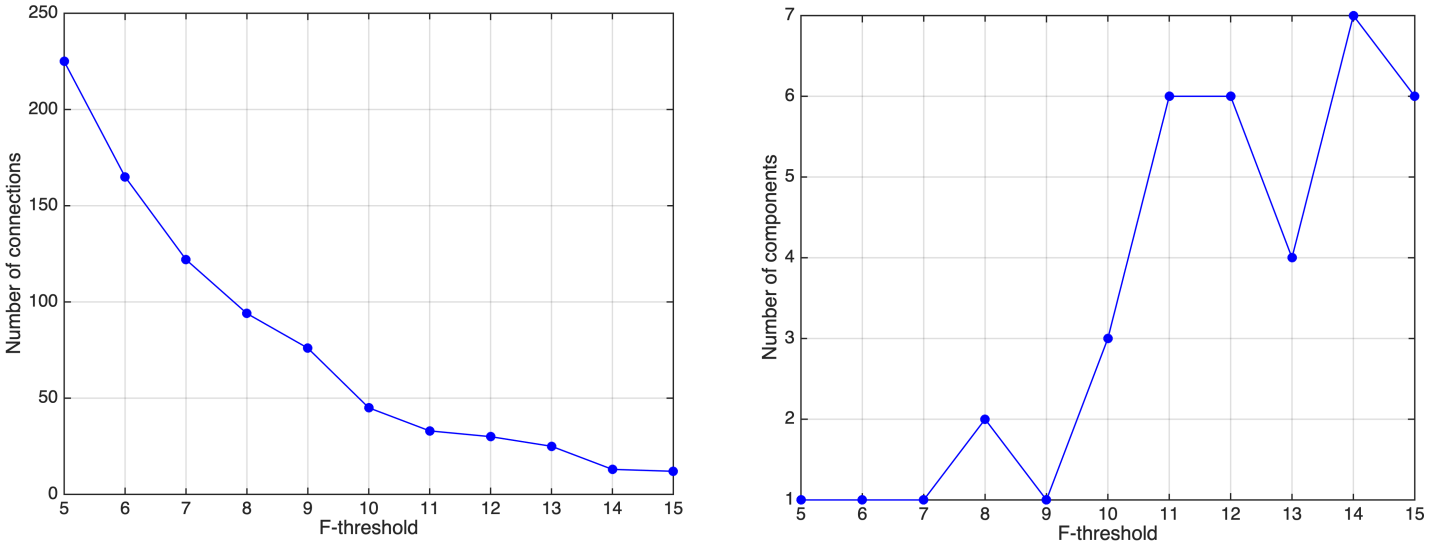

Figure S4. Relationship between F-threshold and number of connections/components, that detected a significant component. The F-threshold used in this study (7.0) was selected based on the maximal F-

threshold that detected a single component with more than two connections. This generated an NBS component with 59% nodes of the network (100 nodes) and 122 links.

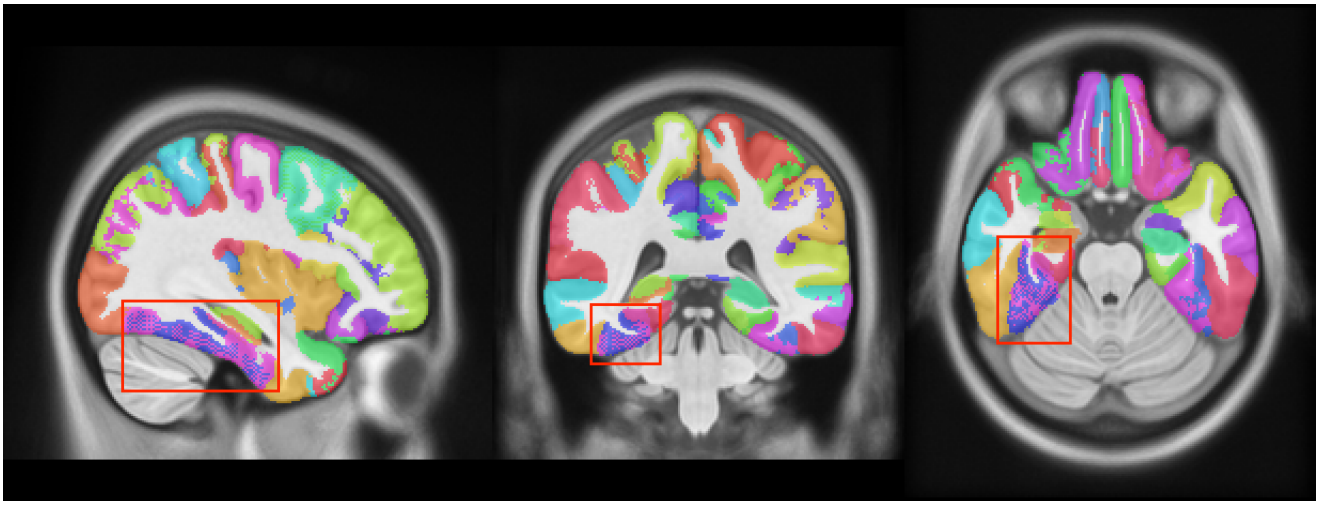

Figure S5. Davies-Bouldin parcellation with the region displaying a checkerboard pattern highlighted.

Table S1. Labels and center of gravity coordinates, in mm, of each region of the Silhouette parcellation

	Center of gravity coordinates (mm)		
Name	x	y	z
Left Caudal Anterior Cingulate 1	-4.71	24.02	24.08
Left Caudal Anterior Cingulate 2	-7.15	17.85	35.08
Left Caudal Middle Frontal 1	-43.34	11.66	38.03
Left Caudal Middle Frontal 2	-35.12	11.33	53.19
Left Cuneus 1	-13.89	-77.10	29.30
Left Cuneus 2	-3.89	-84.27	18.55
Left Entorhinal 1	-21.06	-5.00	-31.00
Left Entorhinal 2	-28.92	-8.75	-34.92
Left Fusiform 1	-35.56	-33.82	-20.03
Left Fusiform 2	-36.54	-55.93	-17.80
Left Inferior Parietal 1	-43.75	-69.80	32.95
Left Inferior Parietal 2	-30.01	-75.87	35.05
Left Inferior Temporal 1	-50.30	-49.66	-13.79
Left Inferior Temporal 2	-49.65	-23.88	-31.85
Left Isthmus Cingulate 1	-12.25	-48.91	5.02
Left Isthmus Cingulate 2	-5.90	-45.06	24.94
Left Lateral Occipital 1	-45.67	-75.76	2.91
Left Lateral Occipital 2	-26.39	-93.82	0.50
Left Lateral Orbitofrontal 1	-23.78	38.27	-19.12
Left Lateral Orbitofrontal 2	-22.46	5.24	-15.80
Left Lingual 1	-12.28	-72.85	-6.28
Left Lingual 2	-18.95	-57.79	1.43
Left Medial Orbitofrontal 1	-6.38	21.79	-19.62
Left Medial Orbitofrontal 2	-5.37	49.93	-16.74
Left Middle Temporal 1	-59.78	-32.12	-10.50

Left Middle Temporal 2	-45.74	8.94	-38.73
Left Middle Temporal 3	-55.78	-36.57	-0.60
Left Parahippocampal 1	-30.02	-29.00	-21.48
Left Parahippocampal 2	-20.53	-33.71	-16.25
Left Paracentral 1	-9.79	-31.39	54.01
Left Paracentral 2	-4.83	-21.84	62.74
Left Pars Opercularis 1	-45.25	14.01	5.88
Left Pars Opercularis 2	-51.21	14.56	18.66
Left Pars Orbitalis 1	-46.34	35.19	-15.26
Left Pars Orbitalis 2	-39.82	26.53	-6.81
Left Pars Triangularis 1	-41.86	26.29	1.99
Left Pars Triangularis 2	-50.85	33.33	5.53
Left Pericalcarine 1	-14.98	-73.68	9.55
Left Pericalcarine 2	-8.86	-89.42	3.42
Left Postcentral 1	-22.17	-33.83	69.91
Left Postcentral 2	-50.83	-21.20	39.50
Left Postcentral 3	-15.17	-45.55	76.45
Left Posterior Cingulate 1	-8.78	-16.54	41.07
Left Posterior Cingulate 2	-3.97	-21.90	36.04
Left Precentral 1	-22.32	-21.57	70.60
Left Precentral 2	-47.76	-4.59	35.59
Left Precuneus 1	-6.99	-59.41	52.34
Left Precuneus 2	-9.53	-58.97	30.30
Left Rostral Anterior Cingulate 1	-4.44	29.35	-5.06
Left Rostral Anterior Cingulate 2	-6.57	43.38	4.70
Left Rostral Middle Frontal 1	-28.73	48.26	19.11
Left Rostral Middle Frontal 2	-26.78	33.93	38.53
Left Rostral Middle Frontal 3	-39.54	43.20	18.05
Left Superior Frontal 1	-2.52	-1.40	64.85
Left Superior Frontal 2	-13.90	35.16	39.18
Left Superior Parietal 1	-23.97	-54.43	65.35
Left Superior Parietal 2	-25.35	-65.63	49.27
Left Superior Temporal 1	-32.87	12.42	-30.24
Left Superior Temporal 2	-53.28	-14.33	-4.89
Left Supramarginal 1	-55.20	-37.98	34.68
Left Supramarginal 2	-58.07	-56.02	26.62
Left Supramarginal 3	-48.28	-45.05	44.20
Left Transverse Temporal 1	-44.57	-25.11	11.38
Left Transverse Temporal 2	-46.05	-18.51	5.84
Left Insula 1	-37.64	-9.66	0.77
Left Insula 2	-36.04	8.76	-0.48
Left Thalamus Proper 1	-13.44	-20.87	9.62
Left Thalamus Proper 2	-13.73	-16.81	3.98
Left Caudate 1	-13.44	8.23	13.07
Left Caudate 2	-16.90	-2.40	16.91
Left Caudate 3	-18.92	-3.33	22.81
Left Caudate 4	-12.17	15.73	-1.87
Left Caudate 5	-17.51	17.78	5.52
Left Putamen 1	-25.93	-0.28	5.94
Left Putamen 2	-26.05	2.38	-5.17
Left Pallidum 1	-22.48	-9.66	1.42
Left Pallidum 2	-18.49	-0.95	-1.86
Left Hippocampus 1	-30.15	-25.52	-10.39
Left Hippocampus 2	-24.93	-21.59	-16.11
Left Amygdala 1	-21.99	-4.71	-20.55
Left Amygdala 2	-27.77	-6.79	-18.27
Left Accumbens Area 1	-10.34	11.45	-7.95
Right Accumbens Area 1	9.69	12.30	-7.62

Right Amygdala 1	25.54	-3.52	-27.22
Right Amygdala 2	19.11	-5.82	-19.27
Right Amygdala 3	21.76	-1.69	-19.35
Right Amygdala 4	27.45	-7.56	-17.68
Right Amygdala 5	24.89	-2.81	-16.60
Right Amygdala 6	29.06	-4.29	-16.56
Right Hippocampus 1	29.20	-25.17	-8.30
Right Hippocampus 2	26.14	-20.98	-15.77
Right Pallidum 1	23.67	-10.37	1.34
Right Pallidum 2	18.46	-0.19	-0.54
Right Putamen 1	23.14	6.79	-0.01
Right Putamen 2	29.76	-3.96	0.23
Right Caudate 1	15.33	3.20	13.88
Right Caudate 2	17.91	19.41	5.20
Right Caudate 3	12.06	18.11	-3.13
Right Caudate 4	18.89	-7.89	22.23
Right Caudate 5	10.19	7.25	10.82
Right Caudate 6	14.31	10.41	12.74
Right Thalamus Proper 1	13.10	-15.59	4.04
Right Thalamus Proper 2	13.42	-19.34	9.69
Right Insula 1	38.28	-4.91	-3.65
Right Insula 2	35.79	6.61	1.84
Right Transverse Temporal 1	46.63	-14.94	4.90
Right Transverse Temporal 2	44.03	-21.14	10.83
Right Supramarginal 1	44.70	-25.22	19.71
Right Supramarginal 2	55.79	-33.34	37.81
Right Superior Temporal 1	30.02	14.75	-33.21
Right Superior Temporal 2	54.48	-10.98	-4.18
Right Superior Parietal 1	21.41	-56.28	65.80
Right Superior Parietal 2	27.12	-65.00	47.14
Right Superior Frontal 1	5.94	47.29	-4.53
Right Superior Frontal 2	4.79	-2.94	62.96
Right Superior Frontal 3	13.61	35.49	37.77
Right Rostral Middle Frontal 1	38.83	47.47	15.39
Right Rostral Middle Frontal 2	38.29	32.15	29.71
Right Rostral Anterior Cingulate 1	6.81	42.18	8.86
Right Rostral Anterior Cingulate 2	4.22	32.89	-2.64
Right Precuneus 1	10.29	-48.01	69.24
Right Precuneus 2	9.62	-58.33	38.25
Right Precentral 1	46.31	-2.15	35.51
Right Precentral 2	59.33	6.07	28.27
Right Precentral 3	25.38	-21.00	67.83
Right Posterior Cingulate 1	8.22	-15.20	41.73
Right Posterior Cingulate 2	4.21	-20.98	36.46
Right Postcentral 1	21.20	-34.63	71.40
Right Postcentral 2	50.99	-17.43	37.36
Right Postcentral 3	11.51	-42.59	78.25
Right Pericalcarine 1	10.66	-90.37	3.78
Right Pericalcarine 2	14.03	-73.38	10.89
Right Pars Triangularis 1	43.23	27.16	2.05
Right Pars Triangularis 2	50.52	35.78	4.29
Right Pars Orbitalis 1	39.01	27.21	-7.13
Right Pars Orbitalis 2	44.63	37.44	-15.29
Right Pars Opercularis 1	43.92	17.05	5.80
Right Pars Opercularis 2	51.20	16.74	16.60
Right Paracentral 1	12.13	-31.00	51.20
Right Paracentral 2	4.51	-22.99	62.16
Right Parahippocampal 1	27.29	-33.47	-16.07

Right Parahippocampal 2	21.86	-28.17	-20.08
Right Middle Temporal 1	57.97	-26.91	-11.75
Right Middle Temporal 2	52.09	-36.30	1.78
Right Medial Orbitofrontal 1	3.72	50.54	-18.15
Right Medial Orbitofrontal 2	5.17	23.78	-19.08
Right Lingual 1	13.45	-68.28	-4.16
Right Lateral Orbitofrontal 1	18.76	9.89	-15.99
Right Lateral Orbitofrontal 2	22.70	40.24	-19.25
Right Lateral Occipital 1	43.59	-65.72	2.06
Right Lateral Occipital 2	31.63	-87.73	1.19
Right Isthmus Cingulate 1	5.31	-43.25	28.77
Right Isthmus Cingulate 2	10.86	-45.77	8.46
Right Inferior Temporal 1	48.96	-28.54	-27.70
Right Inferior Parietal 1	47.64	-63.84	30.98
Right Inferior Parietal 2	44.71	-66.96	14.29
Right Inferior Parietal 3	38.93	-61.11	41.50
Right Fusiform 1	30.67	-43.26	-18.63
Right Fusiform 2	35.97	-46.58	-20.74
Right Entorhinal 1	20.27	-8.02	-32.15
Right Entorhinal 2	21.42	3.41	-30.89
Right Entorhinal 3	25.09	-0.01	-38.45
Right Entorhinal 4	28.66	-5.82	-35.23
Right Entorhinal 5	29.48	-12.87	-33.10
Right Cuneus 1	7.28	-87.98	24.51
Right Cuneus 2	11.38	-72.00	24.17
Right Caudal Middle Frontal 1	38.45	16.57	44.37
Right Caudal Middle Frontal 2	34.67	7.26	53.99
Right Caudal Anterior Cingulate 1	5.66	19.88	30.93
Right Caudal Anterior Cingulate 2	4.93	22.06	23.24

Table S2. Brain regions belonging to the different modules of each timepoint's modularity community structure.

Timepoint 1	
Module	Area
1	Left Entorhinal 1
	Left Entorhinal 2
	Left Fusiform 1
	Left Fusiform 2
	Left Inferior Temporal 1
	Left Inferior Temporal 2
	Left Middle Temporal 1
	Left Middle Temporal 2
	Left Middle Temporal 3
	Left Parahippocampal 1
	Left Parahippocampal 2
	Left Superior Temporal 1
	Left Superior Temporal 2
	Left Transverse Temporal 1
	Left Transverse Temporal 2
	Left Hippocampus 1
	Left Hippocampus 2
	Left Amygdala 1

Timepoint 2	
Module	Area
1	Left Cuneus 1
	Left Cuneus 2
	Left Entorhinal 1
	Left Entorhinal 2
	Left Fusiform 1
	Left Fusiform 2
	Left Inferior Temporal 1
	Left Inferior Temporal 2
	Left Lateral Occipital 1
	Left Lateral Occipital 2
	Left Lingual 1
	Left Lingual 2
	Left Middle Temporal 1
	Left Middle Temporal 2
	Left Middle Temporal 3
	Left Parahippocampal 1
	Left Parahippocampal 2
	Left Pericalcarine 1

	Left Amygdala 2
2	Left Caudal Anterior Cingulate 1
	Left Caudal Anterior Cingulate 2
	Left Caudal Middle Frontal 1
	Left Caudal Middle Frontal 2
	Left Lateral Orbitofrontal 1
	Left Lateral Orbitofrontal 2
	Left Medial Orbitofrontal 1
	Left Medial Orbitofrontal 2
	Left Pars Opercularis 1
	Left Pars Opercularis 2
	Left Pars Orbitalis 1
	Left Pars Orbitalis 2
	Left Pars Triangularis 1
	Left Pars Triangularis 2
	Left Postcentral 1
	Left Postcentral 2
	Left Precentral 1
	Left Precentral 2
	Left Rostral Anterior Cingulate 1
	Left Rostral Anterior Cingulate 2
	Left Rostral Middle Frontal 1
	Left Rostral Middle Frontal 2
	Left Rostral Middle Frontal 3
	Left Superior Frontal 1
	Left Superior Frontal 2
	Left Insula 1
	Left Insula 2
	Left Putamen 1
	Left Putamen 2
	Left Pallidum 1
	Left Pallidum 2
	Left Accumbens Area 1
3	Left Inferior Parietal 1
	Left Inferior Parietal 2
	Left Postcentral 3
	Left Superior Parietal 1
	Left Superior Parietal 2
	Left Supramarginal 1
	Left Supramarginal 2
	Left Supramarginal 3
4	Left Thalamus Proper 1
	Left Thalamus Proper 2
	Left Caudate 1
	Left Caudate 2
	Left Caudate 3
	Left Caudate 4
	Left Caudate 5
5	Right Amygdala 1
	Right Amygdala 2
	Right Amygdala 3
	Right Amygdala 4
	Right Amygdala 5
	Right Amygdala 6
	Right Hippocampus 1
	Right Hippocampus 2
	Left Pericalcarine 2
2	Left Superior Temporal 1
	Left Superior Temporal 2
	Left Transverse Temporal 1
	Left Transverse Temporal 2
	Left Hippocampus 1
	Left Hippocampus 2
	Left Amygdala 1
	Left Amygdala 2
2	Left Caudal Middle Frontal 1
	Left Caudal Middle Frontal 2
	Left Lateral Orbitofrontal 1
	Left Lateral Orbitofrontal 2
	Left Medial Orbitofrontal 1
	Left Medial Orbitofrontal 2
	Left Pars Opercularis 1
	Left Pars Opercularis 2
	Left Pars Orbitalis 1
	Left Pars Orbitalis 2
	Left Pars Triangularis 1
	Left Pars Triangularis 2
	Left Rostral Anterior Cingulate 1
	Left Rostral Anterior Cingulate 2
	Left Rostral Middle Frontal 1
	Left Rostral Middle Frontal 2
	Left Rostral Middle Frontal 3
	Left Superior Frontal 1
	Left Superior Frontal 2
	Left Insula 1
	Left Insula 2
	Left Thalamus Proper 1
	Left Thalamus Proper 2
	Left Caudate 1
	Left Caudate 2
	Left Caudate 3
	Left Caudate 4
	Left Caudate 5
	Left Putamen 1
	Left Putamen 2
	Left Pallidum 1
	Left Pallidum 2
	Left Accumbens Area 1
3	Left Inferior Parietal 1
	Left Inferior Parietal 2
	Left Postcentral 1
	Left Postcentral 2
	Left Postcentral 3
	Left Precentral 1
	Left Precentral 2
	Left Superior Parietal 1
	Left Superior Parietal 2
	Left Supramarginal 1
	Left Supramarginal 2
	Left Supramarginal 3
4	Right Caudate 1
	Right Caudate 2

	Right Superior Temporal 1
	Right Parahippocampal 1
	Right Parahippocampal 2
	Right Inferior Temporal 1
	Right Fusiform 1
	Right Fusiform 2
	Right Entorhinal 1
	Right Entorhinal 2
	Right Entorhinal 3
	Right Entorhinal 4
	Right Entorhinal 5
6	Left Cuneus 1
	Left Cuneus 2
	Left Isthmus Cingulate 1
	Left Isthmus Cingulate 2
	Left Lateral Occipital 1
	Left Lateral Occipital 2
	Left Lingual 1
	Left Lingual 2
	Left Paracentral 1
	Left Paracentral 2
	Left Pericalcarine 1
	Left Pericalcarine 2
	Left Posterior Cingulate 1
	Left Posterior Cingulate 2
	Left Precuneus 1
	Left Precuneus 2
	Right Precuneus 1
	Right Precuneus 2
	Right Posterior Cingulate 1
	Right Posterior Cingulate 2
	Right Pericalcarine 1
	Right Pericalcarine 2
	Right Paracentral 1
	Right Paracentral 2
	Right Lingual 1
	Right Lateral Occipital 1
	Right Lateral Occipital 2
	Right Isthmus Cingulate 1
	Right Isthmus Cingulate 2
	Right Cuneus 1
	Right Cuneus 2
7	Right Insula 1
	Right Insula 2
	Right Transverse Temporal 1
	Right Transverse Temporal 2
	Right Supramarginal 1
	Right Supramarginal 2
	Right Superior Temporal 2
	Right Superior Parietal 1
	Right Superior Parietal 2
	Right Rostral Middle Frontal 1
	Right Rostral Middle Frontal 2
	Right Precentral 1
	Right Precentral 2
	Right Precentral 3

	Right Caudate 4
	Right Caudate 5
	Right Caudate 6
	Right Thalamus Proper 1
	Right Thalamus Proper 2
5	Right Accumbens Area 1
	Right Pallidum 1
	Right Pallidum 2
	Right Putamen 1
	Right Putamen 2
	Right Caudate 3
	Right Insula 1
	Right Insula 2
	Right Superior Frontal 1
	Right Superior Frontal 2
	Right Superior Frontal 3
	Right Rostral Middle Frontal 1
	Right Rostral Middle Frontal 2
	Right Rostral Anterior Cingulate 1
	Right Rostral Anterior Cingulate 2
	Right Precentral 1
	Right Precentral 2
	Right Precentral 3
	Right Pars Triangularis 1
	Right Pars Triangularis 2
	Right Pars Orbitalis 1
	Right Pars Orbitalis 2
	Right Pars Opercularis 1
	Right Pars Opercularis 2
	Right Medial Orbitofrontal 1
	Right Medial Orbitofrontal 2
	Right Lateral Orbitofrontal 1
	Right Lateral Orbitofrontal 2
	Right Caudal Middle Frontal 1
	Right Caudal Middle Frontal 2
6	Left Caudal Anterior Cingulate 1
	Left Caudal Anterior Cingulate 2
	Left Isthmus Cingulate 1
	Left Isthmus Cingulate 2
	Left Paracentral 1
	Left Paracentral 2
	Left Posterior Cingulate 1
	Left Posterior Cingulate 2
	Left Precuneus 1
	Left Precuneus 2
	Right Precuneus 1
	Right Precuneus 2
	Right Posterior Cingulate 1
	Right Posterior Cingulate 2
	Right Postcentral 1
	Right Postcentral 3
	Right Paracentral 1
	Right Paracentral 2
	Right Isthmus Cingulate 1
	Right Isthmus Cingulate 2
	Right Caudal Anterior Cingulate 1

	Right Postcentral 1
	Right Postcentral 2
	Right Postcentral 3
	Right Pars Triangularis 1
	Right Pars Triangularis 2
	Right Pars Orbitalis 1
	Right Pars Orbitalis 2
	Right Pars Opercularis 1
	Right Pars Opercularis 2
	Right Middle Temporal 1
	Right Middle Temporal 2
	Right Inferior Parietal 1
	Right Inferior Parietal 2
	Right Inferior Parietal 3
	Right Caudal Middle Frontal 1
	Right Caudal Middle Frontal 2
8	Right Accumbens Area 1
	Right Pallidum 1
	Right Pallidum 2
	Right Putamen 1
	Right Putamen 2
	Right Caudate 1
	Right Caudate 2
	Right Caudate 3
	Right Caudate 4
	Right Caudate 5
	Right Caudate 6
	Right Thalamus Proper 1
	Right Thalamus Proper 2
	Right Superior Frontal 1
	Right Superior Frontal 2
	Right Superior Frontal 3
	Right Rostral Anterior Cingulate 1
	Right Rostral Anterior Cingulate 2
	Right Medial Orbitofrontal 1
	Right Medial Orbitofrontal 2
	Right Lateral Orbitofrontal 1
	Right Lateral Orbitofrontal 2
	Right Caudal Anterior Cingulate 1
	Right Caudal Anterior Cingulate 2

	Right Caudal Anterior Cingulate 2
	Right Transverse Temporal 1
	Right Transverse Temporal 2
	Right Supramarginal 1
	Right Supramarginal 2
	Right Superior Temporal 2
	Right Superior Parietal 1
	Right Superior Parietal 2
	Right Postcentral 2
	Right Pericalcarine 1
7	Right Pericalcarine 2
	Right Middle Temporal 1
	Right Middle Temporal 2
	Right Lingual 1
	Right Lateral Occipital 1
	Right Lateral Occipital 2
	Right Inferior Parietal 1
	Right Inferior Parietal 2
	Right Inferior Parietal 3
	Right Cuneus 1
	Right Cuneus 2
	Right Amygdala 1
	Right Amygdala 2
	Right Amygdala 3
	Right Amygdala 4
	Right Amygdala 5
	Right Amygdala 6
	Right Hippocampus 1
	Right Hippocampus 2
	Right Superior Temporal 1
8	Right Parahippocampal 1
	Right Parahippocampal 2
	Right Inferior Temporal 1
	Right Fusiform 1
	Right Fusiform 2
	Right Entorhinal 1
	Right Entorhinal 2
	Right Entorhinal 3
	Right Entorhinal 4
	Right Entorhinal 5

CHAPTHER V

General Discussion

1. Discussion

The normal aging process induces changes in brain's structure and function along with alterations in cognition (Cabeza et al., 2017). Trajectories of cognitive performance in aging differ among individuals, with some presenting levels similar or even higher to their middle-aged counterparts whereas others exhibit significant cognitive decline (Habib et al., 2007; Josefsson et al., 2012). Factors such as years of formal education (Habib et al., 2007; Paulo et al., 2011; Santos et al., 2014), physical activity (Josefsson et al., 2012), mood (Santos et al., 2014), social inclusion (Paulo et al., 2011) and genetic and environmental factors (Barter and Foster, 2018) are known to influence inter-individual variability in cognitive aging. Nevertheless, the neural mechanisms which trigger different levels of cognitive abilities in older individuals are still poorly understood. The identification of in-vivo brain biomarkers responsible for the heterogeneity of cognitive trajectories in aging could help provide a healthier cognitive aging for the population and thus reduce the impact of aging in societies.

The advent of neuroimaging techniques enabled the study of the structure and function of the aging brain and the number of studies exploring the relations between the aging effects on the brain and on cognition is growing. Furthermore, the adoption of analytical tools from other fields, (e.g., graph theory and machine learning) motivated the emergence of new techniques in neuroimaging research, such as network analysis and CBP. These new methods can give new insights of the aging brain and generate predictive models of cognitive trajectories in aging (Spreng and Turner, 2019). Despite the growing popularity of these methods, their application in the aging field has been mostly limited to functional data. Particularly, studies exploring the existence of sub-networks with significant age-related changes in WM structural connectivity or applying CBP to WM structural connectivity data to investigate age-related changes in brain's structural network are inexistent. Moreover, despite the number of longitudinal studies is increasing, they still are outnumbered by cross-sectional studies.

The main goal of this thesis was to provide new evidence of brain WM biomarkers of healthy cognitive aging. In order to accomplish this, a sample of older adults, part of a larger sample representative of the Portuguese population, was followed longitudinally with an interval of 4 to 5 years between evaluations. At each evaluation, subjects underwent a multimodal MRI protocol and an extensive battery of neurocognitive testing. Network analysis and CBP methods were applied to the MRI data to unravel new insights about the age-related alterations in brain's structural network and how they associate with cognitive trajectories.

In the first study, we characterized the longitudinal changes of WM microstructural integrity and how these changes were associated with cognitive trajectories. Our results revealed a deterioration of WM integrity between the two evaluations, which is consistent with previous longitudinal studies (Sexton et al., 2014; Vinke et al., 2018). Moreover, we found significant associations between longitudinal changes in WM integrity and longitudinal changes in cognitive scores of memory, executive function and general cognition. These findings again replicate previous work and provide additional support to the "disconnection hypothesis" (Bendlin et al., 2010; Brickman et al., 2012; Carlesimo et al., 2010; Cremers et al., 2016; Davis et al., 2009; Gazes et al., 2016; Hedden et al., 2016; Kennedy and Raz, 2009; Madden et al., 2009; Sasson et al., 2012; Ystad et al., 2011). Although our study only replicates previous findings and uses traditional analysis techniques, it is still prominent for the aging literature since longitudinal studies are yet a minority and also because it allowed us to confirm that the period between evaluations was sufficient to detect changes in WM.

Next, we evaluated the longitudinal changes occurring in WM structural brain networks, both in terms of connectivity and topological properties. Our findings revealed a sub-network with significant changes in SC between timepoints. This sub-network was comprised of both increases and decreases in SC along time. Interestingly, decreases occur predominantly in intra-hemispheric connections and thus are mainly composed of association fibers. On the other hand, increases occur mostly in inter-hemispheric connections and are constituted by different types of WM tracts, such as association, commissural and projection fibers. These findings are in line with the "last-in, first-out" hypothesis, which postulates that regions/connections reaching full maturation later during development are more prone to age-related decline (Raz, 1999). Regarding WM, association fibers have a later peak of maturation in comparison to commissural and projection fibers and previous studies have found steepest declines of WM integrity in aging for this type of fibers (Bender et al., 2016; Benitez et al., 2018; Bennett and Madden, 2014; Brickman et al., 2012; Cox et al., 2016; Davis et al., 2009; Slater et al., 2019). To the best of our knowledge, our study is the first to identify sub-networks with longitudinal alterations in SC in aging and to provide evidence supporting the "last-in, first-out" hypothesis in terms of SC.

Regarding topological properties, our results suggest a decrease in integration and an increase in segregation during aging. Reduced integration was characterized by a decrease in the number of detected connector hubs, which play a key role in inter-modular communication, and also reduced connector-hub inter-modular connectivity. Increased segregation was described by an increase in the number of detected provincial hubs, which are regions with most of their connections within their own module. Our findings

are in line with a recent study (Puxeddu et al., 2020), which found differences in the modular structure of the brain's structural network across the human lifespan. Specifically, Puxeddu and colleagues found increased segregation described by a predominance of hemispheric-specific modules, a decrease in the participation coefficient and an increase in modularity in late lifespan. At older ages, the number of clusters was higher, but their sizes were smaller. A different study which investigated age-related changes in the brain's functional network also found evidence of decreased integration and increased segregation (Sala-Llonch et al., 2014). Overall, these findings also support the theory of a "disconnected" brain in aging.

In the last study, we developed a CBP method to create a new parcellation of the brain based on diffusion MRI data of an aging cohort. We implemented different state-of-the-art clustering techniques (hierarchical and *k*-means clustering) and evaluated their performance alone and in conjunction with data dimensionality reduction methods (Principal Component Analysis (PCA) and Self-Organizing Maps (SOM)). Furthermore, we established a new metric (fingerprint homogeneity) to evaluate the quality of a connectivity-based parcellation. Since the main goal of CBP is to group voxels with similar connectivity profiles (Eickhoff et al., 2015; Reuter et al., 2020), this metric evaluates if this goal was accomplished by attributing higher values if voxels inside a region establish more homogeneous connections (i.e., connections with the same brain regions) and lower values if voxels' connectivity is more heterogeneous (i.e., connections with different brain regions). Our metric has the advantage over other existing metrics (for a review of the existing metrics, see (Arslan et al., 2018)) of taking into account the type of connections each voxel establishes (i.e., homogeneous or heterogenous) but not the connectivity values which could lead to misleading results. Thus, we consider that our metric adequately evaluates a connectivity-based parcellation and could be used for any CBP study. In our study, we obtained higher fingerprint homogeneity scores for the developed CBP in comparison to the initial parcellation, meaning that the final parcellation is composed of parcels with high connectivity homogeneity. This result validates the developed CBP method and so our method could be used to create a parcellation of the human brain using data from any cohort.

Next, we used the developed parcellation to study longitudinal changes of brain's structural network in aging. First, we registered the parcellation to follow-up data of the same cohort and calculated the fingerprint homogeneity. The results were very similar to the baseline, which validates the use of the parcellation for the longitudinal analysis. Then, we applied the same network analysis tools of the previous study to evaluate longitudinal changes in connectivity and topological features of WM structural networks.

Our results once again revealed a sub-network with both decreases and increases in SC along time. Also in line with our previous study, decreases were mainly constituted of intra-hemispheric connections and increases occurred in inter-hemispheric connections. The replication of our previous findings further validates our CBP method and strengthens the importance of this finding, which has not been previously reported in studies of age-related changes in WM structural brain networks.

The analysis of the topological features revealed very interesting and challenging results. More specifically, we found a higher number of connector hubs and connector-hub driven inter-modular connectivity. Although previous fMRI studies report increased integration along aging (Cao et al., 2014; He et al., 2020), the opposite is reported in diffusion MRI studies (Puxeddu et al., 2020) and in our second study. It is our belief that such apparent discrepancy may be explained by the higher resolution of our parcellation, which might have contributed to the identification of a higher number of connector hubs that otherwise would not be captured due to an attenuation of the effects when considering the whole region. Overall, this study provided a new method to investigate brain alterations at higher resolutions which can give new insights regarding our understanding of the brain.

In conclusion, this thesis revealed that aging is characterized by alterations in WM microstructure and WM structural connectivity and also that these changes are associated with cognitive decline. One of the major findings was that connectivity within hemispheres decreases, while connectivity between hemispheres increases, which is in accordance with the "last-in, first-out" hypothesis. Furthermore, we also revealed that, during aging, the brain's structural network suffers a reorganization in terms of integration and segregation, which leads to a more "disconnected" brain. These findings may help identify the main drivers of WM alterations at different cognitive levels, that could lead to the development of new in-vivo brain biomarkers of inter-individual variability in cognitive trajectories.

Finally, this thesis also made a major contribution to the neuroimaging research field by developing a new method to create a connectivity-based parcellation of the brain and a new metric to evaluate the quality of parcellations. We demonstrated the applicability of the method by performing the analysis of longitudinal changes in brain's structural networks during aging. This analysis replicated our previous results (intra-hemispheric connectivity decreases and inter-hemispheric connectivity increases) but also revealed challenging aspects that could be the result of using a high-resolution partition of the brain. Thus, we believe our CBP method can be applied to study any research question and could reveal new

findings that can help advance our knowledge of the brain's structure and function. Additionally, it allowed us to replicate previous findings and disclose new insights about the aging brain.

2. Future Perspectives

The work developed in this thesis provided new evidence about the aging brain and its relationship with cognition. Moreover, new analysis methods for neuroimaging research were developed that may contribute to shed new light regarding brain's organization in health and disease. However, new questions were raised that we intent to address in future studies. Particularly, future work should investigate longitudinal changes in connectivity and topological properties of functional brain networks of the same aging cohort, in order to complement the longitudinal analysis of structural brain networks presented here. This will allow to explore structure-function relationships in aging. Additionally, the CBP method could be employed as a data reduction step in an age prediction framework that may give new insights about brain alterations in normal aging.

3. References

Arslan, S., Ktena, S.I., Makropoulos, A., Robinson, E.C., Rueckert, D., Parisot, S., 2018. Human brain mapping: A systematic comparison of parcellation methods for the human cerebral cortex. NeuroImage 170, 5–30. https://doi.org/10.1016/j.neuroimage.2017.04.014

Barter, J.D., Foster, T.C., 2018. Aging in the Brain: New Roles of Epigenetics in Cognitive Decline. The Neuroscientist 24, 516–525. https://doi.org/10.1177/1073858418780971

Bender, A.R., Völkle, M.C., Raz, N., 2016. Differential aging of cerebral white matter in middle-aged and older adults: A seven-year follow-up. NeuroImage 125, 74–83. https://doi.org/10.1016/j.neuroimage.2015.10.030

Bendlin, B.B., Fitzgerald, M.E., Ries, M.L., Xu, G., Kastman, E.K., Thiel, B.W., Rowley, H.A., Lazar, M., Alexander, A.L., Johnson, S.C., 2010. White Matter in Aging and Cognition: A Cross-Sectional Study of Microstructure in Adults Aged Eighteen to Eighty-Three. Developmental Neuropsychology 35, 257–277. https://doi.org/10.1080/87565641003696775

Benitez, A., Jensen, J.H., Falangola, M.F., Nietert, P.J., Helpern, J.A., 2018. Modeling white matter tract integrity in aging with diffusional kurtosis imaging. Neurobiology of Aging 70, 265–275. https://doi.org/10.1016/j.neurobiolaging.2018.07.006

Bennett, I.J., Madden, D.J., 2014. Disconnected aging: Cerebral white matter integrity and age-related differences in cognition. Neuroscience 276, 187–205. https://doi.org/10.1016/j.neuroscience.2013.11.026

Brickman, A.M., Meier, I.B., Korgaonkar, M.S., Provenzano, F.A., Grieve, S.M., Siedlecki, K.L., Wasserman, B.T., Williams, L.M., Zimmerman, M.E., 2012. Testing the white matter retrogenesis hypothesis of cognitive aging. Neurobiology of Aging 33, 1699–1715. https://doi.org/10.1016/j.neurobiolaging.2011.06.001

Cabeza, R., Nyberg, L., Park, D.C. (Eds.), 2017. Cognitive neuroscience of aging: linking cognitive and cerebral aging, Second edition. ed. Oxford University Press, New York, NY, United States of America.

Cao, M., Wang, J.H., Dai, Z.J., Cao, X.Y., Jiang, L.L., Fan, F.M., Song, X.W., Xia, M.R., Shu, N., Dong, Q., Milham, M.P., Castellanos, F.X., Zuo, X.N., He, Y., 2014. Topological organization of the human brain functional connectome across the lifespan. Developmental Cognitive Neuroscience 7, 76–93. https://doi.org/10.1016/j.dcn.2013.11.004

Carlesimo, G.A., Cherubini, A., Caltagirone, C., Spalletta, G., 2010. Hippocampal mean diffusivity and memory in healthy elderly individuals: A cross-sectional study. Neurology 74, 194–200. https://doi.org/10.1212/WNL.0b013e3181cb3e39

Cox, S.R., Ritchie, S.J., Tucker-Drob, E.M., Liewald, D.C., Hagenaars, S.P., Davies, G., Wardlaw, J.M., Gale, C.R., Bastin, M.E., Deary, I.J., 2016. Ageing and brain white matter structure in 3,513 UK Biobank participants. Nature Communications 7. https://doi.org/10.1038/ncomms13629

Cremers, L.G.M., de Groot, M., Hofman, A., Krestin, G.P., van der Lugt, A., Niessen, W.J., Vernooij, M.W., Ikram, M.A., 2016. Altered tract-specific white matter microstructure is related to poorer cognitive performance: The Rotterdam Study. Neurobiology of Aging 39, 108–117. https://doi.org/10.1016/j.neurobiolaging.2015.11.021

Davis, S.W., Dennis, N.A., Buchler, N.G., White, L.E., Madden, D.J., Cabeza, R., 2009. Assessing the effects of age on long white matter tracts using diffusion tensor tractography. NeuroImage 46, 530–541. https://doi.org/10.1016/j.neuroimage.2009.01.068

Eickhoff, S.B., Thirion, B., Varoquaux, G., Bzdok, D., 2015. Connectivity-based parcellation: Critique and implications. Human Brain Mapping 36, 4771–4792. https://doi.org/10.1002/hbm.22933

Gazes, Y., Bowman, F.D., Razlighi, Q.R., O'Shea, D., Stern, Y., Habeck, C., 2016. White matter tract covariance patterns predict age-declining cognitive abilities. NeuroImage 125, 53–60. https://doi.org/10.1016/j.neuroimage.2015.10.016

Habib, R., Nyberg, L., Nilsson, L.-G., 2007. Cognitive and Non-Cognitive Factors Contributing to the Longitudinal Identification of Successful Older Adults in the *Betula* Study. Aging, Neuropsychology, and Cognition 14, 257–273. https://doi.org/10.1080/13825580600582412

He, L., Wang, X., Zhuang, K., Qiu, J., 2020. Decreased Dynamic Segregation but Increased Dynamic Integration of the Resting-state Functional Networks During Normal Aging. Neuroscience 437, 54–63. https://doi.org/10.1016/j.neuroscience.2020.04.030

Hedden, T., Schultz, A.P., Rieckmann, A., Mormino, E.C., Johnson, K.A., Sperling, R.A., Buckner, R.L., 2016. Multiple Brain Markers are Linked to Age-Related Variation in Cognition. Cerebral Cortex 26, 1388–1400. https://doi.org/10.1093/cercor/bhu238

Josefsson, M., de Luna, X., Pudas, S., Nilsson, L.-G., Nyberg, L., 2012. Genetic and Lifestyle Predictors of 15-Year Longitudinal Change in Episodic Memory. Journal of the American Geriatrics Society 60, 2308–2312. https://doi.org/10.1111/jgs.12000

Kennedy, K.M., Raz, N., 2009. Aging white matter and cognition: Differential effects of regional variations in diffusion properties on memory, executive functions, and speed. Neuropsychologia 47, 916–927. https://doi.org/10.1016/j.neuropsychologia.2009.01.001

Madden, D.J., Spaniol, J., Costello, M.C., Bucur, B., White, L.E., Cabeza, R., Davis, S.W., Dennis, N.A., Provenzale, J.M., Huettel, S.A., 2009. Cerebral White Matter Integrity Mediates Adult Age Differences in Cognitive Performance. Journal of Cognitive Neuroscience 21, 289–302. https://doi.org/10.1162/jocn.2009.21047

Paulo, A.C., Sampaio, A., Santos, N.C., Costa, P.S., Cunha, P., Zihl, J., Cerqueira, J., Palha, J.A., Sousa, N., 2011. Patterns of cognitive performance in healthy ageing in northern portugal: A cross-sectional analysis. PLoS ONE 6, 1–9. https://doi.org/10.1371/journal.pone.0024553

Puxeddu, M.G., Faskowitz, J., Betzel, R.F., Petti, M., Astolfi, L., Sporns, O., 2020. The modular organization of brain cortical connectivity across the human lifespan. NeuroImage 218, 116974. https://doi.org/10.1016/j.neuroimage.2020.116974

Raz, N., 1999. Aging of the brain and its impact on cognitive performance: Integration of structural and functional findings. 2nd ed. Mahwah, N: Lawrence Erlbaum Associates; 2.

Reuter, N., Genon, S., Kharabian Masouleh, S., Hoffstaedter, F., Liu, X., Kalenscher, T., Eickhoff, S.B., Patil, K.R., 2020. CBPtools: a Python package for regional connectivity-based parcellation. Brain Structure and Function 225, 1261–1275. https://doi.org/10.1007/s00429-020-02046-1

Sala-Llonch, R., Junqué, C., Arenaza-Urquijo, E.M., Vidal-Piñeiro, D., Valls-Pedret, C., Palacios, E.M., Domènech, S., Salvà, A., Bargalló, N., Bartrés-Faz, D., 2014. Changes in whole-brain functional networks and memory performance in aging. Neurobiology of Aging 35, 2193–2202. https://doi.org/10.1016/j.neurobiolaging.2014.04.007

Santos, N.C., Costa, P.S., Cunha, P., Portugal-Nunes, C., Amorim, L., Cotter, J., Cerqueira, J.J., Palha, J.A., Sousa, N., 2014. Clinical, physical and lifestyle variables and relationship with cognition and mood in aging: A cross-sectional analysis of distinct educational groups. Frontiers in Aging Neuroscience 6, 1–15. https://doi.org/10.3389/fnagi.2014.00021

Sasson, E., Doniger, G.M., Pasternak, O., Tarrasch, R., Assaf, Y., 2012. Structural correlates of cognitive domains in normal aging with diffusion tensor imaging. Brain Structure and Function 217, 503–515. https://doi.org/10.1007/s00429-011-0344-7

Sexton, C.E., Walhovd, K.B., Storsve, A.B., Tamnes, C.K., Westlye, L.T., Johansen-Berg, H., Fjell, A.M., 2014. Accelerated Changes in White Matter Microstructure during Aging: A Longitudinal Diffusion Tensor Imaging Study. Journal of Neuroscience 34, 15425–15436. https://doi.org/10.1523/JNEUROSCI.0203-14.2014

Slater, D.A., Melie-Garcia, L., Preisig, M., Kherif, F., Lutti, A., Draganski, B., 2019. Evolution of white matter tract microstructure across the life span. Human Brain Mapping 40, 2252–2268. https://doi.org/10.1002/hbm.24522

Spreng, R.N., Turner, G.R., 2019. Structure and function of the aging brain., in: The Aging Brain: Functional Adaptation across Adulthood. American Psychological Association, Washington, DC, US, pp. 9–43. https://doi.org/10.1037/0000143-002

Vinke, E.J., de Groot, M., Venkatraghavan, V., Klein, S., Niessen, W.J., Ikram, M.A., Vernooij, M.W., 2018. Trajectories of imaging markers in brain aging: the Rotterdam Study. Neurobiology of Aging 71, 32–40. https://doi.org/10.1016/j.neurobiolaging.2018.07.001

Ystad, M., Hodneland, E., Adolfsdottir, S., Haász, J., Lundervold, A.J., Eichele, T., Lundervold, A., 2011. Cortico-striatal connectivity and cognition in normal aging: A combined DTI and resting state fMRI study. NeuroImage 55, 24–31. https://doi.org/10.1016/j.neuroimage.2010.11.016